SECOND ORDER WAVE LOADING ON VERTICAL CYLINDERS

by

DAVID M. ELLIX

Thesis submitted to The City University
for the Degree of Doctor of Philosophy
in the Department of Civil Engineering

OCTOBER 1984

SYNOPSIS

The total wave induced loading on a vertical surface-piercing cylinder can be considered to be the sum of the linear drag and inertia components, and a number of second order forces. This study investigates the second order forces, both theoretically and experimentally. The second order waterline, dynamic pressure and Stokes' wave forces have each been shown to make a significant contribution to the theoretical wave loading under certain conditions.

In the experimental facility used, the wave environment was found to include a significant free second harmonic wave. This imposed an additional second order force on the test cylinder, which was dependent on the amplitude and phase of the free wave. An experimental technique has therefore been developed and used to deduce the amplitudes and phases of the individual waves present, from measured wave records. The wave results highlighted some important characteristics of the wave generator and flume.

The wave induced loading on the test cylinders has been measured, and analysed by means of a Fast Fourier Transform to separate the Fourier components of the force. The measured force components were compared with the theoretical forces calculated using the measured wave data. The first order force results were used to compute values for the drag and inertia coefficients. These were in reasonable accord with previous published results.

The theoretical second order force components were the sum

of a large number of forces, which could not be separated experimentally. Numerical comparison between the total theoretical second order force components and the measured results showed good agreement in a large number of cases. The agreement was less good in those cases where the theoretical forces were dominated by the free second harmonic wave. Recommendations are made for further experimentation under conditions in which the free wave amplitude is minimized.

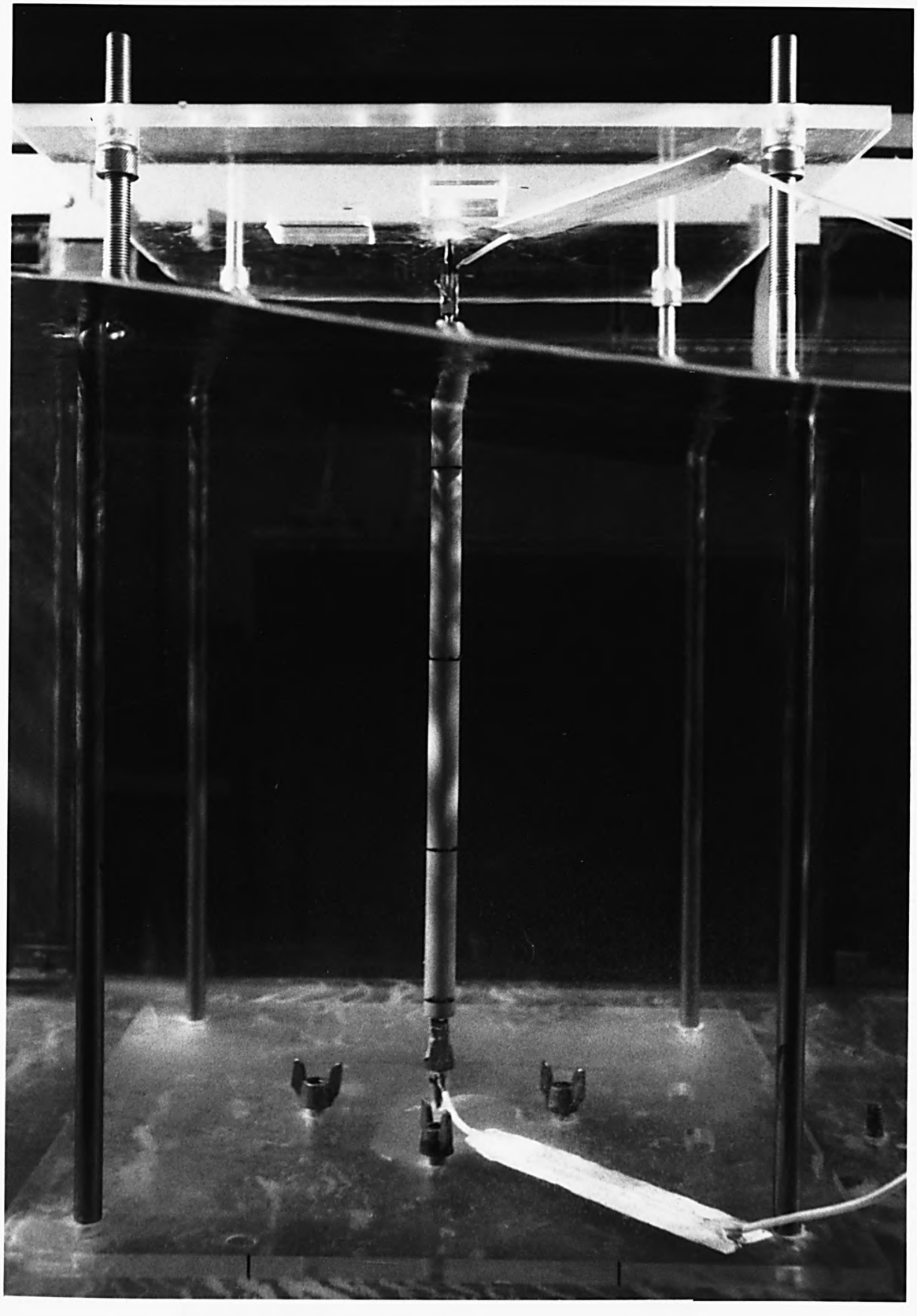

TEST CYLINDER UNDER WAVE ACTION

Acknowledgements

The work reported in this thesis was carried out in The City University, Department of Civil Engineering, under the supervision of Dr. K. Arumugam, to whom I would like to express my gratitude. Thanks are also due to my colleagues at The City University, particularly to [redacted] for his assistance at the beginning of the work.

I would like to thank the laboratory technical staff, especially [redacted] for his help with the design and construction of the testing rig.

I am grateful to [redacted] for his assistance with the design and construction of the electronic filter.

I am indebted to [redacted] for undertaking to type this manuscript.

This work was made possible by the award of maintenance and support grants by the Science and Engineering Research Council.

This thesis is dedicated to my wife, [redacted], for her tolerance and encouragement throughout the period of the study.

CONTENTS

LIST OF FIGURES

LIST OF TABLES

CHAPTER 1 - INTRODUCTION

1.1 Background

The severe wave conditions encountered by offshore structures and the forces which they impose must be clearly understood, and yet simply described, in the development of a useful design technique.

The design wave conditions, statistically determined to represent the worst conditions which will occur during the lifetime of the structure, are commonly simplified to a regular wavetrain of given height and period. Alternatively the use of spectral techniques allows the wave environment, and hence the forces imposed on the structure, to be represented by a spectral density function. The particle kinematics under the wave cannot be exactly described, but may be approximated by either a linear or higher order wave theory, as appropriate to the wave conditions.

Whatever method is used to determine the particle kinematics, the design forces are calculated by Morison's equation. This expression, derived by Morison, O'Brien, Johnson and Schaaf (1950) in response to demand for a simple design formula, expresses the total force as the sum of drag and inertia components, each governed by an empirical coefficient. A great deal of work has since been done to determine suitable values for the drag and inertia coefficients. The results have tended to be rather diverse, with the measured coefficients depending as much on the way in which they were defined and measured, as on anything else.

The uncertainties involved in the application of Morison's equation have lead to the use of large safety factors. As the exploration for oil, particularly in the North Sea, pushes out into deeper, more hostile conditions, the design can become uneconomical. Thus if the oil reserves in these locations are to be fully exploited, a better understanding of the wave loading mechanism is essential.

Lighthill (1979) was critical of Morison's equation and its assumption that the inertia force arises from the linear interaction between the structure and the irrotational flow field, even where the fluid kinematics are described by a highly non-linear theory. He suggested that the mathematical representation of wave induced loading would be improved by the inclusion of a number of second order forces, arising from the non-linear interaction between the structure and the wave.

1.2 Scope of the Present Study

This study sets out to demonstrate the theoretical derivation of Lighthill's second order forces, for the case of a vertical surface-piercing cylinder, and to identify them experimentally.

The theoretical description of wave induced loading is extended from the linear approximation, given by Morison's equation, by considering the effect of a number of second order forces.

The second order-Stokes' wave forces arise from the correction to the velocity potential, which results from the extension of the wave theory to its second order of approximation.

The waterline forces (Lighthill) are calculated by taking the upper limit of the integration of the elemental forces to be the instantaneous free surface, rather than the undisturbed water level.

The second order forces which arise from the convective acceleration, and from the variation in dynamic pressure (Lighthill), are also considered.

The experimental facility used in this study consists of a long rectangular wave flume, with a wedge type wavemaker at one end and an absorbing beach at the other. The wave environment produced in the flume includes a significant free second harmonic wave, which imposes an additional second order force on the test cylinder.

In order to determine the amplitudes and phases of the waves present in the flume, an experimental technique is developed, based on the analysis of wave records by the Fast Fourier Transform. The measured wave data is then used to calculate the theoretical force components, and at the same time identifies several characteristics of the wave generator, the beach and the interaction between the wave components.

The wave loading on the test cylinders is measured by means of force transducers at the top and bottom. The Fast Fourier Transform is used to compute the Fourier compositions of the top and bottom end reactions. These allow the Fourier components of the resultant force to be evaluated, together with their respective depths of action.

The forces on the cylinder are analysed by considering the first, second and third harmonic components separately. The first order wave and force results are used to calculate the drag and inertia coefficients C_m and C_d. The deviation of these coefficients from some previously published results demonstrates the scale effects associated with this study, where the Reynolds' numbers are very low.

The first order coefficients are used in conjunction with the second order wave data to calculate the theoretical second order forces. These are then compared with the measured results. In those cases where the agreement is not very good, the discrepancy is attributed to the limitations in the experimental set up, particularly the presence of the free second harmonic wave.

The measured third order forces are used to test the validity of the mathematical expression for the drag force.

It is recognized that the experimental work has covered only a limited range of conditions in terms of the Reynolds' number, and also that the free second harmonic wave caused problems in a number of tests. Further study to explicitly identify the second order components requires refinements which are listed in the subsequent chapters.

CHAPTER 2 - LITERATURE SURVEY

2.1 Introduction

The state of the art reviews carried out on the subject of wave induced loading; Hogben et al.(1977), Sarpkaya and Isaacson (1981), have demonstrated that the measurement and prediction of wave forces involves two distinct stages.

Firstly, the wave environment must be described in a manner which allows certain parameters of the fluid motion, such as the velocity field beneath the wave, to be either measured, or predicted by a suitable theory.

Secondly, a framework must be developed to relate the forces to the wave environment. This framework must correlate measured wave force data, and allow the prediction of the forces on structures due to other wave environments.

Any sensible review of the literature on the subject must make this same distinction. This chapter therefore deals with the broader subject of waves and wave hydrodynamics, before considering the more specialized area of wave induced loading.

A great deal of work has been done in developing theoretical descriptions of wave motion. The various theories are each applicable over certain ranges of wave conditions, as governed by water depth, wavelength and wave height. Simple theories have been developed which are easily applied to give approximate solutions,

while higher order theories, which are computationally more involved, lead to more accurate solutions.

The situation of waves in a laboratory test facility has been extensively researched. The effects of the wave generator and the wave flume have been considered both analytically and experimentally.

The loading on structures in waves has been of increasing interest since the development of offshore oil fields. Morison et al.(1950) proposed a simple formula, termed Morison's equation, expressing the total load on an element of a vertical cylinder as the sum of two components. Since then, much of the work has been concentrated on empirical determination of the two coefficients in Morison's equation.

Morison's equation has always been subject to the criticism that it over-simplifies the true mechanics of the loading. Recently Lighthill (1979) has suggested that a number of second order effects should be taken into account, in order to give a better representation.

2.2 Wave Hydrodynamics

Much of the classical theoretical work on the hydrodynamics of wave motion was carried out in the second half of the last century. One of the most important papers of this period was by Stokes (1847), reprinted with a supplement in 1880.

Stokes assumed that waves were propagated without change of form, and that the problem could be reduced to one of two dimensions for the case of long-crested waves. He further assumed that the fluid through which the waves travelled was incompressible, homogeneous and inviscid.

The problem was therefore set out as a solution of Laplace's equation of continuity, subject to a number of boundary conditions, and expressed in terms of the velocity potential. The first of the boundary conditions was one of no flow through the rigid bottom on which the fluid rested. Two further conditions were applied at the free surface of the fluid. One expressed the condition that fluid particles initially at the surface remained at the surface, and the other was an application of the unsteady state Bernouilli equation. These three conditions are referred to as the bottom, surface kinematic, and surface dynamic boundary conditions respectively.

Stokes solved the problem to a first order of approximation by neglecting small quantities such as the squares of the particle velocities and the slope of the free surface. In addition he applied the surface boundary conditions at the still water level, rather than at the unknown free surface position.

This derivation, commonly referred to as small amplitude or linear wave theory, predicted the surface profile to be a sinusoid travelling in the positive x-direction without change of shape. The velocity potential determined in this solution showed that the fluid particles moved in closed orbits, with no net

displacement at the end of a complete wave period. The particle orbits were shown to be circular in deep water and elliptical in water of finite depth, and their amplitude was found to decrease with the depth of the particle below the surface.

The celerity of propagation of the waveform was shown to depend on the wavelength and water depth, indicating that water surface waves represent a dispersive system. In this linear approximation, the celerity was found to be independent of the wave height.

Stokes extended his solution to a second order of approximation by substituting the first order velocity potential into the smaller terms neglected in the linear derivation. The surface boundary conditions were effectively applied at the instantaneous free surface by means of a Taylor's series expansion about the undisturbed water level.

The second order solution introduced terms at twice the frequency into both the wave profile and velocity potential. The second order correction to the wave profile had the effect of sharpening the wave crests and flattening the troughs. The particle orbits were no longer closed, but there was now a net velocity in the positive x-direction, termed the drift or mass transport velocity. The linear formula for celerity was shown to be correct to the second order of approximation.

Stokes introduced a perturbation technique, which allowed

the theory to be extended to any order of accuracy, by utlizing the result from the preceeding order. However, as Stokes observed, this process involved increasingly lengthy mathematical effort at the higher orders of approximation.

Standard solutions for Stokes fifth order waves were determined by Skjelbreia and Hendrickson (1961). They demonstrated that the expressions for the wave profile and the velocity potential were Fourier series with twenty unknown coefficients A,B and a perturbation parameter λ. Explicit expressions were given for each of these coefficients and the results were presented in tabular form for a range of depth to wavelength ratios.

The authors assumed that the wave would be described in terms of the water depth, wave height and period. They gave a pair of simultaneous equations to be solved for the wavelength to depth ratio and for the perturbation parameter, in order that the tabulated results could be used for the Fourier coefficients. As noted by Sarpkaya and Isaacson (1981), the development of a computer program based on this formulation of Stokes' fifth order wave theory would not be unduly difficult.

The requirement for convergence in the Stokes wave expansion method is that each term in the velocity potential series is an order of magnitude smaller than the preceeding term. This places a restriction on the wave height in shallow water, beyond which a separate shallow wave expansion must be used.

Steep waves moving in very shallow water are outside the range of the present study, but brief consideration will be given to the wave theories appropriate for these conditions. Korteweg and de Vries (1895) developed a shallow water wave theory in which the wave characteristics were expressed in terms of the Jacobian elliptic function, cn. This was termed the cnoidal wave theory.

The cnoidal wave theory was derived by changing the horizontal and vertical length scales. The vertical ordinate was 'stretched' by non-dimensionalizing the vertical and horizontal by the water depth and wavelength respectively. A typical cnoidal wave profile has short steep crests separated by long flat troughs. Use of the elliptic function maintained the periodicity of the wave profile.

A limiting case of the cnoidal wave is one in which the crests are so far apart that they can be considered as totally separate from one another. In this case the wavelength can be considered to be infinite, and the wave will be defined solely by the undisturbed water depth and the wave height. Solitary waves, as such waves are called, were first reported by Scott Russell (1844) on the basis of experimental observation.

A review of work carried out on the cnoidal and solitary wave theories, including their extension to higher orders of approximation, was given by Sarpkaya and Isaacson (1981).

A numerical method for predicting two dimensional wave characteristics based on a stream function representation was

introduced by Dean (1965). He tackled two separate problems: firstly to provide a fit to a measured wave profile, and secondly to represent a theoretical wave given by its period, wave height and water depth.

The method derived for fitting a measured profile was a least squares perturbation technique to minimize the errors in both the dynamic boundary condition and the fit to the measured profile. In each successive iteration small changes were made to the assumed wavelength and period and to the Fourier coefficients of the stream function expression. After three or four cycles the changes were found to be negligible.

In the second problem of a theoretical wave profile, the period was not an unknown and the solution was of a slightly different form. The stream function representation was shown to have two advantages over the velocity potential method. One set of coefficients defined all the characteristics of the wave system, and the stream function expression exactly satisfied the kinematic free surface boundary condition.

Dean compared the velocity potential and stream function representations for the particular case of a highly non-linear theoretical wave, with both approximations taken to the seventh order. The stream function method gave a better fit to the dynamic surface boundary conditions, and also resulted in a smoother wave profile.

Dean further demonstrated that the stream function method could take account of a uniform current flowing in the x-direction and of a pressure distribution at the surface.

With the number of wave theories available, it is important, from an engineering point of view, that the ranges of validity of each theory should be known. For a particular location, where a proposed structure is to be sited, the wave environment may be specified in terms of a design wave.

The design wave is generally described by its height, period and still water depth. Theoretical and experimental work has been carried out to assess which wave theory is appropriate for different ratios of these parameters.

Dean (1970) undertook a theoretical comparison of a number of wave theories on the basis of the fit to the dynamic surface boundary condition. He considered waves of between 25% and 100% of the breaking height. The wave theories included in Dean's study were linear wave theory, third and fifth order Stokes, first and second order cnoidal, first and second order solitary, and fifth order stream function theory.

Initially considering only the analytical wave theories, Dean found that Stokes fifth order theory gave the best fit in deep water. In shallow water the closest fit was given by first order cnoidal theory, while in the intermediate range the linear wave theory was most applicable. When the numerical stream function theory was included, it was found to give the closest fit to the

dynamic surface boundary condition, in all except the very shallowest water.

In order to test the justification for using boundary condition fit as a guide to the choice of theory, Dean calculated the total drag force on a cylinder in the wave using the different wave theories. In shallow water he found that the cnoidal and linear wave theories, which had both given good fits to the boundary condition, gave vastly different estimates for the force. Thus he concluded that the boundary condition fit might not be an appropriate measure of wave theory validity in shallow water.

Iwagaki and Sakai (1970) compared various wave theories in an experimental study of the horizontal particle velocities. Under a range of wave conditions, the vertical distribution of horizontal velocity under the wave crest was measured by tracing the motion of hydrogen bubbles. The time variation of the horizontal velocity at a fixed level below the surface was recorded using a pair of hot wire anenometers.

These results were compared with the horizontal particle velocities predicted by the linear wave theory, Stokes third order theory, and hyperbolic wave theory representing an approximation of the cnoidal theory.

There was some scatter in the results, but the velocities were closely predicted by Stokes third order theory in deep water, and by the hyperbolic wave theory in shallow water.

Chakrabarti (1980b) performed a series of experiments in which the horizontal and vertical velocities, together with the dynamic pressure, were measured under a range of wave conditions. Waves were generated in relatively deep water, then travelled over a sloping bottom to a shallower test section. For the shorter waves tested, this change in water depth had little or no effect, and the measurements made in the test section showed good agreement with linear wave theory.

However, for the longer waves, the shoaling bottom caused the waves to break down, giving rise to multiple peaks, or solitons, in their profiles. These solitons travelled independently of the main wave, causing the waveform to vary as it travelled down the flume. In comparing these waves with the cnoidal and stream function theories, Chakrabarti assumed that the waves were of constant form. Thus his results and conclusions are subject to the criticism that they have not accounted for the wave conditions existing in the flume.

Other comparisons of the wave theories, as summarized by Sarpkaya and Isaacson (1981), generally agree that deep water waves are well represented by higher order Stokes or stream function theory, and the shallow water waves by cnoidal theory.

2.3 Laboratory Wave Environment

In a laboratory test facility waves are generated at one end of a long rectangular flume. The wave environment in the flume will be subject to effects caused by the wave generator and by the flume itself. Amongst the effects which must be considered are

the generation of free second harmonic waves, and the reflection of waves from the beach at the far end of the flume.

Havelock (1929) considered waves in which the fluid velocity had an assigned value at every point on a given vertical surface. These he described as forced waves. The forcing was shown to impose an additional boundary condition on the fluid motion. This boundary condition was applied on the prescribed surface, which could be considered to be the face of a wave generator.

Havelock analysed the important case in which the surface oscillated horizontally in simple harmonic motion, representing a piston type generator. His solution for this situation, based on small amplitude wave theory, introduced an additional term into the expressions for both the velocity potential and the surface profile. These terms were shown to be large in the immediate vicinity of the generator, but to decay exponentially with the distance from it.

Ursell, Dean and Yu (1960) were concerned with the amplitude of the waves produced by both piston and paddle type wavemakers. Following on from Havelock's (1929) work, they applied the boundary condition of no flow through the face of the generator. Their solution gave expressions for the ratio of wave height to wavemaker stroke for both types of wavemaker. This wave amplitude ratio was shown to depend solely on the ratio of wavelength to water depth in both cases.

The theoretically derived relationship for the wave amplitude ratio was tested experimentally for the piston type wave

generator. The results showed that the theory overestimated the wave amplitude ratio by between 3% and 10%, increasing with wave steepness.

Madsen (1971) analysed the generation of waves by a piston wavemaker to the second order of approximation. By limiting his consideration to long waves, he was able to neglect the exponentially decaying terms in the velocity potential near the generator. The second order velocity potential was assumed to be the sum of two components. The first was found by considering the second order surface boundary conditions, and consequently corresponded to the second order term associated with a Stokes progressive wave. The second component was due to a significant non-linear forcing term in the wavemaker and was shown to give rise to a free second harmonic wave travelling independently of the main wave.

Madsen derived an expression for the amplitude of the free second harmonic wave in terms of the first order wave amplitude, wavelength and water depth. This was tested experimentally for two wave settings by comparing the measured wave profile at two locations in the wave flume with the predicted profile. The agreement was reasonable for waves of moderate steepness, but not as good for the steeper waves.

The author also suggested that introducing a second order component into the wavemaker motion should reduce the amplitude of the free wave. This was based on the intuitive concept that to generate a wave of permanent form, the wavemaker motion should correspond, as closely as possible, to the particle motion under the desired wave. This was tested experimentally with moderate success.

Buhr Hansen and Svendsen (1974) analysed the interaction between the second order Stokes term and the free second harmonic wave. They derived an expression for the theoretical beating effect in the total second harmonic motion. The maximum second harmonic amplitude was shown to be the sum of the Stokes component and the free wave, and the minimum to be the difference.

A series of experiments were carried out in which the variation in the second harmonic wave amplitude was recorded. This was done by taking a continuous record of the output from a wave probe as it moved slowly down the flume. The output was passed through a band-pass filter to remove the first harmonic motion. This gave a record of the second harmonic variation, from which the amplitudes of the two components could be determined.

The measured value of the second order Stokes component was compared to the theoretical value, calculated from the first order wave amplitude, for each test run. The agreement was found to be reasonable.

The measured second harmonic wave amplitudes were compared with the predicted values of Madsen (1971), but showed very poor agreement. It was likely that the shallow water assumption made in Madsen's derivation was not justified in this case, where the depth to wavelength ratio was somewhat greater.

Buhr Hansen and Svendsen were able to make a very considerable reduction in the amplitude of the free second harmonic wave by including a second harmonic component in the wave generator motion,

as had been suggested by Madsen (1971).

The generation of waves by a body oscillating in the water surface is analytically more complex than generation by a moving vertical surface. Possibly for this reason plunger type wavemakers are less widely used in laboratory facilities than are pistons or paddles.

Ursell (1949) analysed the simplest case of a circular cylinder oscillating in the surface of water of infinite depth. The formulation of the problem was similar to that of Havelock (1929), in that an additional boundary condition was imposed on the surface of the wavemaker. In the case of the oscillating cylinder, this boundary condition stated that the velocity component of the fluid normal to the boundary was equal to the corresponding component of the velocity of the cylinder.

The shape of the boundary made it more convenient to express the problem in polar co-ordinates. Ursell used a multipole technique to determine an expression for the amplitude of the generated wave at a distance from the cylinder. The wave amplitude ratio, in this case the ratio of the wave amplitude to the cylinder oscillation amplitude, was shown to depend on the ratio of the cylinder radius to the wavelength.

Wang (1974) considered plungers of more general shape. By using a two parameter conformal transformation, he was able to represent any plunger shape by its depth, breadth and cross sectional area. He showed, similarly to Ursell's case for the cylinder, that

in deep water the wave amplitude ratio for a given plunger geometry depended on the ratio of its breadth to the wavelength. He produced a series of theoretical curves for wave amplitude ratio, covering a range of plunger geometries.

The theoretical relationships were tested experimentally with two triangular plungers of different depth to breadth ratio. The results showed good agreement over the whole range of wave conditions covered.

The theory of wave generation by a plunger type wavemaker has not been successfully extended to its second order of approximation in any published work. Particularly lacking from the literature is any account of the generation of free second harmonic waves or any estimation of their amplitudes. This point has been noted by the writer, Ellix and Arumugam (1984).

A major problem in any wave flume facility is the dissipation of the wave energy at the far end of the flume. This is normally achieved by means of a spending beach, which essentially represents a gradual reduction in the water depth. The mechanism by which the energy is dissipated is generally recognised as being wave breaking, which converts the energy into water circulations or heat. Mahony and Pritchard (1980) suggested that in cases where the slope of the beach was very gradual, viscous effects including bottom friction made a significant contribution to the energy dissipation.

Some observers, for example Buhr Hansen and Svendsen (1974), produced beach layouts which, they assumed, absorbed all of the wave

energy. It is generally accepted however that some energy will be reflected in the form of a small wave travelling back down the flume. The reflected wave is predominantly of the same frequency as the incident wave, and its amplitude is given by a reflection coefficient times that of the incident wave.

Eagleson and Dean (1966) discussed the interaction, or beating, between the incident and reflected waves, and its effect on the particle orbits. The first order wave amplitude was shown to vary down the flume between a maximum of the sum of the incident and reflected waves, and a minimum of the difference.

A simple procedure, based on measurement of the beating effect, was used, for example, by Ursell, Dean and Yu (1960) to estimate the amplitudes of the incident and reflected waves. The wave amplitude was measured at approximately 25 positions in the flume, spread over one wavelength. From the pattern of the variation in the wave motion, the amplitudes of the incident and reflected waves were easily evaluated.

An alternative technique for estimating the amplitudes of the incident and reflected waves was proposed by Goda and Suzuki (1976). The procedure was based on the Fast Fourier Transform, and could be extended to cover random wave tests.

Expressions were developed for the amplitudes of the incident and reflected waves, in terms of the amplitudes and relative phases in records taken from two wave probes a small distance apart.

The technique was tested experimentally for a number of regular wave conditions. The amplitudes of the incident and reflected waves calculated in this manner compared very well with those calculated by the more established maximum and minimum wave amplitude method.

Although this technique gave a very rapid estimation of the wave amplitudes, it was subject to a number of assumptions and limitations. The wavelength was assumed to be known, and the wave probe separation could not be a multiple of half the wavelength. Because records were only taken at two positions in the flume, the results were susceptible to signal noise and randon variations in the wave amplitude.

A method chosen by some observers to eliminate the effect of reflection is the 'burst' method. In this method, the wavemaker is started from rest and produces a small number of waves. All observations are made in the unsteady conditions before any reflected waves have had time to return to the test section. Madsen (1970) considered the variability of the wave height in a short burst of approximately 15 waves. He experimentally observed the wave height to be unstable, and in particular noted that the first and last waves were considerably larger than the others.

Madsen derived a relationship between the height of a given wave and the steady wave height which would be present if the generator was left running. This remains, however, a difficult method to use, and most observers prefer to make small corrections to their results to allow for the reflected wave.

2.4 Wave Loading

In response to demand for a design formula for the loading on offshore structures due to waves, Morison et al.(1950) proposed a formula in which the total force on an element of a vertical cylinder was expressed as the sum of two components. The first component was a drag force, having a similar form to the steady flow situation, and proportional to the square of the fluid velocity. The drag force was represented by a drag coefficient C_d, which it was expected, would assume substantially the same value as for steady flow.

The second force component was due to the pressure field causing the fluid acceleration. This force was proportional to the accelerative force exerted on the mass of water displaced by the cylinder. A coefficient was introduced into the expression for this force to account for the added mass effects of the flow of water around the cylinder. This was termed the coefficient of mass, C_m, later referred to as the inertia coefficient.

A major criticism of Morison's equation is that it assumes that the two force components are respectively equal to zero at the instants of zero velocity and acceleration in the wave cycle. Morison et al. conducted a series of experiments in which the total moment exerted on a vertical cylinder was recorded over a number of wave cycles. The measured moments at the times of zero velocity and acceleration, as determined from the wave profile and linear theory, were used to evaluate C_m and C_d respectively. In spite of the foregoing criticism, the authors found that the remainder of

the moment trace, calculated using these coefficients, agreed very well with the measured trace.

Morison's equation has been, and remains, the main technique used in the estimation of wave forces on structures, in cases where the structure is small relative to the wavelength. Where the size of the structure becomes a greater proportion of the wavelength, scattering effects become significant and a diffraction technique, such as that of MacCamy and Fuchs (1954), must be employed. The use of diffraction theory to estimate the wave forces on large bodies was examined at length by Sarpkaya and Isaacson (1981), and will not be considered further in this review.

The widespread use of Morison's equation has led to great interest in ascertaining appropriate values for the drag and inertia coefficients. In the absence of any adequate theoretical description, the coefficients have been determined by a variety of experimental techniques. The experimental programmes undertaken can be broadly classified into three categories.

In the most fundamental series of experiments, the complex kinematics of the fluid under a wave were replaced by a simple harmonic oscillation of water past the body. This was achieved by Sarpkaya (1976) by oscillating water in a U-tube past a fixed cylinder, and by Garrison et al.(1977) by moving a cylinder through still water. This form of experimentation is subject to the criticism that the kinematics are oversimplified and that the results obtained cannot be applied directly to waves. It has, however, allowed the wave force mechanism to be tested over a wide

range of simulated conditions.

Experiments carried out under laboratory wave conditions give a better representation of the wave structure interaction. In tests, such as those of Chakrabarti et al.(1976) on vertical cylinders, the particle kinematics can be described by a suitable wave theory. These experiments are carried out under controlled repeatable conditions, but are subject to significant scale effects.

Several studies have been carried out to measure the forces exerted on a test structure under actual sea conditions. The test structures were located some distance offshore and the loading under storm conditions was recorded. These real sea tests give a good representation of wave forces under the conditions which a prototype structure would encounter. The results are, however, difficult to correlate, because the wave environment is highly irregular, and subject to currents of unknown magnitude.

A critical review of the work on the determination of Morison's coefficients was presented by Hogben, Miller, Searle and Ward (1977). They considered the range of test conditions covered, the trends and scatter in the results for C_m and C_d, and recommended values to be taken under various wave conditions. A few of the important papers are discussed below.

Keulegan and Carpenter (1958) carried out a series of experiments to investigate the dependence of the Morison coefficients on the period parameter. This parameter, which subsequent observers termed the Keulegan Carpenter number, KC, expressed the

ratio of the particle motion to the cylinder diameter. Their experiments were carried out with horizontal cylinders positioned under the node of a standing wave. Since the fluid motion was assumed to be uni-directional and simple harmonic, this study fits into the same category as the later U-tube experiments.

The Keulegan Carpenter number is an important parameter in assessing the relative magnitudes of the drag and inertia forces. For constant drag and inertia coefficients, the ratio of drag to inertia force is directly proportional to KC. Thus at low values of KC the inertia force dominates, while at higher values the loading is predominantly drag.

The results for C_m and C_d indicated the existence of a critical Keulegan Carpenter number at which C_m reached a minimum, while C_d was at its maximum. The authors gave a physical explanation for this in terms of separation effects. This was based on an examination of the eddy shedding frequency, and was supported by flow visualization tests.

At low values of KC, no vortices were shed during the wave cycle. The drag coefficient was therefore relatively low, while the inertia coefficient approximated to its theoretical values of 2. Conversely at very high values of KC, a continuous von Karman street of vortices was shed from alternate sides of the cylinder. Under these conditions the drag coefficient tended towards its steady flow value. The critical Keulegan Carpenter number was shown to correspond to the formation and shedding of a single eddy in each half cycle.

Keulegan and Carpenter stated that they could find no trend with Reynolds' Number, Re, in either of the coefficients. However, their results were re-analysed by Sarpkaya (1976a) using an additional dimensionless variable known as the frequency parameter, β, which is the ratio of the Reynolds' number to the Keulegan Carpenter number. In this way, Sarpkaya was able to show that the results of Keulegan and Carpenter for C_m and C_d did indeed have clearly defined trends with Reynolds' number.

Sarpkaya performed a series of experiments in which the forces on cylinders, due to the harmonically oscillating flow in a U-tube, were measured. The use of the frequency parameter as an intermediate step in assessing Reynolds' number dependence was very convenient for Sarpkaya, and for other observers carrying out U-tube experiments. The period of oscillation was constant for any given U-tube arrangement, thus the frequency parameter varied solely with the cylinder diameter.

Sarpkaya was able to identify the variation of the Morison coefficients with both KC and Re. As the Reynolds' number increased, the drag coefficient reduced to a minimum, the value of which depended on KC, and then began to increase with further increases in Re. The inertia coefficient was found to increase with Re, reach a maximum, and then gradually approach a constant value of about 1.75. The two coefficients were found to be independent of Reynolds' number for values below about 20,000, which may explain the conclusions reached by Keulegan and Carpenter. Sarpkaya's results for the variation of C_m and C_d with KC showed very much the same trends as those of Keulegan and Carpenter.

The variations of the two coefficients with Reynolds' number was independently observed by Garrison, Field and May (1977) at about the same time as Sarpkaya. They carried out a series of tests in which a cylinder was oscillated through still water. The hydrodynamics were somewhat different in this case, in that the pressure field due to fluid acceleration was absent. Thus there was no Froude-Krylov force, and the inertia force was due solely to added mass effects. The effective inertia coefficient recorded in this arrangement was equivalent to $C_m - 1$.

The advantage of this set up was that the speed of the oscillation could be varied while its amplitude was left unchanged. In this way a range of Reynolds' numbers could be covered for constant values of the Keulegan Carpenter number.

After making allowance for the hydrodynamic differences, the results of Garrison et al. for the variation of C_m and C_d with Re were substantially the same as those of Sarpkaya (1976).

Maull and Milliner (1978) adopted a different approach in the analysis of their U-tube force results. They proposed the use of a total force coefficient expressing the non-dimensionalized r.m.s. force on the cylinder. Two possible non-dimensionalising parameters were considered, differing by a factor of KC squared. Depending on which parameter was chosen, the total force coefficient would tend to infinity at either very high or very low values of the Keulegan Carpenter number. Choosing the former option, the authors developed an expression relating the total force coefficient C_F to the Morison coefficients C_m and C_d.

Maull and Milliner demonstrated that their measured results for C_F were consistent with the use of constant values of C_m and C_d, of 2.0 and 1.45, throughout the range of Keulegan Carpenter numbers used. The implication of this finding was that the r.m.s. value of total force was less susceptible to changes in C_m and C_d with KC, than were the individual drag and inertia components.

A series of experiments were carried out by Chakrabarti, Wolbert and Tam (1976) and Chakrabarti (1980a) in which the forces on vertical cylinders under laboratory wave conditions were measured. The loading in short test sections of the cylinder at depths below the water surface was recorded under a range of wave conditions. From the measured wave profile the particle kinematics at the depths of the test sections were calculated, using linear wave theory in the earlier study, and stream function theory in the later. For each set of results the Morison coefficients, Keulegan Carpenter and Reynolds' numbers were calculated.

The authors compared their results for C_m and C_d against Keulegan Carpenter number with those of Sarpkaya (1976a), taken from his U-tube results for a similar range in Reynolds' number. They found that the values of the drag coefficient from the two classes of experiments showed very good agreement for Keulegan Carpenter numbers below about 40. There was, however, considerable discrepancy in the values of C_m for Keulegan Carpenter numbers less than 15. The inertia coefficient measured in the wave tests was appreciably higher than was found in the uni-directional flow tests.

In both studies Chakrabarti (et al.) found that the range of Reynolds' number covered was too small, and the scatter in the results too great, for the variation of the Morison coefficients with Reynolds' number to be inferred.

The total force on the cylinder was measured, and compared with a value calculated from the observed drag and inertia coefficients. In calculating the total integrated force on the cylinder, the drag and inertia coefficients were taken as functions of KC, and allowed to vary over the length of the cylinder. The correlation between the measured and calculated force was found to be very good.

Jen (1968) was concerned with the wave forces on a vertical cylinder in the inertia dominated regime. Fourier analysis was used to separate the total loading into in-phase and quadrature components at the first five harmonics of the wave frequency. The first order quadrature component was used in conjunction with linear wave theory to evaluate the inertia coefficient. C_m did not vary significantly from its theoretical value, and the r.m.s. force on the cylinder was in good agreement with that calculated assuming pure inertia loading and a coefficient of 2.0.

In his consideration of the drag loading, Jen did not attempt to evaluate C_d. The r.m.s. drag force was calculated as the sum of all of the Fourier components not attributable to inertia loading, and was shown to be far smaller than the inertia force.

It is interesting to note that the author offered no explanation for the second harmonic quadrature force component, which

under some wave conditions was quite significant.

The use of the drag and inertia coefficients obtained from uni-directional flow tests for the estimation of the forces on vertical cylinders under wave conditions was criticised by Ramberg and Niedzwecki (1979). Their main criticism was of the assumption of constant C_m and C_d along the length of the cylinder. The authors were also critical of the use of parameters, such as the Keulegan Carpenter number, calculated using particle velocities at the still water level. Drag and inertia coefficients assumed from the surface Keulegan Carpenter number could be inappropriate for the overall loading situation.

A small number of tests were carried out in which the drag and inertia coefficients were determined from the wave loading on a vertical cylinder. These coefficients were compared with Sarpkaya's (1976a) U-tube results for similar values of the Keulegan Carpenter number and the frequency parameter. The U-tube results were significantly greater than the wave results, with the overprediction principally in the drag constribution. The discrepancy in the inertia loading was successfully removed by allowing for a linear variation of C_m with depth. This was not possible in the case of the drag loading. The authors gave a possible explanation for the large difference between the observed and predicted drag force, this being the variation in velocity along the cylinder length.

Stansby, Bullock and Short (1983) undertook a comparison between the force coefficients obtained from tests in U-tubes and

those from vertical cylinders in waves. Their results, taken from short sections of a vertical cylinder under wave loading, were compared with the corresponding results of Sarpkaya (1976a). In their comparison, the authors introduced the orbital shape parameter, Λ, expressing the ratio of the amplitudes of the vertical and horizontal particle velocities. This parameter varied between 1.0 in deep water waves and 0.0 in U-tubes.

The results showed a clear trend for the variation of the drag coefficient with the orbital shape parameter. Under shallow water wave conditions, with low values of Λ, the two values for C_d were in good agreement, while in deep water, as Λ approached unity, C_d was up to 50% lower in waves than in the U-tube. The authors' results for C_m displayed a broad band of scatter around Sarpkaya's values, from which no obvious trends could be inferred.

To eliminate the scatter in C_m and C_d the results were also compared in terms of the r.m.s. total force coefficient C_F. With the exception of the case where the particle orbits were very nearly circular, the wave test and U-tube values for C_F were in very good agreement. In the deep water conditions, however, with Λ equal to 0.9, C_F was some 25% below the equivalent U-tube value.

The experimental programmes which have been carried out to measure the loading on test structures under real sea conditions have tended to entail the gathering of data over the course of a number of months or years. For this reason such projects have been very expensive, and usually jointly funded by oil companies and governmental departments. The major problem in all of these test

programmes has been in correlating the measured wave profile and force data.

Evans (1969) reported two programmes of experiments performed in the Gulf of Mexico between 1954 and 1963. Two techniques were used in computing the drag and inertia force coefficients, both of which analysed the data one wave at a time. In the first method C_m and C_d were calculated from points in the wave cycle at which the particle velocity and acceleration, as given by the wave profile and Stokes' fifth order wave theory, were respectively assumed to be zero. The second method was a least squares fit of the Morison coefficients to the measured forces over each full wave cycle.

The results obtained for C_m and C_d by both techniques showed extreme scatter, and the author was unable to correlate the results with either Keulegan Carpenter or Reynolds' number. The only useful way in which the results could be presented was as probability distributions of the Morison coefficients with the number of waves observed. From these, mean and modal values of C_m and C_d were presented.

Other reports of real sea tests, for example Wiegel, Beebe and Moon (1957), have noted similar scatter in the measured forces and force coefficients. The uncertainty in the results places a severe limitation on the viability of using the real sea environment for full scale testing.

The major defect in any laboratory tests carried out on wave induced loading is the effect of scale on the Reynolds' number. The

Reynolds' number is the most important parameter governing the separation of the boundary layer and the formation of a wake, and has a strong influence on the drag coefficient in both steady and oscillating flow. Typical laboratory Reynolds' numbers are two or three orders of magnitude smaller than occur for the prototype under real loading conditions. Thus drag coefficients obtained from laboratory tests may not be applicable for the design of offshore structures.

A series of experiments were carried out at the Hydraulics Research Station (1981) which attempted to simulate high Reynolds' numbers in small scale tests. The authors noted that at Re higher than a critical value of approximately 2×10^5, the flow is fully turbulent and C_d becomes independent of Reynolds' number. Following the success of earlier work in steady flow, they attempted to 'trip' the boundary layer into turbulence at lower values of the Reynolds' number, by means of small wires attached along the length of the cylinder.

The tests were carried out in a U-tube and covered a variety of trip wire diameters and configurations. The results showed that under certain conditions the critical value of Reynolds' number could be reduced. However, they did not match the success of the steady flow tests, and the critical Reynolds' number could not be reduced below 1×10^5.

An additional series of experiments were carried out which attempted to introduce turbulence by injecting water into the boundary layer. This was done by applying a static head of water through the

porous surface of the cylinder. The results of this were most disappointing and had no measurable effect on the drag coefficient.

It has been noted that once a structure has been located offshore, it can quickly become encrusted with marine growth. This growth has two effects on the structural members - an increase in effective diameter, and a roughening of the surface. Provided that an estimate can be made of the total build up, the increased diameter can easily be accounted for in the calculation of the loading on the member. The surface roughness, however, can greatly effect the mechanics of the wave loading, and may be best accounted for by making appropriate corrections to the drag and inertia coefficients.

Sarpkaya (1976b) conducted a series of experiments in which the forces on artificially roughened cylinders were measured in harmonically oscillating flow. The roughness was achieved by attaching grains of sand to the cylinder surface. A range of relative roughnesses, expressing the ratio of sand grain to cylinder diameter, of between 1/800 and 1/50 was covered. The effect of surface roughness on the drag and inertia coefficients was quite marked.

The drag coefficient was found to reach a minimum value at a lower value of Reynolds' number than for the smooth cylinder. The value of C_d at this critical Reynolds' number increased with increasing relative roughness. At larger values of Re, the drag coefficient increased rapidly before reaching a steady value considerably higher than for the smooth cylinder.

The inertia coefficient for the roughened cylinders had a maximum value at the Reynolds' number corresponding to minimum C_d in each case. At high Reynolds' numbers, the inertia coefficient tended towards a value somewhat lower than the smooth cylinder case, with the difference increasing with relative roughness.

Gaston and Ohmart (1979) carried out experiments to examine the effect of surface roughness on the wave loading on vertical cylinders. They found the drag coefficient to be significantly effected by roughness, having a value almost twice as high for rough as for smooth cylinders. Most of the increase in C_d occurred for the initial transition between smooth and rough cylinders, with further increases in relative roughness having little effect. The inertia coefficient was less sensitive to surface roughness, being only a few percent higher for rough than for smooth cylinders.

The force on a body under wave motion or oscillatory flow, acting in the direction of the motion, is known as the in line or longitudinal force. In addition to this, there is a force perpendicular to the motion called the transverse or lift force. The lift force arises from the asymmetric shedding of vortices from the surface of the body. In analogy with the in line drag force, the lift force is considered to be proportional to the particle velocity squared, and is governed by the lift coefficient C_L.

One of the earliest studies of lift forces was by Bidde (1971). The development of the lift force was considered in terms of the eddy shedding regimes, as observed with flow visualization. At very

low Keulegan Carpenter numbers, no separation occurred, and hence no lift force was expected. As KC increased, a single eddy was shed from one side of the cylinder, marking the onset of lift. For larger values of KC a clear von Karman street of vortices became visible, before turbulence in the surface disguised the pattern of eddies.

Bidde conducted a series of experiments in which the longitudinal and lift forces on a vertical cylinder were recorded. The results were presented as the ratio of maximum lift to longitudinal force. As had been expected, no lift force was recorded for Keulegan Carpenter numbers below approximately 4. Above this value of KC, the lift force increased, reaching a maximum of 60% of the longitudinal force in some cases. The results indicated that the lift force may have reached a peak at KC of about 15, but there were insufficient results above this value for any precise conclusions to be drawn.

Isaacson and Maull (1976) presented what they considered to be an extension of Bidde's work on lift forces. The results of their study were presented in the form of the r.m.s. lift coefficient. The lift coefficient was found to be zero for KC less than 5, reach a peak value for KC of about 12, and approach a steady value of about 0.3 at higher Keulegan Carpenter numbers. The peak value of the lift coefficient varied between 0.5 and 1.2, and was dependent on the relative water depth. This water depth dependence was explained by the variation of KC along the length of the cylinder, and by the use of surface values in its determination.

The authors undertook a Fourier analysis of the lift force in order to establish its frequency composition. They found that for KC less than 15, the lift force was predominantly at twice the incident wave frequency. The third harmonic was the major component for Keulegan Carpenter numbers between 15 and 25, which was the upper limit of the observations. They suggested that the ratio of the lift frequency to the wave frequency would be given by N+1, where N was the number of vortices shed in each half wave cycle.

The fundamental physical mechanisms giving rise to forces on structures in waves were considered at length by Lighthill (1979). The fluid motion around the structure was analysed into two components, the first of which was the irrotational flow field, which described the wave in the absence of the structure. The second component was the vortex motion, associated with any vorticity which had been shed from the surface of the structure, and which contained the 'memory' of the fluid.

Lighthill was critical of the use of Morison's equation and its assumption that the inertia force was due to the linear interaction between the irrotational flow field and the structure. In Morison's formulation the drag force was associated with the increase in the kinetic energy of the vortex motion. Even where the irrotational flow had been described by a higher order theory, it was assumed to interact linearly with the structure to give the inertia force. Thus any non-linearities in the wave loading were associated with the shed vorticity and hence with the drag force. The author suggested that there were non-linearities in the force arising from the irrotational flow, and that to ignore them would lead to a

false estimate for the drag coefficient.

Lighthill derived two main second order forces from the non-linear interaction between a surface - piercing structure and the irrotational flow field. These were shown to exist even when the wave was decribed by linear theory. The largest of these forces, the waterline force, was due to the integration of the pressure between the still water level and the instantaneous free surface. The second of Lighthill's forces was caused by the horizontal gradient of the particle velocity, and was given by the resultant of the dynamic pressure acting over the body's surface. The second order forces were calculated for the simple case of a vertical surface-piercing cylinder in deep water. With a moderately steep wave, the second order forces amounted to almost 20% of the first order inertia force, and attributing all non-linearities to drag implied a doubling of C_d.

For submerged bodies, such as vertical elements and horizontal cylinders, the waterline force is not present and Lighthill's correction reduces to the dynamic pressure force. In harmonically oscillating flow, there is no horizontal gradient of velocity, and neither of the second order forces is present. Thus any experimental study aimed at identifying the two non-linear force components must involve the measurement of the forces on a surface-piercing cylinder under wave action. No reports have yet been published of work carried out with this intention.

CHAPTER 3 - THEORETICAL DEVELOPMENT

This chapter deals with the theoretical background to the present study. Consideration is given to the development of wave theory to a suitable order of approximation, and to the flume effects of reflected and free second harmonic waves. The theoretical expression for the wave loading on a vertical surface-piercing cylinder is developed from the linear Morison's equation. Each of the additional force components, including those due to the reflected and free waves and those proposed by Lighthill (1979) is considered in turn, in order to derive the total non-linear loading.

3.1 Wave Theory

3.1.1 Choice of Wave Theory

The ranges of wave conditions, under which the various available wave theories are appropriate, are governed by the ratios of water depth, wave height and period. A typical representation of the ranges of validity is shown in Figure 3.2. This has been taken from Sarpkaya and Isaacson (1981) after Le Mehaute (1976), with only the analytical theories considered. The range of wave conditions covered in this study are also shown. The clear indication is that Stokes' second order theory would be the most appropriate in this case.

A further indication of which wave theory should be applied

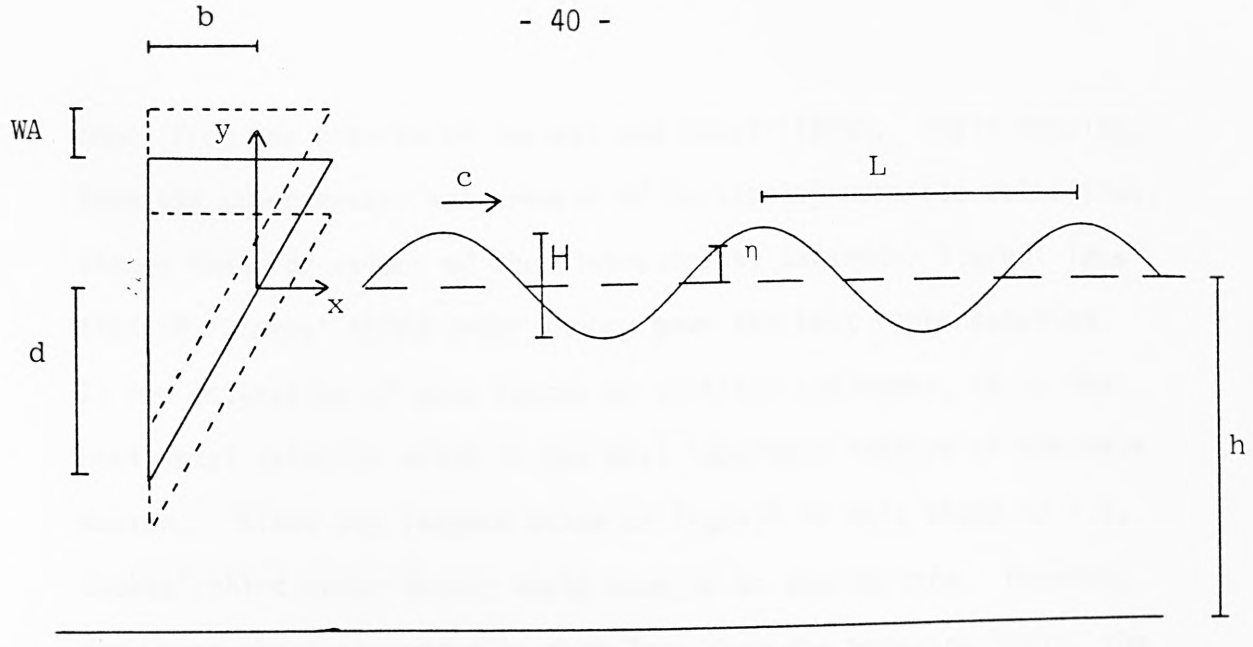

Wave Theory Definition Sketch

Figure 3·1

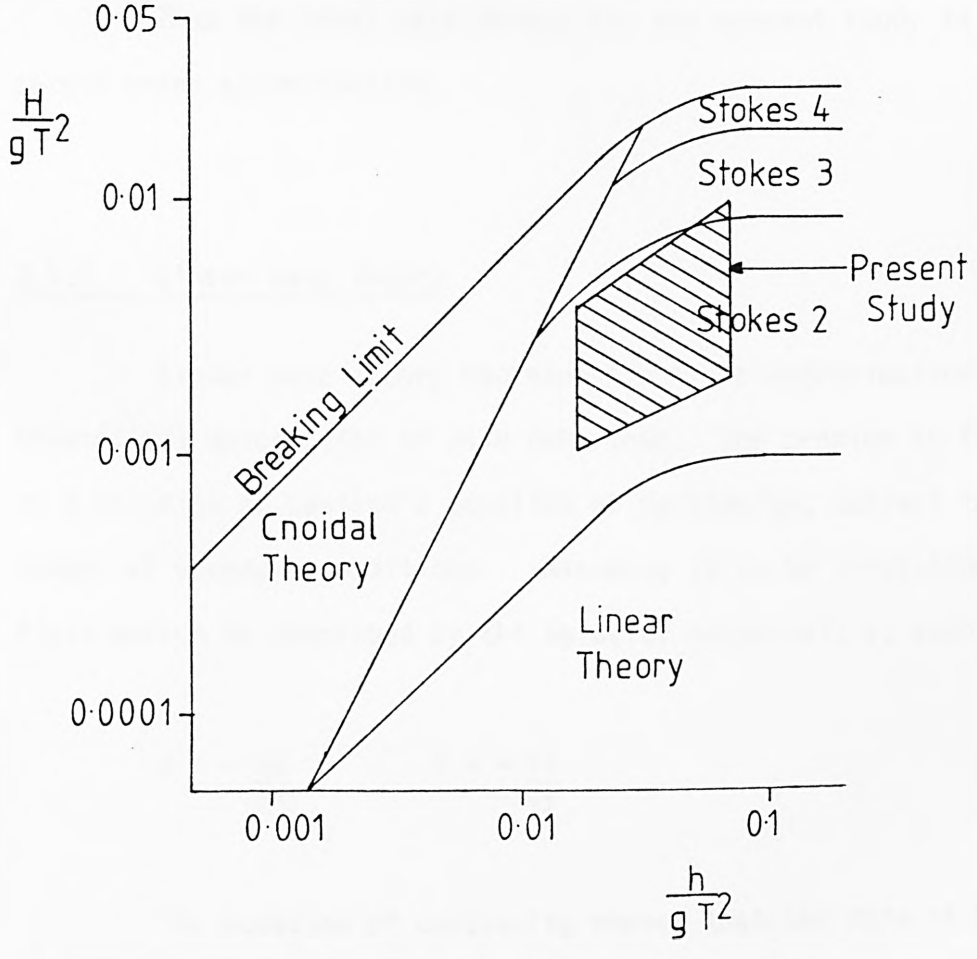

Validity of Wave Theories

Figure 3·2

comes from the results of Iwagaki and Sakai (1970). Their results, from the experimental measurement of horizontal particle velocities, showed that for values of the dimensionless parameter $T(g/h)^{\frac{1}{2}}$ less than 10, Stokes' third order theory gave the best representation. In the estimation of wave forces on vertical cylinders, it is the horizontal velocity which is the most important feature of the wave motion. Since the largest value of $T(g/h)^{\frac{1}{2}}$ in this study is 7.5, Stokes' third order theory would seem to be appropriate. However, for waves whose steepness is much less than the breaking limit, the third order correction to the horizontal velocity becomes negligible, and second order theory gives an identical result.

Thus the ideal wave theory for the present study is Stokes' second order approximation.

3.1.2 Linear Wave Theory

Linear wave theory represents a first approximation to the theoretical description of wave behaviour. The problem is formulated as a solution of Laplace's equation of continuity, subject to a number of boundary conditions. Assuming it to be irrotational, the fluid motion is described by the velocity potential, ϕ, such that;

$$u = -\frac{\partial \phi}{\partial x} \quad ; \qquad v = -\frac{\partial \phi}{\partial y} \tag{3-1}$$

The equation of continuity states that the rate of flow into an elemental space equals the rate of flow out. Assuming the flow to be two-dimensional;

$$\frac{\partial u}{\partial x} + \frac{\partial v}{\partial y} = 0 \qquad \text{for all } (x,y)$$

$$\frac{\partial^2 \phi}{\partial x^2} + \frac{\partial^2 \phi}{\partial y^2} = 0 \tag{3-2}$$

The bottom boundary condition is one of no flow through the solid bottom on which the fluid rests. Thus, the vertical velocity must be zero at y = -h;

$$\frac{\partial \phi}{\partial y} = 0 \quad @\ y = -h \tag{3-3}$$

The kinematic free surface boundary condition states that there is no flow across the surface, i.e. that particles at the surface remain at the surface. This condition is imposed by equating the vertical velocity of the particles in the surface with that of the surface.

$$\frac{dy}{dt} = \frac{d\eta}{dt} \quad @\ y = \eta$$

Noting that,

$$\frac{d\eta}{dt} = \frac{\partial \eta}{\partial t} + \frac{\partial \eta}{\partial x}\frac{\partial x}{\partial t}$$

gives,

$$-\frac{\partial \phi}{\partial y} = \frac{\partial \eta}{\partial t} - \frac{\partial \eta}{\partial x}\frac{\partial \phi}{\partial x} \quad @\ y = \eta \tag{3-4}$$

The dynamic free surface boundary condition represents an application of the unsteady-state Bernoulli equation.

$$\frac{P}{\rho g} + \frac{u^2 + v^2}{2g} + y - \frac{1}{g}\frac{\partial \phi}{\partial t} = 0 \quad @\ y = \eta$$

Variations in the atmospheric pressure will be very small for changes in η, thus the pressure term, P, at the surface will be negligible. Then;

$$\eta = \frac{1}{g}\left(\frac{\partial \phi}{\partial t} - \frac{1}{2}\left(\left(\frac{\partial \phi}{\partial x}\right)^2 + \left(\frac{\partial \phi}{\partial y}\right)^2\right)\right) \quad @\ y = \eta \qquad (3\text{-}5)$$

In linear theory, the amplitude of the wave is assumed to be small, and the two free surface boundary conditions are simplified. The slope of the free surface, $\frac{\partial \eta}{\partial x}$, is assumed to be negligible for all values of x. Additionally it is assumed that the water particle velocities, $\frac{\partial \phi}{\partial x}$ and $\frac{\partial \phi}{\partial y}$, are small and hence that their squares are negligible. The boundary conditions are further simplified by applying them not at the (unknown) free surface position, $y = \eta$, but at the still water level, $y = 0$. Thus the linearized surface boundary conditions become;

$$-\frac{\partial \phi}{\partial y} = \frac{\partial \eta}{\partial t} \quad @\ y = 0 \qquad (3\text{-}4a)$$

$$\eta = \frac{1}{g}\left(\frac{\partial \phi}{\partial t}\right) \quad @\ y = 0 \qquad (3\text{-}5a)$$

The general solution of Laplace's equation (3-2) is found by a separation of variables to give ϕ as a function of x, y and t. Applying the bottom (3-3), and dynamic free surface (3-5a) boundary conditions then yield the solution;

$$\eta = a_I \cos(kx - \omega t) \tag{3-6}$$

$$\phi = -\frac{g a_I}{\omega} \frac{\cosh k(y+h)}{\cosh kh} \sin(kx - \omega t) \tag{3-7}$$

The velocities in the fluid under the wave are then given by

$$u = -\frac{\partial \phi}{\partial x} = \frac{a_I g k}{\omega} \frac{\cosh k(y+h)}{\cosh kh} \cos(kx - \omega t)$$

$$v = -\frac{\partial \phi}{\partial y} = \frac{a_I g k}{\omega} \frac{\sinh k(y+h)}{\cosh kh} \sin(kx - \omega t) \tag{3-8}$$

The physical significance of this result is that the surface profile is represented by a sinusoid travelling in the positive x-direction. The trajectories of the fluid particles are given by closed ellipses (circles in deep water) whose amplitudes decay with depth below the surface.

Consideration of the kinematic free surface boundary condition (3-4a) gives an expression for the celerity at which the waveform travels;

$$c^2 = \frac{\omega^2}{k^2} = \frac{g}{k} \tanh kh \tag{3-9}$$

Equation (3-9) is the dispersion relationship and expresses the fact that waves of different wavelengths travel at different celerities. In general, longer waves travel faster then shorter

waves, and any wave travels faster in deep than in shallow water.

3.1.3 Stokes' Second Order Theory

In proceeding to the second order of approximation, the first order solution for ϕ (3-7) is substituted into the smaller terms neglected in the linearization of the surface boundary conditions (3-4) and (3-5). A Taylor's series expansion is used to effectively apply these boundary conditions at a second order approximation of the instantaneous free surface position. A detailed mathematical derivation has been given, for example, by Dean and Eagleson (1966), and only the result will be considered here. The solution becomes;

$$\eta = a_I \cos(kx - \omega t) + a_2 \cos 2(kx - \omega t) \tag{3-10}$$

where $$a_2 = \frac{\cosh kh(2 + \cosh 2kh)}{4 \sinh^3 kh} \, ka_I^2$$

$$\phi = \phi_1 + \phi_2 = - \frac{ga_I}{\omega} \frac{\cosh k(y+h)}{\cosh kh} \sin(kx - \omega t)$$

$$- \frac{3}{8} \omega a_I^2 \frac{\cosh 2k(y+h)}{\sinh^4 kh} \sin 2(kx - \omega t) \tag{3-11}$$

$$c^2 = \frac{g}{k} \tanh kh \tag{3-9}$$

The horizontal particle velocity becomes;

$$u = u_1 + u_2 = a_I \frac{gk}{\omega} \frac{\cosh k(y+h)}{\cosh kh} \cos(kx - \omega t)$$

$$+ \frac{3}{4} k\omega a_I^2 \frac{\cosh 2k(y+h)}{\sinh^4 kh} \cos 2(kx - \omega t) \tag{3-12}$$

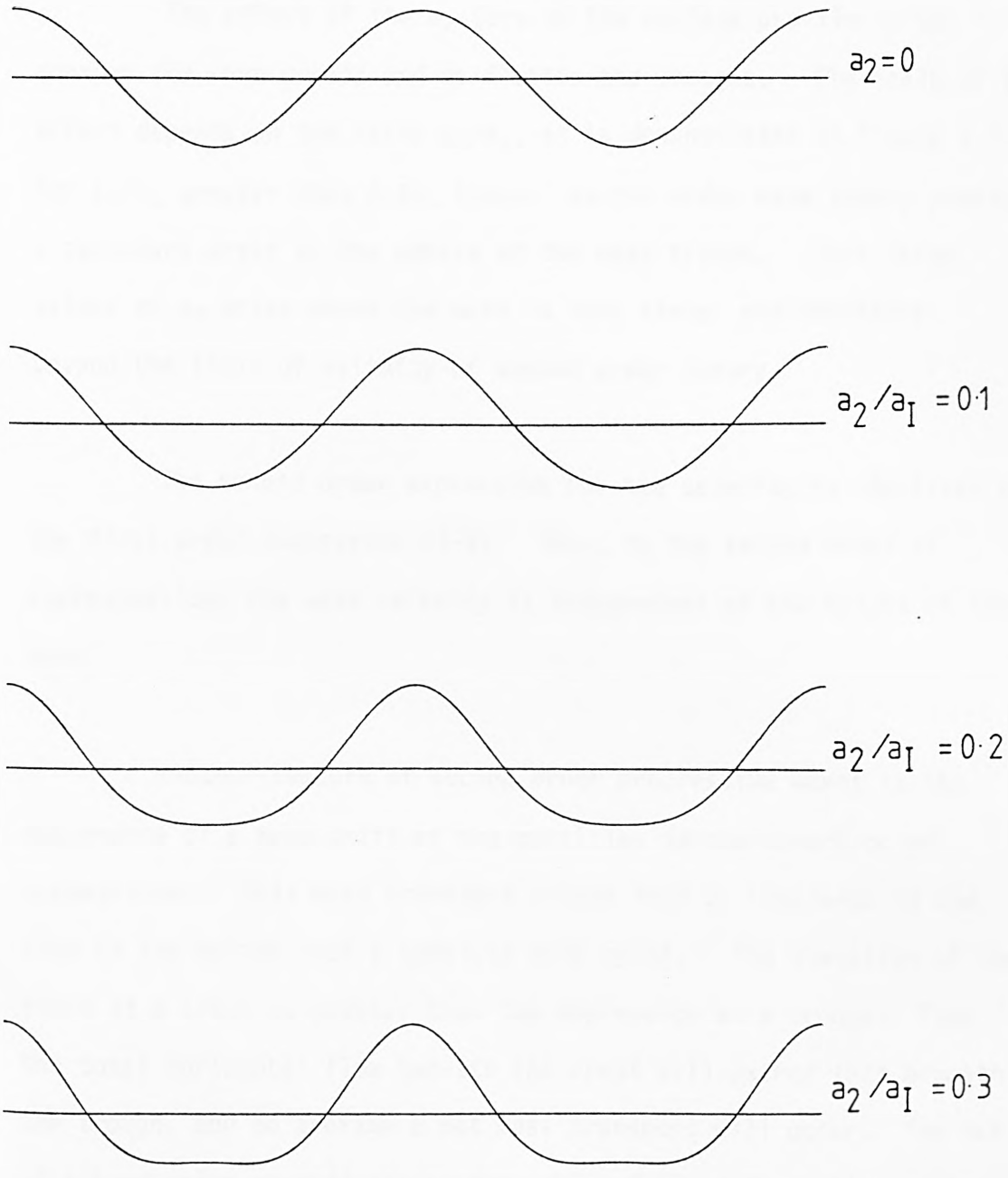

$$\eta = a_I \cos wt + a_2 \cos 2wt$$

Second Order Wave Profiles

Figure 3.3

The effect of the a_2 term on the surface profile is to sharpen the wave crests and to flatten the troughs. The scale of the effect depends on the ratio a_2/a_I, as is demonstrated in Figure 3.3. For a_2/a_I greater than 0.25, Stokes' second order wave theory predicts a secondary crest at the centre of the wave trough. Such large values of a_2 arise where the wave is very steep, and therefore beyond the limit of validity of second order theory.

The second order expression for the celerity is identical to the first order expression (3-9). Thus, to the second order of approximation, the wave celerity is independent of the height of the wave.

Another feature of second order progressive waves is the occurrence of a mean drift of the particles in the direction of propagation. This mass transport arises from an inbalance in the flux of the motion over a complete wave cycle. The elevation of the fluid at a crest is greater than the depression at a trough. Thus the total horizontal flux beneath the crest will exceed that beneath the trough, and on average a net mass transport will occur. The use of a Lagrangian co-ordinate system, which follows the motion of an individual particle, gives an expression for the mass transport velocity;

$$u_t = c(ka_I)^2 \frac{\cosh 2k(y+h)}{2\sinh^2 kh} \qquad (3\text{-}13)$$

In a closed system, such as a wave flume, this expression would imply a gradual build up of water at one end. Since this situation cannot exist in reality, the net drift of the water is assumed to

be balanced by a uniform current flowing in the opposite direction. The mass transport velocity at the free surface in a wave flume is therefore given by;

$$U_t = \frac{c(ka_I)^2}{2\sinh^2 kh} \left(\cosh 2kh - \frac{\sinh 2kh}{2kh}\right) \qquad (3\text{-}14)$$

3.1.4 Wave Flume Effects

In the generation of waves by an oscillating piston, paddle or wedge, the fluid velocity is defined at all times for all points on the wavemaker surface. This imposes an additional boundary condition on the solution for the velocity potential, and the waves produced are called forced waves.

In the linear solutions of Ursell, Dean and Yu (1960) for pistons and paddles, and Wang (1974) for wedges, the additional boundary condition gave rise to an expression for the wave amplitude, a_I. The wave amplitude in each case was found to be directly proportional to the amplitude of the wavemaker motion and dependent on the wavelength, water depth and wavemaker geometry. For example, for a wedge type wavemaker in deep water;

$$a_I = WA \cdot f(kb, b/d) \qquad (3\text{-}15)$$

where WA is the amplitude of the wedge oscillation.

In the second order approximation the wavemaker boundary condition becomes incompatible with the Stokes' form of velocity potential (3-11). The discrepancy in the second order component of

the velocity potential gives rise to a linear wave a twice the fundamental frequency

$$\eta_{22} = a_{22}\cos(k_{22}x - 2\omega t + \beta) \tag{3-16}$$

$$\phi_{22} = \frac{-a_{22}g \cosh k_{22}(y+h)}{2\omega \cosh k_{22}h} \sin(k_{22}x - 2\omega t + \beta) \tag{3-17}$$

This wave, termed the free second harmonic wave, travels independently at a celerity which is given by the dispersion relationship and which is somewhat slower than the main wave

$$C_{22}^2 = \left(\frac{2\omega}{k_{22}} \right)^2 = \frac{g}{k_{22}} \tanh k_{22}h \tag{3-18}$$

An expression for the amplitude of the free second harmonic wave produced by a piston wavemaker was given by Madsen (1971). No such derivation has been given for a_{22} in the case of a wedge, but it is expected to be a function of wedge amplitude, water depth and frequency.

An additional feature of wave flume testing is the occurrence of a reflected wave travelling in the negative x-direction. This wave is caused by the imperfect absorption of the incident wave energy by the beach at the far end of the flume. The main component of the reflected wave is at the fundamental incident wave frequency, and it travels with a celerity equal and opposite to that of the incident wave. Because the reflected wave is generally small, it is assumed to be adequately described by linear wave theory.

Thus,

$$\eta_R = a_R \cos(kx + \omega t + \alpha) \tag{3-19}$$

$$\phi_R = \frac{a_R g \cosh k(y+h)}{\omega \cosh kh} \sin(kx + \omega t + \alpha) \tag{3-20}$$

The amplitudes of the incident and reflected waves are related by the reflection coefficient;

$$K_R = \frac{a_R}{a_I} \times 100\% \tag{3-21}$$

The reflection coefficient depends on water depth, wavelength, wave height and beach geometry. In the absence of any accurate theoretical description, K_R must be found empirically for each wave flume and set of experiments.

A second reflected wave component occurs at twice the fundamental frequency. This may be the result of energy transfer between the harmonics in the mechanism of wave absorption, and/or reflection of the incident second harmonic components. The reflected free second harmonic wave travels at a celerity equal and opposite to that of the incident free second harmonic wave. The amplitude of this wave is very small and linear theory applies;

$$\eta_{22R} = a_{22R} \cos(k_{22}x + 2\omega t + \gamma) \tag{3-22}$$

The total wave motion in a wave flume therefore consists

of a second order Stokes' wave, whose amplitude is proportional to the wavemaker amplitude, a free second harmonic wave, and reflected waves at both the fundamental and second harmonic frequencies.

3.2 Linearized Wave Loading

3.2.1 Morison's Equation

The total force exerted on a vertical cylinder by surface wave action is found by initially considering a small element, δ_y, of the cylinder at a depth below the free surface. The force on this element will be due to its response to a fluctuating fluid velocity. Where the cylinder diameter is small relative to the wavelength and scattering effects are negligible, Morison et al. (1950) suggested that the force on the element is the instantaneous summation of two distinct components.

The first of the force components is the drag force, analogous to the drag force on a body in uniform flow. This force acts over the frontal area of the element, D x δ_y, and is proportional to the square of the instantaneous fluid velocity, u^2. It is caused by separation of the flow from some point on the cylinder surface, creating a low pressure region behind it. The position at which separation occurs, the way in which it occurs, and the resultant wake width all influence the pressure difference and hence the drag force. A major difference between wave motion and uniform flow is that the wave is swept back past the cylinder each time the flow reverses. These effects are accounted for by the introduction of

an empirical drag coefficient C_d. Thus;

$$F_d = \tfrac{1}{2}\rho C_d D \delta y \; u|u| \tag{3-23}$$

with u^2 being replaced by $u|u|$ to maintain the directionality of the drag force.

The second component is the inertia force which is proportional to the instantaneous fluid acceleration, $\frac{\partial u}{\partial t}$. The acceleration causes a pressure gradient in the fluid which acts on the displaced volume, $V = \pi D^2/4 \times \delta y$, of the element. The Froude-Krylov part of the inertia force has a similar form to the buoyancy force acting on a submerged body, and is given by the mass of fluid displaced by the element times the acceleration, $\rho V \frac{\partial u}{\partial t}$.

In addition, the acceleration of the fluid increases the kinetic energy of the flow field around the cylinder. This in turn imposes a force on the cylinder, which is given by $M_a \frac{\partial u}{\partial t}$ (see Lamb (1932) Art. 68). The result of this is that the pressure distribution caused by the acceleration effectively acts on a mass greater than the displaced mass of the fluid. M_a is therefore termed the added mass, and the total inertia force on the element becomes;

$$F_i = (\rho V + M_a) \frac{\partial u}{\partial t} \tag{3-24}$$

In ideal flow M_a is equal to ρV, but in practice it is accounted for by an empirical coefficient of mass, C_m also referred to as the inertia coefficient

$$C_m = 1 + \frac{M_a}{\rho V} \tag{3-25}$$

Thus;

$$F_i = C_m \rho V \frac{\partial u}{\partial t}$$

$$= \rho \frac{\pi D^2}{4} C_m \frac{\partial u}{\partial t} \delta y \tag{3-26}$$

The summation of the drag and inertia forces gives Morison's equation for the force on a vertical element due to wave motion;

$$F_e = F_d + F_i = \tfrac{1}{2}\rho C_d D\, u|u|\delta y + \frac{\rho\pi D^2}{4} C_m \frac{\partial u}{\partial t} \delta y \tag{3-27}$$

In the simplest application of Morison's equation for wave forces, the wave is assumed to be of small amplitude, and therefore to be described by linear wave theory

$$\eta = a_I \cos(kx - \omega t) \tag{3-6}$$

$$u = \frac{a_I g k \cosh k(y+h)}{\omega \cosh kh} \cos(kx - \omega t) \tag{3-8}$$

Assuming the origin of x to be positioned at the centre line of the cylinder, the kx term can be omitted and the particle kinematics are given by;

$$u = \frac{a_I g k \cosh k(y+h)}{\omega \cosh kh} \cos \omega t$$

$$\frac{\partial u}{\partial t} = - a_I g k \frac{\cosh k(y+h)}{\cosh kh} \sin \omega t \qquad (3\text{-}28)$$

Thus the elemental drag and inertia forces become;

$$F_d = \tfrac{1}{2}\rho C_d D \left(\frac{a_I g k \cosh k(y+h)}{\omega \cosh kh}\right)^2 \cos \omega t |\cos \omega t| \delta y \qquad (3\text{-}29)$$

$$F_i = - \frac{\rho \pi D^2}{4} C_m a_I g k \frac{\cosh k(y+h)}{\cosh kh} \sin \omega t \, \delta y \qquad (3\text{-}30)$$

The total drag and inertia forces are found by integration of the elemental forces between the bottom and the surface. In the linear approximation the surface is taken as the still water level, y=0.

$$FT = FD + FI = \tfrac{1}{2}\rho D \int_{-h}^{0} C_d \, u|u| dy + \frac{\rho \pi D^2}{4} \int_{-h}^{0} C_m \frac{\partial u}{\partial t} dy \qquad (3\text{-}31)$$

In the above expression the coefficients C_m and C_d are taken to vary with depth, i.e. to be functions of y, and are therefore placed inside the integrals. Conversely if the coefficients are assumed to be constant over the length of the cylinder, an assumption which may be necessary if their vertical distributions are unknown, they may be left outside the integrals. Evaluation of the integrals in this case gives;

$$FD = \frac{1}{4} \rho C_d D a_I^2 g \left(\frac{\sinh 2kh + 2kh}{\sinh 2kh} \right) \cos \omega t |\cos \omega t| \qquad (3\text{-}32)$$

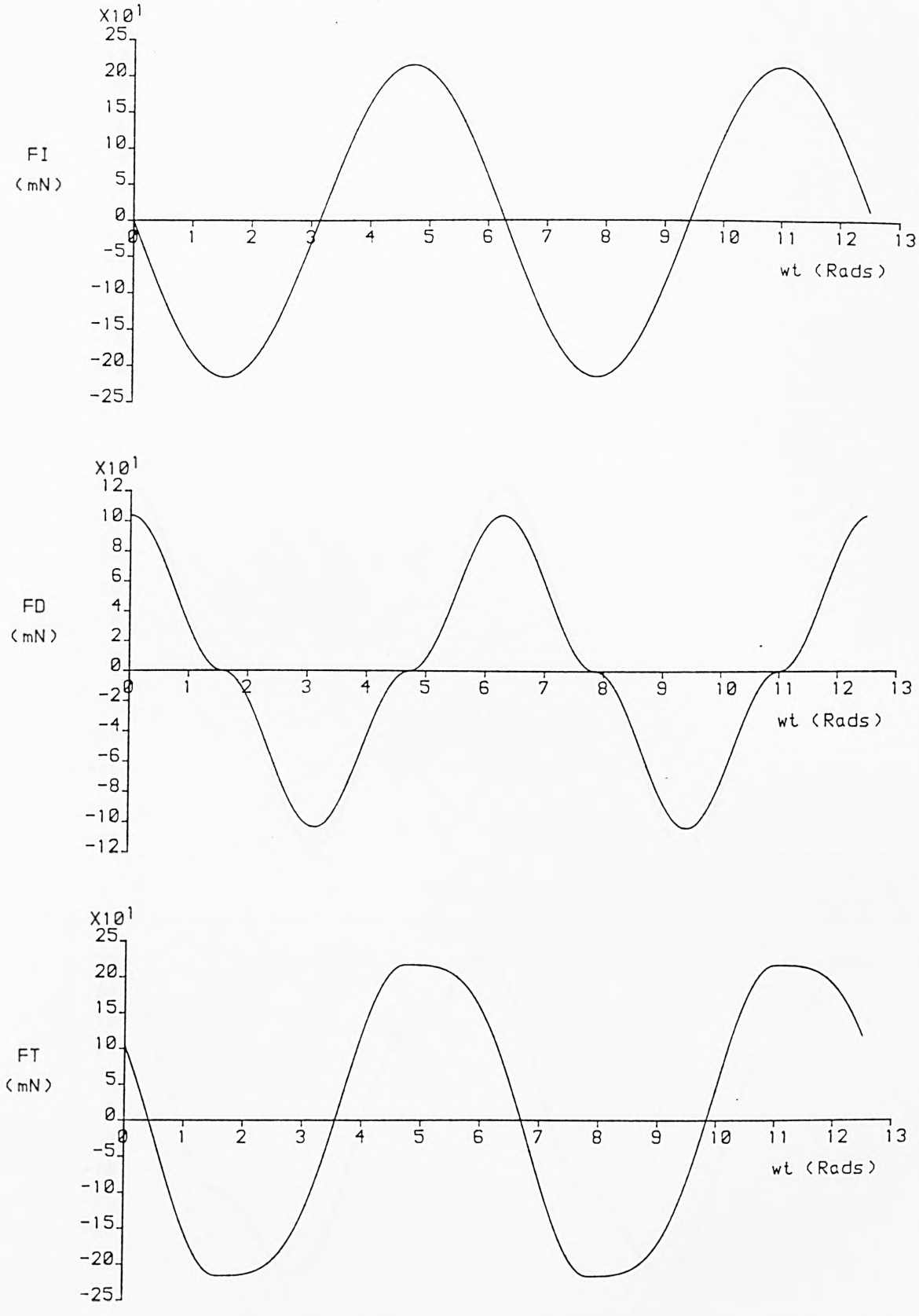

THEORETICAL FORCES ON 25.0mm CYLINDER; CM= 2.0; CD= 1.2

WAVE CONDITIONS: h= 500.0mm; Freq= .60Hz; WL= 3244.1mm; Wave Amp= 30.0mm

DIMENSIONLESS PARAMETERS: KC= 7.91; ka= .058; kh= .968

LOW KEULEGAN CARPENTER NUMBER: INERTIA FORCE DOMINATES

Figure 3.4

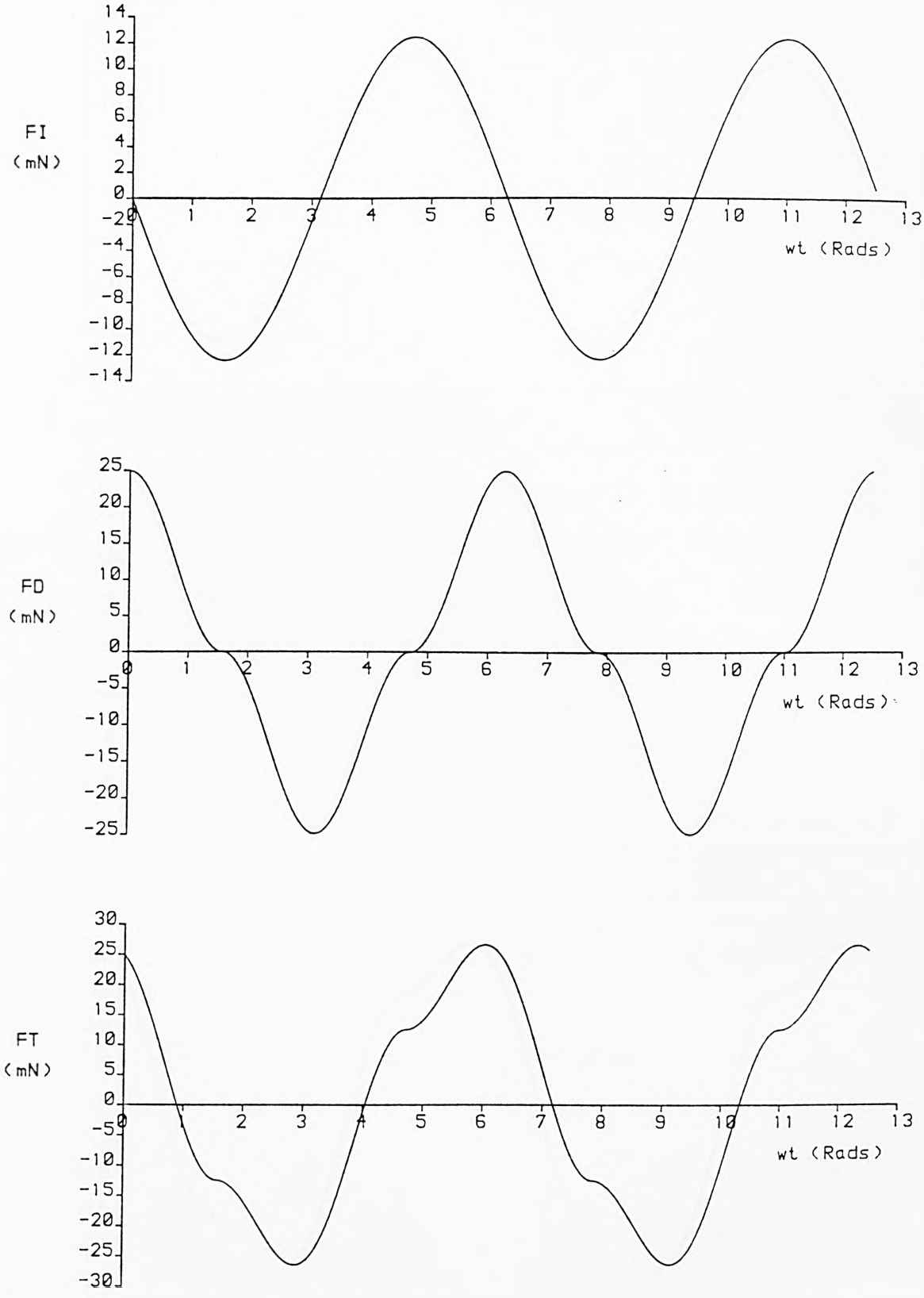

THEORETICAL FORCES ON 6.0mm CYLINDER; CM= 2.0; CD= 1.2

WAVE CONDITIONS: h= 500.0mm; Freq= .60Hz; WL= 3244.1mm; Wave Amp= 30.0mm

DIMENSIONLESS PARAMETERS: KC= 32.98; ka= .058; kh= .968

HIGH KEULEGAN CARPENTER NUMBER: DRAG FORCE DOMINATES

Figure 3.5

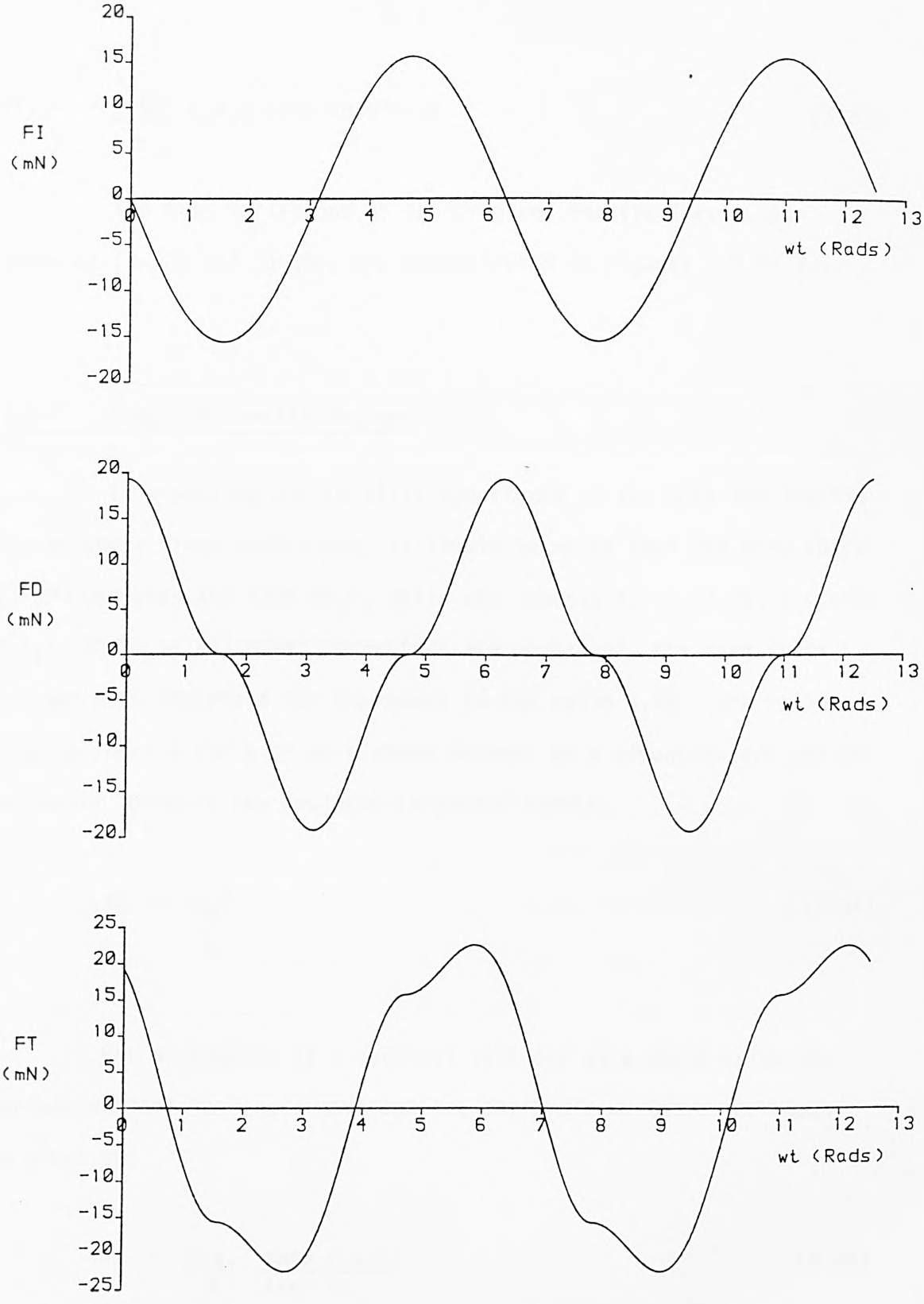

THEORETICAL FORCES ON 6.0mm CYLINDER; CM= 2.0; CD= 1.2

WAVE CONDITIONS: h= 500.0mm; Freq= .90Hz; WL= 1811.1mm; Wave Amp= 30.0mm

DIMENSIONLESS PARAMETERS: KC= 20.33; ka= .104; kh= 1.735

MID RANGE KEULEGAN CARPENTER NUMBER: FD & FI OF SIMILAR MAGNITUDE

Figure 3.6

$$FI = -\frac{\rho\pi D^2}{4} C_m a_I g \tanh kh \sin \omega t \qquad (3\text{-}33)$$

The time variations of the drag and inertia forces, as given by (3-32) and (3-33), are demonstrated in Figures 3.4 to 3.6.

3.2.2 Drag and Inertia Regimes

In assessing the relative importance of the drag and inertia forces under given conditions, it should be noted that the drag force (3-29) contains the term Da_I^2, while the inertia force (3-30) includes D^2a_I. Thus, if all other parameters are unchanged, the drag force becomes more important for increases in the ratio a_I/D. The ratio of drag to inertia force on an element depends on a dimensionless period parameter known as the Keulegan Carpenter number.

$$KC = \frac{u_m T}{D} \qquad (3\text{-}34)$$

For an element of a vertical cylinder at a depth below the surface subject to linear wave action, the Keulegan Carpenter number is given by;

$$KC = \frac{2\pi a_I}{D} \frac{\cosh k(y+h)}{\sinh kh} \qquad (3\text{-}35)$$

The ratio of maximum drag to inertia force on the element is given by;

$$\frac{F_{dmax}}{F_{imax}} = \frac{2a_I \, C_d \cosh k(y+h)}{\pi D \, C_m \sinh kh}$$

$$= \frac{KC}{\pi^2} \frac{C_d}{C_m} \qquad (3\text{-}36)$$

In assigning an equivalent parameter governing the total force on a vertical cylinder, it has been common practice to use the Keulegan Carpenter number calculated using free surface values for u_m, (see Ramberg and Niedzwecki(1979)).

$$KCS = \frac{2\pi a_I}{D \tanh kh} \qquad (3\text{-}37)$$

The use of this parameter does not, however, account for the vertical distribution of the forces, and it does not uniquely define the ratio of the total drag and inertia forces. Identical values of KCS can result from quite different wave conditions. In this study an alternative parameter, KCI, is proposed, such that the ratio of total drag to inertia force on the cylinder is given by an equation of the same form as that for an element (3-36). Thus;

$$\frac{FD_{max}}{FI_{max}} = \frac{KCI}{\pi^2} \frac{C_d}{C_m} \qquad (3\text{-}38)$$

From (3-32) and (3-33);

$$\frac{FD_{max}}{FI_{max}} = \frac{C_d \; a_I \; (\sinh 2kh + 2kh)}{C_m \; 2\pi D \quad \sinh^2 kh} \qquad (3\text{-}39)$$

Thus;

$$KCI = \frac{\pi a_I \ (\sinh 2kh + 2kh)}{2D \qquad \sinh^2 kh} \tag{3-40}$$

In the shallow water limit, the expressions for KCS and KCI are identical, since KC does not vary with depth. Conversely in deep water, KCI has only half the value of KCS. The use of KCI is a convenient technique for assessing an'integrated average' value of the Keulegan Carpenter number for a vertical cylinder.

The effect of the Keulegan Carpenter number on the relative magnitudes of the drag and inertia forces is demonstrated in the total force traces in Figures 3.4 to 3.6. The total drag and inertia forces on a vertical cylinder have been determined for the given wave conditions and with assumed values of C_m and C_d. The values given for the Keulegan Carpenter number have been calculated as KCI (3-40). At values of KC less than about 8, the loading is inertia dominated, while for KC greater than 30 the drag force dominates. At intermediate Keulegan Carpenter numbers the drag and inertia forces are of the same order of magnitude.

3.3 Non-linear Force Components

In the foregoing analysis of wave loading using Morison's equation, certain simplifying assumptions and linearizations were made. This section examines these assumptions and derives a number of additional force components. Some of the forces discussed below,

such as that due to the free second harmonic wave, are perfectly linear, but are an order of magnitude smaller than the first order Morison forces. The other force components are non-linear for one of two reasons. Some, such as the second order Stokes' wave force, are due to the interaction between the cylinder and a non-linear wave component. Others, such as the waterline force, are due to the non-linear interaction between the cylinder and the linear wave kinematics.

Since each of these force components represents a correction to the simplified Morison's equation, it is convenient to collect them all together under the general heading of "non-linear". They are considered individually, and each constitutes a second order correction to the loading. Cross terms, such as the waterline line force due to the second order Stokes' wave, are considered to be of a higher order and are not taken into account.

3.3.1 Forces Due to Second Order Stokes' Wave

In Section 3.2.1, the wave kinematics were assumed to be described by linear theory. If the second order approximation is considered;

$$\phi = \frac{-ga_I}{\omega} \frac{\cosh k(y+h)}{\cosh kh} \sin(kx - \omega t)$$

$$-\frac{3}{8} \omega a_I^2 \frac{\cosh 2k(y+h)}{\sinh^4 kh} \sin 2(kx - \omega t) \qquad (3\text{-}11)$$

Taking origin of x at the cylinder, the particle kinematics will be given by;

$$u = \frac{a_I g k}{\omega} \frac{\cosh k(y+h)}{\cosh kh} \cos\omega t + \frac{3}{4} \omega a_I^2 k \frac{\cosh 2k(y+h)}{\sinh^4 kh} \cos 2\omega t \qquad (3\text{-}41)$$

$$\frac{\partial u}{\partial t} = - a_I g k \frac{\cosh k(y+h)}{\cosh kh} \sin\omega t - \frac{3}{2} \omega^2 a_I^2 k \frac{\cosh 2k(y+h)}{\sinh^4 kh} \sin 2\omega t \qquad (3\text{-}42)$$

The second order terms in the expressions for u and $\frac{\partial u}{\partial t}$ effect the drag and inertia forces. In evaluating the correction to the inertia force it is noted that the force varies linearly with the instantaneous acceleration. Thus the total inertia force will be modified by the inclusion of a component due to the second term in $\frac{\partial u}{\partial t}$ (3-42).

$$FI2 = - \frac{3}{16} \rho\pi D^2 C_m \omega^2 a_I^2 \frac{\sinh 2kh}{\sinh^4 kh} \sin 2\omega t \qquad (3\text{-}43)$$

The correction of the drag force is complicated by the fact that it does not vary linearly with u, but is proportional to $u|u|$. In the second order approximation,

$$u|u| = \left(\frac{a_I g k}{\omega} \frac{\cosh k(y+h)}{\cosh kh} \cos\omega t + \frac{3}{4} \omega a_I^2 k \frac{\cosh k(y+h)}{\sinh^4 kh} \cos 2\omega t \right)$$

$$\times \left| \frac{a_I g k}{\omega} \frac{\cosh k(y+h)}{\cosh kh} \cos \omega t + \frac{3}{4} \omega a_I^2 k \frac{\cosh 2k(y+h)}{\sinh^4 kh} \cos 2\omega t \right| \qquad (3\text{-}44)$$

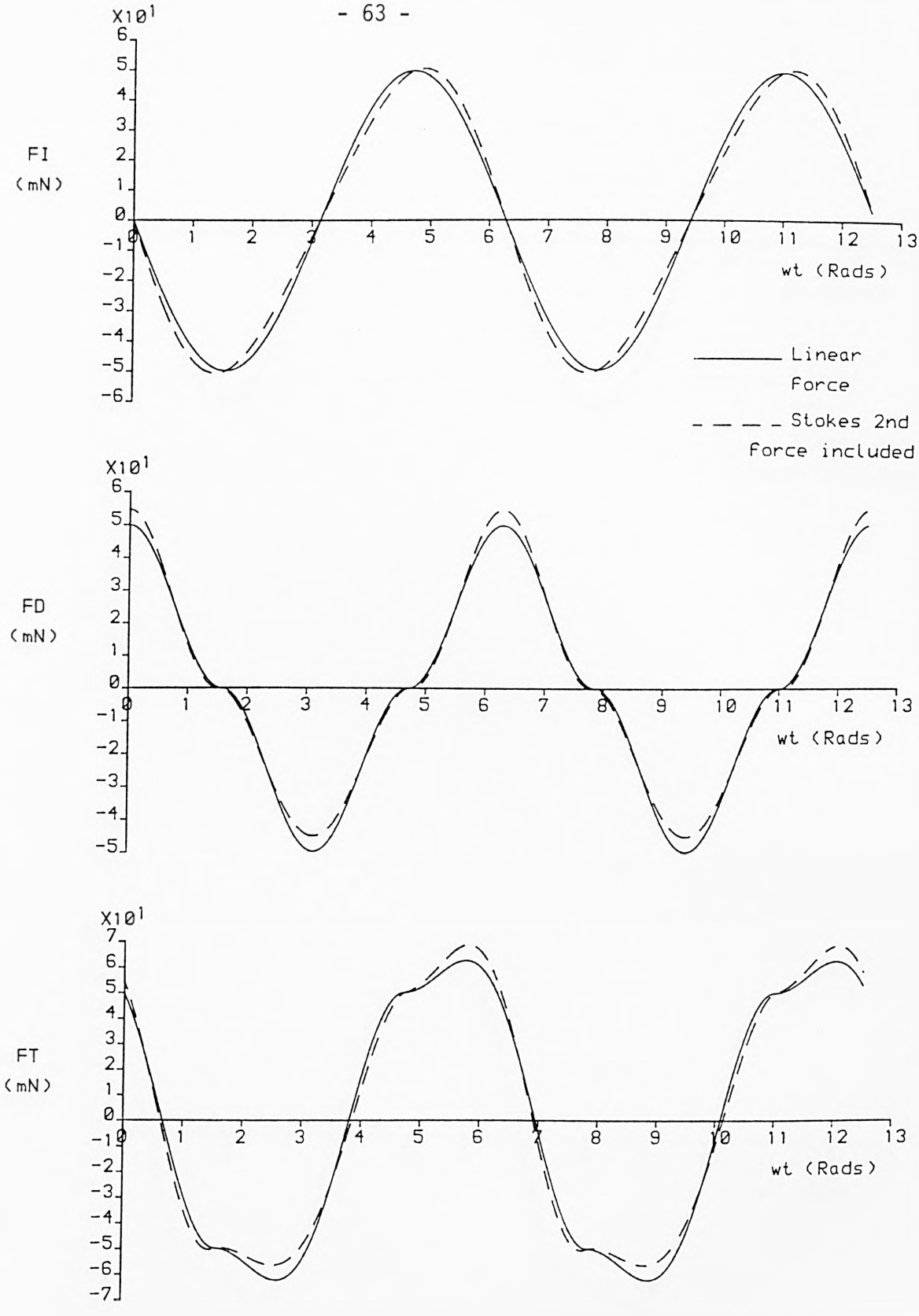

THEORETICAL FORCES ON 12.0mm CYLINDER; CM= 2.0; CD= 1.2

WAVE CONDITIONS: h= 500.0mm; Freq= .60Hz; WL= 3244.1mm; Wave Amp= 30.0mm

DIMENSIONLESS PARAMETERS: KC= 16.49; ka= .058; kh= .968

DEMONSTRATING EFFECT OF STOKES 2ND ORDER WAVE: A2= 2.541mm

Figure 3.7

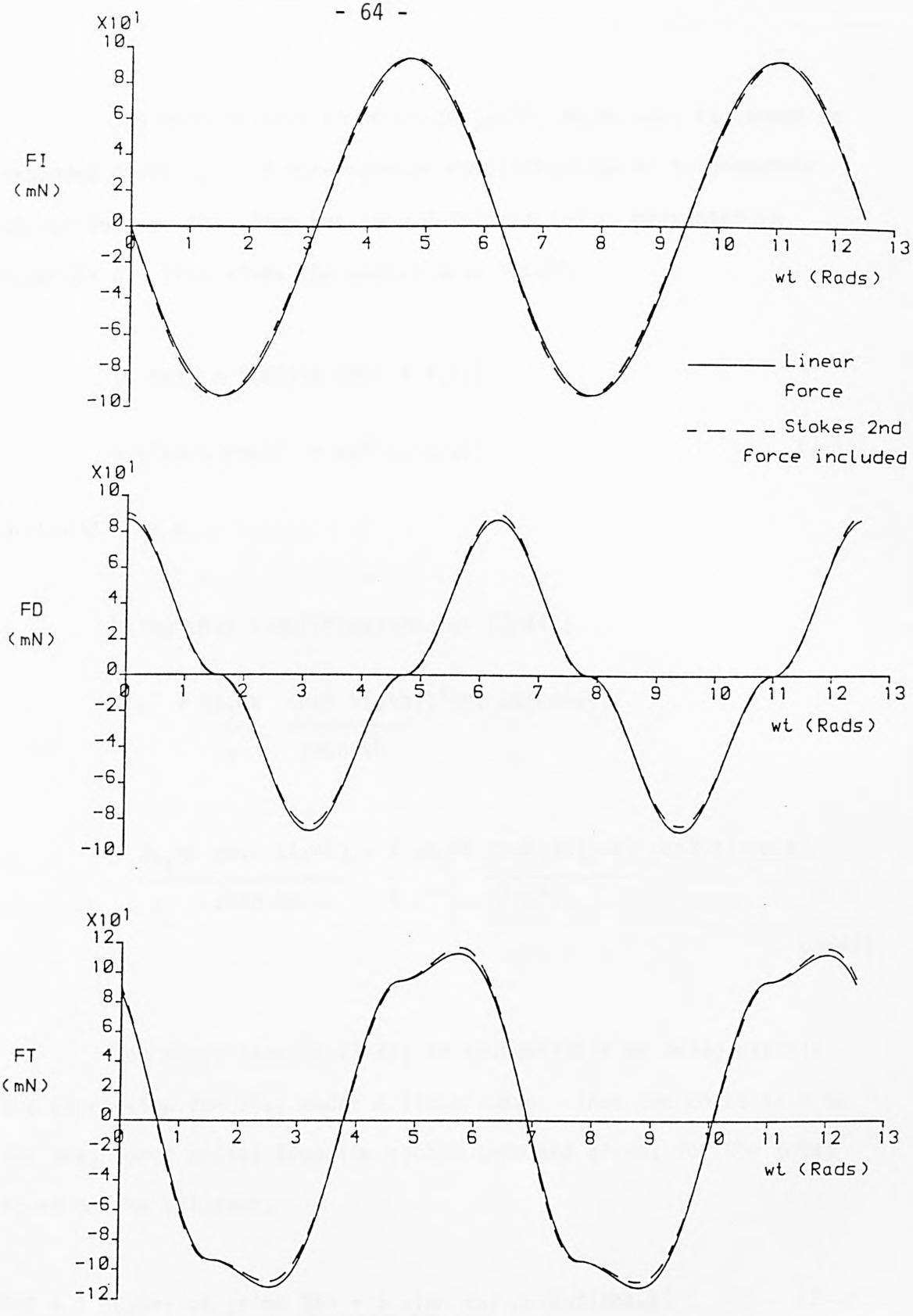

THEORETICAL FORCES ON 12.0mm CYLINDER; CM= 2.0; CD= 1.2

WAVE CONDITIONS: h= 500.0mm; Freq= .90Hz; WL= 1811.1mm; Wave Amp= 45.0mm

DIMENSIONLESS PARAMETERS: KC= 15.25; ka= .156; kh= 1.735

DEMONSTRATING EFFECT OF STOKES 2ND ORDER WAVE: A2= 4.483mm

Figure 3.8

The modulus term in equation (3-44) means that it cannot be expanded directly. A non-rigorous simplification of trignometric expressions of this form has been developed and is presented in Appendix 3. This gives the approximate result;

$$(a\cos\theta + f(\theta))|a\cos\theta + f(\theta)|$$

$$= a^2\cos\theta|\cos\theta| + 2af(\theta)|\cos\theta| \qquad (3\text{-}45)$$

provided $f << a$.

Using this simplification for (3-44);

$$u|u| = \left(\frac{a_I gk}{\omega}\,\frac{\cosh k(y+h)}{\cosh kh}\right)^2 \cos\omega t|\cos\omega t| + \frac{2a_I gk}{\omega}\,\frac{\cosh k(y+h)}{\cosh kh} \times \frac{3}{4}\,\omega a_I{}^2 k\,\frac{\cosh 2k(y+h)}{\sinh^4 kh}\cos 2\omega t|\cos\omega t| \qquad (3\text{-}46)$$

The first term in (3-46) in recognizable as being exactly the expression for $u|u|$ under a linear wave. Thus the correction to the drag force arises from the second term and gives, for the total force on the cylinder;

$$FD2 = \frac{1}{8}\rho C_d D a_I{}^3 gk\,\frac{(\sinh 3kh + 3\sinh kh)}{\cosh kh\,\sinh^4 kh}\cos 2\omega t|\cos\omega t| \qquad (3\text{-}47)$$

The effect of the second order wave on the drag, inertia and total forces on a vertical cylinder is demonstrated in Figures 3.7 and 3.8. In Figure 3.7, the water is relatively shallow, kh less than 1,

and the second order correction to the velocity potential is significant. Under these conditions the second order drag and inertia forces are as much as 10% of the linear forces. As the relative water depth, kh, increases the second order component of the velocity potential decreases. Under the conditions in Figure 3.8, the correction to the surface profile, a_2, is significant, but the second order force components are very small.

Thus, the second order corrections to the drag and inertia forces are most important where the water depth to wavelength ratio is small.

3.3.2 Convective Acceleration

In the expression for the inertia force on a vertical element (3-26), the acceleration is assumed to be given solely by the local component, $\frac{\partial u}{\partial t}$. However, the total acceleration in the fluid is the sum of the local and convective components.

$$\frac{du}{dt} = \frac{\partial u}{\partial t} + u\frac{\partial u}{\partial x} + v\frac{\partial u}{\partial y} \qquad (3\text{-}48)$$

Using linear wave theory to describe the particle kinematics, the two components of the convective acceleration are given by;

$$u\frac{\partial u}{\partial x} = \left(\frac{a_I g k \cosh k(y+h)}{\omega \cosh kh}\right)^2 k \cos\omega t \sin\omega t \qquad (3\text{-}49)$$

$$v\frac{\partial u}{\partial y} = \left(\frac{a_I g k \sinh k(y+h)}{\omega \cosh kh}\right)^2 k \cos\omega t \sin\omega t \qquad (3\text{-}50)$$

If the inertia force is taken to be proportional to the total rather than the local acceleration, the force due to the convenctive acceleration must be included

$$FCA = \frac{\rho\pi D^2}{4} C_m \int_{-h}^{o} \left(u \frac{\partial u}{\partial x} + v \frac{\partial u}{\partial y}\right) dy$$

$$= \frac{\rho\pi D^2}{4} C_m a_I{}^2 gk \left(\frac{kh}{\sinh 2kh}\right) \sin 2\omega t \qquad (3\text{-}51)$$

The magnitude of the convective acceleration force is found by considering the deep and shallow water limits of (3-51). In intermediate to deep water, as kh increases, the value of kh/sinh 2 kh rapidly approaches zero and the convective acceleration force vanishes. In shallow water the ratio of FCA to FI is found from (3-33) and (3-51) to be proportional to the wave steepness, ka_I

$$\frac{FCA}{FI} = \frac{ka_I}{2} \qquad (3\text{-}52)$$

The convective acceleration force under the steepest shallow water wave conditions covered by the present study is shown in Figure 3.9. This demonstrates that FCA can be neglected throught the study.

An alternative formulation for the convective acceleration force was given by Isaacson (1979). He noted that the force due to the vertical component of the horizontal convective acceleration, $v \frac{\partial u}{\partial y}$, would not include any added mass effects. Thus the convective acceleration force would be given by;

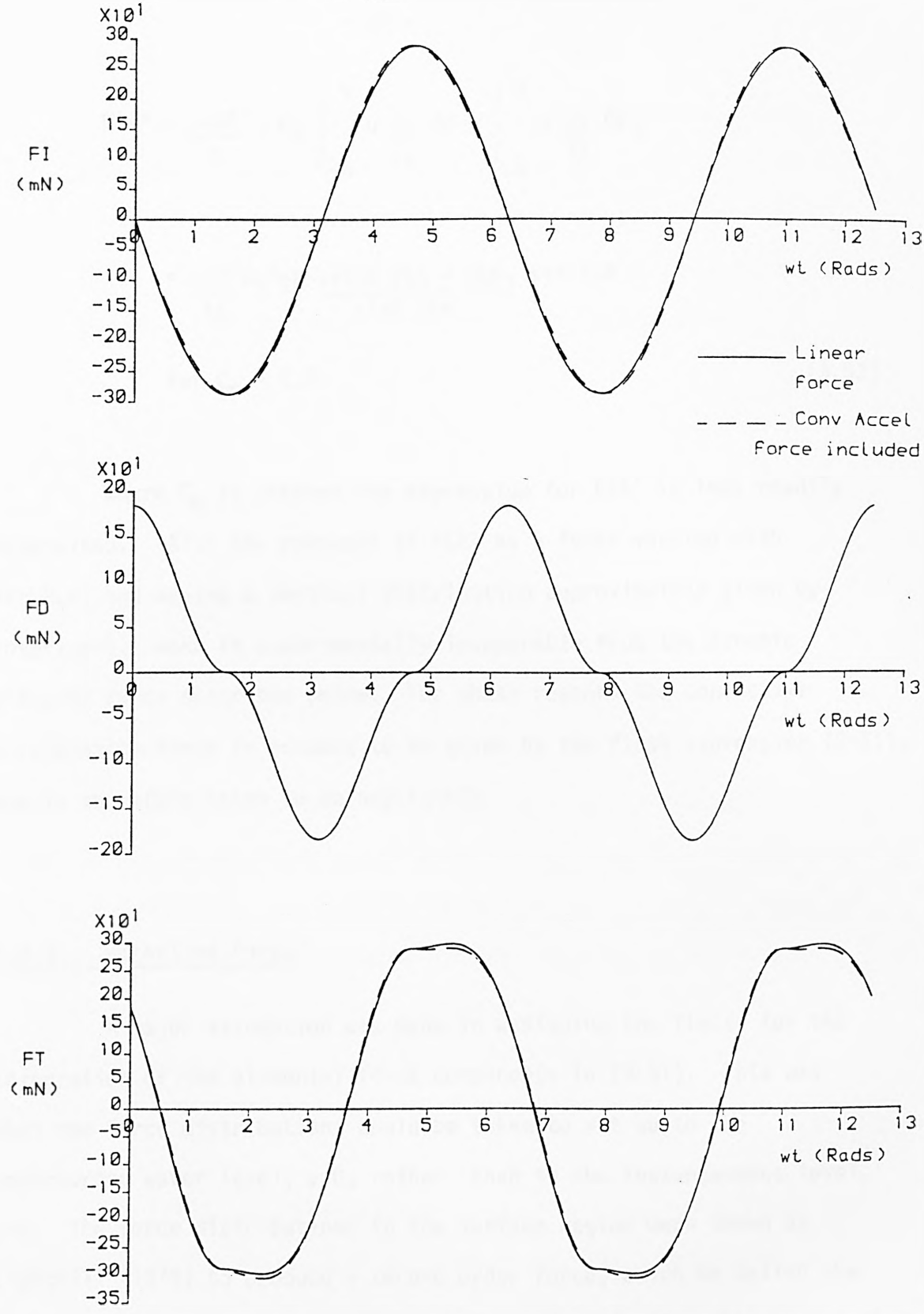

THEORETICAL FORCES ON 25.0mm CYLINDER; CM= 2.0; CD= 1.2

WAVE CONDITIONS: h= 500.0mm; Freq= .60Hz; WL= 3244.1mm; Wave Amp= 40.0mm

DIMENSIONLESS PARAMETERS: KC= 10.55; ka= .077; kh= .968

DEMONSTRATING EFFECT OF CONVECTIVE ACCELERATION

Figure 3.9

$$FCA' = \frac{\rho\pi D^2}{4}\left(C_m \int_{-h}^{o} u\frac{\partial u}{\partial x}\,dy + \int_{-h}^{o} v\frac{\partial u}{\partial y}\,dy\right)$$

$$= \frac{\rho\pi D^2 a_I{}^2 gk}{16}\left(\frac{\sinh 2kh + 6kh}{\sinh 2kh}\right)\sin 2\omega t$$

for $C_m = 2.0$ (3.53)

Where C_m is unknown the expression for FCA' is less readily determined. Also the presence of FCA' as a force varying with $\sin 2\omega t$, and having a vertical distribution approximately given by $\cosh^2 k(y+h)$, make it experimentally inseperable from the dynamic pressure force described below. For these reasons the convective acceleration force is assumed to be given by the first expression (3-51), and is therefore taken to be negligible.

3.3.3 Waterline Force

A major assumption was made in assigning the limits for the integration of the elemental force components in (3-31). This was that the force distributions could be taken to act up to the undisturbed water level, $y=0$, rather than to the instantaneous level, $y=\eta$. The force distributions in the surface region were shown by Lighthill (1979) to produce a second order force, which he called the waterline force. This force was evaluated by integrating the transient and hydrostatic pressures around the cylinder in the region $y=0$ to $y=\eta$.

A more simplistic approach was suggested by Verley (1975), and this has been adopted in the derivation below. The particle velocity and acceleration, calculated at the undisturbed water level are considered to act on an element of variable height, $\eta = a_I \cos\omega t$. Noting that η is, at different times, positive and negative;

$$FWD = \tfrac{1}{2}\rho C_d D \eta u_o |u_o|$$

$$= \tfrac{1}{2}\rho C_d D a_I{}^3 \left(\frac{gk}{\omega}\right)^2 \cos^2\omega t |\cos\omega t| \qquad (3\text{-}54)$$

$$FWI = \frac{\rho\pi D^2}{4} C_m \eta \frac{\partial u_o}{\partial t}$$

$$= -\frac{\rho\pi D^2}{8} C_m a_I{}^2 gk \sin 2\omega t \qquad (3\text{-}55)$$

Lighthill's expression for the waterline force was of the same form as FWI (3-55), except that C_m was given by its theoretical value of 2.0. A discrepancy arises at this point from the fact that Lighthill did not consider the drag force in the waterline region and hence found no force equivalent to FWD. However, Lighthill's work covered the inertia dominated regime, in which small corrections to the drag force would have little effect on the total loading.

The effect of the waterline force on the total loading is demonstrated in Figures 3.10 to 3.12. Where the wave steepness is very small, as in Figure 3.10, the waterline region is a correspondingly small proportion of the total length of the cylinder. The waterline force is not therefore a significant part of the total loading. In Figures 3.11 and 3.12 the wave is considerably steeper and the waterline components have a marked effect on the drag and inertia

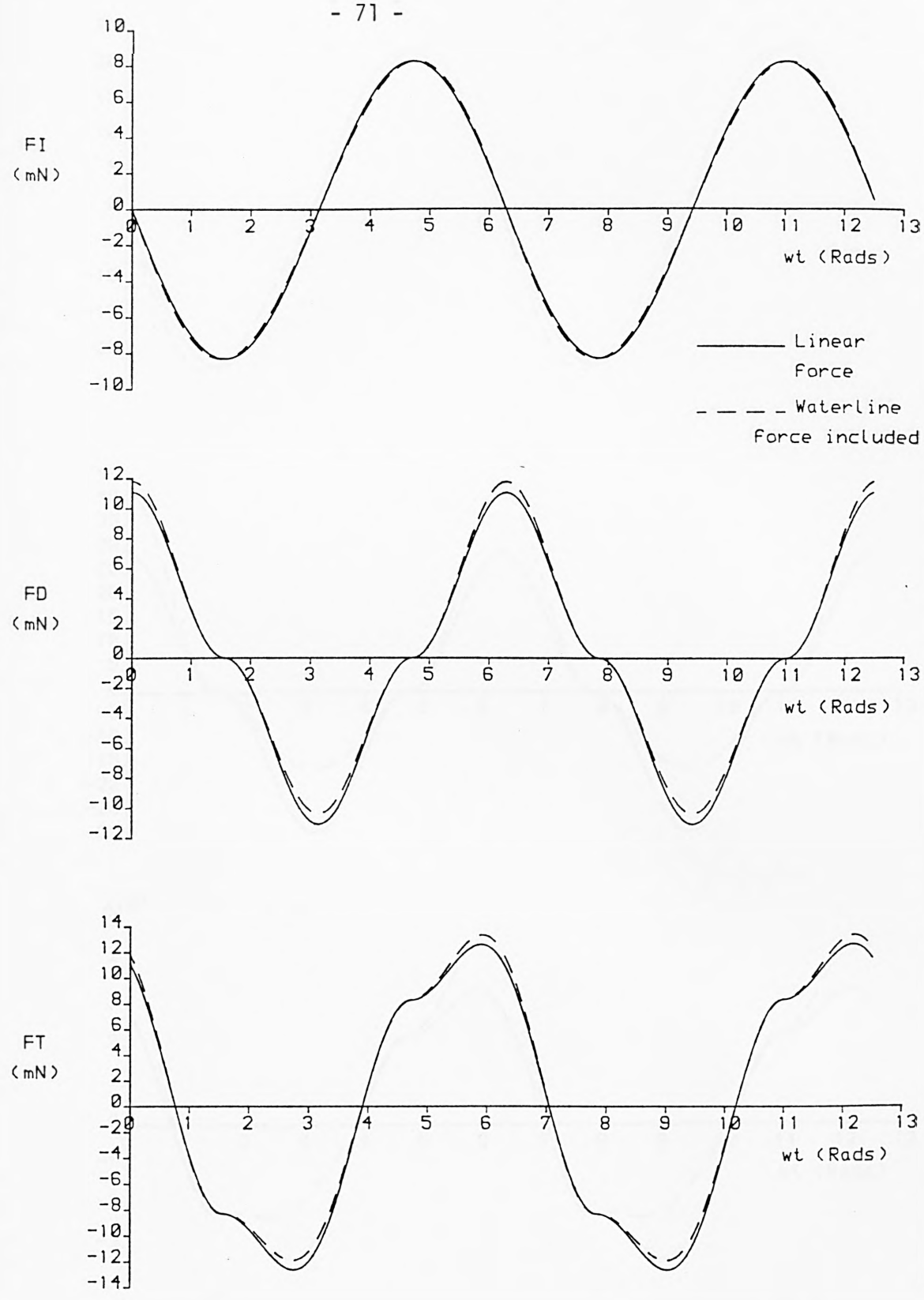

THEORETICAL FORCES ON 6.0mm CYLINDER; CM= 2.0; CD= 1.2

WAVE CONDITIONS: h= 500.0mm; Freq= .60Hz; WL= 3244.1mm; Wave Amp= 20.0mm

DIMENSIONLESS PARAMETERS: KC= 21.98; ka= .039; kh= .968

DEMONSTRATING EFFECT OF WATERLINE FORCE

Figure 3.10

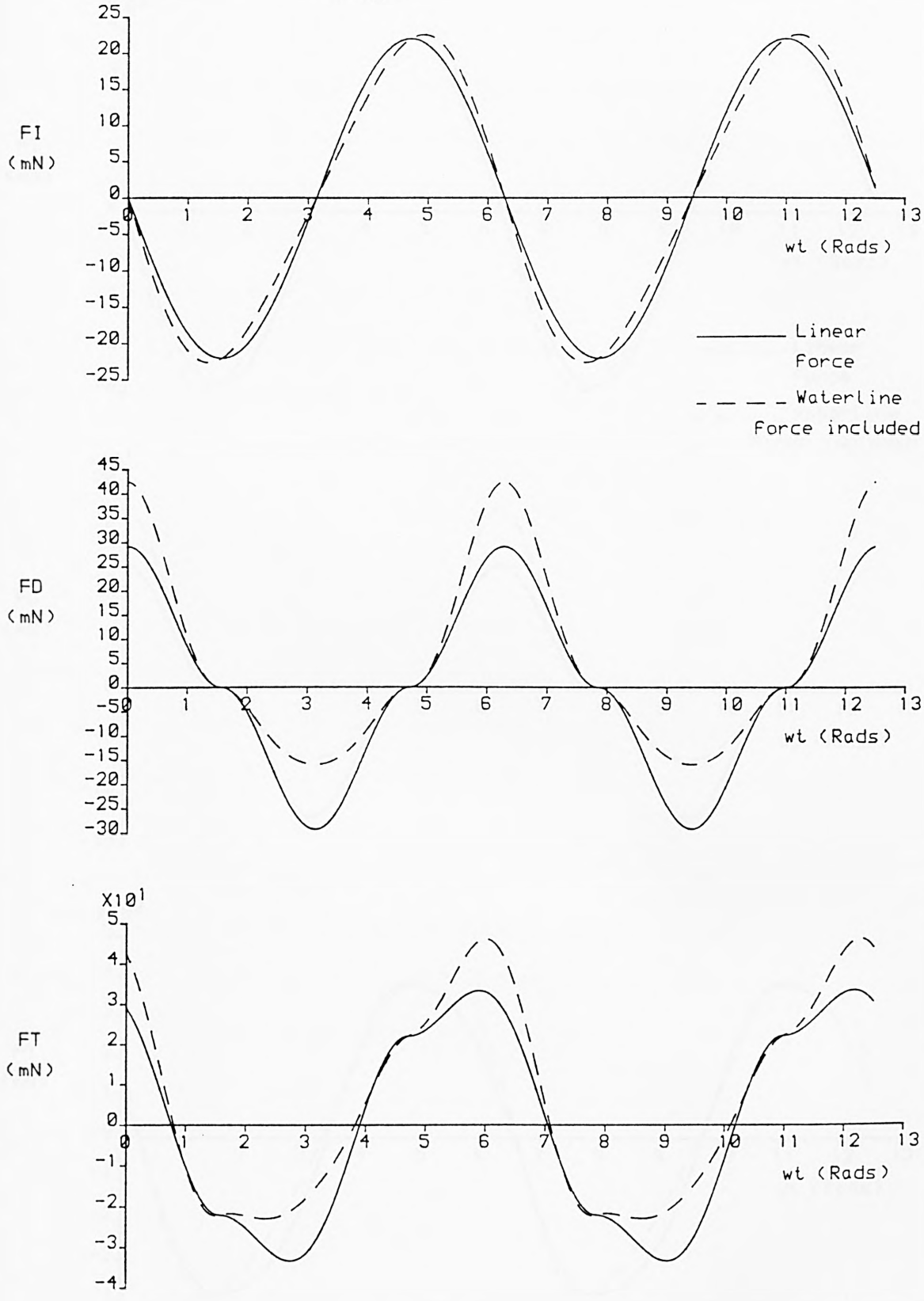

THEORETICAL FORCES ON 6.0mm CYLINDER; CM= 2.0; CD= 1.2

WAVE CONDITIONS: h= 500.0mm; Freq= 1.20Hz; WL= 1077.9mm; Wave Amp= 40.0mm

DIMENSIONLESS PARAMETERS: KC= 21.79; ka= .233; kh= 2.915

DEMONSTRATING EFFECT OF WATERLINE FORCE

Figure 3.11

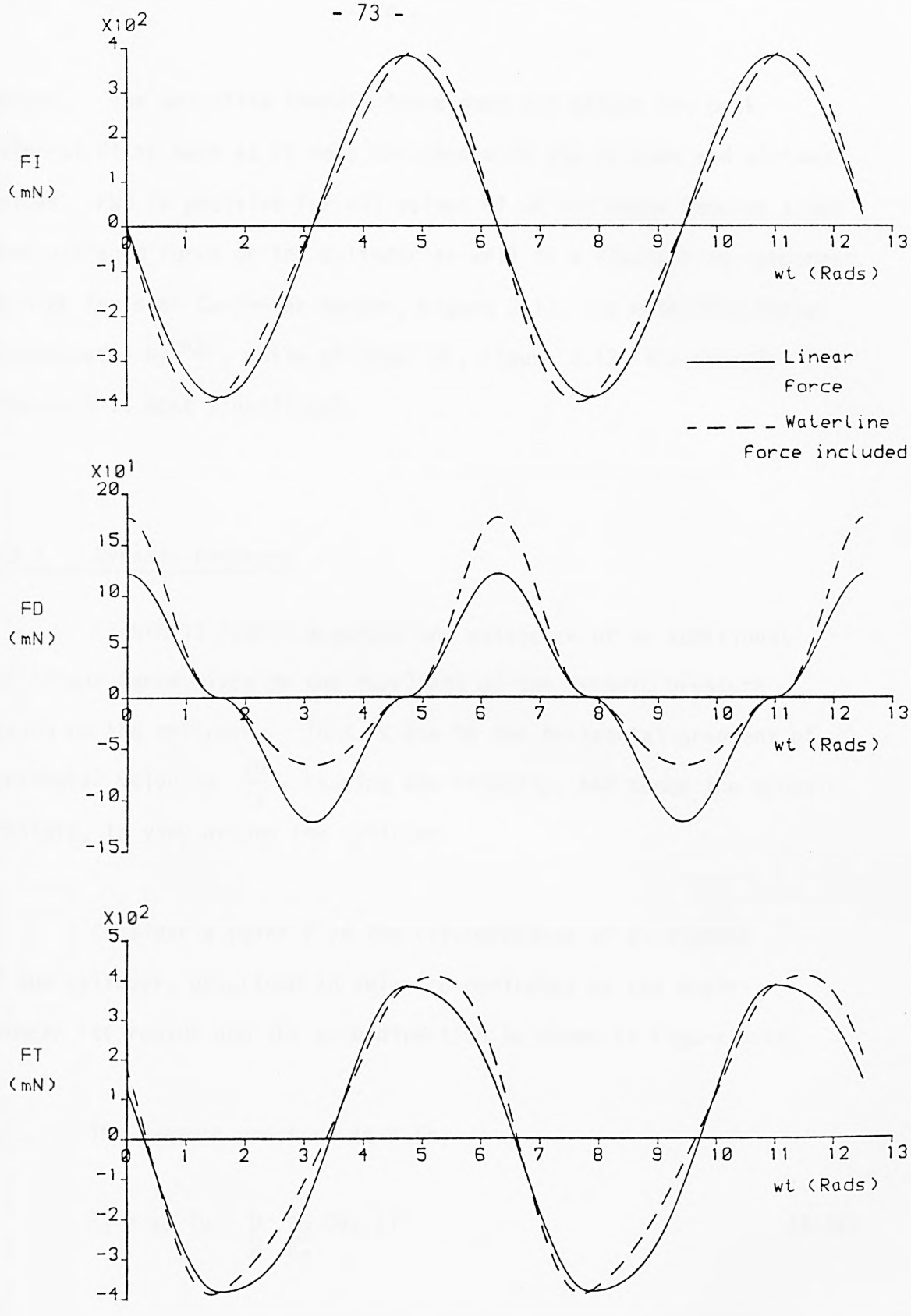

THEORETICAL FORCES ON 25.0mm CYLINDER; CM= 2.0; CD= 1.2

WAVE CONDITIONS: h= 500.0mm; Freq= 1.20Hz; WL= 1077.9mm; Wave Amp= 40.0mm

DIMENSIONLESS PARAMETERS: KC= 5.23; ka= .233; kh= 2.915

DEMONSTRATING EFFECT OF WATERLINE FORCE

Figure 3.12

forces. The waterline inertia force does not effect the peak value of FI as much as it does the phases of the maximum and minimum values. FWD is positive for all values of ωt and hence imposes a net time-averaged force on the cylinder as well as a fluctuating component. At high Keulegan Carpenter number, Figure 3.11, the waterline force is dominated by F_{WD}, while at lower KC, Figure 3.12, the inertia component is most significant.

3.3.4 Dynamic Pressure

Lighthill (1979) proposed the existence of an additional non-linear force given by the resultant of the dynamic pressure acting on the cylinder. This is due to the horizontal gradient of horizontal velocity, $\frac{\partial u}{\partial x}$, causing the velocity, and hence the dynamic pressure, to vary around the cylinder.

Consider a point P on the circumference of an element of the cylinder, described in polar co-ordinates by the angle between its radius and the wave direction as shown in Figure 3.13.

The dynamic pressure at P is;

$$P_d = \tfrac{1}{2}\rho \left(u - \frac{D}{2} \frac{\partial u}{\partial x} \cos\theta\right)^2 \qquad (3\text{-}56)$$

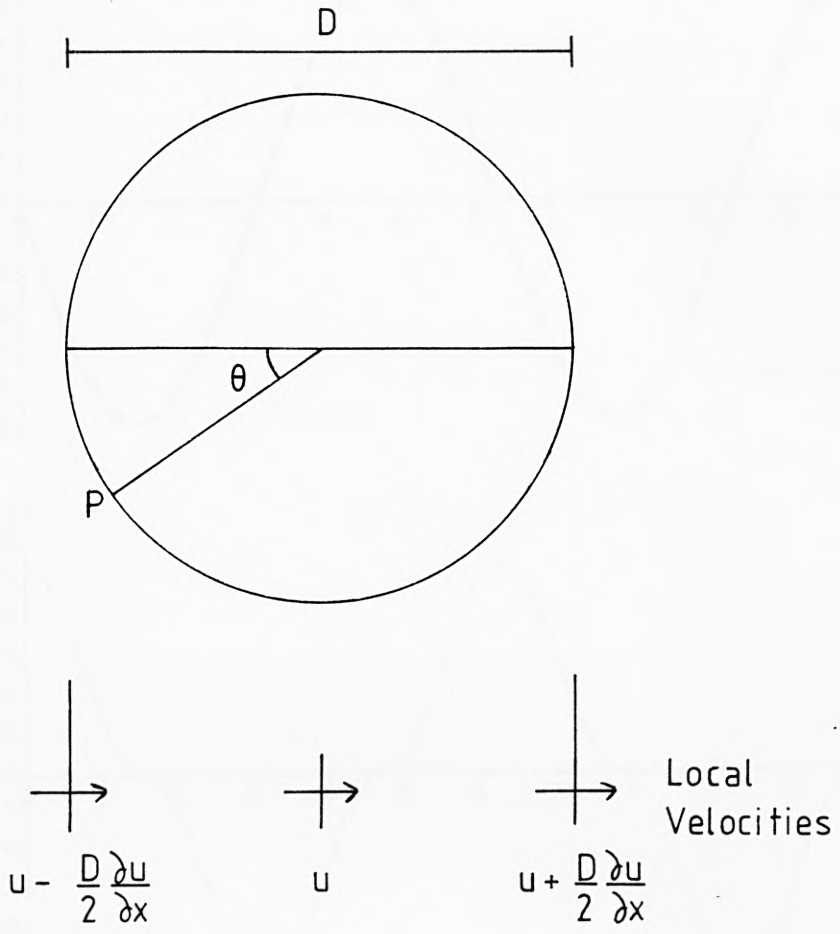

Dynamic Pressure Variation

Figure 3.13

The resultant force on the element due to the dynamic pressure is found by integrating the longitudinal component of P_d around the circumference;

$$F_{dp} = \int_0^{2\pi} \tfrac{1}{2}\rho\left(u - \frac{D}{2}\frac{\partial u}{\partial x}\cos\theta\right)^2 \frac{D}{2}\cos\theta \, d\theta \, \delta y$$

$$= -\frac{\rho\pi D^2}{4} u \frac{\partial u}{\partial x} \delta y \qquad (3\text{-}57)$$

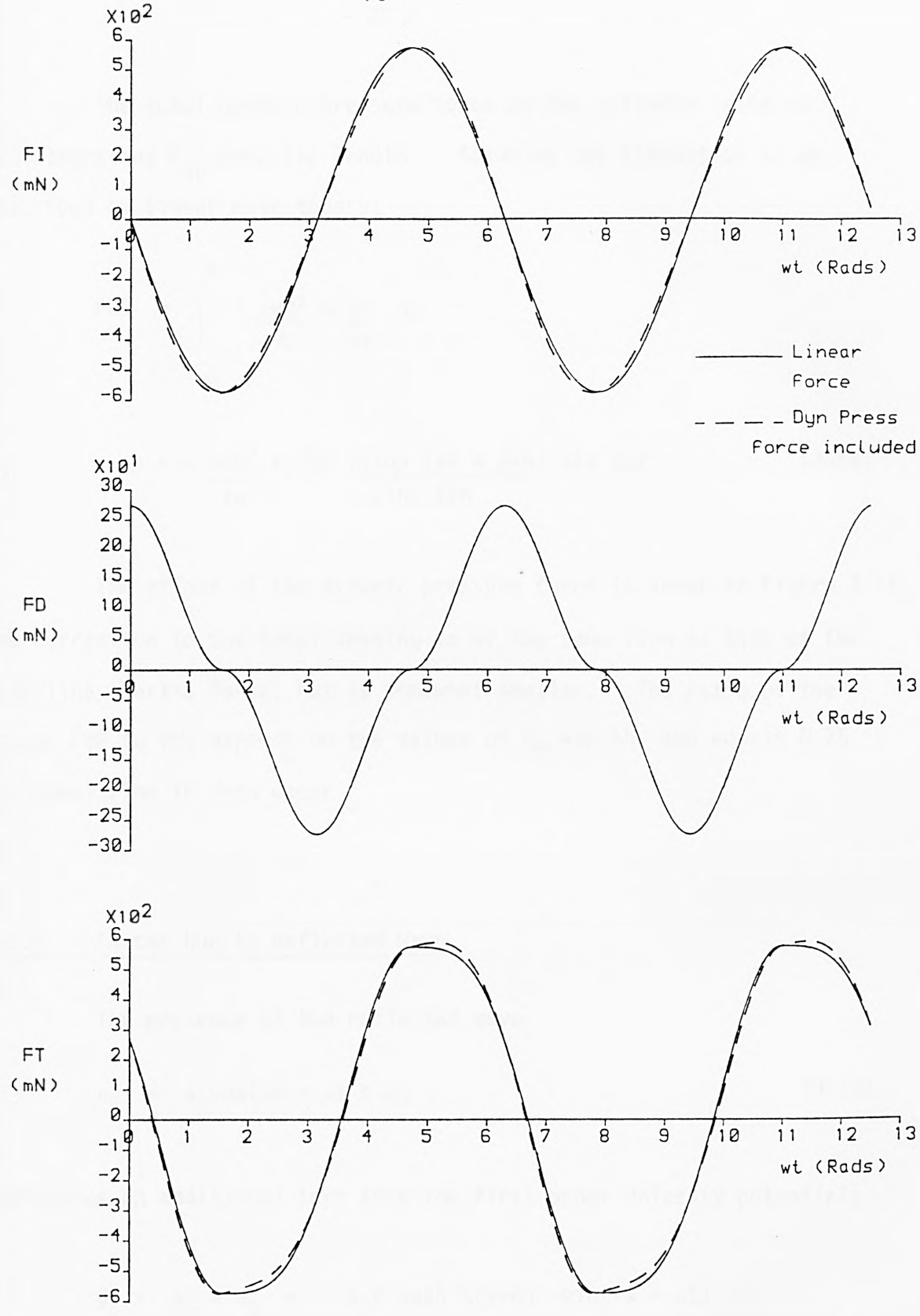

THEORETICAL FORCES ON 25.0mm CYLINDER; CM= 2.0; CD= 1.2

WAVE CONDITIONS: h= 500.0mm; Freq= 1.20Hz; WL= 1077.9mm; Wave Amp= 60.0mm

DIMENSIONLESS PARAMETERS: KC= 7.84; ka= .350; kh= 2.915

DEMONSTRATING EFFECT OF DYNAMIC PRESSURE

Figure 3.14

The total dynamic pressure force on the cylinder is found by integrating F_{dp} over its length. Assuming the kinematics to be described by linear wave theory;

$$FDP = \int_{-h}^{o} - \frac{\rho\pi D^2}{4} u \frac{\partial u}{\partial x} dy$$

$$= - \frac{\rho\pi D^2}{16} a_I{}^2 gk \frac{(\sinh 2kh + 2kh)}{\sinh 2kh} \sin 2\omega t \qquad (3\text{-}58)$$

The effect of the dynamic pressure force is shown in Figure 3.14. The correction to the total loading is of the same form as that of the waterline inertia force, but is somewhat smaller. The ratio of the forces FDP to FWI depends on the values of C_m and kh, and equals 0.25 for ideal flow in deep water.

3.3.5 Forces Due to Reflected Wave

The presence of the reflected wave

$$\eta_R = a_R \cos(kx + \omega t + \alpha) \qquad (3\text{-}19)$$

introduces an additional term into the first order velocity potential;

$$\phi = \phi_1 + \phi_R = - \frac{a_I g \cosh k(y+h)}{\omega \cosh kh} \sin(kx - \omega t)$$

$$+ \frac{a_R g \cosh k(y+h)}{\omega \cosh kh} \sin(kx + \omega t + \alpha) \qquad (3\text{-}59)$$

With the cylinder positioned at the origin of x, the particle kinematics are given by;

$$u = u_1 + u_R = \frac{a_I gk \cosh k(y+h)}{\omega \cosh kh} \cos \omega t - \frac{a_R gk \cosh k(y+h)}{\omega \cosh kh} \cos(\omega t + \alpha) \quad (3\text{-}60)$$

$$\frac{\partial u}{\partial t} = - a_I gk \frac{\cosh k(y+h)}{\cosh kh} \sin\omega t + a_R gk \frac{\cosh k(y+h)}{\cosh kh} \sin(\omega t + \alpha) \quad (3\text{-}61)$$

In assessing the effect of the reflect wave on the loading, the observations made in Section 3.3.1, regarding the linearity of the inertia force and the dependence of the drag force on $u|u|$, are noted. The expression derived from (3-60) for $u|u|$ is simplified using (3-45), and the forces due to the reflected wave are given by;

$$FDR = -\tfrac{1}{2}\rho C_d D a_I a_R g \left(\frac{\sinh 2kh + 2kh}{\sinh 2kh}\right) \cos(\omega t + \alpha)|\cos\omega t| \quad (3\text{-}62)$$

$$FIR = \frac{\rho\pi D^2}{4} C_m a_R g \tanh kh \sin(\omega t + \alpha) \quad (3\text{-}63)$$

The form of the correction to the loading due to FDR and FIR depends on the phase angle, α, while the magnitude of the effect is proportional to the reflection coefficient, K_R. The effect of the reflected wave on the total force on a vertical cylinder is shown in Figures 3.15 to 3.17 for different values of α, and for a reflection coefficient of 10%.

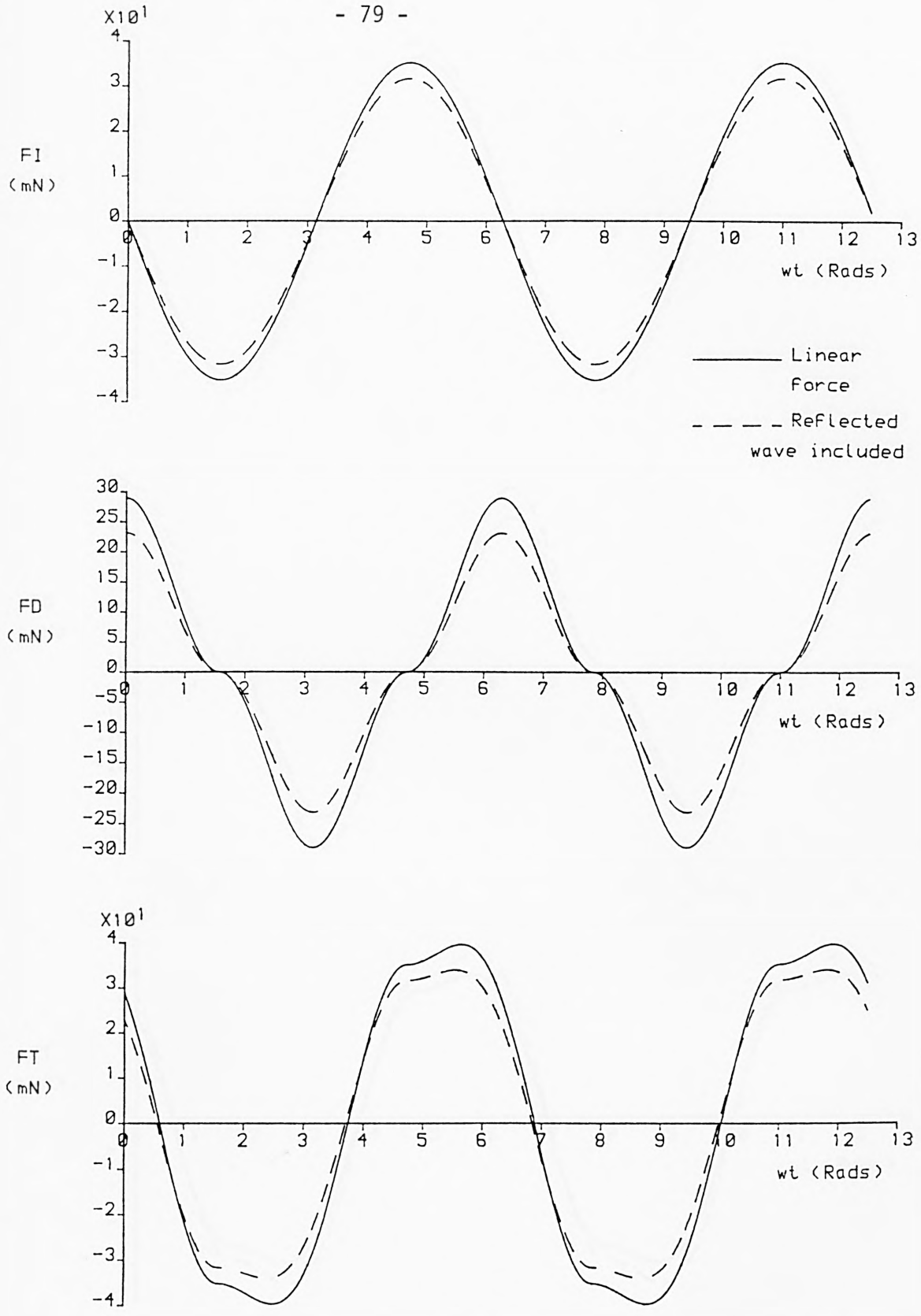

THEORETICAL FORCES ON 9.0mm CYLINDER; CM= 2.0; CD= 1.2

WAVE CONDITIONS: h= 500.0mm; Freq= .90Hz; WL= 1811.1mm; Wave Amp= 30.0mm

DIMENSIONLESS PARAMETERS: KC= 13.56; ka= .104; kh= 1.735

DEMONSTRATING EFFECT OF REFLECTED WAVE: KR= 10.0%; ALPHA= .000Rads

Figure 3.15

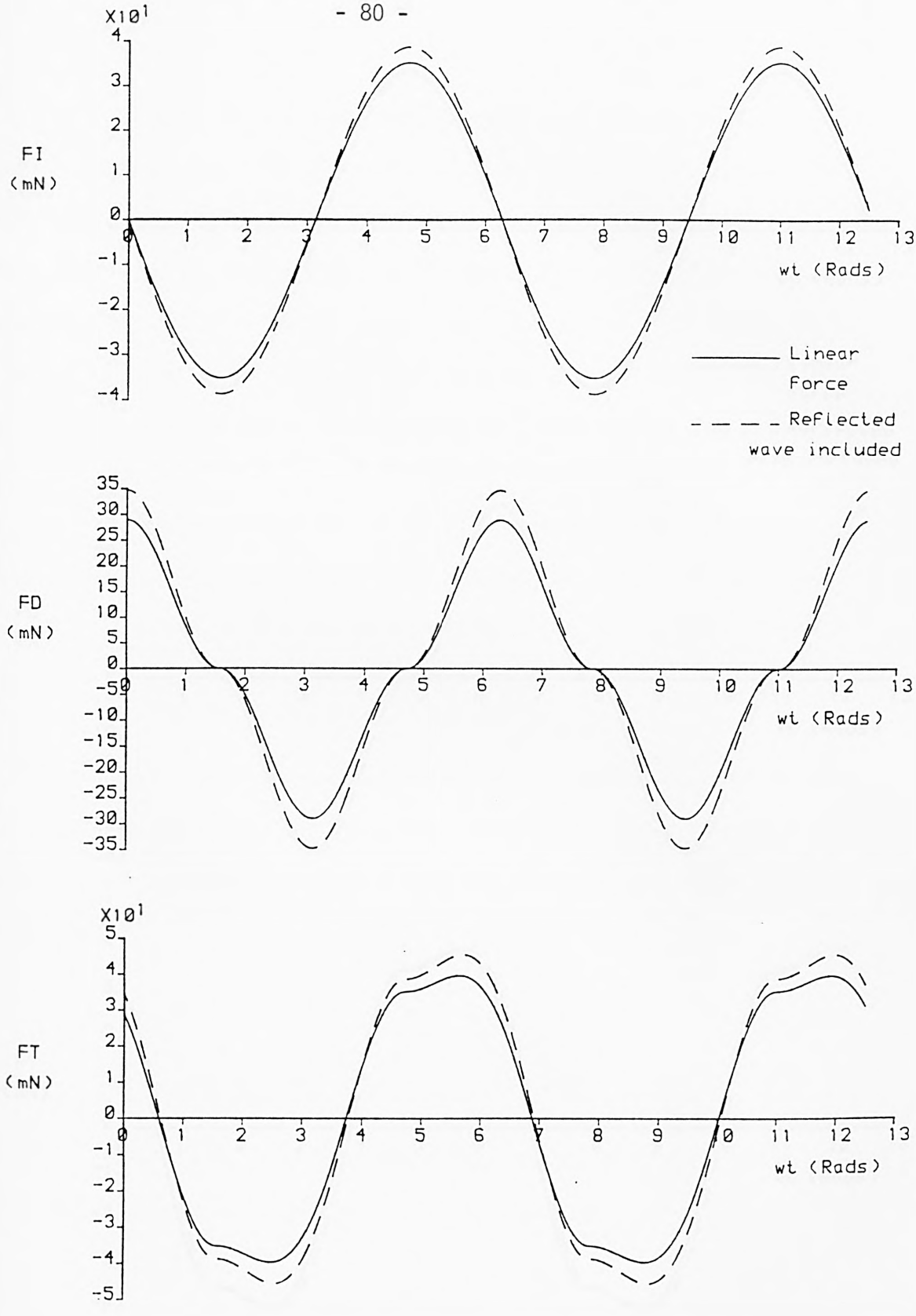

THEORETICAL FORCES ON 9.0mm CYLINDER; CM= 2.0; CD= 1.2

WAVE CONDITIONS: h= 500.0mm; Freq= .90Hz; WL= 1811.1mm; Wave Amp= 30.0mm

DIMENSIONLESS PARAMETERS: KC= 13.56; ka= .104; kh= 1.735

DEMONSTRATING EFFECT OF REFLECTED WAVE: KR= 10.0%; ALPHA= 3.142Rads

Figure 3.16

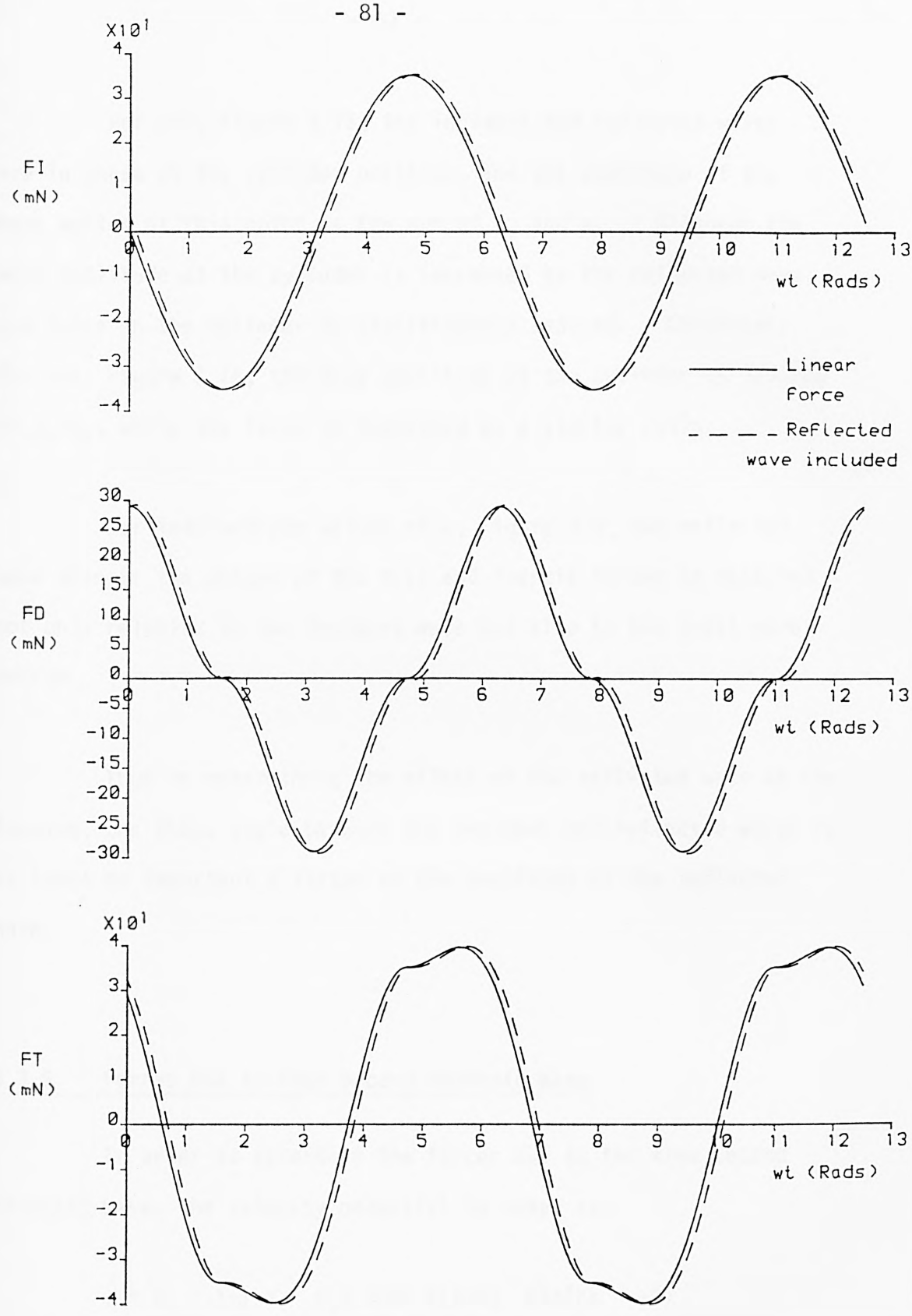

THEORETICAL FORCES ON 9.0mm CYLINDER; CM= 2.0; CD= 1.2

WAVE CONDITIONS: h= 500.0mm; Freq= .90Hz; WL= 1811.1mm; Wave Amp= 30.0mm

DIMENSIONLESS PARAMETERS: KC= 13.56; ka= .104; kh= 1.735

DEMONSTRATING EFFECT OF REFLECTED WAVE: KR= 10.0%; ALPHA= 1.571Rads

Figure 3.17

For $\alpha=0$, Figure 3.15, the incident and reflected waves are in phase at the cylinder position, and the amplitude of the wave motion at this point is the sum of a_I and a_R. Although the wave amplitude at the cylinder is increased by the reflected wave, the force on the cylinder is significantly reduced. Conversely for $\alpha=\pi$, Figure 3.16, the wave amplitude at the cylinder is reduced to a_I-a_R, while the force is increased by a similar ratio.

For intermediate values of α, Figure 3.17, the reflected wave changes the phases of the drag and inertia forces as measured not only relative to the incident wave but also to the total wave motion.

Thus in determining the effect of the reflected wave on the loading, the phase angle between the incident and reflected waves is at least as important a factor as the amplitude of the reflected wave.

3.3.6 Forces Due to Free Second Harmonic Wave

In order to ascertain the forces due to the free second harmonic wave, the velocity potential is taken as;

$$\phi = \phi_1 + \phi_{22} = - \frac{a_I g}{\omega} \frac{\cosh k(y+h)}{\cosh kh} \sin(kx - \omega t)$$

$$- \frac{a_{22} g}{2\omega} \frac{\cosh k_{22}(y+h)}{\cosh k_{22} h} \sin(k_{22}x - 2\omega t + \beta) \qquad (3\text{-}64)$$

The particle kinematics are;

$$u = u_1 + u_{22} = \frac{a_I g k \cosh k(y+h)}{\omega \cosh kh} \cos\omega t + \frac{a_{22} g k_{22} \cosh k_{22}(y+h)}{2\omega \cosh k_{22} h} \cos(2\omega t - \beta) \quad (3\text{-}65)$$

$$\frac{\partial u}{\partial t} = - a_I g k \frac{\cosh k(y+h)}{\cosh kh} \sin\omega t - a_{22} g k_{22} \frac{\cosh k_{22}(y+h)}{\cosh k_{22} h} \sin(2\omega t - \beta) \quad (3\text{-}66)$$

The expression attained for $u|u|$ is simplified by the relationship (3-45), and the total forces on the cylinder due to the free second harmonic wave are given by;

$$FD22 = \frac{1}{4} \frac{\rho C_d D a_I a_{22} g k_{22}}{\sinh kh \cosh k_{22} h} \left(\frac{\sinh(k_{22}+ k)h}{(k_{22}+ k)} + \frac{\sinh(k_{22} - k)h}{(k_{22}- k)} \right) x \cos(2\omega t - \beta) |\cos\omega t| \quad (3\text{-}67)$$

$$FI22 = - \frac{\rho \pi D^2}{4} C_m a_{22} g \tanh k_{22} h \sin(2\omega t - \beta) \quad (3\text{-}68)$$

The effect of the free second harmonic wave on the total wave loading depends on the phase angle, β, and its magnitude on the amplitude, a_{22}. This is demonstrated in Figures 3.18 to 3.20 for different values of β.

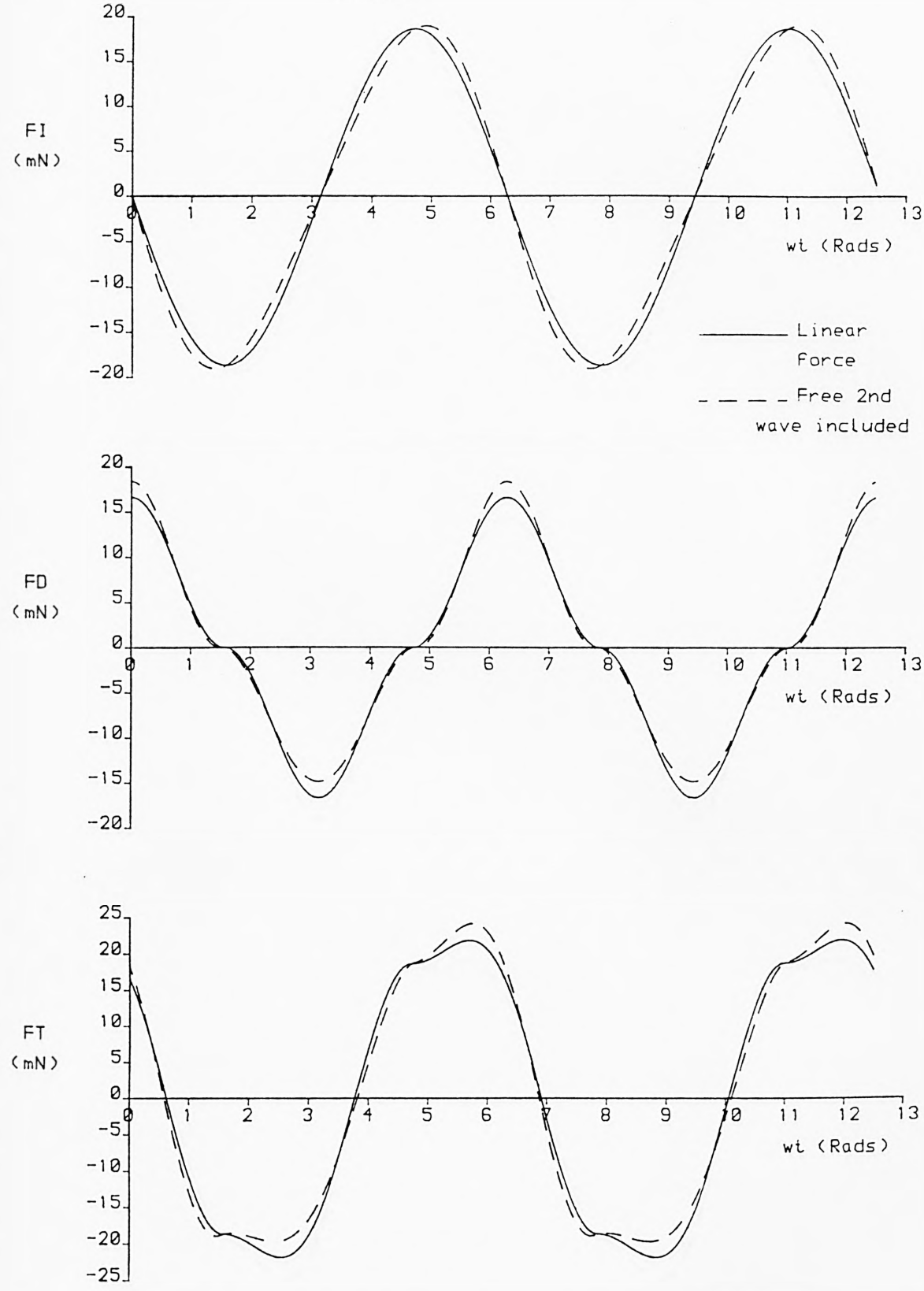

THEORETICAL FORCES ON 9.0mm CYLINDER; CM= 2.0; CD= 1.2

WAVE CONDITIONS: h= 500.0mm; Freq= .60Hz; WL= 3244.1mm; Wave Amp= 20.0mm

DIMENSIONLESS PARAMETERS: KC= 14.66; ka= .039; kh= .968

DEMONSTRATING EFFECT OF FREE 2ND WAVE: A22= 1.50mm; BETA= .000Rads

Figure 3.18

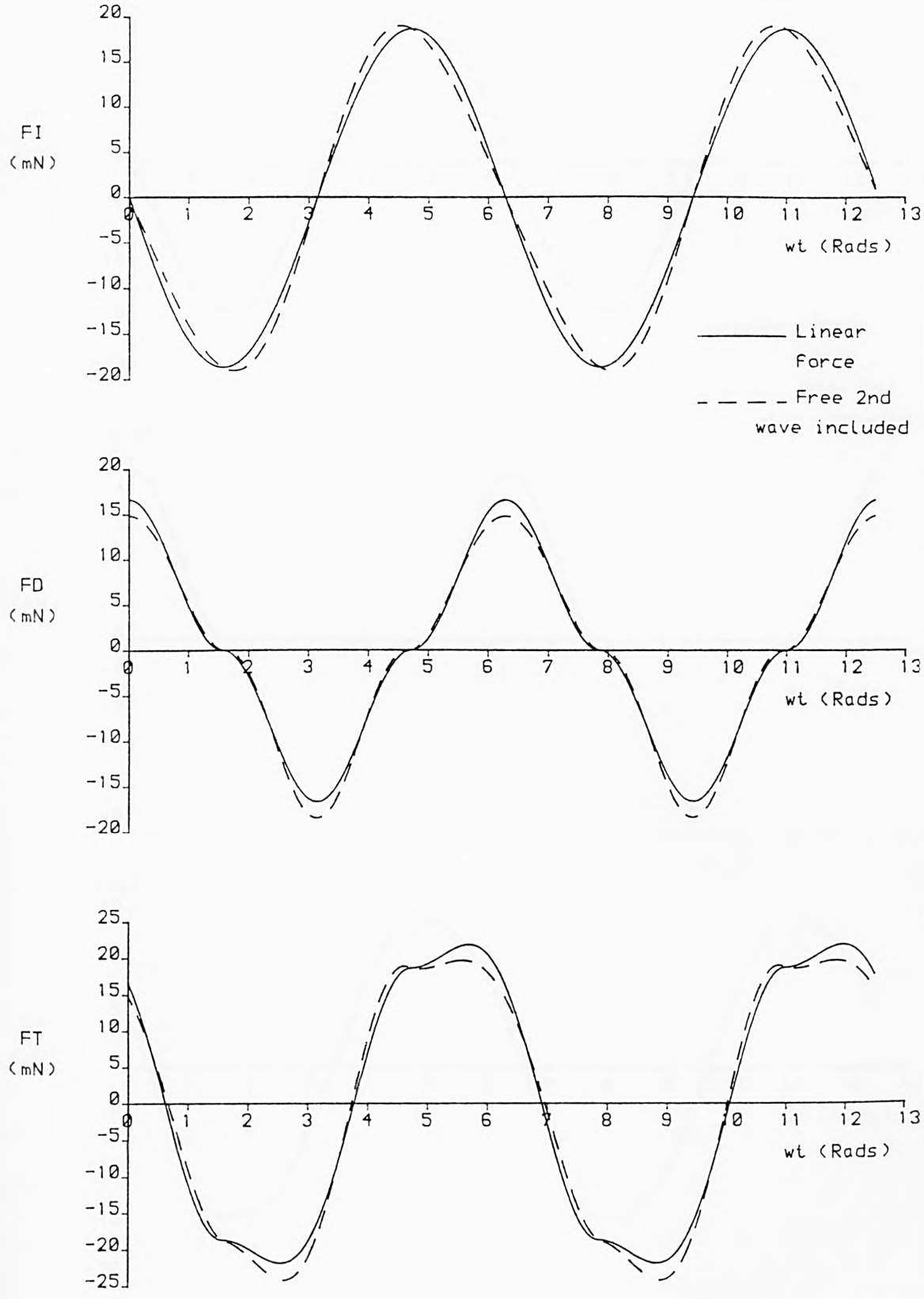

THEORETICAL FORCES ON 9.0mm CYLINDER; CM= 2.0; CD= 1.2

WAVE CONDITIONS: h= 500.0mm; Freq= .60Hz; WL= 3244.1mm; Wave Amp= 20.0mm

DIMENSIONLESS PARAMETERS: KC= 14.66; ka= .039; kh= .968

DEMONSTRATING EFFECT OF FREE 2ND WAVE: A22= 1.50mm; BETA= 3.142Rads

Figure 3.19

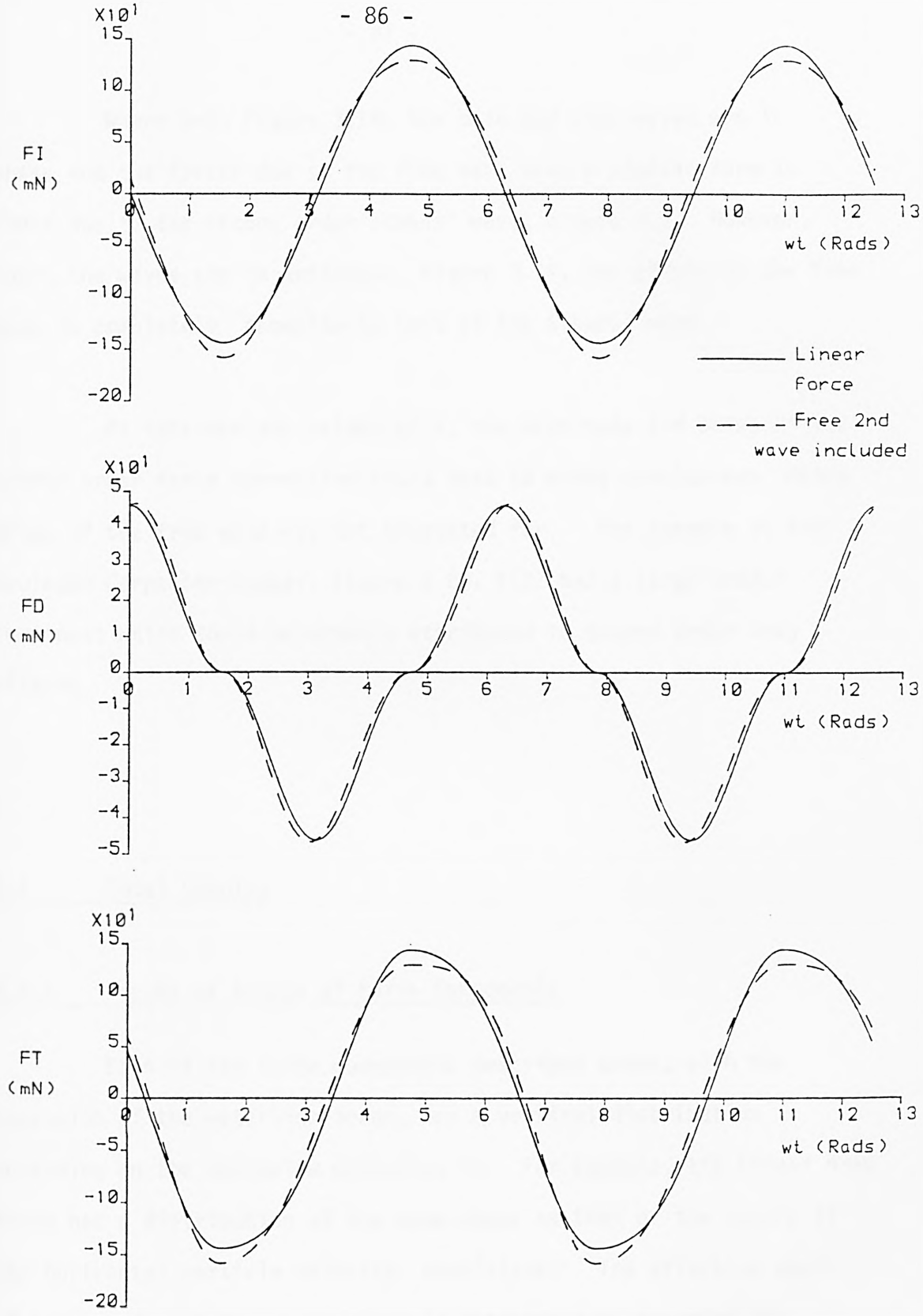

THEORETICAL FORCES ON 25.0mm CYLINDER; CM= 2.0; CD= 1.2

WAVE CONDITIONS: h= 500.0mm; Freq= .60Hz; WL= 3244.1mm; Wave Amp= 20.0mm

DIMENSIONLESS PARAMETERS: KC= 5.28; ka= .039; kh= .968

DEMONSTRATING EFFECT OF FREE 2ND WAVE: A22= 1.50mm; BETA= 1.571Rads

Figure 3.20

Where $\beta=0$, Figure 3.18, the main and free waves are in phase and the forces due to the free wave have a similar form to those due to the second order Stokes' wave, Figure 3.7. However, where the waves are in antiphase, Figure 3.19, the effect of the free wave is completely opposite to that of the Stokes' wave.

At intermediate values of β, the magnitude and phase of the second order force correction could lead to wrong conclusions being drawn if the free wave was not accounted for. For example at high Keulegan Carpenter number, Figure 3.20, FI22 has a large $\cos 2\omega t$ component which could be wrongly attributed to second order drag effects.

3.4 Total Loading

3.4.1 Depths of Action of Force Components

Each of the force components described above, with the exception of the waterline force, has a vertical distribution depending on the mechanism producing it. For example, the linear drag force has a distribution of the same shape as that of the square of the horizontal particle velocity, $\cosh^2 k(y+h)$. The effective depth of action of each force component is determined by equating the moment due to the force distribution with the moment due to the resultant force, as is demonstrated in Figure 3.21.

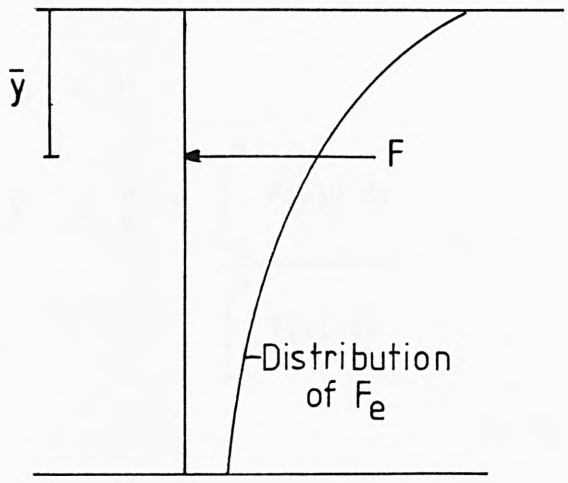

F acts through centroid of distribution

Effective Depth of Action

Figure 3.21

Consider any one of the force components. The force on an element is given by,

$$F_e = A\, f(y) \tag{3-69}$$

where f(y) represents the vertical distribution.

The total force is;

$$F = A \int_{-h}^{o} f(y)dy \tag{3-70}$$

and the total moment about y=0 is given by;

$$M = A \int_{-h}^{o} f(y)y\, dy \tag{3-71}$$

If the resultant force acts at a depth of $y=\bar{y}$, then;

$$F\bar{y} = M$$

$$\bar{y} = \frac{M}{F} = \frac{\int_{-h}^{o} f(y)y\,dy}{\int_{-h}^{o} f(y)\,dy} \qquad (3\text{-}72)$$

For each of the force components, the distribution $f(y)$ is known, and the effective depth of action is found from (3-72). The results of this are presented in Table 3.1.

Force Component	Depth of action ($\bar{y}$)
FI, FIR	$\frac{-1}{k \tanh kh} + \frac{1}{k \sinh kh}$
FD, FDR, FDP	$\frac{1}{2k}\left(\frac{-2(kh)^2 - \cosh 2kh + 1}{\sinh 2kh + 2kh}\right)$
FI2	$\frac{-1}{2k \tanh 2kh} + \frac{1}{2k \sinh 2kh}$
FD2	$\frac{1}{k}\left(\frac{-9 \cosh kh - \cosh 3kh + 10}{9 \sinh kh + 3 \sinh 3kh}\right)$
FWI, FWD	0.0
FI22	$\frac{-1}{k_{22} \tanh k_{22} h} + \frac{1}{k_{22} \sinh k_{22} h}$
FD22	$\dfrac{\frac{(1 - \cosh(k_{22}-k)h)}{(k_{22} - k)^2} + \frac{(1 - \cosh(k_{22}+k)h)}{(k_{22} + k)^2}}{\frac{\sinh(k_{22} - k)h}{k_{22} - k} + \frac{\sinh(k_{22} + k)h}{k_{22} + k}}$

Depths of Action of Force Components

Table 3.1

3.4.2 Frequency Composition of Force Components

In assessing the total load on the cylinder, it is necessary to know the frequency compositions of the force components. This is relatively simple for the inertia components, since most of the terms are either sin ωt or sin $2\omega t$. The phase angles, α and β, in the reflected and free wave inertia forces are accounted for by;

$$\sin(\omega t + \alpha) = \sin \omega t \cos\alpha + \cos \omega t \sin\alpha \qquad (3\text{-}73)$$

The drag loading, however, is complicated by the presence of terms such as $\cos \omega t|\cos \omega t|$. Even the first order drag force in Figure 3.5 has a distinctly non-linear time variation due to this term. A Fourier series for $\cos \omega t|\cos \omega t|$ is derived by considering it to be the product of $\cos^2\omega t$ and a cosine square wave. The cosine square wave is a function which has a value of unity for positive values of $\cos \omega t$, and minus unity for negative $\cos \omega t$. The Fourier series for a cosine square wave is given by;

$$\frac{4}{\pi} \cos \omega t - \frac{4}{3\pi} \cos 3\omega t + \frac{4}{5\pi} \cos 5\omega t - \frac{4}{7\pi} \cos 7\omega t + ...$$

Thus;

$$\cos \omega t|\cos \omega t|$$

$$= \cos^2\omega t \times \text{square wave}$$

$$= \frac{8}{3\pi} \cos \omega t + \frac{8}{15\pi} \cos 3\omega t - \frac{8}{105\pi} \cos 5\omega t + ... \qquad (3\text{-}74)$$

In a similar manner the Fourier series for the other drag force components have been determined and these are presented in Table 3.2.

Force Component	$f(\omega t)$	Fourier Series
FD	$\cos\omega t\lvert\cos\omega t\rvert$	$\frac{8}{3\pi}\cos\omega t + \frac{8}{15\pi}\cos 3\omega t - \frac{8}{105\pi}\cos 5\omega t$
FD2	$\cos 2\omega t\lvert\cos\omega t\rvert$	$\frac{2}{3\pi} + \frac{28}{15\pi}\cos 2\omega t + \frac{76}{105\pi}\cos 4\omega t$
FWD	$\cos^2\omega t\lvert\cos\omega t\rvert$	$\frac{8}{6\pi} + \frac{8}{5\pi}\cos 2\omega t + \frac{8}{35\pi}\cos 4\omega t$
FDR	$\cos(\omega t+\alpha)\lvert\cos\omega t\rvert$	$\frac{8}{3\pi}\cos\omega t\cos\alpha - \frac{4}{3\pi}\sin\omega t\sin\alpha$ $\frac{+8}{15\pi}\cos 3\omega t\cos\alpha - \frac{4}{5\pi}\sin 3\omega t\sin\alpha$ $\frac{-8}{105\pi}\cos 5\omega t\cos\alpha + \frac{4}{21\pi}\sin 5\omega t\sin\alpha$
FD22	$\cos(2\omega t-\beta)\lvert\cos\omega t\rvert$	$\frac{2}{3\pi}\cos\beta + \frac{28}{15\pi}\cos 2\omega t\cos\beta + \frac{32}{15\pi}\sin 2\omega t\sin\beta$ $+ \frac{76}{105\pi}\cos 4\omega t\cos\beta + \frac{64}{105\pi}\sin 4\omega t\sin\beta$

Fourier Series for Drag Force Components

Table 3.2

3.4.3 Total Non-Linear Loading

The total wave loading on a vertical cylinder is assumed to be given by the simple summation of the linear and non-linear force components. The resultant and depth of action of each of the Fourier components of the total force are found by consideration of the Fourier Series of the force components. For example the cos $2\omega t$ component of the total force is the resultant of appropriate proportions of FWD, FD2, FD22 and FI22.

In taking the simple summation of the drag force components, the relationship (3-45) is assumed to be applicable where $f(\theta)$ is the sum of a number of trigonemetrical terms. In Appendix 3, this is shown to be the case provided the total value of $f(\theta)$ remains small relative to a. The full expression for $u|u|$ becomes;

$$u|u| = (u_1 + u_R + u_2 + u_{22})|u_1 + u_R + u_2 + u_{22}|$$

$$= u_1|u_1| + 2u_R|u_1| + 2u_2|u_1| + 2u_{22}|u_1| \qquad (3\text{-}75)$$

and the linear superposition of the drag force components is valid.

The total force on a cylinder under practical experimental combinations of incident, reflected and free second harmonic waves has been calculated for a number of cases and these are presented both numerically and graphically in Figures 3.22 to 3.25. The wave conditions used for this were taken from the results of the wave experiments which were carried out, and which are reported in Chapter 5.

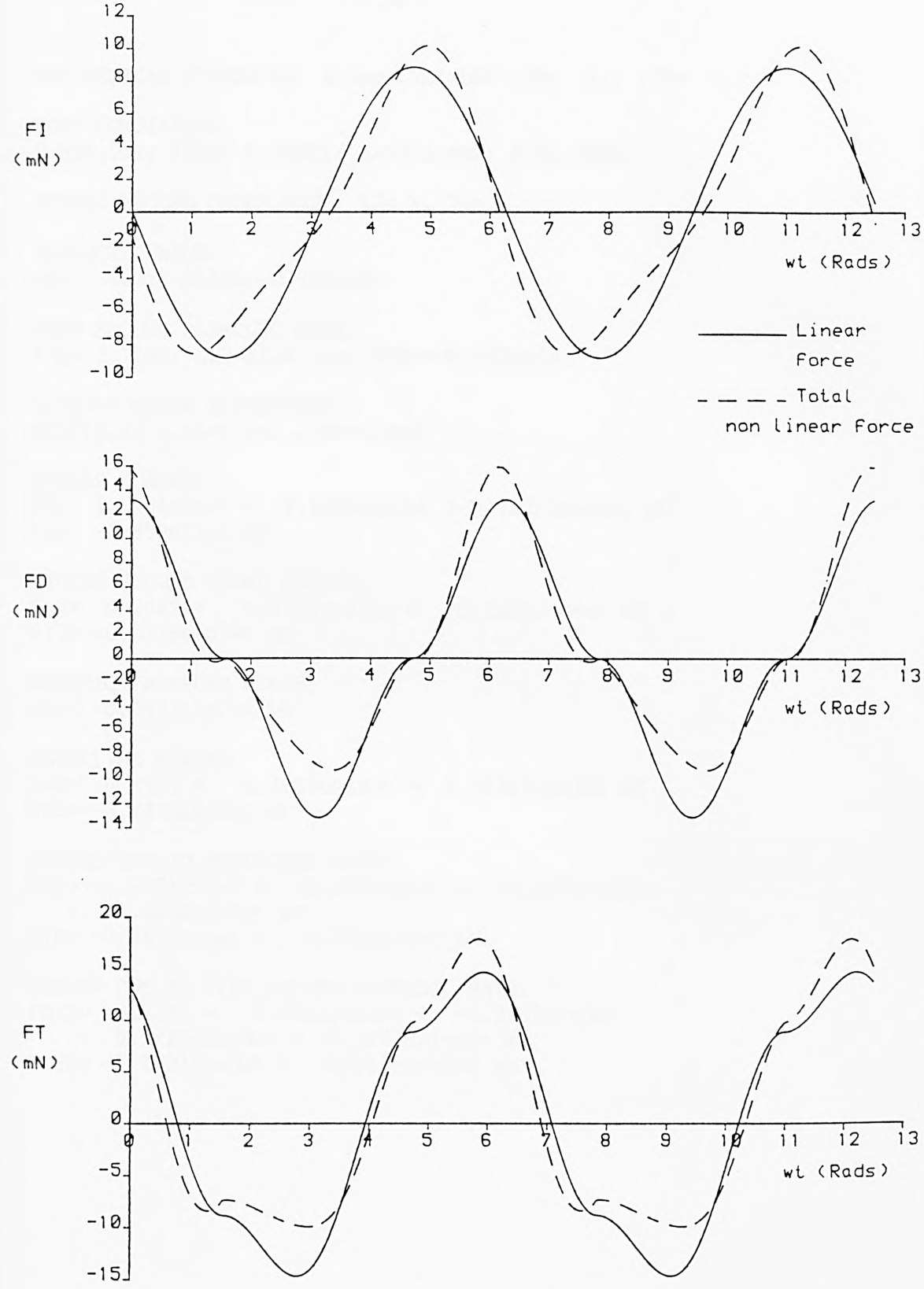

THEORETICAL FORCES ON 6.0mm CYLINDER; CM= 2.0; CD= 1.2

WAVE CONDITIONS: h= 500.0mm; Freq= .586Hz; WL= 3342.6mm; Wave Amp= 21.7mm

A2= 1.370mm; AR= 1.017mm; ALPHA= -.745Rads; A22= 2.736mm; BETA= -.902Rads

DIMENSIONLESS PARAMETERS: KC= 24.53; ka= .041; kh= .940

TOTAL LINEAR AND NON-LINEAR FORCE

Figure 3.22

THEORETICAL FORCES ON 6.0mm CYLINDER ;CM= 2.0 ;CD= 1.2

WAVE CONDITIONS:
H=500.0mm; FREQ= 0.586Hz; L=3342.6mm; A=21.70mm

STOKES SECOND ORDER WAVE: A2= 1.37mm

REFLECTED WAVE:
AR= 1.02mm; ALPHA=-0.745Rads

FREE SECOND HARMONIC WAVE:
A22= 2.74mm; L22=1128.0mm; BETA=-0.902Rads

DIMENSIONLESS PARAMETERS:
KCI=24.53 ; KA=0.041 ; KH=0.940

LINEAR FORCES:
FD= 11.204coswt + 2.2409cos3wt +-0.32013cos5wt mN
FI= -8.850sinwt mN

STOKES SECOND ORDER FORCES:
FD2= 0.2047 + 0.5733cos2wt + 0.2223cos4wt mN
FI2= -0.6263sin2wt mN

DYNAMIC PRESSURE FORCE:
FDP= -0.0974sin2wt mN

WATERLINE FORCES:
FWD= 0.3916 + 0.4699cos2wt + 0.06713cos4wt mN
FWI= -0.2455sin2wt mN

FORCES DUE TO REFLECTED WAVE:
FDR= -0.7721coswt + -0.3560sinwt + -0.1544cos3wt
+ -0.2136sin3wt mN
FIR= -0.2812coswt + 0.3049sinwt mN

FORCES DUE TO FREE SECOND HARMONIC WAVE:
FD22= 0.3151 + 0.8822cos2wt + -1.2767sin2wt
+ 0.34206cos4wt + -0.36478sin4wt mN
FI22= -1.1821cos2wt + -0.9335sin2wt mN

(fig. 3.22)

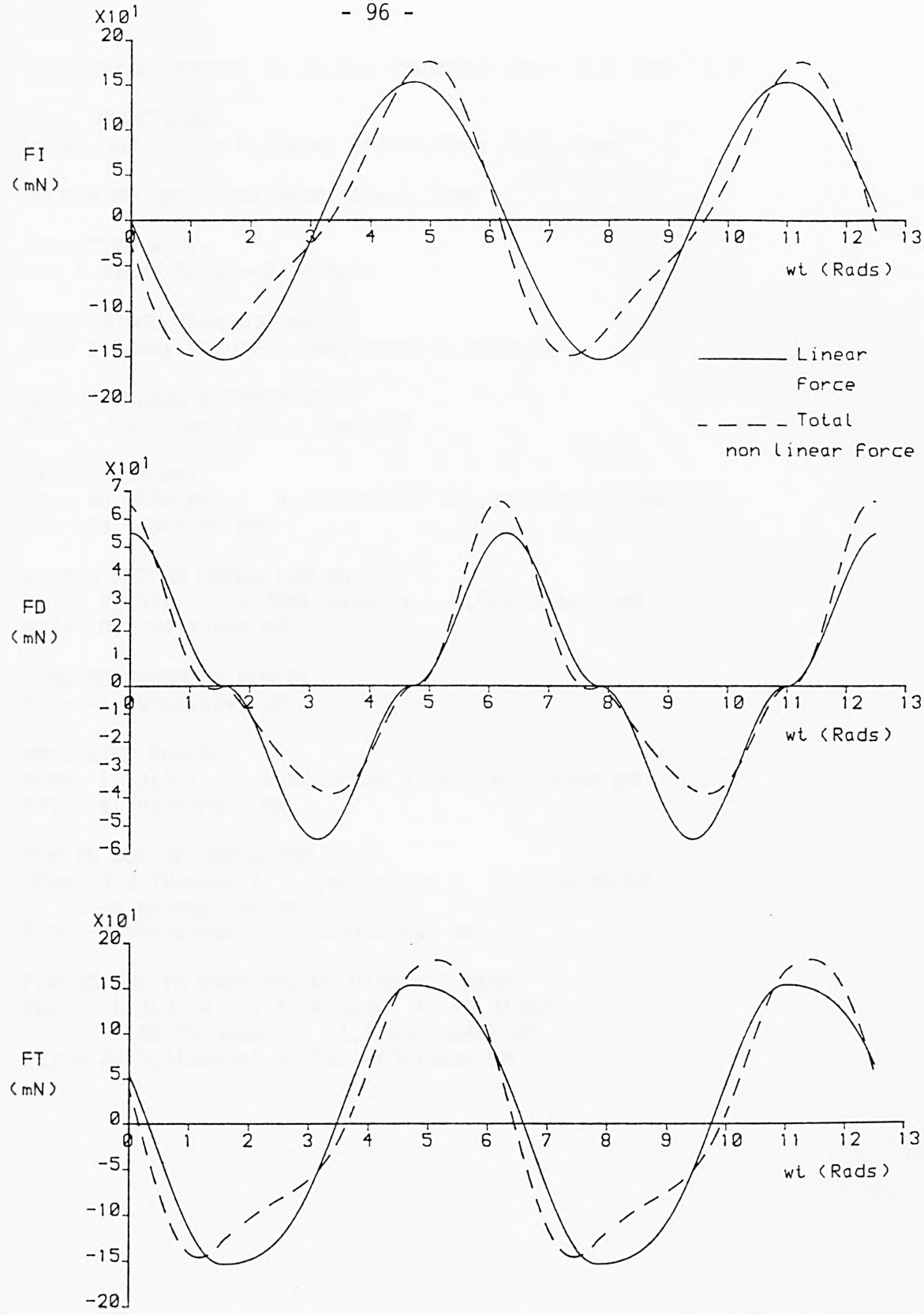

THEORETICAL FORCES ON 25.0mm CYLINDER; CM= 2.0; CD= 1.2

WAVE CONDITIONS: h= 500.0mm; Freq= .586Hz; WL= 3342.6mm; Wave Amp= 21.7mm

A2= 1.370mm; AR= 1.017mm; ALPHA= -.745Rads; A22= 2.736mm; BETA= -.902Rads

DIMENSIONLESS PARAMETERS: KC= 5.89; ka= .041; kh= .940

TOTAL LINEAR AND NON-LINEAR FORCE

Figure 3.23

THEORETICAL FORCES ON 25.0mm CYLINDER ;CM= 2.0 ;CD= 1.2

WAVE CONDITIONS:
H=500.0mm; FREQ= 0.586Hz; L=3342.6mm; A=21.70mm

STOKES SECOND ORDER WAVE: A2= 1.37mm

REFLECTED WAVE:
AR= 1.02mm; ALPHA=-0.745Rads

FREE SECOND HARMONIC WAVE:
A22= 2.74mm; L22=1128.0mm; BETA=-0.902Rads

DIMENSIONLESS PARAMETERS:
KCI= 5.89 ; KA=0.041 ; KH=0.940

LINEAR FORCES:
FD= 46.685coswt + 9.3371cos3wt +-1.33386cos5wt mN
FI=-153.643sinwt mN

STOKES SECOND ORDER FORCES:
FD2= 0.8531 + 2.3886cos2wt + 0.9262cos4wt mN
FI2=-10.8724sin2wt mN

DYNAMIC PRESSURE FORCE:
FDP= -1.6916sin2wt mN

WATERLINE FORCES:
FWD= 1.6317 + 1.9581cos2wt + 0.27972cos4wt mN
FWI= -4.2624sin2wt mN

FORCES DUE TO REFLECTED WAVE:
FDR= -3.2170coswt + -1.4832sinwt + -0.6434cos3wt
+ -0.8899sin3wt mN
FIR= -4.8813coswt + 5.2936sinwt mN

FORCES DUE TO FREE SECOND HARMONIC WAVE:
FD22= 1.3127 + 3.6756cos2wt + -5.3198sin2wt
+ 1.42525cos4wt + -1.51993sin4wt mN
FI22=-20.5231cos2wt + -16.2060sin2wt mN

(fig. 3.23)

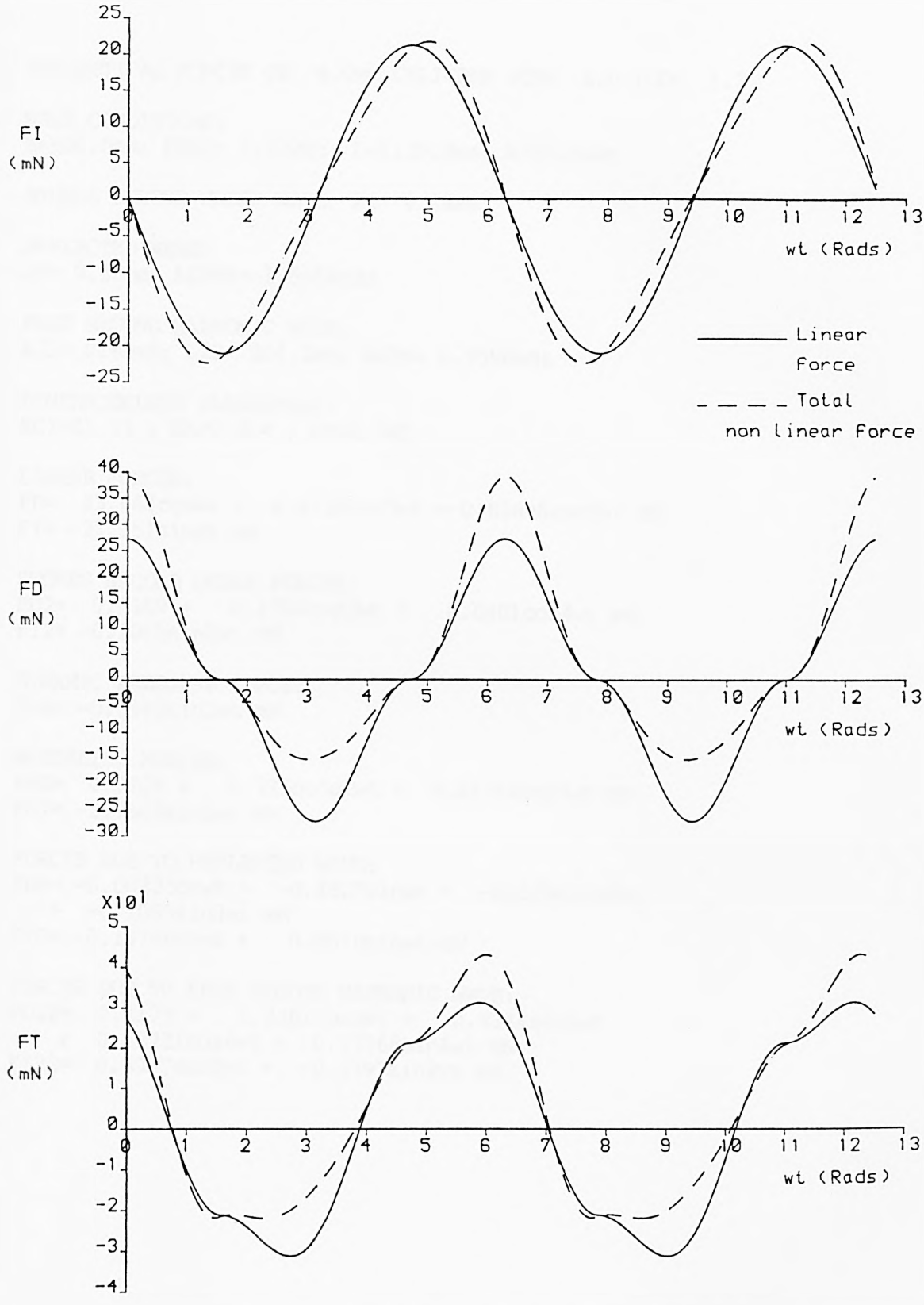

THEORETICAL FORCES ON 6.0mm CYLINDER; CM= 2.0; CD= 1.2

WAVE CONDITIONS: h= 500.0mm; Freq= 1.172Hz; WL= 1128.0mm; Wave Amp= 38.4mm

A2= 4.238mm; AR= .304mm; ALPHA= -1.565Rads; A22= .878mm; BETA= .959Rads

DIMENSIONLESS PARAMETERS: KC= 21.13; ka= .214; kh= 2.785

TOTAL LINEAR AND NON-LINEAR FORCE

Figure 3.24

THEORETICAL FORCES ON 6.0mm CYLINDER ;CM= 2.0 ;CD= 1.2

WAVE CONDITIONS:
H=500.0mm; FREQ= 1.172Hz; L=1128.0mm; A=38.42mm

STOKES SECOND ORDER WAVE: A2= 4.24mm

REFLECTED WAVE:
AR= 0.30mm; ALPHA=-1.565Rads

FREE SECOND HARMONIC WAVE:
A22= 0.88mm; L22= 284.2mm; BETA= 0.959Rads

DIMENSIONLESS PARAMETERS:
KCI=21.13 ; KA=0.214 ; KH=2.785

LINEAR FORCES:
FD= 23.064coswt + 4.6128cos3wt +-0.65896cos5wt mN
FI= -21.151sinwt mN

STOKES SECOND ORDER FORCES:
FD2= 0.0369 + 0.1034cos2wt + 0.0401cos4wt mN
FI2= -0.1051sin2wt mN

DYNAMIC PRESSURE FORCE:
FDP= -0.5943sin2wt mN

WATERLINE FORCES:
FWD= 4.7709 + 5.7250cos2wt + 0.81786cos4wt mN
FWI= -2.2805sin2wt mN

FORCES DUE TO REFLECTED WAVE:
FDR= -0.0022coswt + -0.1825sinwt + -0.0004cos3wt
+ -0.1095sin3wt mN
FIR= -0.1674coswt + 0.0010sinwt mN

FORCES DUE TO FREE SECOND HARMONIC WAVE:
FD22= 0.1172 + 0.3281cos2wt + 0.5344sin2wt
+ 0.12721cos4wt + 0.15268sin4wt mN
FI22= 0.3987cos2wt + -0.2797sin2wt mN

(fig. 3.24)

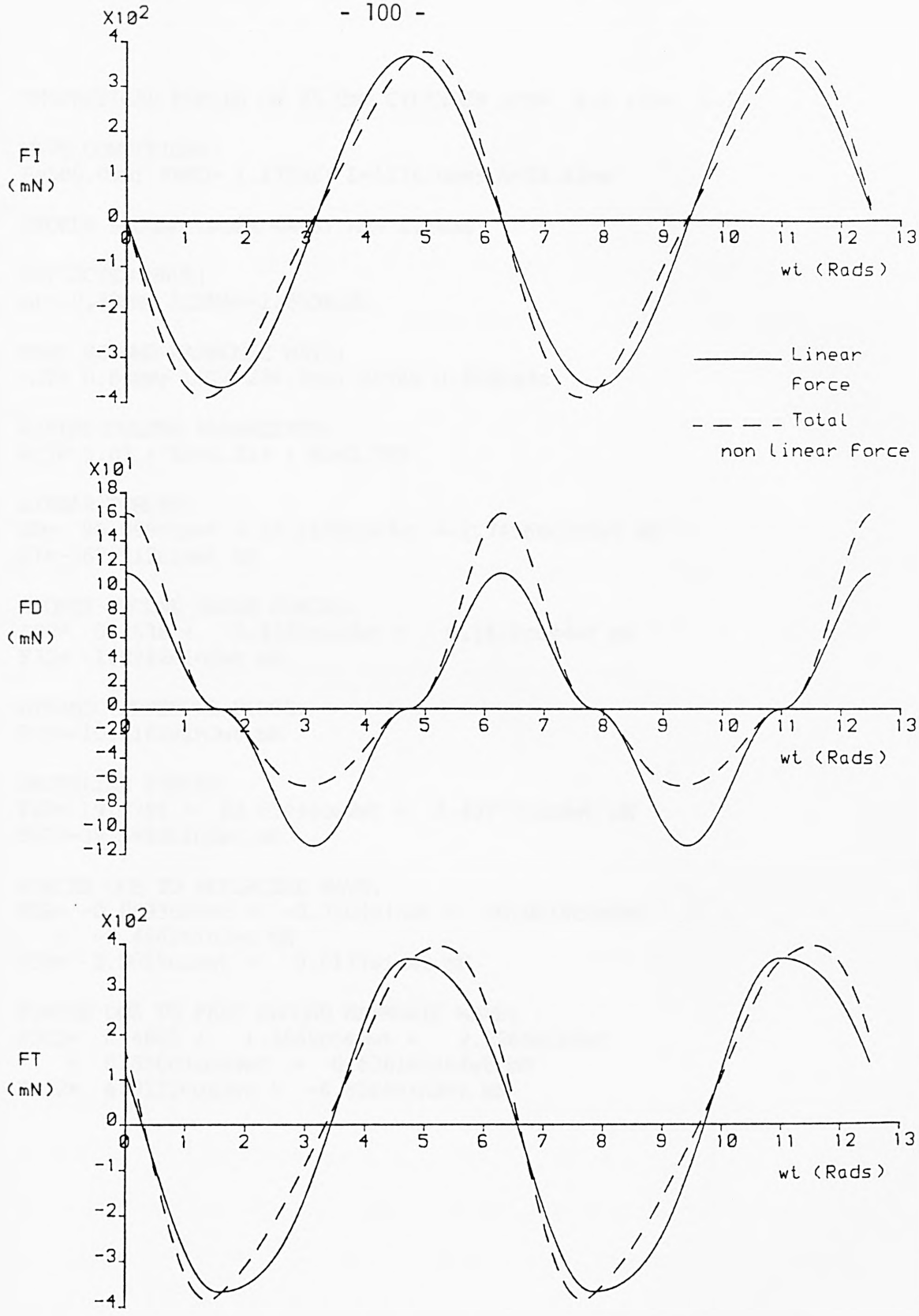

THEORETICAL FORCES ON 25.0mm CYLINDER; CM= 2.0; CD= 1.2

WAVE CONDITIONS: h= 500.0mm; Freq= 1.172Hz; WL= 1128.0mm; Wave Amp= 38.4mm

A2= 4.238mm; AR= .304mm; ALPHA= -1.565Rads; A22= .878mm; BETA= .959Rads

DIMENSIONLESS PARAMETERS: KC= 5.07; ka= .214; kh= 2.785

TOTAL LINEAR AND NON-LINEAR FORCE

Figure 3.25

THEORETICAL FORCES ON 25.0mm CYLINDER ;CM= 2.0 ;CD= 1.2

WAVE CONDITIONS:
H=500.0mm; FREQ= 1.172Hz; L=1128.0mm; A=38.42mm

STOKES SECOND ORDER WAVE: A2= 4.24mm

REFLECTED WAVE:
AR= 0.30mm; ALPHA=-1.565Rads

FREE SECOND HARMONIC WAVE:
A22= 0.88mm; L22= 284.2mm; BETA= 0.959Rads

DIMENSIONLESS PARAMETERS:
KCI= 5.07 ; KA=0.214 ; KH=2.785

LINEAR FORCES:
FD= 96.099coswt + 19.2198cos3wt +-2.74568cos5wt mN
FI=-367.212sinwt mN

STOKES SECOND ORDER FORCES:
FD2= 0.1538 + 0.4307cos2wt + 0.1670cos4wt mN
FI2= -1.8242sin2wt mN

DYNAMIC PRESSURE FORCE:
FDP=-10.3182sin2wt mN

WATERLINE FORCES:
FWD= 19.8786 + 23.8544cos2wt + 3.40777cos4wt mN
FWI=-39.5922sin2wt mN

FORCES DUE TO REFLECTED WAVE:
FDR= -0.0093coswt + -0.7604sinwt + -0.0019cos3wt
+ -0.4562sin3wt mN
FIR= -2.9055coswt + 0.0177sinwt mN

FORCES DUE TO FREE SECOND HARMONIC WAVE:
FD22= 0.4882 + 1.3669cos2wt + 2.2266sin2wt
+ 0.53003cos4wt + 0.63618sin4wt mN
FI22= 6.9222cos2wt + -4.8566sin2wt mN

(fig. 3.25)

Clearly the estimate of wave loading will be considerably in error in each case if the non-linear effects are not taken into account. In Figures 3.22 and 3.23, the wave conditions are a long, shallow water, wave with a considerable degree of reflection and a substantial free second harmonic wave. The non-linear effects are therefore dominated by the forces due to the reflected and free waves.

The conditions in Figures 3.24 and 3.25 are a short steep wave in effectively deep water. The reflection coefficient is small and there is very little free wave activity. Thus the major non-linear effects are the waterline and dynamic pressure forces.

3.4.4 Application to Design

In the design of a structure for offshore applications, the wave environment at the proposed location is assumed to be described by a design wave, with given amplitude, period and water depth. Under such conditions of a single regular wave train, the linear forces on a vertical cylinder are given by Morison's equation, FI and FD. The non linear force components consist of the waterline forces FWI and FWD, the dynamic pressure force FDP, and the second order Stokes' wave forces, FD2 and FI2. Under design conditions the wave flume effects of the reflected and free second harmonic waves, and hence the forces due to them, will be absent.

The effect of the non linear forces on the wave loading on a vertical cylinder under design conditions is demonstrated in

Figures 3.26 to 3.29. The non linear inertia forces are all sin $2\omega t$ components, while the non linear drag forces are both predominantly cos $2\omega t$. Thus the second order forces add together to produce a large effect on the force traces.

For the shorter waves, Figures 3.26 and 3.27, the non linear loading is dominated by the waterline and dynamic pressure forces. As the waves become longer and the water relatively shallower, Figures 3.28 and 3.29, the second order Stokes' forces become more significant.

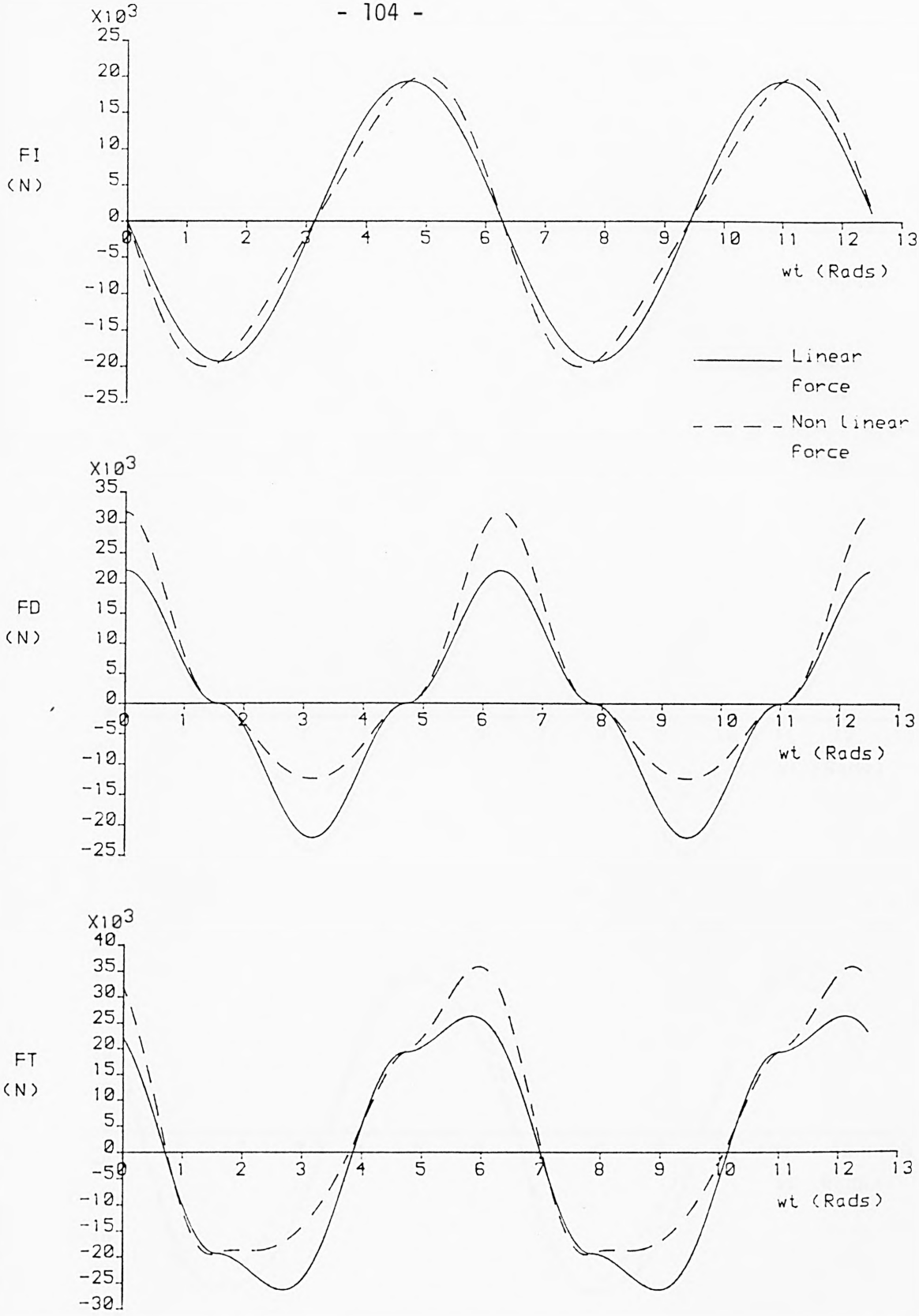

DESIGN FORCES ON .60m CYLINDER; CM= 2.0; CD= 1.2

WAVE CONDITIONS: h= 50.0m; T= 8.0Sec; WL= 99.56m; Wave Amp= 3.50m

DIMENSIONLESS PARAMETERS: KC= 18.81; ka= .221; kh= 3.155

NON LINEAR DESIGN FORCES

Figure 3.26

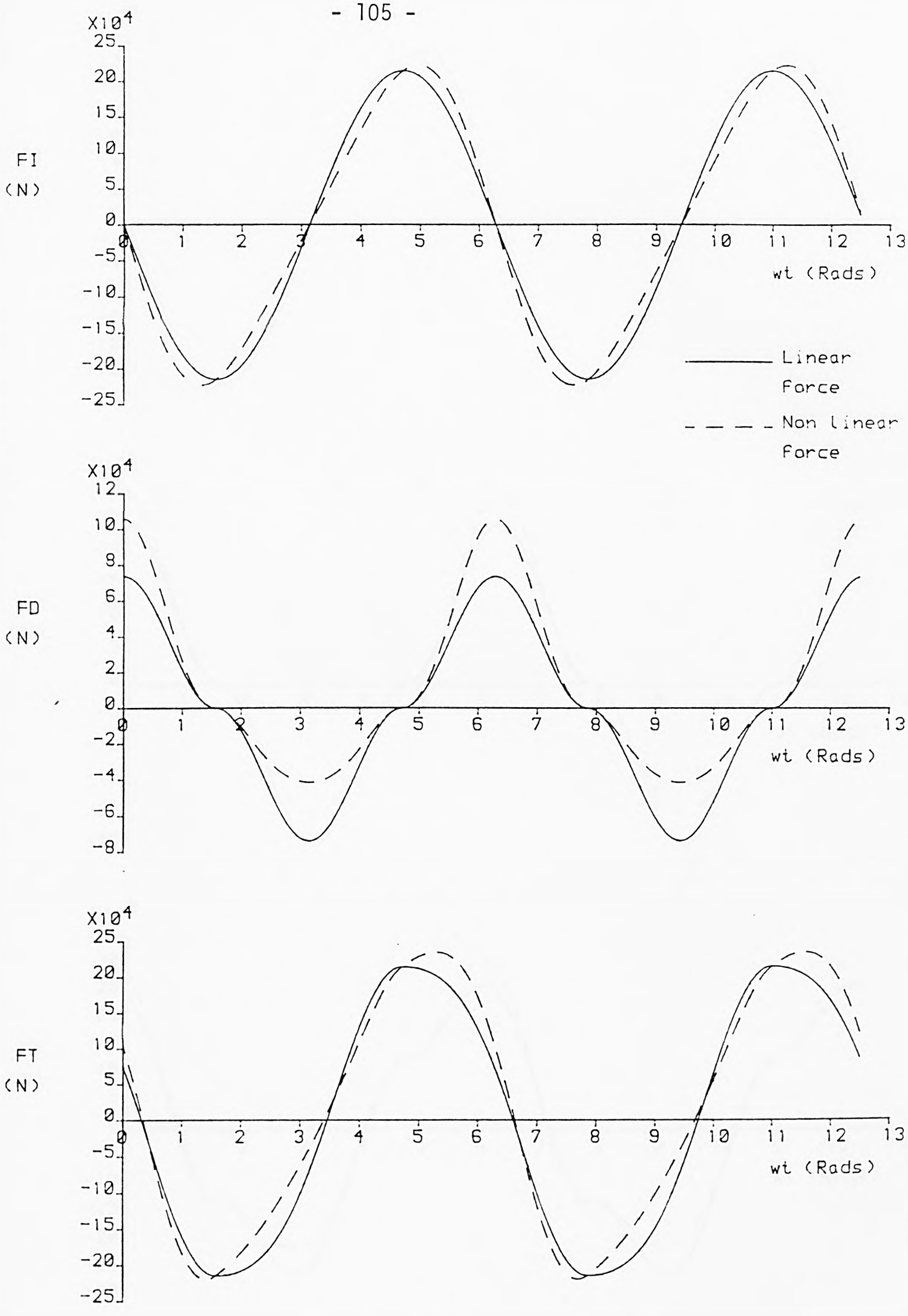

DESIGN FORCES ON 2.00m CYLINDER; CM= 2.0; CD= 1.2

WAVE CONDITIONS: h= 50.0m; T= 8.0Sec; WL= 99.56m; Wave Amp= 3.50m

DIMENSIONLESS PARAMETERS: KC= 5.64; ka= .221; kh= 3.155

NON LINEAR DESIGN FORCES

Figure 3·27

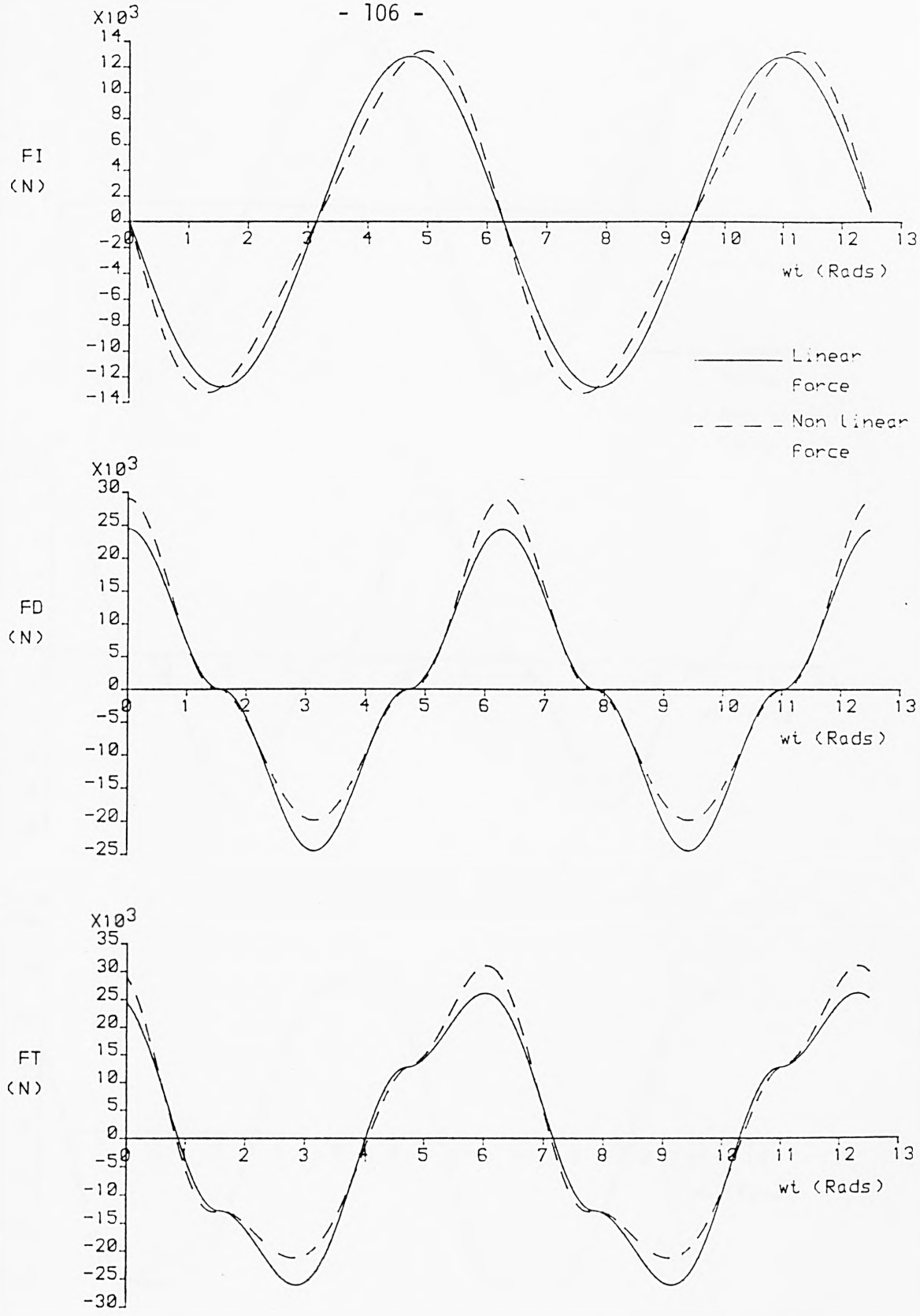

DESIGN FORCES ON .60m CYLINDER; CM= 2.0; CD= 1.2

WAVE CONDITIONS: h= 50.0m; T= 16.0Sec; WL= 307.81m; Wave Amp= 3.00m

DIMENSIONLESS PARAMETERS: KC= 31.40; ka= .061; kh= 1.021

NON LINEAR DESIGN FORCES

Figure 3.28

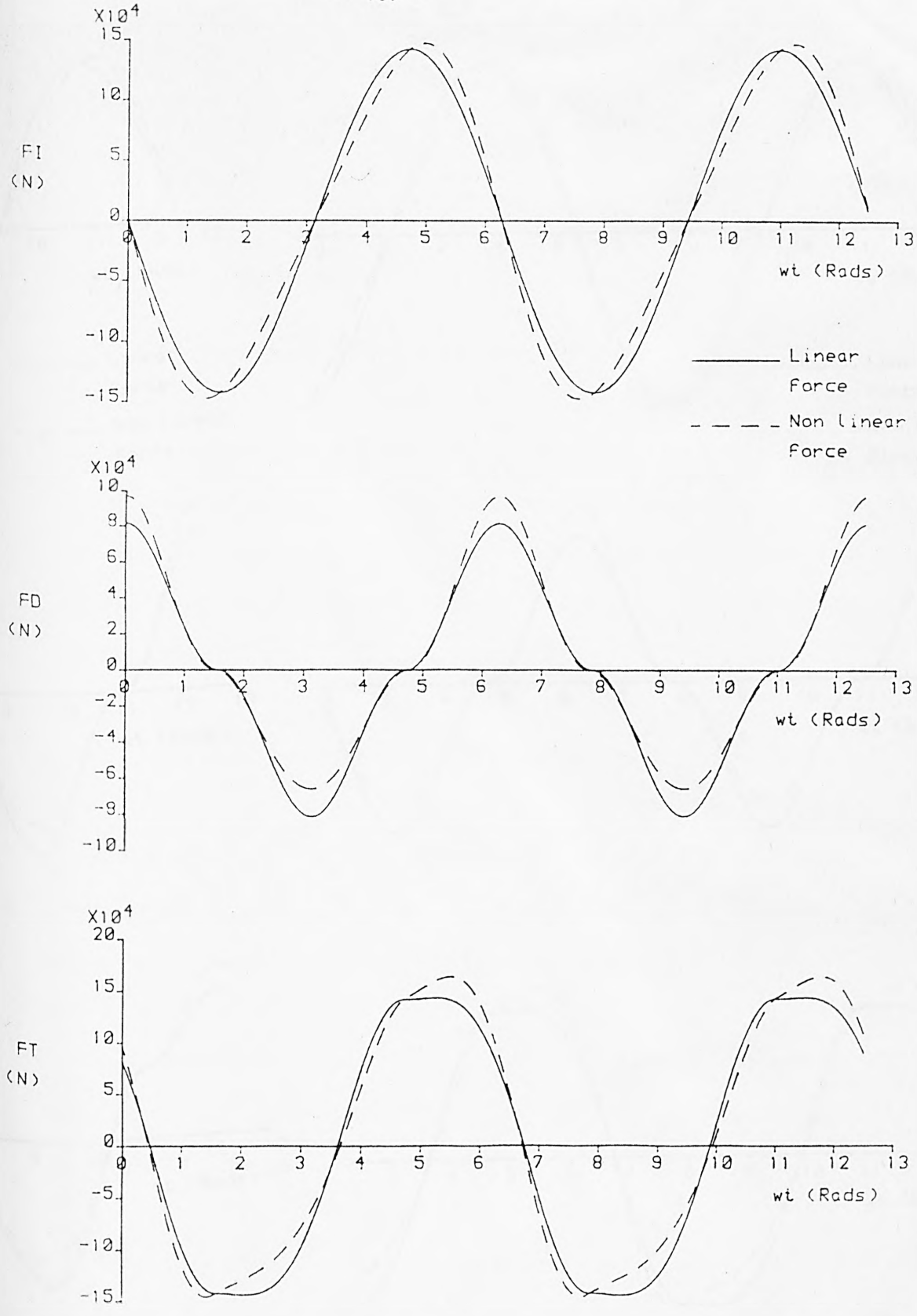

DESIGN FORCES ON 2.00m CYLINDER; CM= 2.0; CD= 1.2

WAVE CONDITIONS: h= 50.0m; T= 16.0Sec; WL= 307.91m; Wave Amp= 3.00m

DIMENSIONLESS PARAMETERS: KC= 9.42; ka= .061; kh= 1.021

NON LINEAR DESIGN FORCES

Figure 3.29

CHAPTER 4 - EXPERIMENTAL INVESTIGATION

4.1 Introduction

The purpose of the experimentation was to investigate the non-linear wave induced loading on vertical cylinders, having a range of diameters and under a range of wave conditions. The Fourier Transform of the total force on the cylinder, and the depths of action of the force components, were determined, allowing the second order loading predictions put forward by Lighthill (1979) to be tested.

A major problem with the experimental programme was found to arise from the laboratory wave flume itself. Ideally, such experiments should be carried out under conditions of a single regular wave train travelling in the positive x-direction. In practice, however, the wave environment produced, even with the wavemaker oscillating at a single frequency, was found to include significant free second harmonic and reflected waves. Clearly, in considering the total wave loading on the cylinder, the forces due to these additional waves must be accounted for.

The experimental programme was, therefore, split into two distinct sections. The first requirement was to analyse the wave environment in the flume in order to identify and evaluate all of the waves present. The second section of the experimentation was to record the forces induced on a number of vertical cylinders under these known wave conditions.

In correlating the measured waves and forces, it was assumed that the velocity distribution could be obtained directly from the wave profile, by means of velocity potential theory. Second order Stokes' theory was used for the primary wave, while the free second harmonic and reflected waves were assumed to satisfy small amplitude linear wave theory. No direction measurement of the velocities under the wave was made.

4.2 Experimental Apparatus

4.2.1 Wave Flume

The experiments were carried out in a glass-sided flume 750 mm wide and approximately 20 metres long. The water was at a constant depth of 500 mm throughout the testing, as shown in Figure 4.1.

Waves were generated by means of a wedge oscillating vertically in the surface of the water, and driven by a variable speed motor, via an eccentric mounting. The mounting converted the rotation of the motor into a purely sinusoidal motion of the wedge. At its mean position the wedge had a submerged depth of 300 mm and had a d/b ratio of 1.6. The motion of the water in the region behind the wedge was suppressed by a sheet of plywood floating in the surface; of which the lateral motion was restrained by vertical guides.

At the far end of the flume there was a beach, designed to absorb as much as possible of the incident wave energy, and

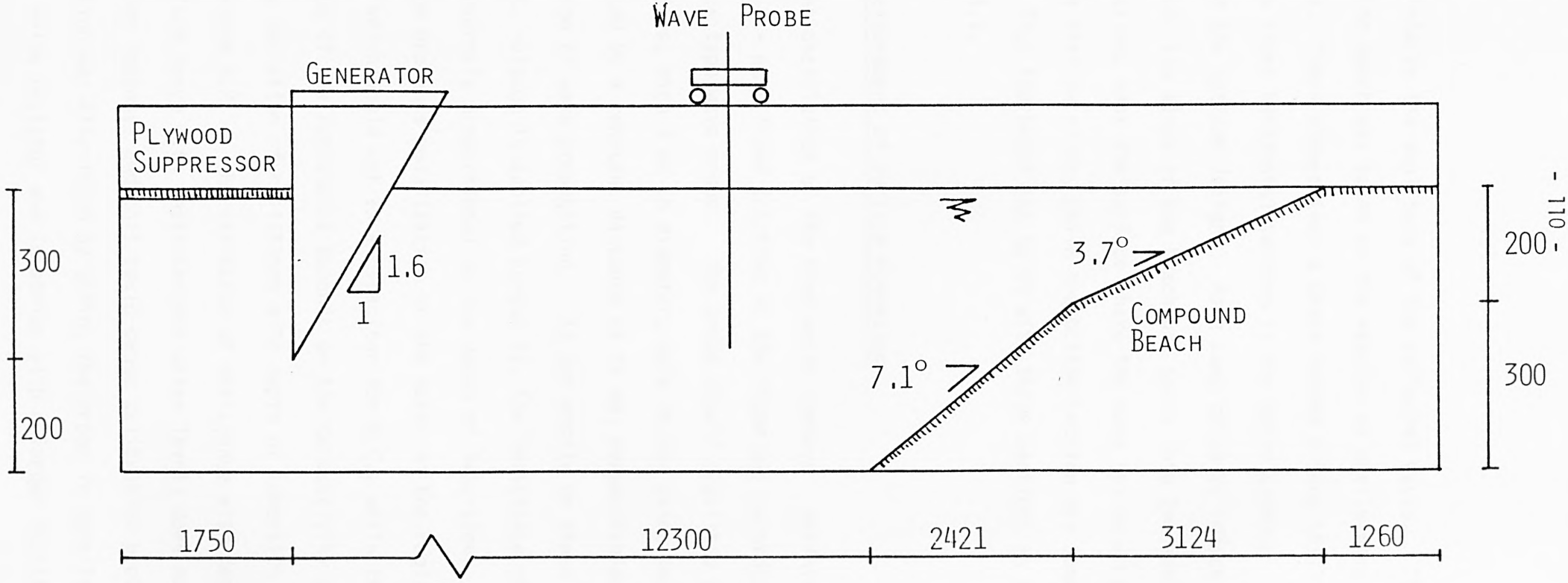

WAVE FLUME LAYOUT

Figure 4.1

hence to minimize the amplitude of the reflected waves. The layout of the beach was based on the results of preliminary experiments. These showed that a beach having a long shallow slope and a short horizontal section in the water surface represented the optimum design. As a compromise to reduce its total length, the slope of the beach was split into two sections. The top section, near the surface where the wave action was greatest, was given a shallow slope, while the bottom section was somewhat steeper. Thus the beach was built with three sections as shown in Figure 4.1.

4.2.2 Measurement of surface elevation

The oscillation of the free water surface - defining the wave profile - at a fixed location in the flume was recorded using a resistance type wave probe. The probe itself consisted of two vertical wires, each 3 mm in diameter, held in the water surface and separated by a constant distance of 25 mm, perpendicular to the direction of wave propagation. It can easily be shown that, when an A.C. voltage is applied across it, the resistance of the probe is inversely proportional to the depth of immersion. The A.C. voltage prevents polarization of the water in the region of the probe, which would act as a capacitor for D.C., while the actual value of the resistance depends on the conductivity of the water. The variation of resistance with depth of immersion is shown in Figure 4.2. The variation of resistance with depth of immersion (and hence with instantaneous water level) does not give a linear response and this could cause calibration problems. This situation was alleviated by wiring the probe in parallel with a low value resistor and in series with a larger resistor.

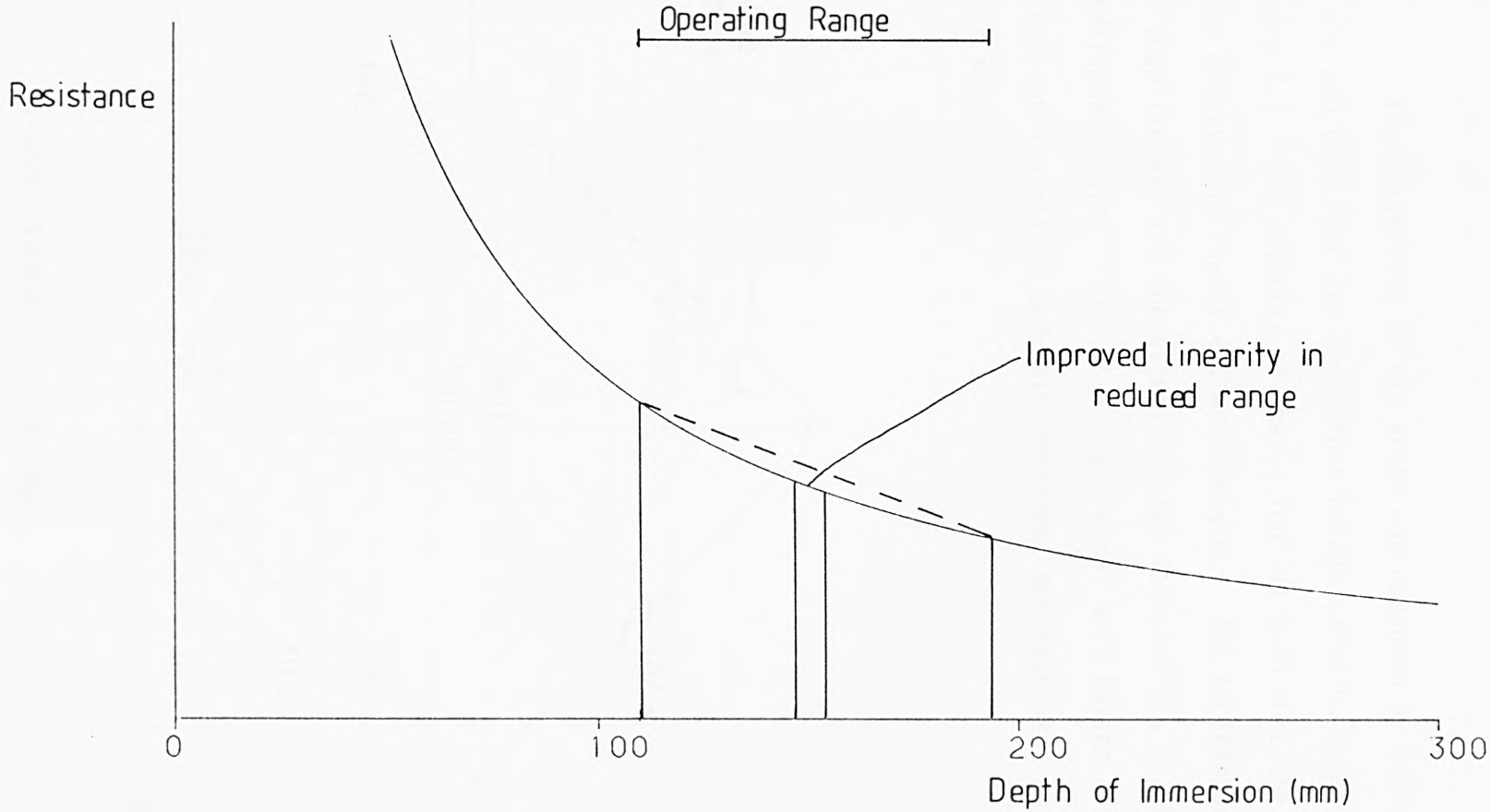

Wave Probe Resistance

Figure 4.2

This had the effect of reducing the change in resistance for a given change in depth, and greatly enhanced the linearity as shown in Figure 4.2.

The resistance of the probe was measured by wiring it up as one arm of a four arm Wheatstone bridge circuit, as shown in Figure 4.3. The polarity of the wiring was such that the negative slope observed in Figure 4.2 was removed. The excitation voltage was supplied by, and the signal voltage detected by, an SE995 bridge conditioning unit. This is a six-channel unit having a range of bridge configurations and gain settings, and excellent gain and phase response.

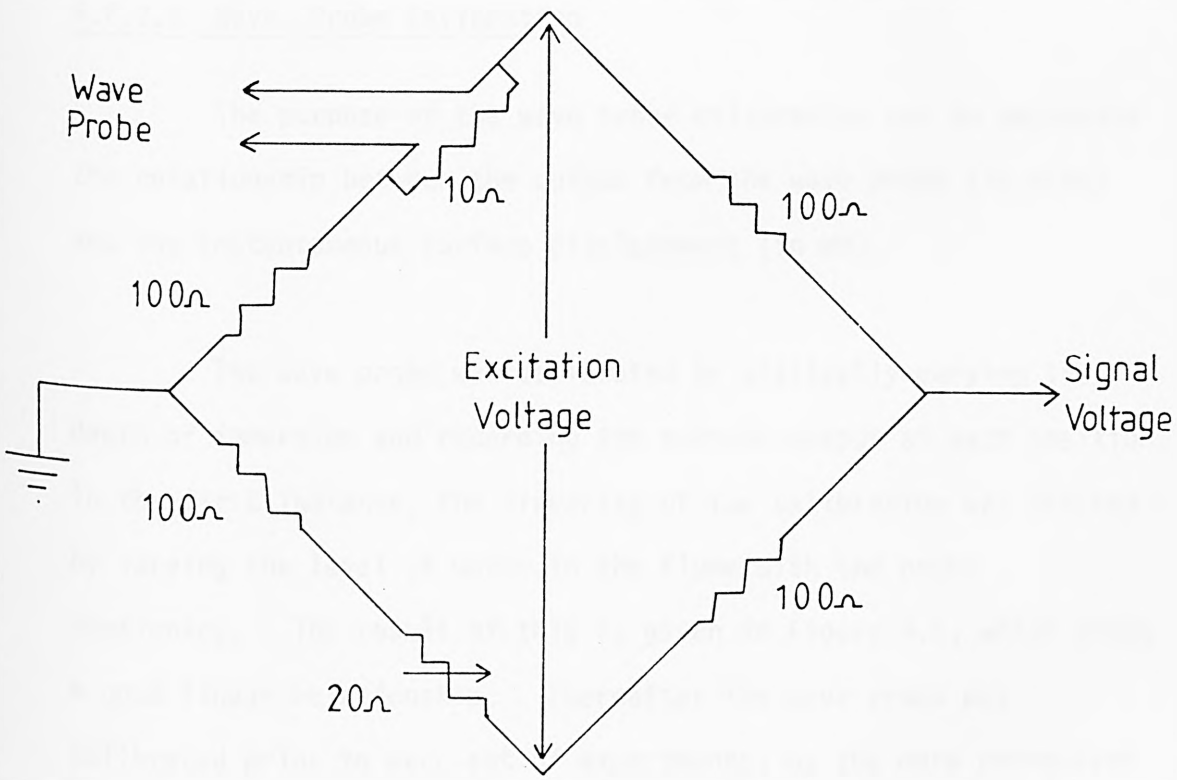

4-arm Wheatstone Bridge

Figure 4.3

The method of data collection is now considered. The fluctuating voltage outputs from the SE995 channels were monitored by a high speed scanner module coupled to a PDP-11 mini-computer. The scanner performed an analogue to digital conversion of the signal voltages, which could then be scanned at regular intervals, the data being written in binary form to a diskfile. The scanner had a range of sensitivities, or coarse gain settings, which could be selected to suit the signal strength. The data was then converted to decimal form to give numerical values in 'bits' proportional to the signal voltages. The appropriate calibration factors were applied to these records to give values of free surface displacement in mm (or force in mN as appropriate). The flow diagram for data collection is shown in Figure 4.4.

4.2.2.1 Wave Probe Calibration

The purpose of the wave probe calibration was to determine the relationship between the output from the wave probe (in bits) and the instantaneous surface displacement (in mm).

The wave probe was calibrated by statically varying its depth of immersion and recording the scanner output at each position. In the first instance, the linearity of the calibration was checked by varying the level of water in the flume with the probe stationary. The result of this is given in Figure 4.5, which shows a good linear relationship. Thereafter the wave probe was calibrated prior to each set of experiments, by the more convenient procedure of raising and lowering the probe through still water. A calibration constant was determined in each case by a linear

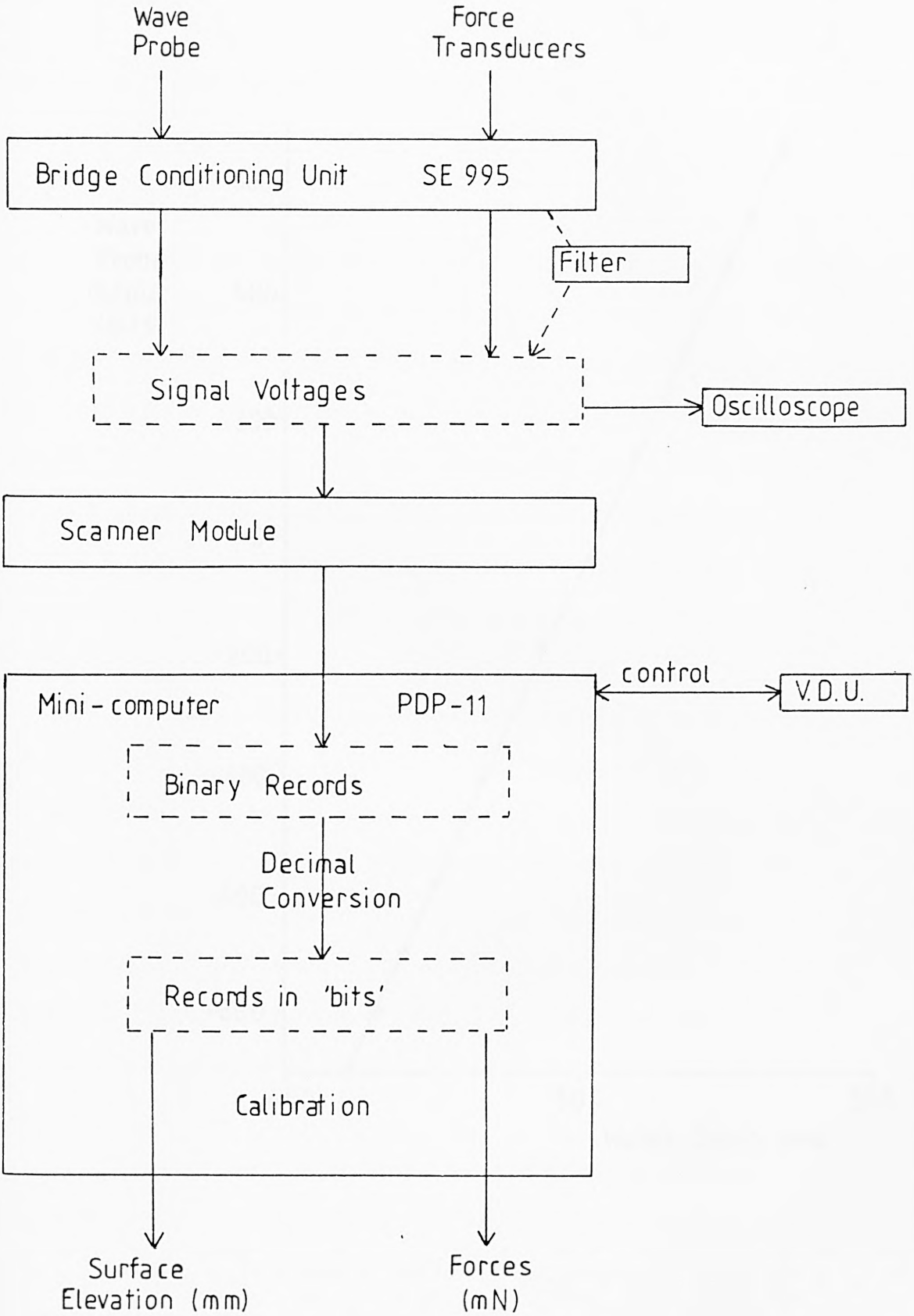

Collection of Data

Figure 4.4

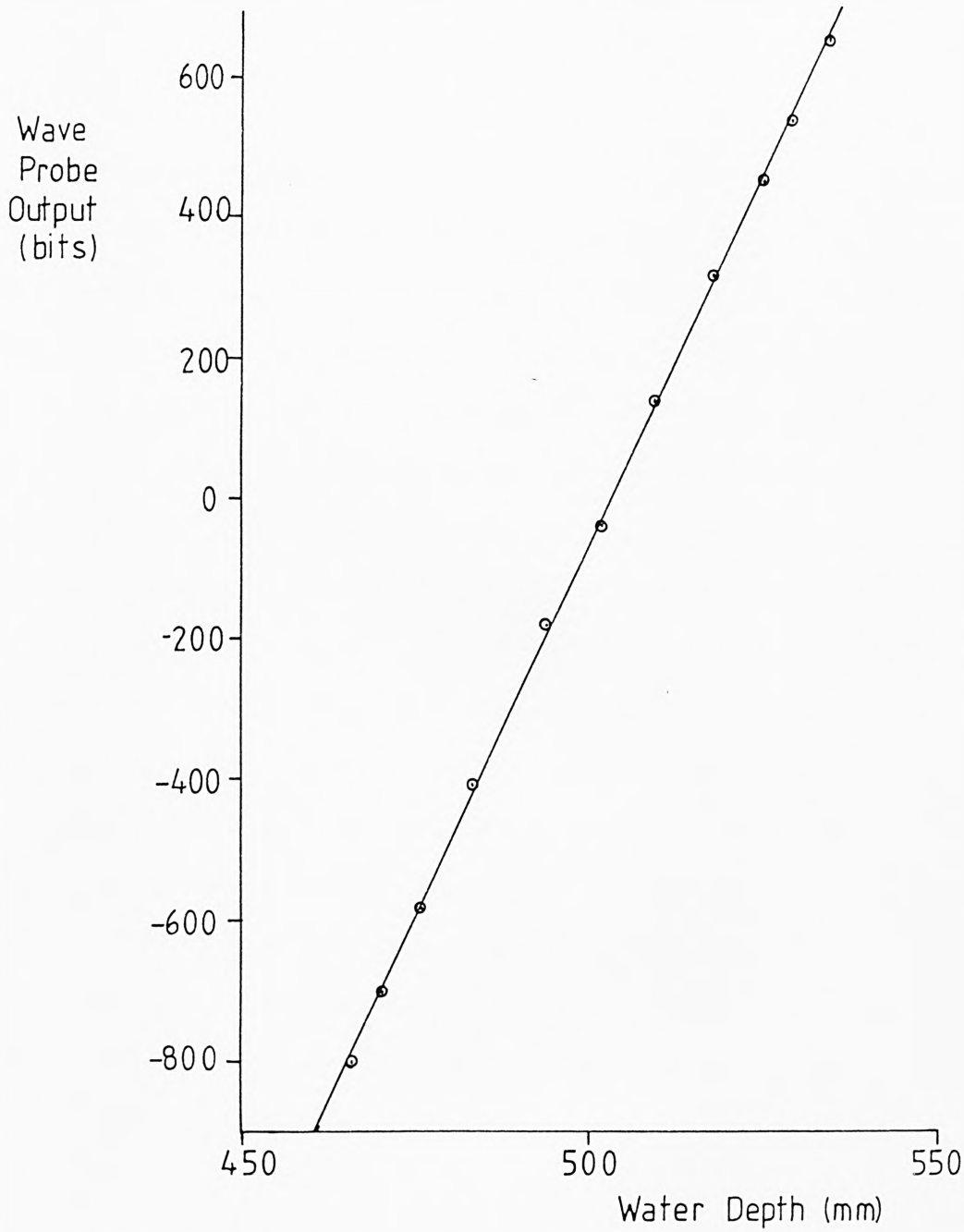

Wave Probe Calibration

Figure 4.5

regression fit to the calibration data points.

4.2.3 Test Cylinders

As previously stated, the object of the experiments was to measure the forces induced by wave action on vertical cylinders. A rig was designed and constructed which would hold the cylinder in place and detect the forces on it. Initial calculations showed that, because of the small scale of the testing, the total force on the cylinder would be very small. This meant that the technique, adopted for example by Chakrabarti (1980), of measuring the force on short test sections of the cylinder would be impractical.

As it was a requirement that not only the force components, but also their resultant depths of action, should be measured, it was decided to hold the cylinder in a simply-supported manner and record the top and bottom end reactions. In order that the rig would be adaptable for the various cylinder diameters, it was designed to hold a thin brass rod between two pin-joints. This rod acted as a central core, over which P.V.C. sleeves of appropriate outside diameters could be fixed.

The final design of the cylinder fixing rig is shown in Figure 4.6. Held in this manner the test cylinder would extend from a point above the highest wave crest to a point as close as possible to the bottom of the flume.

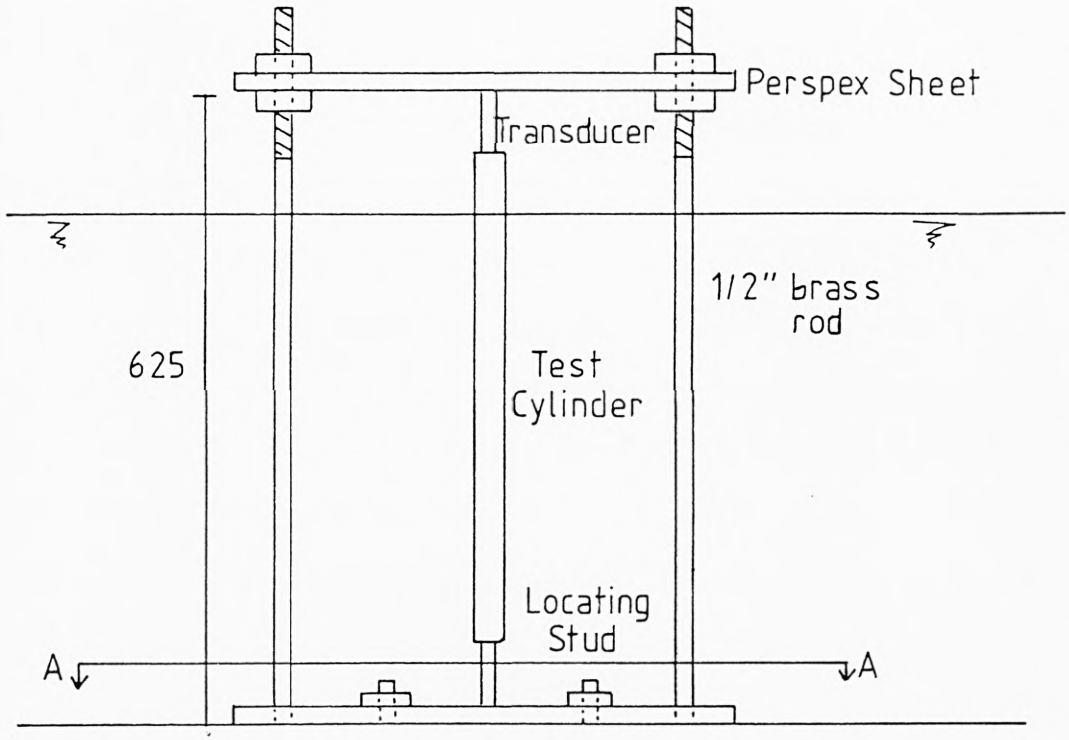

Side Elevation

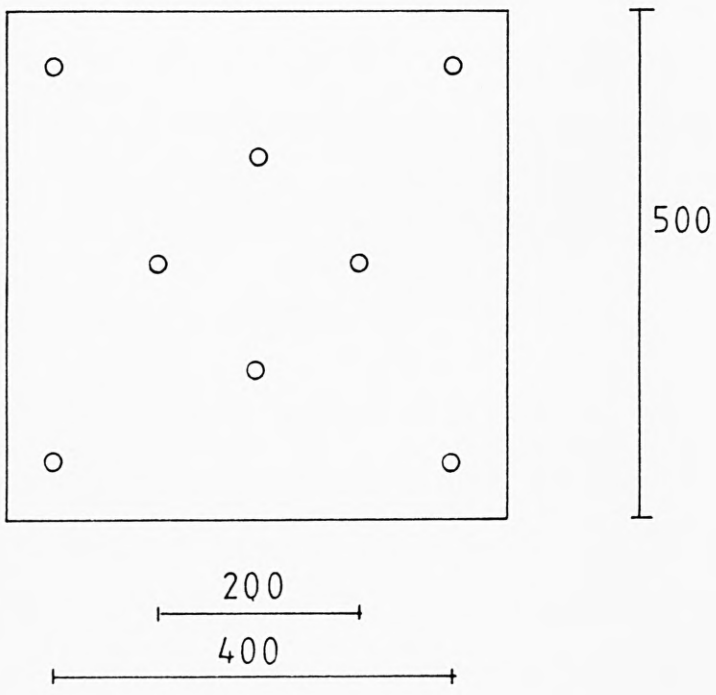

Section A-A

Test Cylinder Fixing Rig

Figure 4.6

4.2.4 Measurement of Forces

Preliminary calculations carried out showed that the maximum force exerted on the test cylinder would be between 10 and 100 mN, depending on its diameter and on the wave conditions. Highly sensitive force measuring equipment was therefore required.

No force transducers of the required sensitivity were found to be commercially available, and it was therefore necessary to design and construct suitable transducers. This design is shown in Figure 4.7.

The end reaction, passed through the pin joint, was detected as a bending strain in the short cantilever length of the force transducer. By using Kyowa semi-conductor strain gauges with their large gauge factors, it was possible, by utilizing the gain of SE995 and sensitivity of the scanner, to produce a measurable signal for even the smallest loading case.

4.2.4.1 Force Transducer Calibration

The purpose of the force transducer calibration was to establish a relationship between the outputs from the two transducers and the resultant force on the cylinder together with its depth of action. The calibration procedure needed to give information, not only about the sensitivities of the two strain gauge pairs, but also about the behaviour of the pin joints.

If the joints could be assumed to behave as perfect pins, that is that they were frictionless and passed no bending moment, the

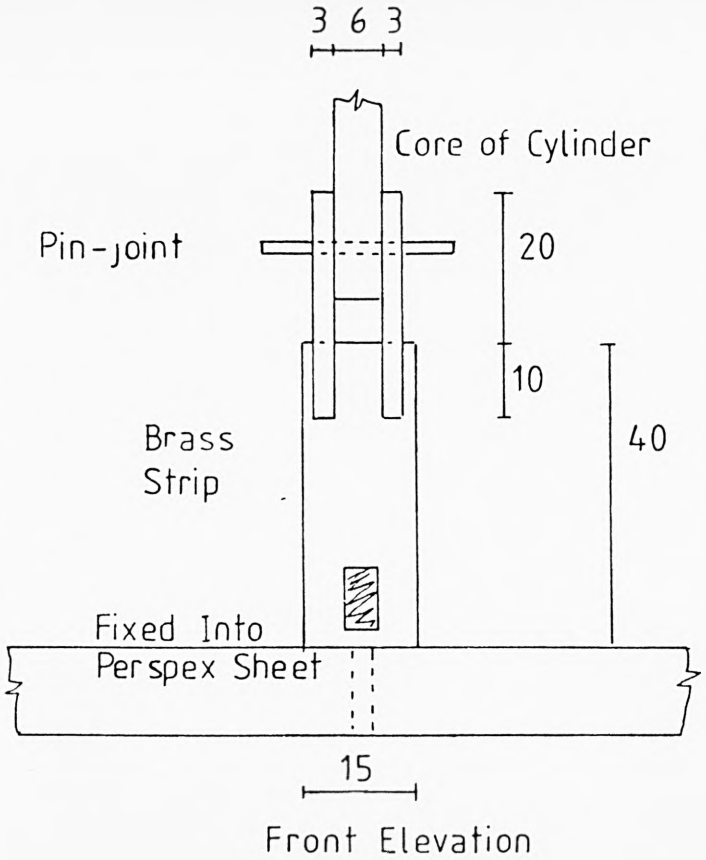

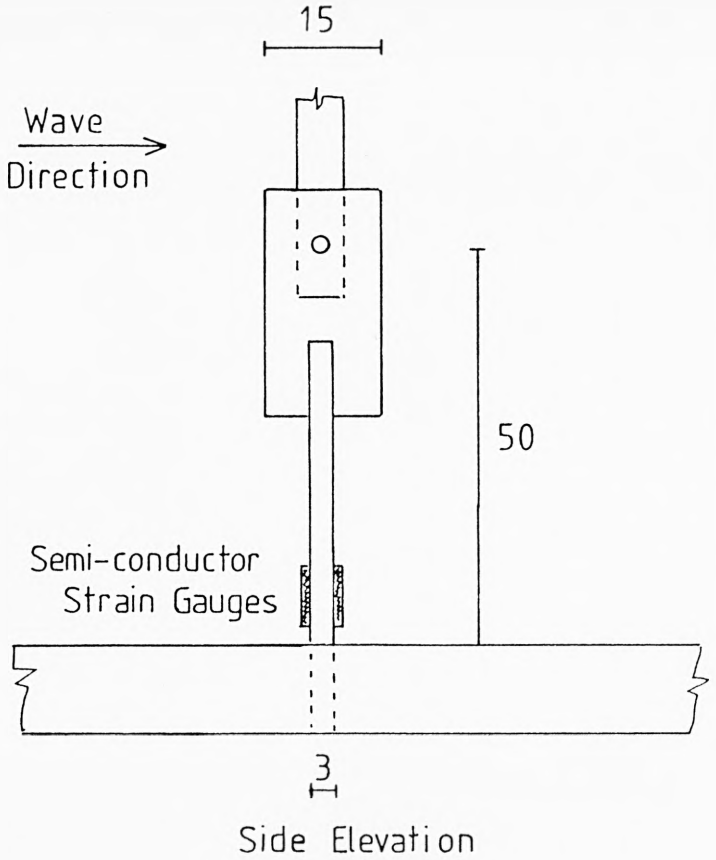

Force Transducer Design

Figure 4.7

cylinder would be truly simply-supported. Conversely, any friction in the joints would introduce a degree of fixity into the cylinder arrangement. The most obvious way of detecting any fixity in the pin joints was to consider the influence lines of the force transducer outputs. The influence lines represent the variation in the sensitivities of the transducers to loads applied at different positions between the two pin joints. Calibration was therefore carried out by applying loads at a number of positions on the cylinder as shown in Figure 4.8. This was carried out with the cylinder rig fixed out of the water prior to each set of experiments.

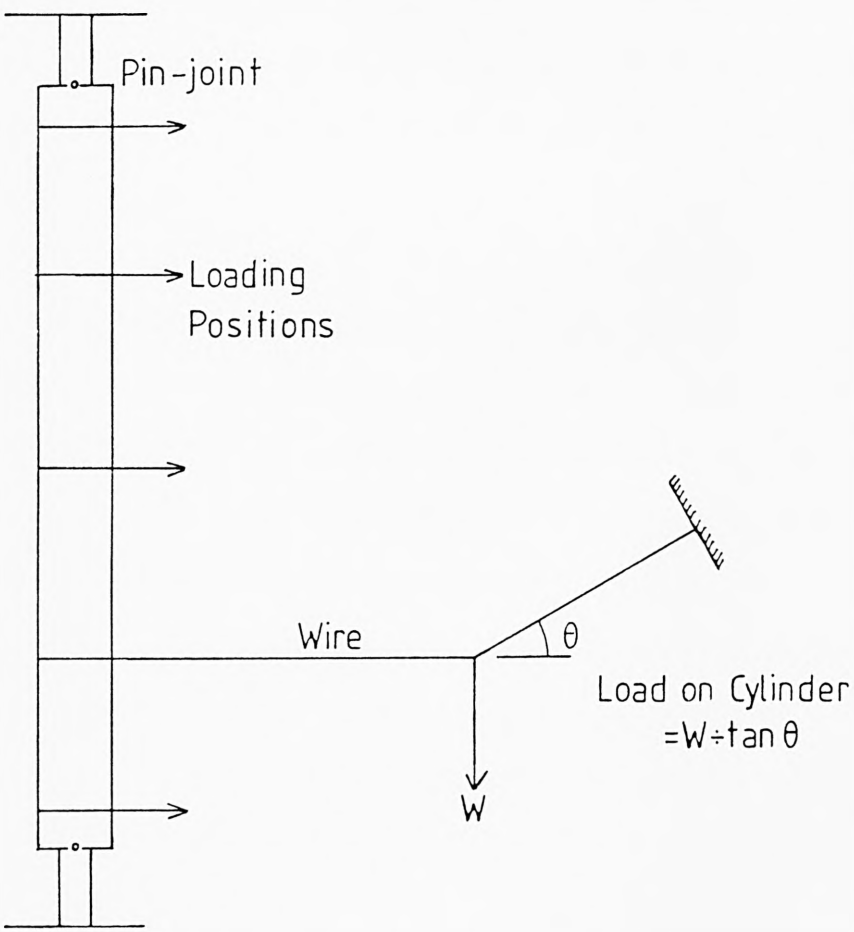

Force Transducer Calibration Arrangment

Figure 4.8

At each loading position the procedure was to apply varying loads to the cylinder and record the output from the two transducers. The three wire, triangle of forces, arrangement for applying the loads was used, because the loads were too small to allow the use of pulleys. A problem with the force transducer arrangement observed at this time was that of instrumental drift. The balance position of the transducer output was found to vary considerably with time, a problem attributable to the very high sensitivity of the equipment. To overcome this problem the effect of each load on the transducer was found by recording the output before the load was applied, with the load applied and after it had been removed, and taking the average difference. The sensitivity of each transducer to loads applied at each position was then evaluated by a linear regression fit to the observed readings.

The variation of sensitivity, in bits/mN, with depth of action, (measured down from the top pin joint) in mm, defined the influence line for each transducer. The equations of the influence lines were found by a least squares cubic fit as shown in Figure 4.9. A cubic fit was chosen because the equation of the influence line for a fixed ended beam is of that order, while that for a simply-supported beam is linear. From the shape of the influence lines in Figure 4.9 it is clear that the cylinder was predominantly simply-supported, but that some fixity was present.

With the influence lines defined, any pair of readings from the top and bottom transducers would give two equations, which could then be solved for the resultant force and its depth of action.

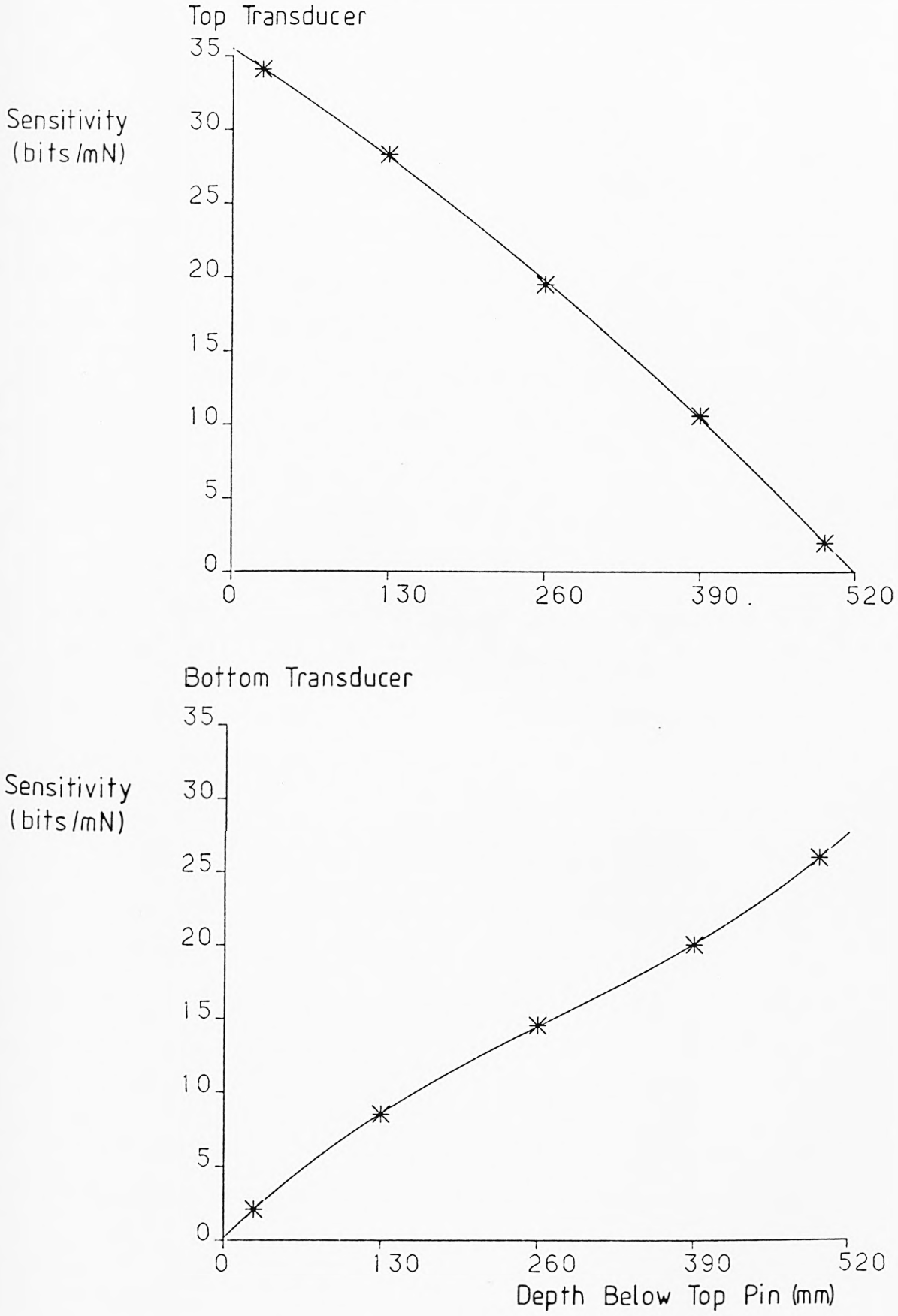

Force Transducer Calibration - Influence Lines

Figure 4.9

4.2.4.2 Filtering of Force Transducer Output

In a number of the experiments carried out, the force transducer output was found to include a high level of noise. This was a combination of 'bounce' of the cylinder at its natural frequency, and mains noise at 50 Hz. It was therefore necessary to introduce an electronic filter into the output which would pass the signal, but not the relatively high frequency noise.

The circuit diagram of the filter is shown in Figure 4.10. The first stage is a simple 10 times amplifier, while the second two stages are a fourth order low-pass filter. The components in the filter stages were chosen for a cut-off frequency of 10 Hz and for optimum linear gain and phase response. Two filter channels were constructed, one for each force transducer.

The variations with frequency of the gain and phase delay of the filter were determined by a series of experiments comparing input and output signals. Although both channels were nominally identical, wide tolerances in the electronic components meant that each had to be tested separately.

The gain results are shown in Figure 4.11. There was some difference between the two channels, but both showed an approximately linear fall to 96% of the D.C. gain at 4 Hz, and a rapid fall off in the gain beyond 7 or 8 Hz.

The phase results are shown in Figure 4.12. Both channels had linear phase reponses up to approximately 4 Hz. This implied

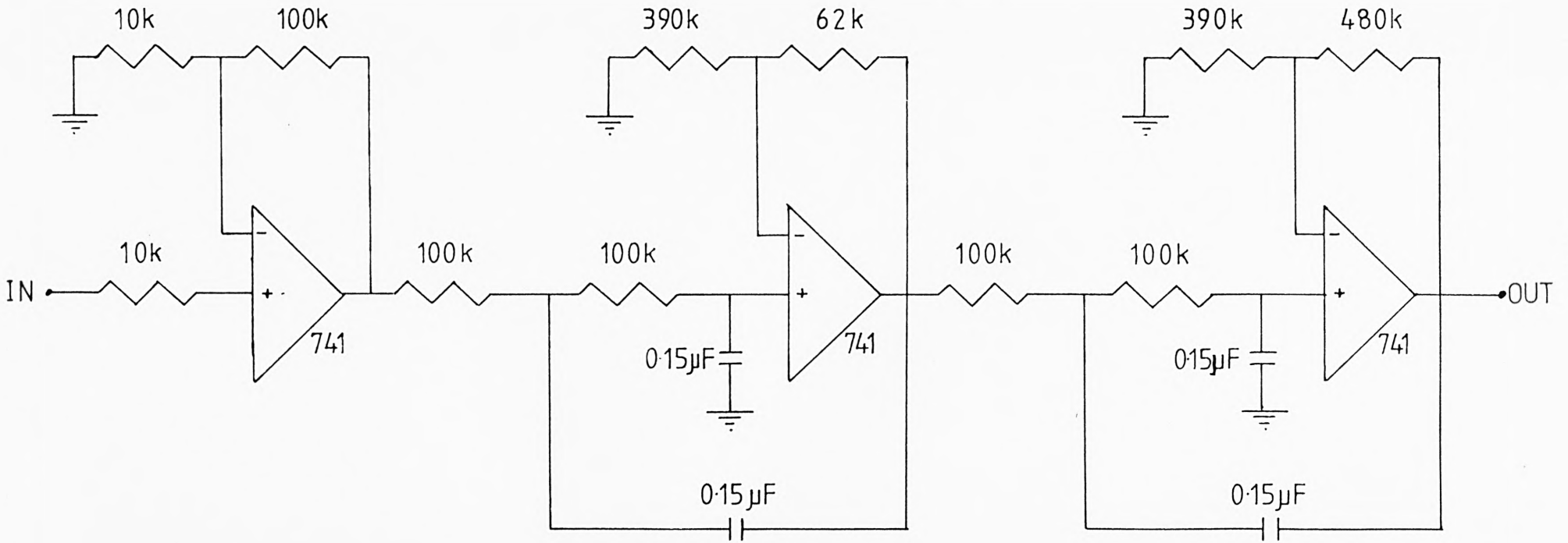

Fourth Order Lo-Pass Filter

Figure 4·10

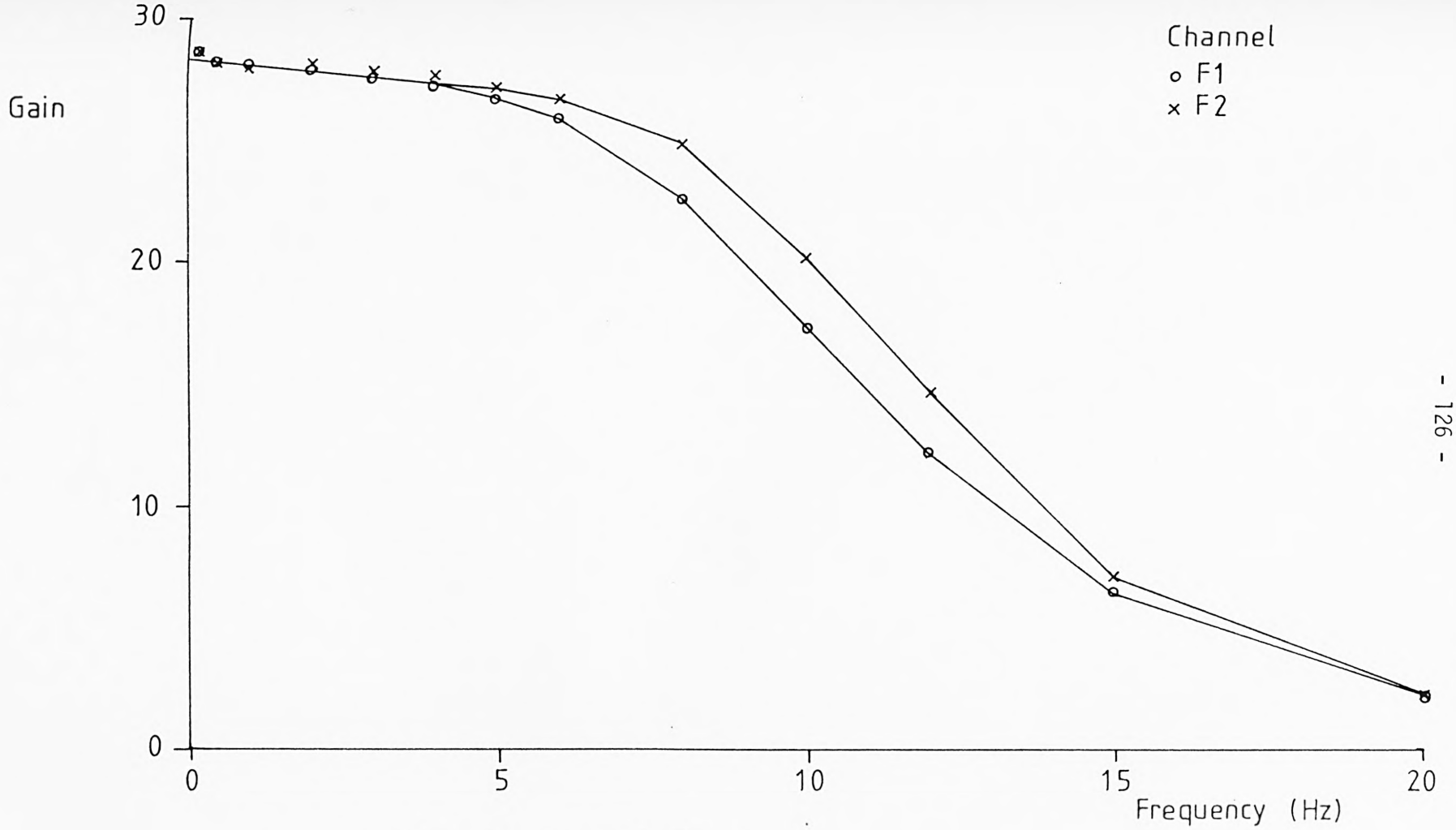

Gain Response of Filter

Figure 4.11

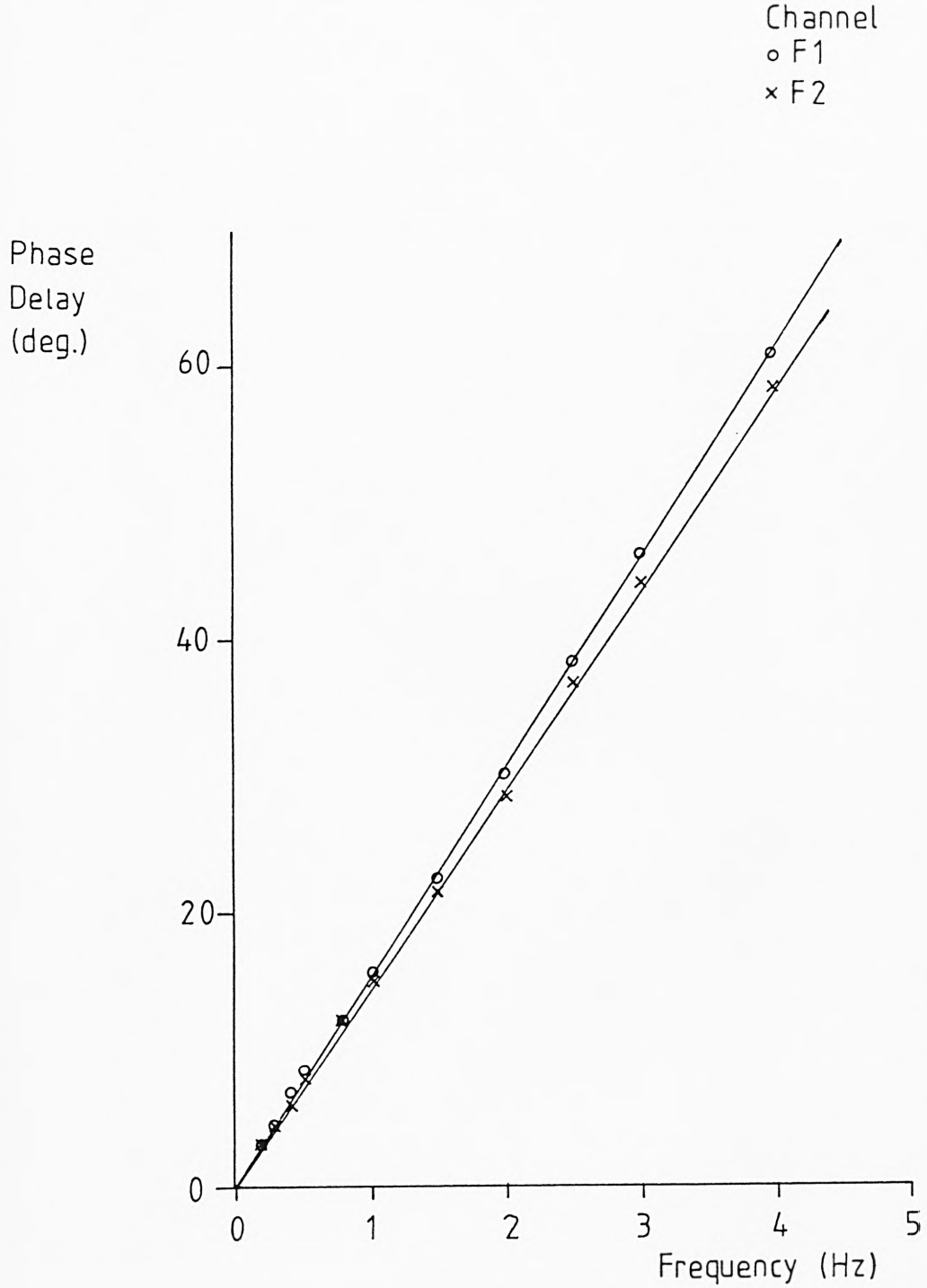

Phase Response of Filter

Figure 4.12

a constant time delay of 0.042 seconds for channel F1 and 0.040 seconds for channel F2.

The effect of the filter on the transducer output is demonstrated in the oscillograph traces in Figure 4.13. The signal to noise ratio was vastly improved, while the small time delay can be seen by comparing the phases of the two traces.

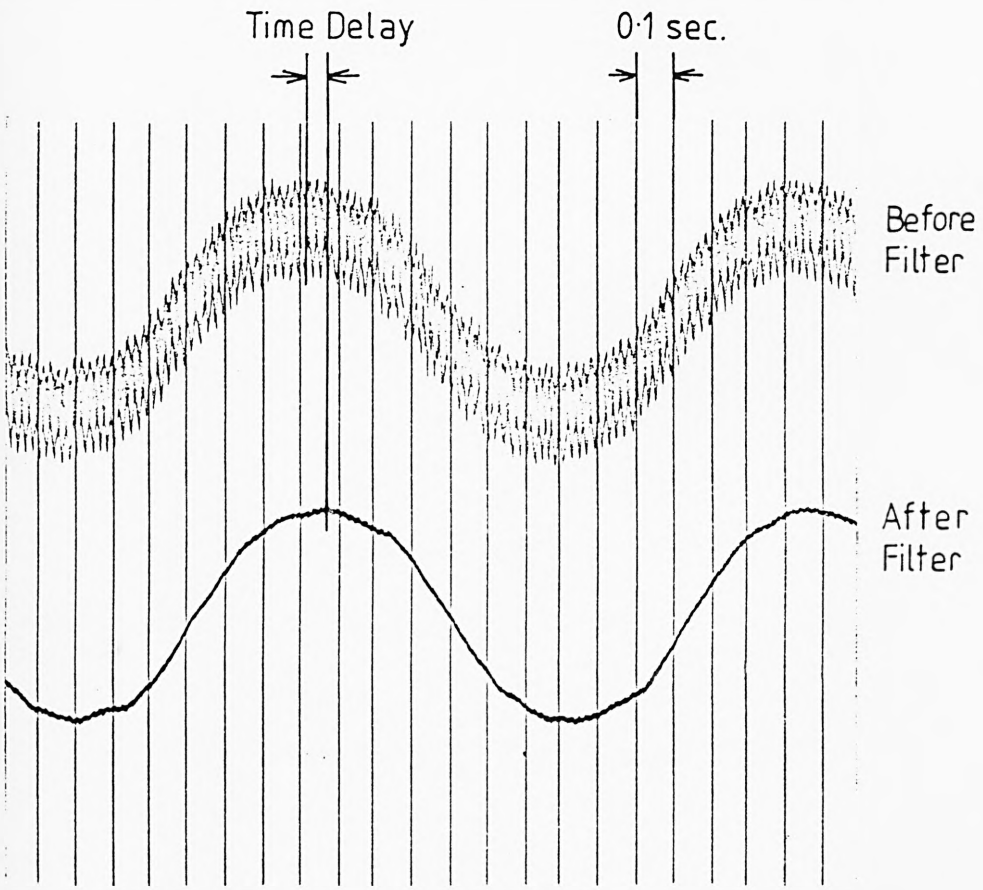

Effect of Filter on Force Transducer Output

Figure 4·13

4.3 Waveform Experiments

A technique has been developed for identifying and evaluating the waves present in a laboratory flume, by observing the change in the shape of the wave, or waveform, as it travels down the flume. The technique and the results of the experimentation have been presented in a paper by the writer, Ellix and Arumugam (1984).

4.3.1 Waveform Analysis

In analysing the total wave motion in the flume, to the second order of approximation, there are several wave components which must be considered. The incident wave, travelling in the positive x-direction away from the generator, comprises a second order Stokes wave travelling without change of shape, together with a free second harmonic wave:

$$\eta = a_I \cos(kx - \omega t) + a_2 \cos 2(kx - \omega t) + a_{22} \cos(k_{22}x - 2\omega t + \beta) \qquad (4\text{-}1)$$

The reflected wave, returning from the beach, has components at both the fundamental and second harmonic frequencies:

$$\eta_R = a_R \cos(kx + \omega t + \alpha) + a_{22R} \cos(k_{22}x + 2\omega t + \gamma) \qquad (4\text{-}2)$$

The shape of the waveform at any position in the flume depends on the magnitudes of the individual components and on their relative phases at that position. The analysis of the waveform variation down the flume is carried out by consideration of the

first and second order wave components separately.

4.3.1.1 First Order Components

The first order wave motion consists of the fundamental frequency incident and reflected waves,

$$\eta_1 = a_I\cos(kx - \omega t) + a_R\cos(kx + \omega t + \alpha) \qquad (4\text{-}3)$$

In considering only the shape of the waveform at a single position, x, the time base can be arbitrarily set such that an incident wave crest passes at t equals zero.

Thus,

$$(kx - \omega t) = 0 \quad \text{at } t = 0$$

Then,

$$\eta_1 = a_I\cos\omega t + a_R\cos(\omega t + 2kx + \alpha)$$

$$= (a_I + a_R\cos(2kx + \alpha))\cos\omega t - a_R\sin(2kx + \alpha)\sin\omega t$$

$$= A_1\cos(\omega t - \delta) \qquad (4\text{-}4)$$

where $A = \sqrt{(a_I + a_R\cos(2kx + \alpha))^2 + (a_R\sin(2kx + \alpha))^2}$

= amplitude of first order wave motion

and $\delta = \tan^{-1}\left(\dfrac{-a_R\sin(2kx + \alpha)}{a_I + a_R\cos(2kx + \alpha)}\right)$

= phase angle by which the incident wave peak leads the total wave peak.

For the purpose of the waveform experimentation, two non-rigorous simplifying assumptions are made, which can be shown to be reasonable as long as $a_I^2 >> a_R^2$. The first assumption is that the second term in A_1 is negligible, and the second is that δ is zero for all values of x. Thus equation (4-4) reduces to:

$$\eta_1 = (a_I + a_R\cos(2kx + \alpha))\cos\omega t$$

Thus if the envelope of first order amplitude down the flume is considered, it would consist of a mean value of a_I, plus a sinusoidal variation having an amplitude of a_R and a wavelength of L_R, equal to L/2. This represents the beating effect between two waves travelling with equal and opposite velocities.

The angle α is the phase difference between the incident and reflected first order waves at the origin of x. The origin of x may be located, for example, at the wave generator, or as will be convenient for the force experiments, at the centre line of the test cylinder.

4.3.1.2 Second Order Components

The second order wave motion comprises the second order Stokes component and the incident and reflected free second harmonic waves.

$$\eta_2 = a_2\cos2(kx - \omega t) + a_{22}\cos(k_{22}x - 2\omega t + \beta) + a_{22R}\cos(k_{22}x + 2\omega t + \gamma) \qquad (4\text{-}5)$$

To maintain compatibility between the first and second order terms, the same time base must be used as described above. Then,

$$\eta_2 = [\, a_2 + a_{22}\cos(k_B x + \beta) + a_{22R}\cos(k_{2R} x + \gamma)]\cos 2\omega t$$
$$+ [\, a_{22}\sin(k_B x + \beta) - a_{22R}\sin(k_{2R} x + \gamma)]\sin 2\omega t \qquad (4\text{-}6)$$

where

$$k_B = k_{22} - 2k$$

$$k_{2R} = k_{22} + 2k$$

From equation (4-6) it is clear that, to evaluate the unknown second order wave parameters, it is necessary to consider the second harmonic component of the wave in two parts; that which is in-phase with the fundamental component - the $\cos 2\omega t$ term -, and that which is in quadrature - the $\sin 2\omega t$ term.

The in-phase second harmonic amplitude envelope has a mean value of a_2 plus a sinusoidal variation having an amplitude of a_{22} and a wavelength of $L_B = 2\pi/k_B$. This represents the beating effect between two waves travelling in the same direction at different speeds.

The quadrature envelope has a similar beating pattern, but has a zero mean and its sinusoidal variation lags that in the in-phase envelope by $L_B/4$.

Both envelopes include an additional term due to beating

between the incident and reflected second order waves. In both cases this variation has an amplitude of a_{22R} and a wavelength of $L_{2R} = 2\pi/k_{2R}$.

4.3.2 Experimental Procedure

The technique entailed the observation of the waveform shape at a number of discrete locations along the centre line of the flume. From these discrete data points, the pattern of waveform variation down the flume could be identified.

The selection of observation locations varied with the wave conditions. They were always in the central portion of the flume, approximately half way between the generator and the beach. The total spread of the points was set to cover at least one and a quarter of the longest beat wavelenghts (L_B), while their spacing was such that there would be at least four points to every one of the shortest beat wavelengths (L_{2R}). Thus, for each wave setting an average 20 locations were used, separated by between 50 and 200 mm.

With the wave probe at each location in turn, a record was taken of the waveform over a number of cycles. These records were then calibrated and analysed using a Fast Fourier Transform, described in Appendix 1, to give the magnitudes of the fundamental, second harmonic in-phase and second harmonic quadrature wave components, in mm, at the respective positions in the flume. This procedure was carried out twice at each location to give some measure of the variability of the waveform. The result of each

waveform run was, therefore, a tabulation of the three Fourier components of the wave against the position in the flume. An example is shown in Table 4.1. X in this case is measured on a tape running backwards up the flume with zero at the beach.

4.3.2.1 Range of Testing

A limitation on the wave frequencies which could be used was imposed by a combination of the Fast Fourier Transform, and the available scanning rates on the PDP-11. To operate efficiently, the F.F.T. requires a power of 2 number of data points covering an exact whole number of cycles, while the PDP-11 could only have multiples of 0.02 seconds as the delay time between successive scans. In order that a good range of frequencies could be covered, and that the F.F.T. should have sufficient points to give a reliable result, it was decided to take 128 points with a delay time of 0.08 seconds. This gave a total sample time of 10.24 seconds, and meant that only those frequencies having a whole number of cycles in that time could be used. Thus the fundamental wave frequencies covered in the experiments were; 0.586, 0.684, 0.781, 0.879, 0.977, 1.074 and 1.172 Hz.

The frequency of the wavemaker was adjusted by means of a variator coupled to the motor gearing, and was 'tuned in' by monitoring the output from a wave probe on a Gould TC22 Time Counter. With some care, it was possible to achieve the desired periods, and hence frequencies, to within 0.2%.

The other variable parameter was the amplitude of the

wave motion, and this was governed by the amplitude of the wedge oscillations. The wedge amplitude was set by changing the eccentricity of its mounting onto the motor. To cover a range of wave steepnesses, wedge amplitudes of between 20 and 70 mm, in steps of 10 mm, were used at each frequency. A few of the largest waves were found to be unstable, while a few of the smaller ones were too small to measure. These wave conditions were therefore omitted from the study, but a good range between long, shallow water waves and short, steep, deep water waves was covered.

4.3.3 Analysis of Data

The results of the form of Table 4.1 were analysed by considering separately the variations of A1, A2 and B2 with X. Each variation was analysed using the least squares sine fitting routine described in Appendix 2. One sine component was fitted to A1 against x and two were fitted to each of A2 and B2 against x. The axis of x was modified to run forwards up the flume with its origin at the wavemaker. As well as the numerical coefficients of the sine fitting, the results were presented graphically as shown in Figure 4.14.

The amplitudes of the various incident and reflected wave components, together with the beat wavelengths, were determined from the sine fitting results. An example is demonstrated in Figure 4.14.

WAVEFORM VARIATION: WEDGE AMP. 50.0MM; FREQ. 0.586HZ
WATER DEPTH 500.0MM; WAVELENGTH 3350.0MM

X(M)	A1(MM)	A2(MM)	B2(MM)
12.000	14.06	1.05	1.24
12.000	14.07	1.06	1.27
11.800	14.22	0.26	1.19
11.800	14.21	0.24	1.18
11.600	14.58	-0.18	1.36
11.600	14.60	-0.15	1.40
11.400	14.96	-0.29	0.91
11.400	14.98	-0.29	0.92
11.200	15.15	-0.78	0.19
11.200	15.14	-0.72	0.19
11.000	15.01	-0.99	-0.08
11.000	15.00	-1.00	-0.13
10.800	14.69	-0.52	-0.44
10.800	14.69	-0.50	-0.42
10.600	14.27	-0.21	-1.14
10.600	14.27	-0.18	-1.14
10.400	13.97	-0.20	-1.37
10.400	13.97	-0.12	-1.39
10.200	14.00	0.45	-1.19
10.200	14.03	0.42	-1.15
10.000	14.41	1.03	-1.45
10.000	14.42	1.04	-1.47
9.800	14.85	1.19	-1.41
9.800	14.89	1.20	-1.43
9.600	15.05	1.50	-0.65
9.600	15.07	1.50	-0.68
9.400	15.00	2.14	-0.26
9.400	14.99	2.13	-0.30
9.200	14.62	2.02	0.02
9.200	14.62	2.02	-0.01
9.000	14.13	1.61	0.75
9.000	14.15	1.63	0.75
8.800	13.88	1.66	1.26
8.800	13.90	1.69	1.27
8.600	13.93	1.38	1.06
8.600	13.95	1.40	1.04
8.400	14.26	0.62	1.27
8.400	14.21	0.59	1.27
8.200	14.72	0.32	1.58
8.200	14.74	0.36	1.62
8.000	15.05	0.03	1.19
8.000	15.07	0.07	1.18
7.800	15.11	-0.71	0.65
7.800	15.10	-0.76	0.62
7.600	14.86	-1.05	0.43
7.600	14.89	-1.04	0.40
7.400	14.55	-0.67	-0.07
7.400	14.51	-0.67	-0.12

Table 4.1 Waveform Variation

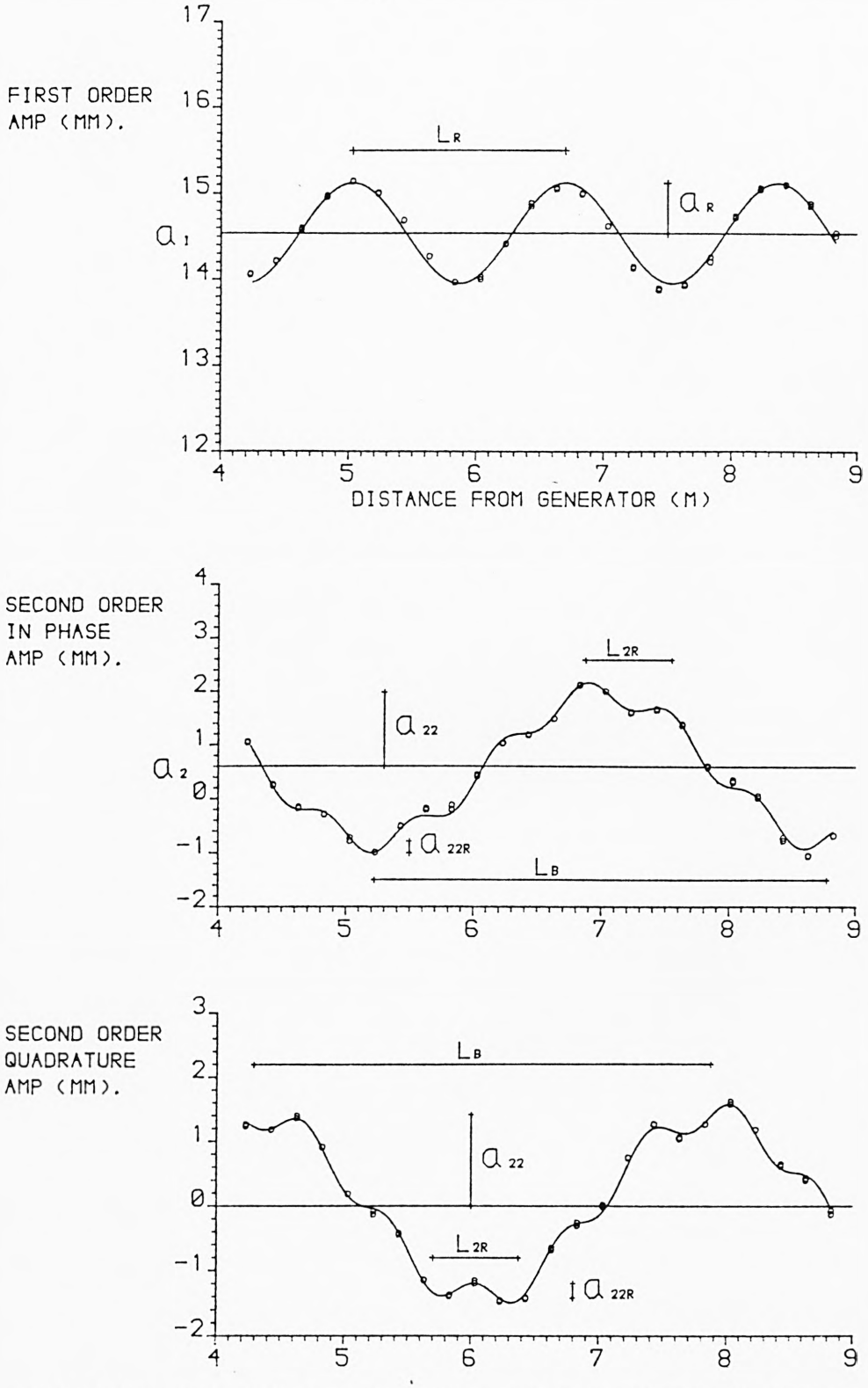

WAVEFORM VARIATION: WEDGE AMP. 50.0MM; FREQ. 0.586HZ

WATER DEPTH 500.0MM; WAVELENGTH 3350.0MM

Analysis of Waveform Variation

Figure 4.14

4.4 Wave Loading Experiments

4.4.1 Wave Environment

The importance of quantifying the wave environment when carrying out any wave loading experiments has been demonstrated in Chapter 3. The effect of the reflected and free second harmonic waves was shown to depend not only on their magnitudes, but also on their phases relative to the primary wave. As a result of this it was necessary to measure the wave activity in the flume at the same time as recording the forces on the test cylinders.

The waveform results showed that the reflected free second harmonic wave was negligible in comparison to the total wave motion, (see Chapter 5 and Ellix and Arumugam, 1984) and this was therefore not considered in the loading experiments.

4.4.2 Experimental Procedure

To determine the wave environment, it was necessary to carry out a waveform experimental run for each cylinder and wave condition combination. With the cylinder in place, a waveform run was performed centred on the cylinder and covering suitable upstream and downstream lengths. The presence of the fixing rig restricted the wave probe to positions greater than 300 mm away from the cylinder, with the exception of a single location in line with it. For the higher frequency shorter waves, this left a significant gap in the waveform data.

Three sets of records were taken of the forces on the

cylinder; before, in the middle of, and after, the waveform run. The output from a wave probe in line with the cylinder, as well as those from the top and bottom force transducers, was recorded. As with the waveform experiments the sample time was set at 10.24 seconds with 128 data points.

The F.F.T. was used to compute the uncalibrated Fourier components of the top and bottom force transducer outputs. The first, second and third harmonic, in phase and quadrature components were calculated for each transducer. The transforms were evaluated with their phases relative to the total first order wave motion, as recorded by the in-line wave probe.

Instrumental drift of the force transducer output continued to be a problem throughout the testing. Frequent rebalancing of the bridge conditioning unit was necessary, and as a result the time-averaged force on the cylinder could not be measured. Analysis of the loading results had to depend on the fluctuating components of the forces.

4.4.2.1 Range of Experiments

The wave force experiments were carried out over a similar range of wave conditions as the waveform experiments. A total of fifteen wave settings were used to cover all of the frequencies and a range of wave steepnesses.

The cylinder diameters were chosen to cover a range of loading conditions in the drag and inertia regime, as governed by the

Keulegan-Carpenter number KCI. The smallest cylinder diameter for which the forces were measurable, was 9.55 mm. The loading on this cylinder was drag dominated for most wave conditions, though the inertia force was always significant. Two other cylinders of diameters 21.45 and 33.56 mm were also used, to give a range of KCI between 2.0 and 20.0.

4.4.3 Analysis of Data

4.4.3.1 Waveform Data

The results of the waveform runs with the cylinder in place were analysed as described in Section 4.3.3. The amplitudes of the waves a_I, a_R and a_{22} were computed, and with the origin of x positioned at the cylinder centre line, the calculated angles of α and β represented the phases of the waves at the cylinder position. In those cases where the gap in the data caused by the cylinder fixing rig was a problem, it was necessary to constrain the range of values of k in the sine fitting routine in order to produce a sensible fit.

Thus the wave environment around the cylinder was determined, including all significant components to the second order of approximation.

4.4.3.2 Corrections to Force Transforms

A number of corrections had to be made to the Fourier Transforms of the force transducer outputs to make them compatible

with the wave data. These are considered below in the order in which they were applied.

(i) Correction for Filter.

In those cases where the transducer outputs were passed through the filter, they were subjected to the gain and phase delay of its circuits. The force transducer calibrations had been carried out with the filter in line, but since this was a static procedure, the gain of the filter corresponded to its D.C. value as shown in Figure 4.11. Each of the components of the force transforms, acting at its appropriate frequency was subject to a gain somewhat less than the D.C. value. It was therefore necessary to multiply all of the components by a factor equal to the ratio of the D.C. gain to the gain at that frequency.

The filter channels also introduced a time delay into the force transducer outputs, giving a phase change that varied with frequency as shown in Figure 4.12. To account for this phase delay it was necessary to adjust the relative magnitudes of the in-phase and quadrature components of the transforms at each frequency. This constituted a simple trigonometrical adjustment.

(ii) Correction for Force on Bottom Force Transducer

The bottom force transducer, though small and positioned near the flume bottom, was subject to a measurable force caused by water motion in that region. To eliminate this effect from the force readings, a series of experiments were carried out with no cylinder in the rig, so that the forces imposed on the bottom transducer could be measured. The Fourier Transform of the bottom transducer

output for each of these tests gave values of the force components, which were then deducted from the respective transforms in the wave loading experiments. Only forces at the fundamental frequency were found to be significant.

(iii) Correction for Phase of Wave Motion

As stated in Section 4.4.1, the transforms were calculated with their phases relative to the total first order wave motion. It was desirable, however, that they should be relative to the incident first order wave. The phases of the transforms were therefore adjusted by an angle δ, as defined under equation (4-4) and calculated at the cylinder position. Again this was a simple trigonometrical adjustment of the relative magnitudes of the in-phase and quadrature components at each frequency.

4.4.3.3 Resultant Force Components

The corrected transforms of the force transducer outputs were used to determine the resultant force components acting on the cylinder. Each Fourier component - first, second and third order, in-phase and quadrature - was considered separately. The respective components of the top and bottom transforms were taken as pairs of readings, which, in conjunction with the calibration influence line coefficients, gave pairs of equations in the force components and their depths of action.

Solution of these equations gave a total of six force components acting on the cylinder, together with their respective points of action.

4.5 Estimation of Experimental Error

A measure of the reliability of the experimental results is found by considering the probable magnitude of the experimental error. Three broad areas of possible error existed in this testing - errors in the wave setting, errors in the measurement of the wave and errors in the measurement of the forces.

Errors in the wave setting would be relatively unimportant, provided that all the features of the wave were being measured. Since only the wave profile was measured, it is worth considering the effect of these errors. The water depth was measured by means of a scale on the glass side of the flume, and could be recorded to within $\pm$ 1 mm or 0.2%. The significance of the water depth came in the evaluation of tanh kh. For the shorter waves, small changes in water depth had no effect whatever on tanh kh, while for the longest waves used, this variability in depth led to an uncertainty in tanh kh of only $\pm$ 0.1%.

The small uncertainty in the wave frequency discussed previously can be shown to have no measurable effect on the components of the wave and force Fourier Transforms. A more significant error was probable, however, in the measurement of the wedge amplitude. This was read directly from a tape fixed to the motor mounting, and could only be read to $\pm$ 1 mm. Thus the typical uncertainty in the wedge amplitude was $\pm$ 3%, leading to a lack of repeatability in the wave settings, and necessitating a separate waveform run on every test.

Any errors in the measurement of the wave profile would result from uncertainty in the calibration of the wave probe. The justification for a linear calibration is demonstrated in Figure 4.5. In raising and lowering the wave probe through the water surface, its position was measured at each point to within $\pm$ 0.5 mm. Such small random errors in the individual points had a limited effect on the calculation of the calibration constant, for which a least squares analysis was used. It is probable therefore that the calibration constants for the wave probe were accurate to within 1%.

Two major sources of error existed in the calibration of the force transducers. The inclination of the tie wire was measured by eye using a protractor, and was correct to $\pm$ 0.5^{o}. This gave an uncertainty in the tangent of the angle, and hence in the force on the cylinder, of $\pm$ 2%. The other source of calibration error was in the position of application of the force on the cylinder's length. The required points of application were marked by lines around the cylinder, but the fixing technique meant that the actual points could be as much as 2 mm away. The uncertainty in the calibration influence lines is therefore reasonably estimated at $\pm$ 3%.

The uncertainties in the wave and force measurements discussed above are realistic estimates of the errors in the first order results. The smaller second and third order results were almost certainly subject to higher relative errors.

CHAPTER 5 - RESULTS AND DISCUSSION

5.1 Waveform Results

The results of the sine fitting analyses of the waveform variations are presented both numerically and graphically in Figures 5.1 to 5.15, for a range of the wave conditions covered. Referring to the graphical results, it is clear that in the majority of cases the fitting of one sine component to the first order variation, and two to each of the second order variations, gives a good fit to the measured data. Random errors in the data points and local peculiarities in the variations, Figures 5.11 and 5.8, cause the fitted sine curves to deviate from some of the individual points, while still giving a good estimation of their variations. These local deviations justify the use of the time consuming technique of taking records of the wave at a number of locations, rather than the more rapid method of Goda and Suzuki (1976), which relies on wave records from just two positions. Under the steepest wave conditions covered in this study, Figure 5.15, the waveform was somewhat unstable, causing scatter in the first order amplitude.

From the numerical results, the amplitudes of the wave components and the beat wavelengths were found as follows. From the first order fit, a_I was the mean value, a_R was the amplitude of the variation, S, and L gave the beat wavelength, L_R. a_2 was given by the mean value in the second order in phase fit. The in phase and quadratic fits gave two estimates for a_{22} and L_B, as the

respective values of S and L. Similarly, two estimates for a_{22R} and L_{2R} were given by the additional terms in the second order fits.

The measured amplitudes of the wave components from all of the waveform experiments are given in Table 5.1.

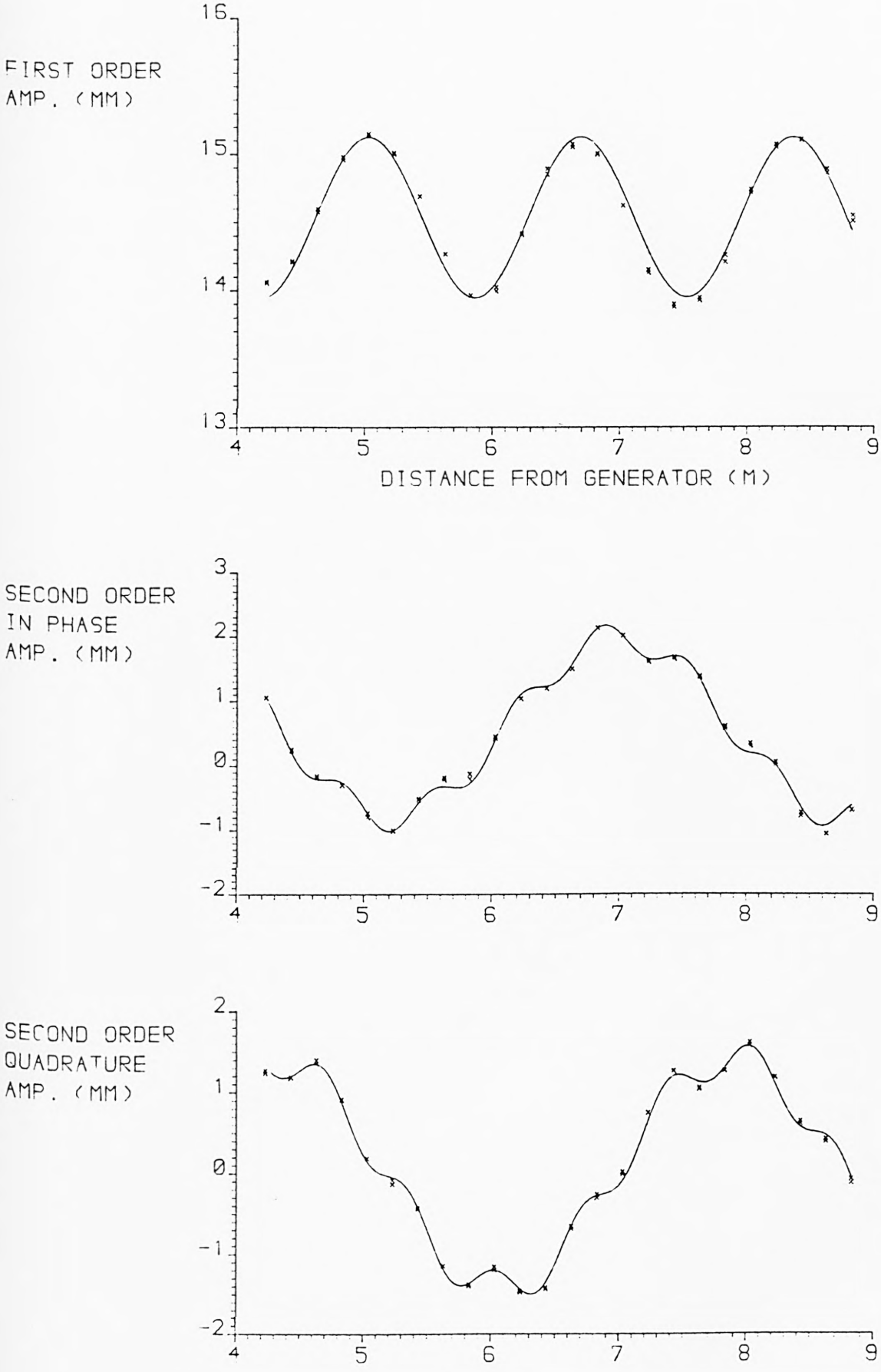

WAVEFORM VARIATION: WEDGE AMP. 50.0MM; FREQ. 0.586HZ
WATER DEPTH 500.0MM; WAVELENGTH 3350.0MM

Figure 5.1

WAVEFORM VARIATION: WEDGE AMP. 50.0MM; FREQ. 0.586HZ
WATER DEPTH 500.0MM; WAVELENGTH 3350.0MM

FIRST ORDER FIT

K= 3.768 L= 1.668
MEAN= 14.538
A= 0.583 B= 0.063 S= 0.586
SUM OF ERROR**2= 0.222 STAND. DEV.= 0.068

MAX. & MIN. POSITIONS
5.032 5.865 6.699 7.533 8.367

SECOND ORDER IN PHASE FIT

K= 1.770 L= 3.550
MEAN= 0.606
A= 1.366 B= -0.248 S= 1.388
SUM OF ERROR**2= 1.407 STAND. DEV.= 0.171

MAX. & MIN. POSITIONS
3.449 5.224 6.999 8.775 10.550

ADDITIONAL TERM

K= 9.341 L= 0.673
MEAN= -0.005
A= 0.042 B= 0.215 S= 0.219
SUM OF ERROR**2= 0.221 STAND. DEV.= 0.068

MAX. & MIN. POSITIONS
5.865 6.201 6.538 6.874 7.210

SECOND ORDER QUADRATURE FIT

K= 1.754 L= 3.582
MEAN= -0.003
A= 0.454 B= 1.340 S= 1.415
SUM OF ERROR**2= 1.278 STAND. DEV.= 0.163

MAX. & MIN. POSITIONS
2.500 4.291 6.082 7.872 9.663

ADDITIONAL TERM

K= 9.354 L= 0.672
MEAN= -0.000
A= 0.220 B= -0.020 S= 0.221
SUM OF ERROR**2= 0.142 STAND. DEV.= 0.054

MAX. & MIN. POSITIONS
5.700 6.036 6.372 6.707 7.043

(fig. 5.1)

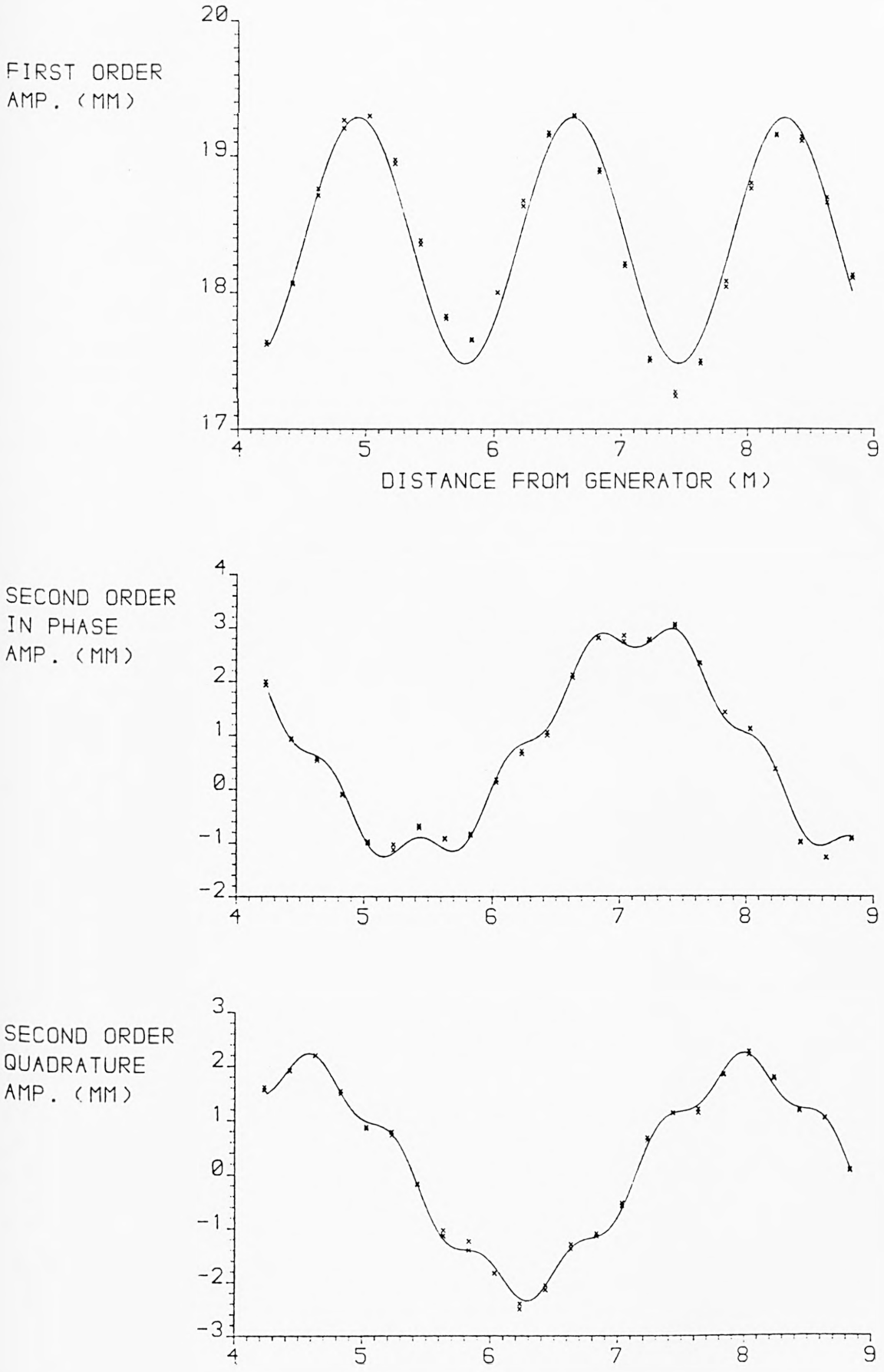

WAVEFORM VARIATION: WEDGE AMP. 60.0MM; FREQ. 0.586HZ
WATER DEPTH 500.0MM; WAVELENGTH 3360.0MM

Figure 5.2

WAVEFORM VARIATION: WEDGE AMP. 60.0MM; FREQ. 0.586HZ
WATER DEPTH 500.0MM; WAVELENGTH 3360.0MM

FIRST ORDER FIT

K= 3.743 L= 1.679
MEAN= 18.380
A= 0.843 B= -0.319 S= 0.901
SUM OF ERROR**2= 0.969 STAND. DEV.= 0.142

MAX. & MIN. POSITIONS
4.940 5.779 6.619 7.458 8.298

SECOND ORDER IN PHASE FIT

K= 1.788 L= 3.513
MEAN= 0.871
A= 2.018 B= 0.479 S= 2.074
SUM OF ERROR**2= 2.902 STAND. DEV.= 0.246

MAX. & MIN. POSITIONS
3.644 5.401 7.157 8.914 10.671

ADDITIONAL TERM

K= 9.227 L= 0.681
MEAN= -0.002
A= 0.301 B= -0.050 S= 0.305
SUM OF ERROR**2= 0.668 STAND. DEV.= 0.118

MAX. & MIN. POSITIONS
5.770 6.111 6.451 6.792 7.132

SECOND ORDER QUADRATURE FIT

K= 1.801 L= 3.488
MEAN= -0.048
A= -0.547 B= 1.955 S= 2.030
SUM OF ERROR**2= 2.135 STAND. DEV.= 0.211

MAX. & MIN. POSITIONS
2.767 4.511 6.255 7.999 9.743

ADDITIONAL TERM

K= 9.269 L= 0.678
MEAN= 0.002
A= 0.061 B= -0.266 S= 0.273
SUM OF ERROR**2= 0.357 STAND. DEV.= 0.086

MAX. & MIN. POSITIONS
5.956 6.295 6.634 6.973 7.312

(fig. 5.2)

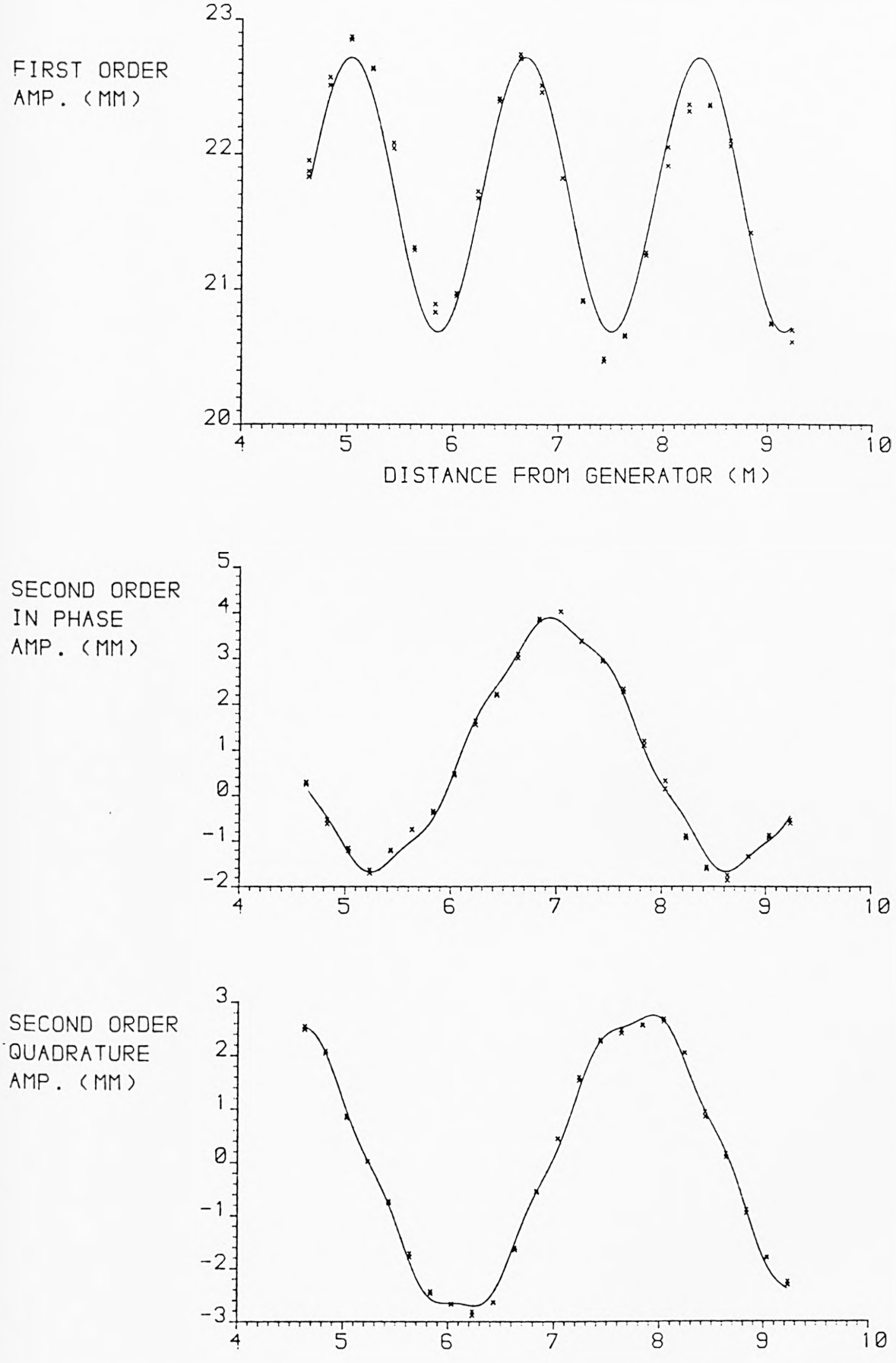

WAVEFORM VARIATION: WEDGE AMP. 70.0MM; FREQ. 0.586HZ
WATER DEPTH 500.0MM; WAVELENGTH 3335.0MM

Figure 5.3

WAVEFORM VARIATION: WEDGE AMP. 70.0MM; FREQ. 0.586HZ
WATER DEPTH 500.0MM; WAVELENGTH 3335.0MM

FIRST ORDER FIT

K= 3.808 L= 1.650
MEAN= 21.700
A= 0.970 B= 0.307 S= 1.017
SUM OF ERROR**2= 1.454 STAND. DEV.= 0.174

MAX. & MIN. POSITIONS
5.031 5.856 6.681 7.506 8.331

SECOND ORDER IN PHASE FIT

K= 1.857 L= 3.384
MEAN= 1.110
A= 2.456 B= 1.086 S= 2.685
SUM OF ERROR**2= 1.585 STAND. DEV.= 0.182

MAX. & MIN. POSITIONS
3.608 5.300 6.992 8.684 10.376

ADDITIONAL TERM

K= 9.328 L= 0.674
MEAN= 0.005
A= 0.032 B= 0.137 S= 0.141
SUM OF ERROR**2= 1.097 STAND. DEV.= 0.151

MAX. & MIN. POSITIONS
5.870 6.207 6.543 6.880 7.217

SECOND ORDER QUADRATURE FIT

K= 1.846 L= 3.403
MEAN= -0.010
A= -0.746 B= 2.686 S= 2.787
SUM OF ERROR**2= 1.028 STAND. DEV.= 0.146

MAX. & MIN. POSITIONS
2.699 4.400 6.102 7.803 9.504

ADDITIONAL TERM

K= 9.624 L= 0.653
MEAN= -0.005
A= -0.058 B= 0.130 S= 0.142
SUM OF ERROR**2= 0.575 STAND. DEV.= 0.109

MAX. & MIN. POSITIONS
5.756 6.083 6.409 6.735 7.062

(fig. 5.3)

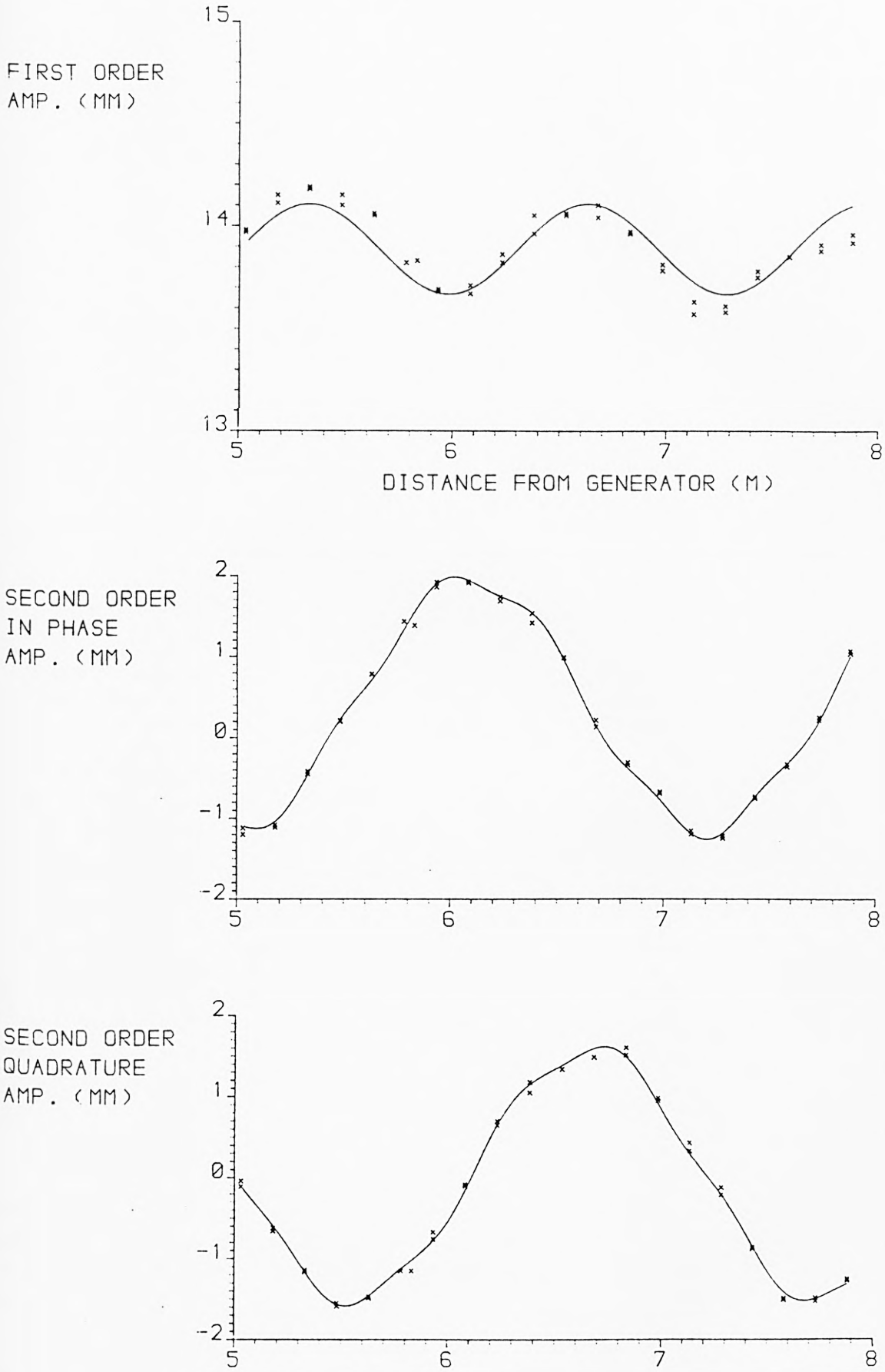

WAVEFORM VARIATION: WEDGE AMP. 50.0MM; FREQ. 0.684HZ
WATER DEPTH 500.0MM; WAVELENGTH 2720.0MM

Figure 5.4

WAVEFORM VARIATION: WEDGE AMP. 50.0MM; FREQ. 0.684HZ
WATER DEPTH 500.0MM; WAVELENGTH 2720.0MM

FIRST ORDER FIT

K= 4.820 L= 1.303
MEAN= 13.887
A= 0.187 B= 0.115 S= 0.219
SUM OF ERROR**2= 0.257 STAND. DEV.= 0.080

MAX. & MIN. POSITIONS
5.329 5.980 6.632 7.284 7.935

SECOND ORDER IN PHASE FIT

K= 2.846 L= 2.208
MEAN= 0.406
A= 0.107 B= -1.551 S= 1.555
SUM OF ERROR**2= 0.360 STAND. DEV.= 0.095

MAX. & MIN. POSITIONS
3.888 4.992 6.096 7.199 8.303

ADDITIONAL TERM

K= 12.440 L= 0.505
MEAN= -0.000
A= 0.014 B= -0.106 S= 0.107
SUM OF ERROR**2= 0.136 STAND. DEV.= 0.058

MAX. & MIN. POSITIONS
5.946 6.198 6.451 6.703 6.956

SECOND ORDER QUADRATURE FIT

K= 2.861 L= 2.196
MEAN= 0.043
A= 1.518 B= 0.309 S= 1.549
SUM OF ERROR**2= 0.349 STAND. DEV.= 0.093

MAX. & MIN. POSITIONS
4.463 5.561 6.659 7.757 8.855

ADDITIONAL TERM

K= 11.896 L= 0.528
MEAN= -0.002
A= 0.071 B= -0.068 S= 0.098
SUM OF ERROR**2= 0.158 STAND. DEV.= 0.063

MAX. & MIN. POSITIONS
6.010 6.274 6.538 6.802 7.066

(fig. 5.4)

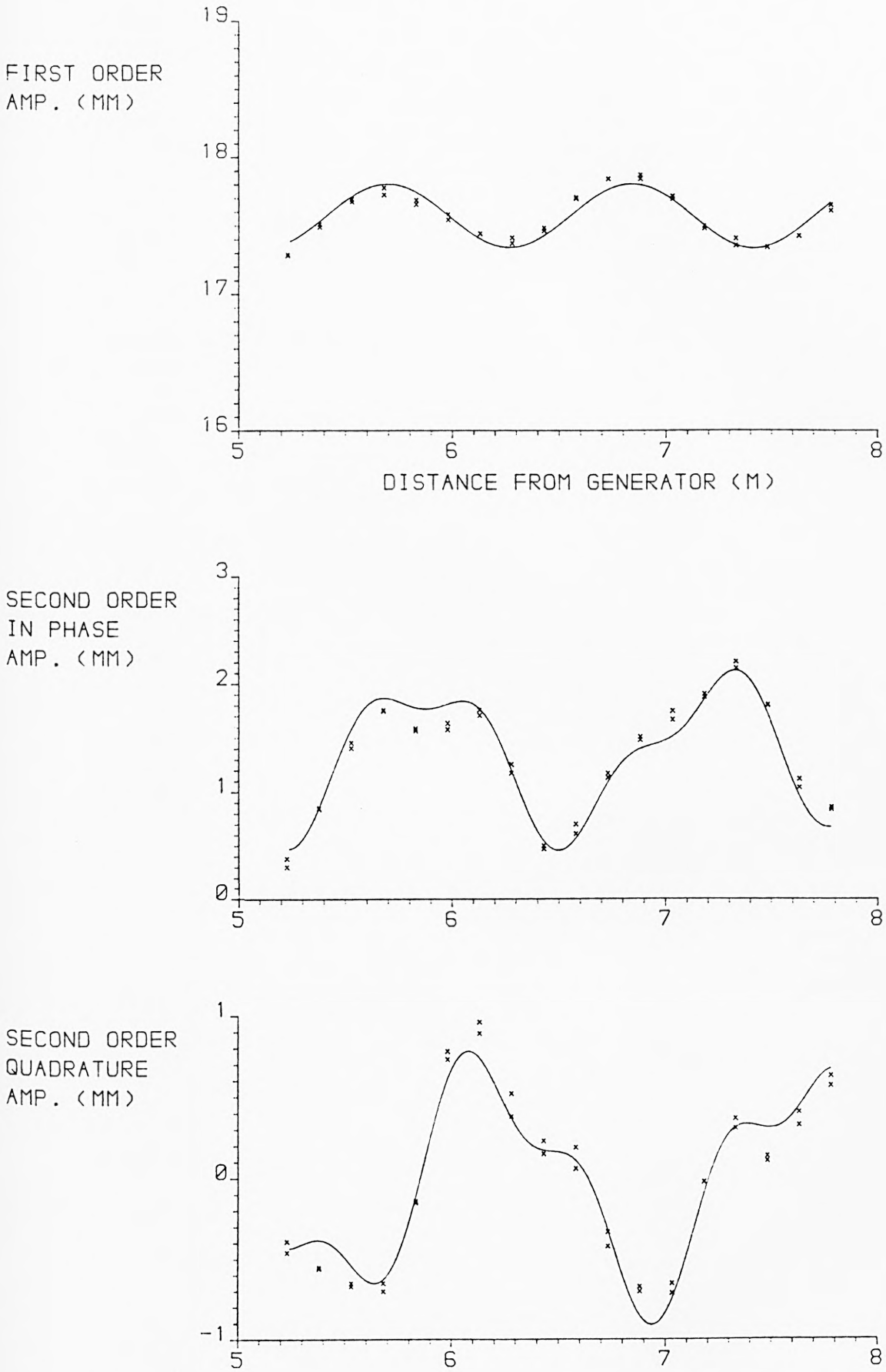

WAVEFORM VARIATION: WEDGE AMP. 40.0MM; FREQ. 0.781HZ
WATER DEPTH 500.0MM; WAVELENGTH 2260.0MM

Figure 5.5

WAVEFORM VARIATION: WEDGE AMP. 40.0MM; FREQ. 0.781HZ
WATER DEPTH 500.0MM; WAVELENGTH 2260.0MM

FIRST ORDER FIT

K= 5.489 L= 1.145
MEAN= 17.569
A= 0.226 B= -0.034 S= 0.229
SUM OF ERROR**2= 0.106 STAND. DEV.= 0.054

MAX. & MIN. POSITIONS
5.124 5.696 6.269 6.841 7.414

SECOND ORDER IN PHASE FIT

K= 4.581 L= 1.372
MEAN= 1.310
A= -0.099 B= 0.656 S= 0.664
SUM OF ERROR**2= 1.487 STAND. DEV.= 0.203

MAX. & MIN. POSITIONS
5.176 5.862 6.548 7.234 7.920

ADDITIONAL TERM

K= 10.397 L= 0.604
MEAN= 0.017
A= 0.056 B= 0.225 S= 0.231
SUM OF ERROR**2= 0.525 STAND. DEV.= 0.121

MAX. & MIN. POSITIONS
5.868 6.171 6.473 6.775 7.077

SECOND ORDER QUADRATURE FIT

K= 4.336 L= 1.449
MEAN= -0.010
A= -0.083 B= 0.643 S= 0.648
SUM OF ERROR**2= 1.550 STAND. DEV.= 0.208

MAX. & MIN. POSITIONS
4.740 5.464 6.189 6.913 7.638

ADDITIONAL TERM

K= 10.256 L= 0.613
MEAN= -0.003
A= 0.134 B= -0.213 S= 0.252
SUM OF ERROR**2= 0.440 STAND. DEV.= 0.111

MAX. & MIN. POSITIONS
6.028 6.334 6.641 6.947 7.253

(fig. 5.5)

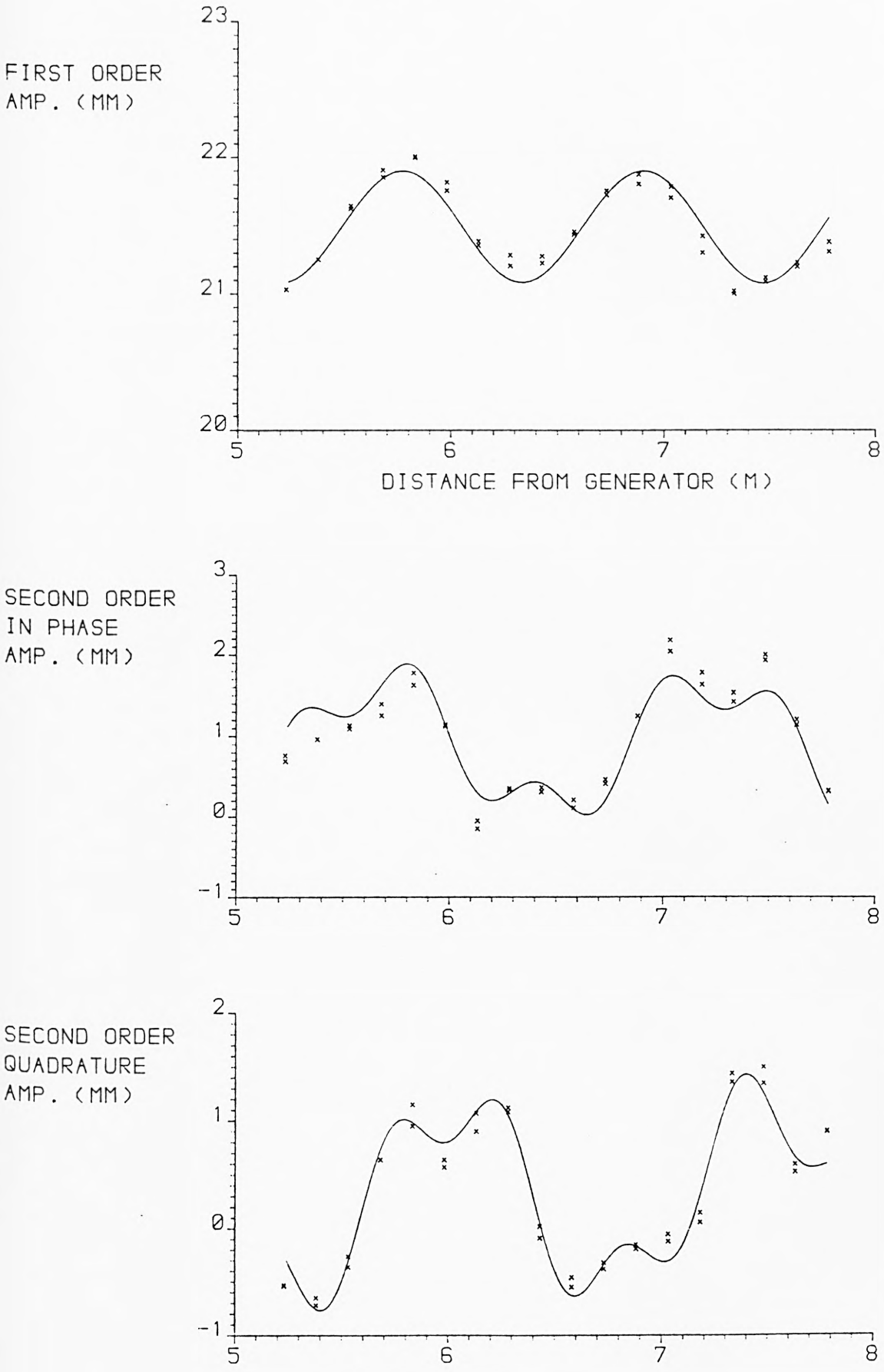

WAVEFORM VARIATION: WEDGE AMP. 50.0MM; FREQ. 0.781HZ
WATER DEPTH 500.0MM; WAVELENGTH 2260.0MM

Figure 5.6

WAVEFORM VARIATION: WEDGE AMP. 50.0MM; FREQ. 0.781HZ
WATER DEPTH 500.0MM; WAVELENGTH 2260.0MM

FIRST ORDER FIT

K= 5.559 L= 1.130
MEAN= 21.487
A= 0.319 B= 0.252 S= 0.407
SUM OF ERROR**2= 0.381 STAND. DEV.= 0.103

MAX. & MIN. POSITIONS
5.207 5.772 6.337 6.902 7.468

SECOND ORDER IN PHASE FIT

K= 3.998 L= 1.572
MEAN= 0.894
A= -0.643 B= -0.490 S= 0.809
SUM OF ERROR**2= 4.404 STAND. DEV.= 0.350

MAX. & MIN. POSITIONS
4.878 5.663 6.449 7.235 8.021

ADDITIONAL TERM

K= 10.973 L= 0.573
MEAN= -0.011
A= 0.106 B= 0.331 S= 0.348
SUM OF ERROR**2= 2.185 STAND. DEV.= 0.246

MAX. & MIN. POSITIONS
5.841 6.127 6.414 6.700 6.986

SECOND ORDER QUADRATURE FIT

K= 4.269 L= 1.472
MEAN= 0.304
A= 0.715 B= 0.469 S= 0.855
SUM OF ERROR**2= 3.149 STAND. DEV.= 0.296

MAX. & MIN. POSITIONS
5.287 6.023 6.759 7.495 8.231

ADDITIONAL TERM

K= 11.409 L= 0.551
MEAN= 0.007
A= -0.259 B= 0.249 S= 0.359
SUM OF ERROR**2= 0.880 STAND. DEV.= 0.156

MAX. & MIN. POSITIONS
5.991 6.266 6.541 6.817 7.092

(fig. 5.6)

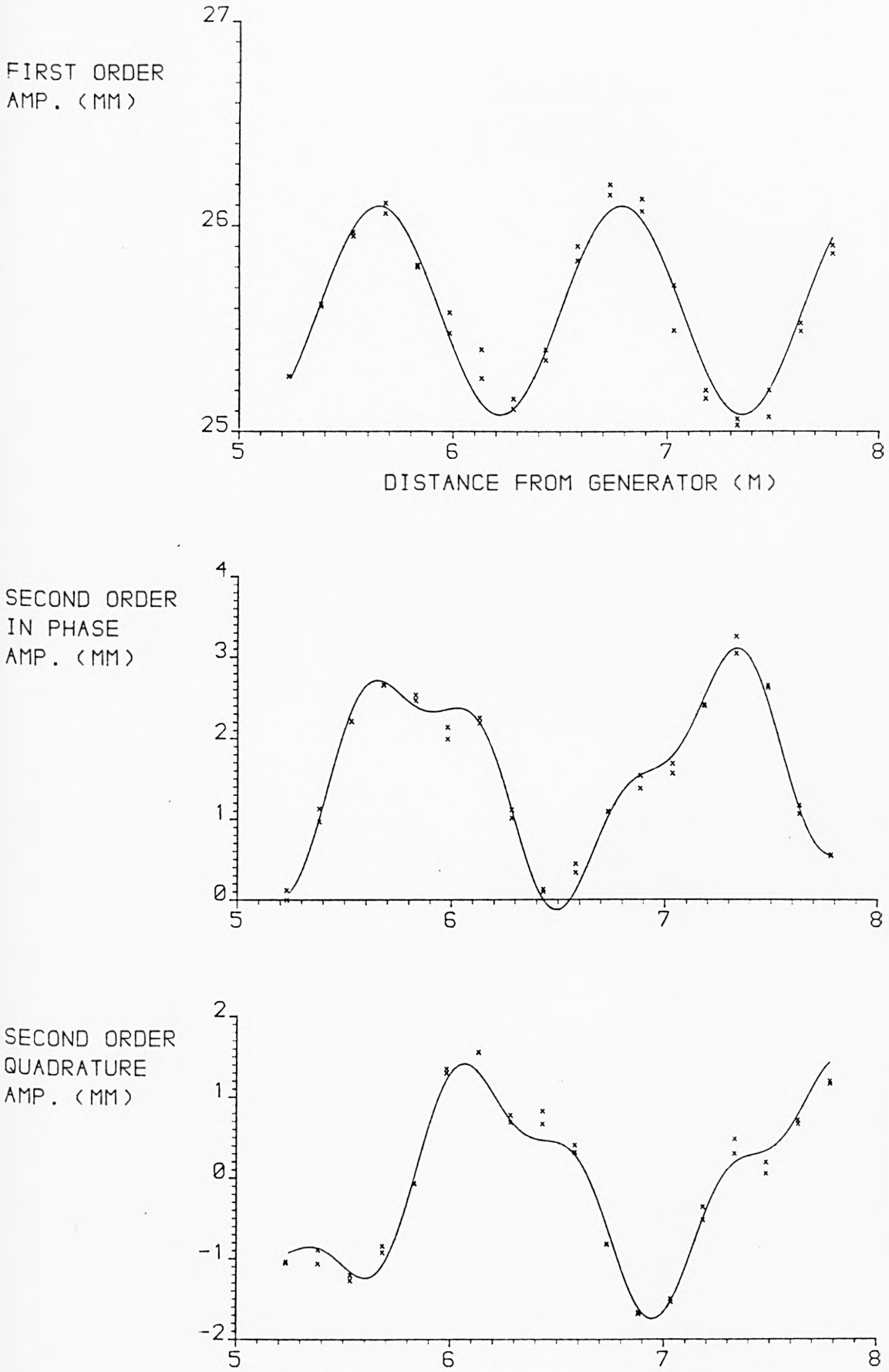

WAVEFORM VARIATION: WEDGE AMP. 60.0MM; FREQ. 0.781HZ
WATER DEPTH 500.0MM; WAVELENGTH 2270.0MM

Figure 5.7

WAVEFORM VARIATION: WEDGE AMP. 60.0MM; FREQ. 0.781HZ
WATER DEPTH 500.0MM; WAVELENGTH 2270.0MM

FIRST ORDER FIT

K= 5.532 L= 1.136
MEAN= 25.588
A= 0.501 B= -0.080 S= 0.508
SUM OF ERROR**2= 0.266 STAND. DEV.= 0.086

MAX. & MIN. POSITIONS
5.082 5.650 6.218 6.786 7.354

SECOND ORDER IN PHASE FIT

K= 4.334 L= 1.450
MEAN= 1.490
A= 1.266 B= 0.108 S= 1.271
SUM OF ERROR**2= 3.860 STAND. DEV.= 0.327

MAX. & MIN. POSITIONS
5.093 5.818 6.543 7.268 7.992

ADDITIONAL TERM

K= 10.379 L= 0.605
MEAN= 0.030
A= 0.177 B= 0.382 S= 0.421
SUM OF ERROR**2= 0.677 STAND. DEV.= 0.137

MAX. & MIN. POSITIONS
5.860 6.163 6.466 6.769 7.071

SECOND ORDER QUADRATURE FIT

K= 4.084 L= 1.538
MEAN= -0.038
A= 1.252 B= 0.176 S= 1.264
SUM OF ERROR**2= 4.215 STAND. DEV.= 0.342

MAX. & MIN. POSITIONS
4.649 5.418 6.188 6.957 7.726

ADDITIONAL TERM

K= 10.073 L= 0.624
MEAN= -0.010
A= -0.304 B= -0.307 S= 0.432
SUM OF ERROR**2= 0.990 STAND. DEV.= 0.166

MAX. & MIN. POSITIONS
6.004 6.316 6.628 6.940 7.252

(fig. 5.7)

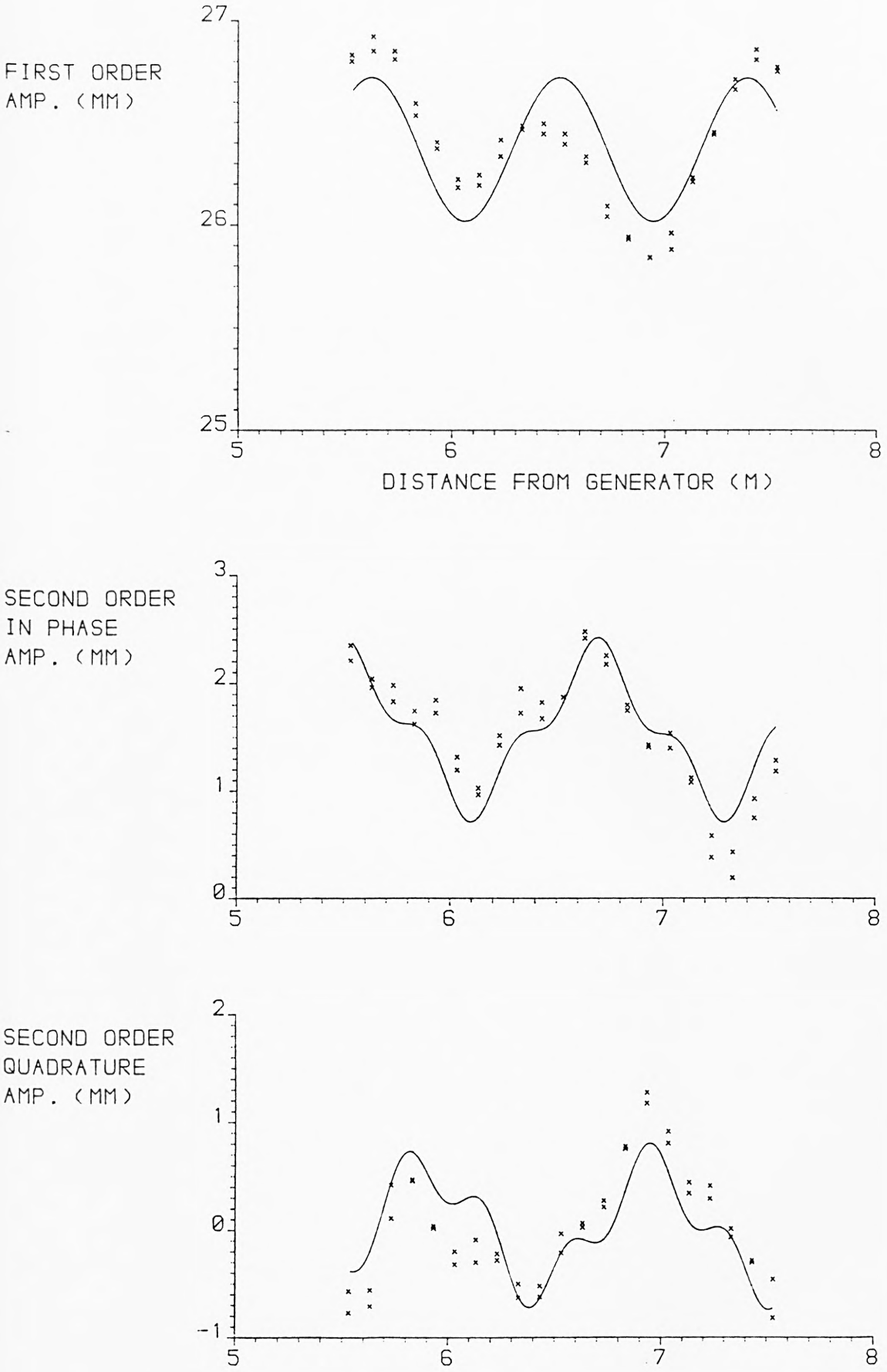

WAVEFORM VARIATION: WEDGE AMP. 50.0MM; FREQ. 0.879HZ
WATER DEPTH 500.0MM; WAVELENGTH 1890.0MM

Figure 5.8

WAVEFORM VARIATION: WEDGE AMP. 50.0MM; FREQ. 0.879HZ
WATER DEPTH 500.0MM; WAVELENGTH 1890.0MM

FIRST ORDER FIT

K= 7.122 L= 0.882
MEAN= 26.367
A= -0.249 B= 0.247 S= 0.351
SUM OF ERROR**2= 1.428 STAND. DEV.= 0.184

MAX. & MIN. POSITIONS
5.625 6.066 6.507 6.948 7.389

SECOND ORDER IN PHASE FIT

K= 5.355 L= 1.173
MEAN= 1.576
A= -0.194 B= -0.622 S= 0.651
SUM OF ERROR**2= 3.993 STAND. DEV.= 0.308

MAX. & MIN. POSITIONS
5.517 6.103 6.690 7.277 7.863

ADDITIONAL TERM

K= 15.721 L= 0.400
MEAN= -0.008
A= -0.001 B= -0.208 S= 0.208
SUM OF ERROR**2= 3.068 STAND. DEV.= 0.270

MAX. & MIN. POSITIONS
6.094 6.294 6.494 6.694 6.894

SECOND ORDER QUADRATURE FIT

K= 5.926 L= 1.060
MEAN= 0.018
A= -0.502 B= -0.214 S= 0.545
SUM OF ERROR**2= 5.331 STAND. DEV.= 0.356

MAX. & MIN. POSITIONS
5.370 5.900 6.430 6.960 7.491

ADDITIONAL TERM

K= 16.421 L= 0.383
MEAN= 0.014
A= 0.148 B= 0.185 S= 0.237
SUM OF ERROR**2= 4.159 STAND. DEV.= 0.315

MAX. & MIN. POSITIONS
6.176 6.368 6.559 6.750 6.942

(fig. 5.8)

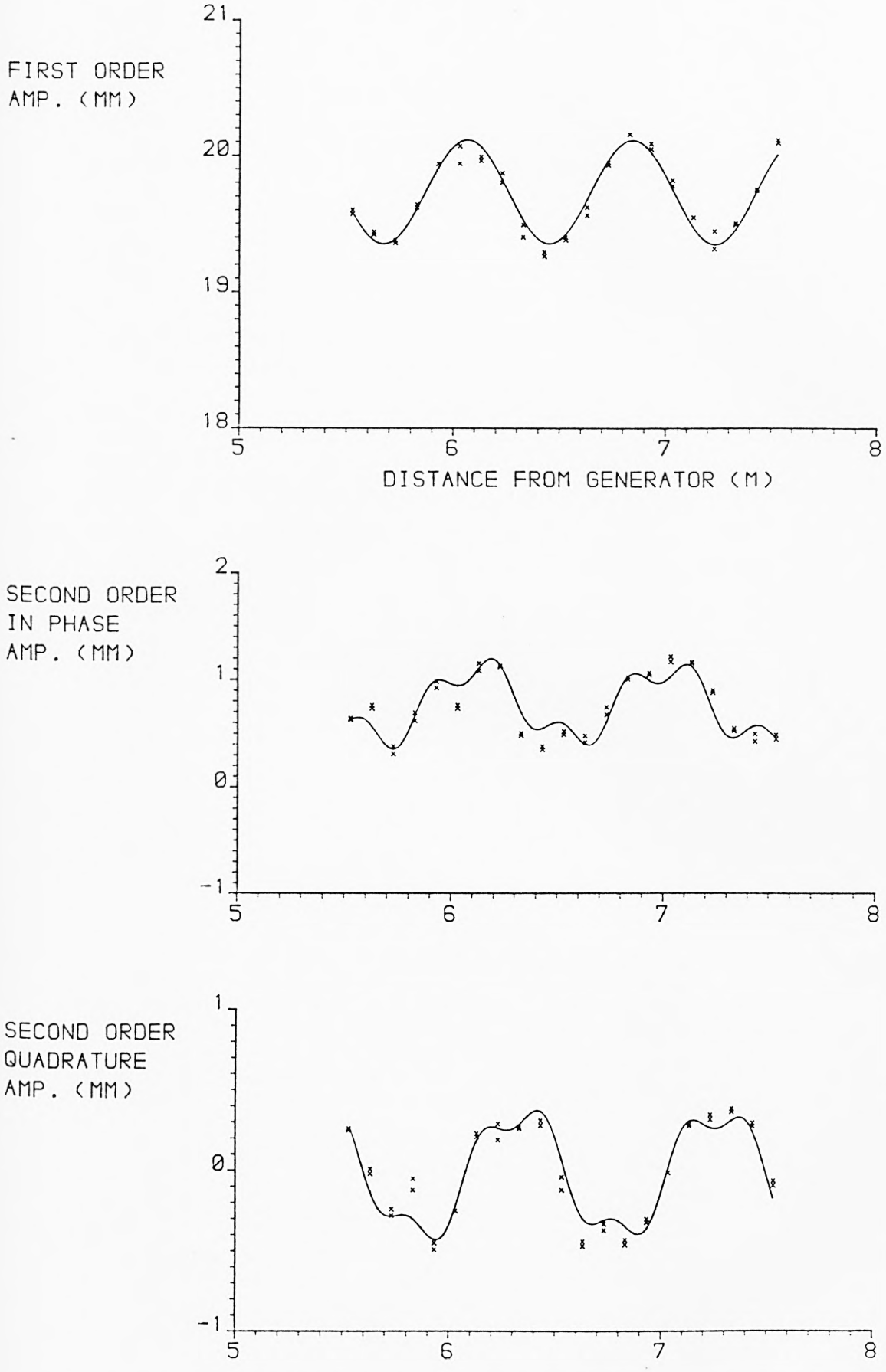

WAVEFORM VARIATION: WEDGE AMP. 30.0MM; FREQ. 0.977HZ
WATER DEPTH 500.0MM; WAVELENGTH 1585.0MM

Figure 5.9

WAVEFORM VARIATION: WEDGE AMP. 30.0MM; FREQ. 0.977HZ
WATER DEPTH 500.0MM; WAVELENGTH 1585.0MM

FIRST ORDER FIT

K= 8.072 L= 0.778
MEAN= 19.733
A= 0.100 B= -0.368 S= 0.382
SUM OF ERROR**2= 0.165 STAND. DEV.= 0.063

MAX. & MIN. POSITIONS
5.677 6.066 6.455 6.844 7.233

SECOND ORDER IN PHASE FIT

K= 7.046 L= 0.892
MEAN= 0.787
A= 0.205 B= -0.261 S= 0.332
SUM OF ERROR**2= 0.888 STAND. DEV.= 0.145

MAX. & MIN. POSITIONS
5.668 6.113 6.559 7.005 7.451

ADDITIONAL TERM

K= 20.376 L= 0.308
MEAN= -0.004
A= 0.087 B= 0.105 S= 0.137
SUM OF ERROR**2= 0.514 STAND. DEV.= 0.111

MAX. & MIN. POSITIONS
6.210 6.364 6.519 6.673 6.827

SECOND ORDER QUADRATURE FIT

K= 6.708 L= 0.937
MEAN= -0.019
A= 0.007 B= -0.388 S= 0.388
SUM OF ERROR**2= 0.564 STAND. DEV.= 0.116

MAX. & MIN. POSITIONS
5.389 5.857 6.325 6.794 7.262

ADDITIONAL TERM

K= 19.612 L= 0.320
MEAN= -0.001
A= 0.062 B= 0.085 S= 0.105
SUM OF ERROR**2= 0.329 STAND. DEV.= 0.088

MAX. & MIN. POSITIONS
6.135 6.296 6.456 6.616 6.776

(fig. 5.9)

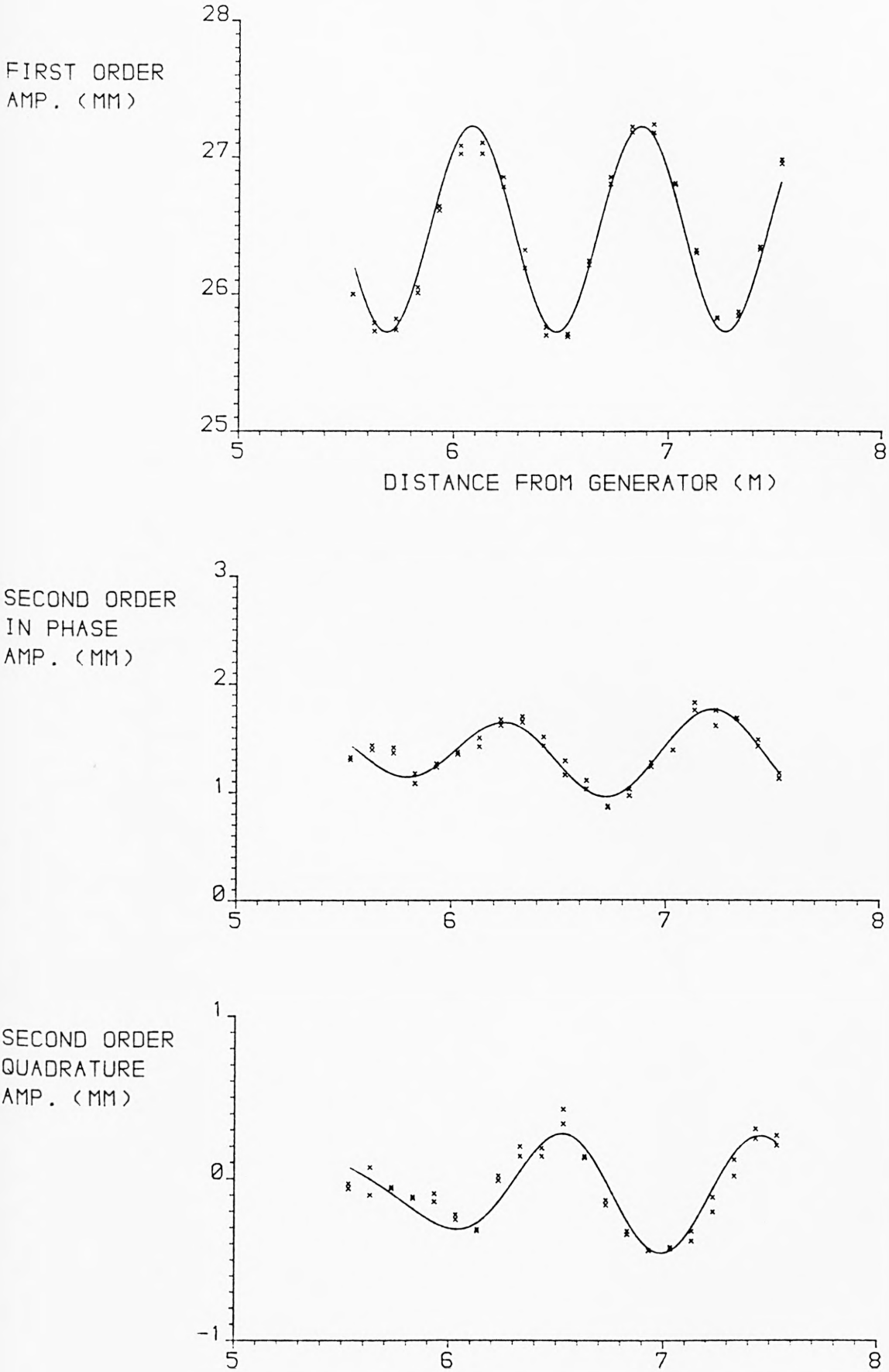

WAVEFORM VARIATION: WEDGE AMP. 40.0MM; FREQ. 0.977HZ
WATER DEPTH 500.0MM; WAVELENGTH 1585.0MM

Figure 5.10

WAVEFORM VARIATION: WEDGE AMP. 40.0MM; FREQ. 0.977HZ
WATER DEPTH 500.0MM; WAVELENGTH 1585.0MM

FIRST ORDER FIT

K= 7.942 L= 0.791
MEAN= 26.474
A= -0.274 B= -0.699 S= 0.751
SUM OF ERROR**2= 0.436 STAND. DEV.= 0.102

MAX. & MIN. POSITIONS
5.689 6.084 6.480 6.875 7.271

SECOND ORDER IN PHASE FIT

K= 6.711 L= 0.936
MEAN= 1.372
A= -0.085 B= -0.305 S= 0.317
SUM OF ERROR**2= 0.584 STAND. DEV.= 0.118

MAX. & MIN. POSITIONS
5.343 5.811 6.279 6.747 7.215

ADDITIONAL TERM

K= 4.387 L= 1.432
MEAN= -0.024
A= 0.098 B= 0.056 S= 0.113
SUM OF ERROR**2= 0.334 STAND. DEV.= 0.089

MAX. & MIN. POSITIONS
5.132 5.848 6.565 7.281 7.997

SECOND ORDER QUADRATURE FIT

K= 6.039 L= 1.040
MEAN= -0.064
A= 0.052 B= 0.282 S= 0.286
SUM OF ERROR**2= 0.547 STAND. DEV.= 0.114

MAX. & MIN. POSITIONS
5.432 5.952 6.473 6.993 7.513

ADDITIONAL TERM

K= 8.412 L= 0.747
MEAN= -0.005
A= 0.058 B= -0.083 S= 0.101
SUM OF ERROR**2= 0.336 STAND. DEV.= 0.089

MAX. & MIN. POSITIONS
5.862 6.235 6.609 6.982 7.356

(fig. 5.10)

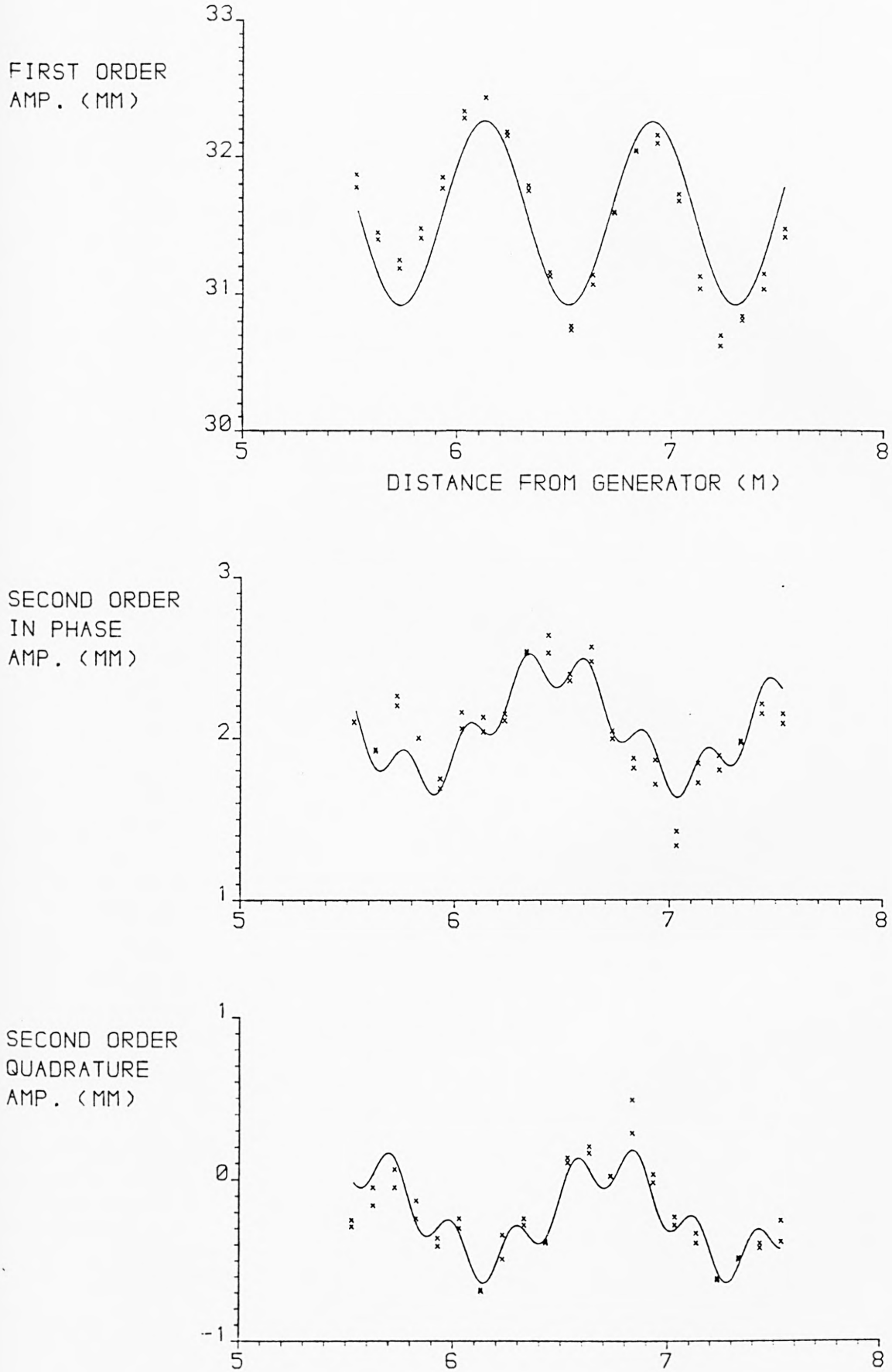

WAVEFORM VARIATION: WEDGE AMP. 50.0MM; FREQ. 0.977HZ
WATER DEPTH 500.0MM; WAVELENGTH 1590.0MM

Figure 5.11

WAVEFORM VARIATION: WEDGE AMP. 50.0MM; FREQ. 0.977HZ
WATER DEPTH 500.0MM; WAVELENGTH 1590.0MM

FIRST ORDER FIT

K= 8.051 L= 0.780
MEAN= 31.590
A= 0.400 B= -0.536 S= 0.669
SUM OF ERROR**2= 2.160 STAND. DEV.= 0.227

MAX. & MIN. POSITIONS
5.738 6.128 6.518 6.909 7.299

SECOND ORDER IN PHASE FIT

K= 5.114 L= 1.229
MEAN= 2.111
A= -0.013 B= 0.342 S= 0.342
SUM OF ERROR**2= 1.280 STAND. DEV.= 0.175

MAX. & MIN. POSITIONS
5.229 5.843 6.457 7.072 7.686

ADDITIONAL TERM

K= 22.478 L= 0.280
MEAN= -0.002
A= -0.082 B= -0.108 S= 0.136
SUM OF ERROR**2= 0.893 STAND. DEV.= 0.146

MAX. & MIN. POSITIONS
6.191 6.330 6.470 6.610 6.750

SECOND ORDER QUADRATURE FIT

K= 5.466 L= 1.150
MEAN= -0.211
A= 0.179 B= -0.234 S= 0.295
SUM OF ERROR**2= 1.002 STAND. DEV.= 0.154

MAX. & MIN. POSITIONS
5.580 6.155 6.729 7.304 7.879

ADDITIONAL TERM

K= 22.227 L= 0.283
MEAN= 0.005
A= 0.024 B= 0.140 S= 0.142
SUM OF ERROR**2= 0.581 STAND. DEV.= 0.118

MAX. & MIN. POSITIONS
6.282 6.423 6.564 6.706 6.847

(fig. 5.11)

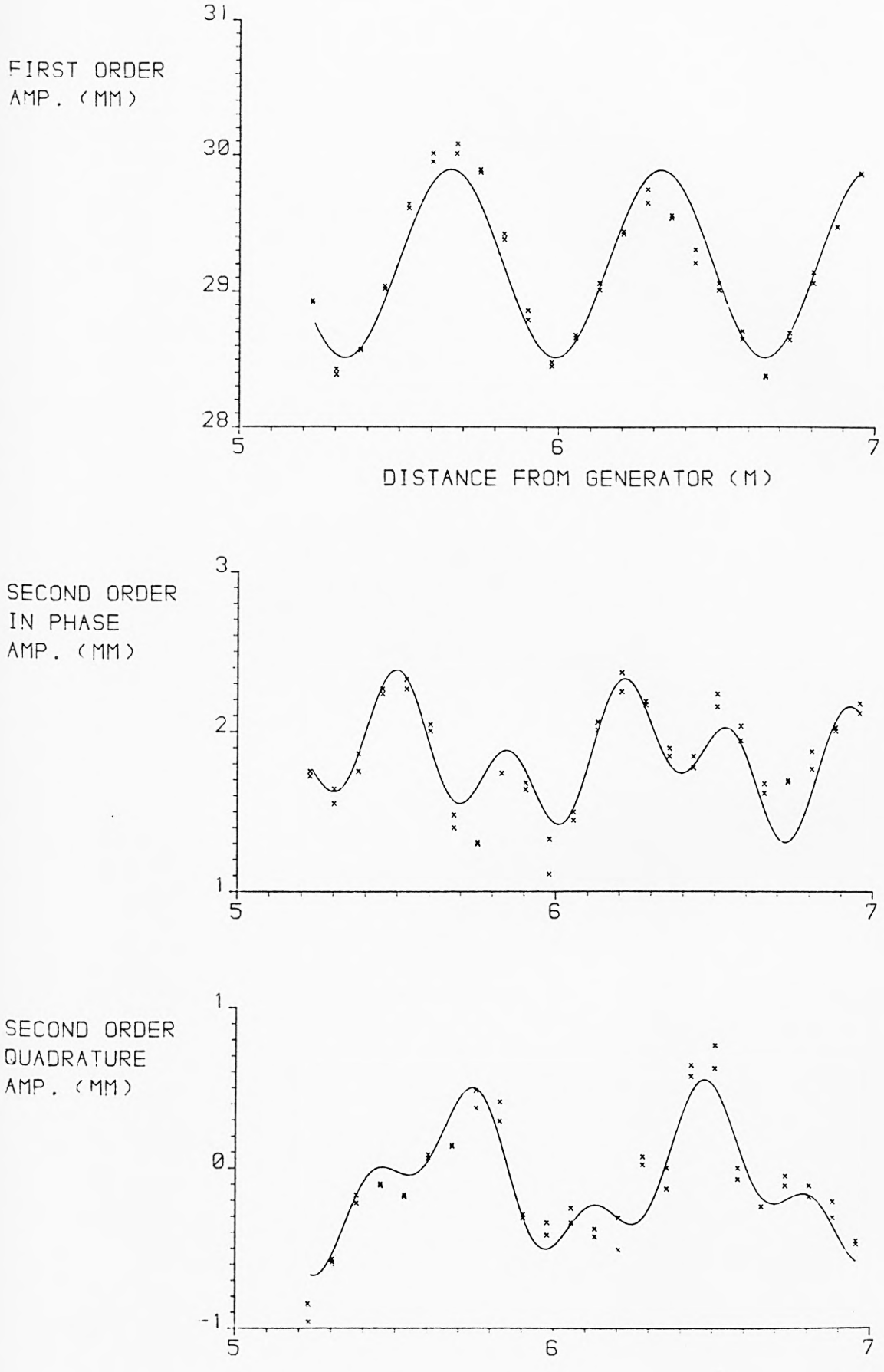

WAVEFORM VARIATION: WEDGE AMP. 40.0MM; FREQ. 1.074HZ
WATER DEPTH 500.0MM; WAVELENGTH 1340.0MM

Figure 5-12

WAVEFORM VARIATION: WEDGE AMP. 40.0MM; FREQ. 1.074HZ
WATER DEPTH 500.0MM; WAVELENGTH 1340.0MM

FIRST ORDER FIT

K= 9.520 L= 0.660
MEAN= 29.204
A= -0.607 B= -0.327 S= 0.690
SUM OF ERROR**2= 1.037 STAND. DEV.= 0.147

MAX. & MIN. POSITIONS
5.992 6.322 6.652 6.982 7.312

SECOND ORDER IN PHASE FIT

K= 17.929 L= 0.350
MEAN= 1.842
A= -0.090 B= -0.271 S= 0.286
SUM OF ERROR**2= 2.541 STAND. DEV.= 0.230

MAX. & MIN. POSITIONS
6.203 6.378 6.553 6.728 6.904

ADDITIONAL TERM

K= 7.778 L= 0.808
MEAN= -0.001
A= 0.060 B= -0.248 S= 0.255
SUM OF ERROR**2= 1.095 STAND. DEV.= 0.151

MAX. & MIN. POSITIONS
5.887 6.291 6.695 7.099 7.503

SECOND ORDER QUADRATURE FIT

K= 7.811 L= 0.804
MEAN= -0.074
A= 0.365 B= 0.165 S= 0.400
SUM OF ERROR**2= 2.302 STAND. DEV.= 0.219

MAX. & MIN. POSITIONS
5.685 6.087 6.490 6.892 7.294

ADDITIONAL TERM

K= 17.841 L= 0.352
MEAN= 0.005
A= -0.151 B= 0.166 S= 0.224
SUM OF ERROR**2= 1.078 STAND. DEV.= 0.150

MAX. & MIN. POSITIONS
6.117 6.293 6.469 6.645 6.821

(fig. 5.12)

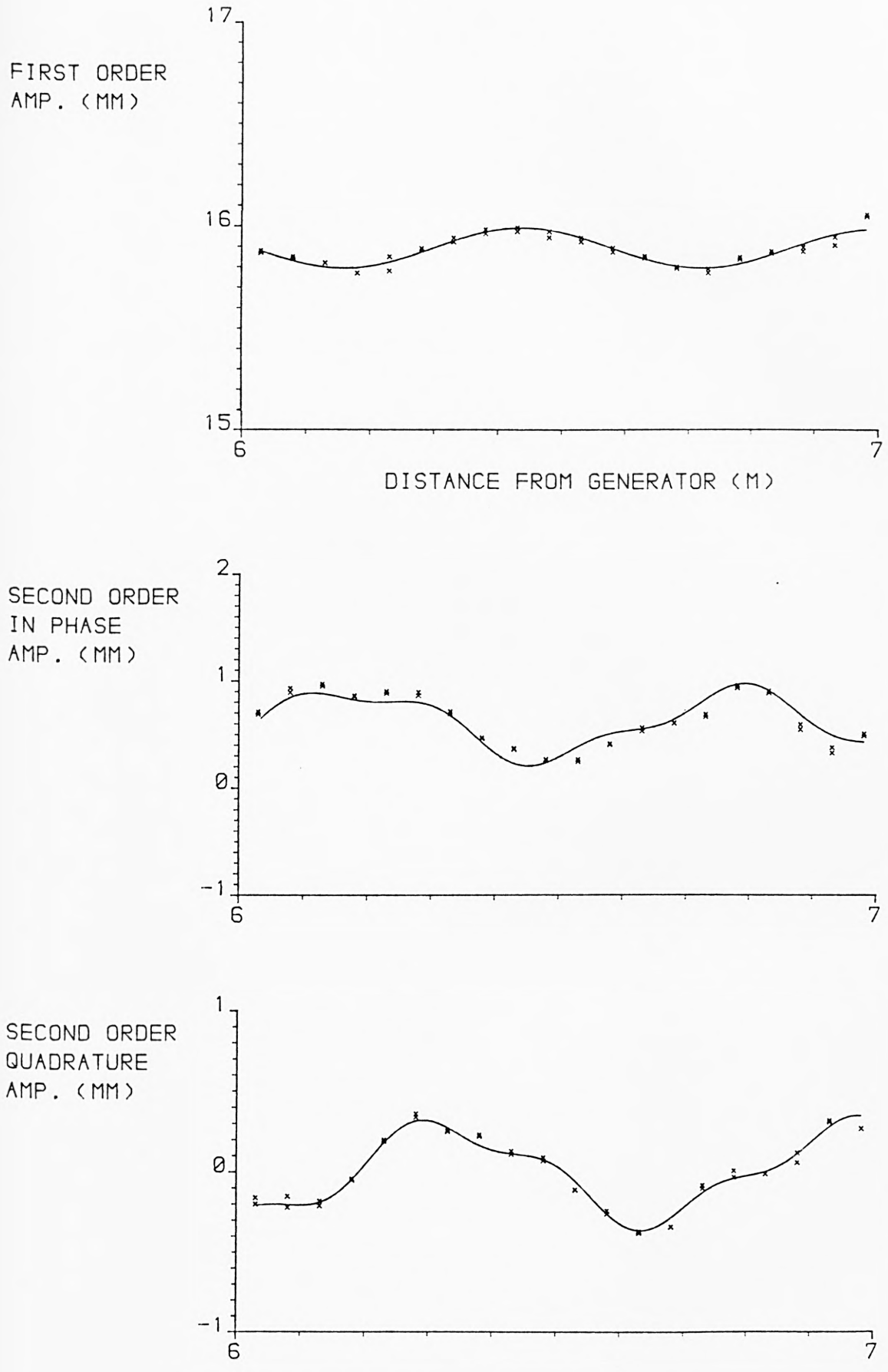

WAVEFORM VARIATION: WEDGE AMP. 20.0MM; FREQ. 1.172HZ
WATER DEPTH 500.0MM; WAVELENGTH 1135.0MM

Figure 5.13

WAVEFORM VARIATION: WEDGE AMP. 20.0MM; FREQ. 1.172HZ
WATER DEPTH 500.0MM; WAVELENGTH 1135.0MM

FIRST ORDER FIT

K= 11.264 L= 0.558
MEAN= 15.891
A= -0.094 B= -0.024 S= 0.097
SUM OF ERROR**2= 0.026 STAND. DEV.= 0.025

MAX. & MIN. POSITIONS
5.879 6.158 6.437 6.716 6.995

SECOND ORDER IN PHASE FIT

K= 10.438 L= 0.602
MEAN= 0.592
A= -0.027 B= 0.310 S= 0.312
SUM OF ERROR**2= 0.450 STAND. DEV.= 0.106

MAX. & MIN. POSITIONS
5.878 6.179 6.480 6.781 7.082

ADDITIONAL TERM

K= 26.121 L= 0.241
MEAN= -0.001
A= -0.007 B= 0.091 S= 0.091
SUM OF ERROR**2= 0.290 STAND. DEV.= 0.085

MAX. & MIN. POSITIONS
6.317 6.437 6.558 6.678 6.798

SECOND ORDER QUADRATURE FIT

K= 9.893 L= 0.635
MEAN= -0.003
A= 0.277 B= -0.058 S= 0.283
SUM OF ERROR**2= 0.183 STAND. DEV.= 0.068

MAX. & MIN. POSITIONS
6.013 6.330 6.648 6.965 7.283

ADDITIONAL TERM

K= 26.663 L= 0.236
MEAN= -0.004
A= -0.060 B= -0.050 S= 0.078
SUM OF ERROR**2= 0.055 STAND. DEV.= 0.037

MAX. & MIN. POSITIONS
6.271 6.389 6.507 6.624 6.742

(fig. 5.13)

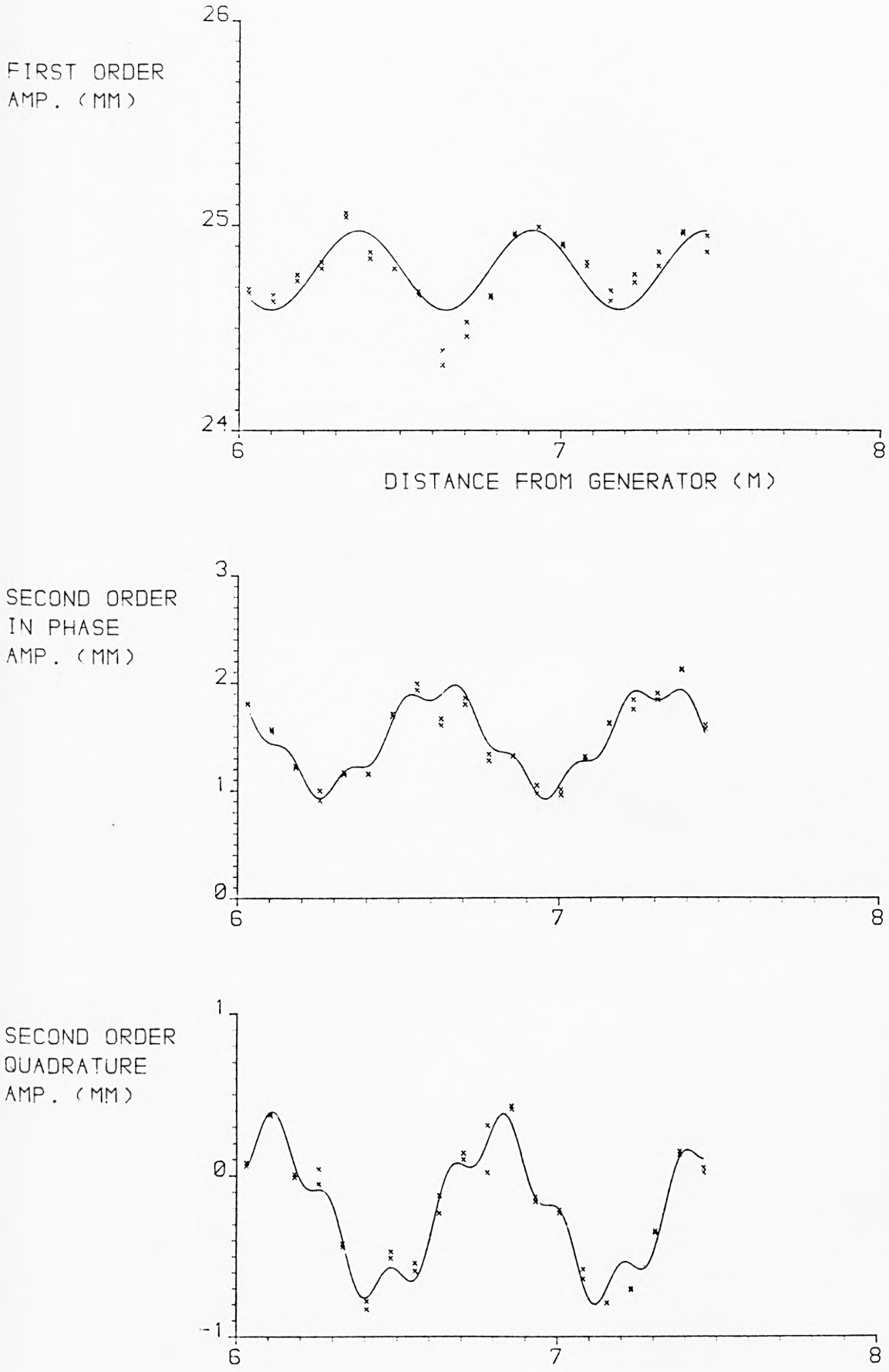

WAVEFORM VARIATION: WEDGE AMP. 30.0MM; FREQ. 1.172HZ
WATER DEPTH 500.0MM; WAVELENGTH 1140.0MM

Figure 5.14

WAVEFORM VARIATION: WEDGE AMP. 30.0MM; FREQ. 1.172HZ
WATER DEPTH 500.0MM; WAVELENGTH 1140.0MM

FIRST ORDER FIT

K= 11.599 L= 0.542
MEAN= 24.781
A= 0.010 B= -0.193 S= 0.193
SUM OF ERROR**2= 0.359 STAND. DEV.= 0.095

MAX. & MIN. POSITIONS
5.828 6.099 6.369 6.640 6.911

SECOND ORDER IN PHASE FIT

K= 9.118 L= 0.689
MEAN= 1.483
A= -0.362 B= -0.290 S= 0.464
SUM OF ERROR**2= 0.647 STAND. DEV.= 0.127

MAX. & MIN. POSITIONS
5.931 6.276 6.620 6.965 7.310

ADDITIONAL TERM

K= 35.645 L= 0.176
MEAN= 0.002
A= 0.099 B= -0.029 S= 0.103
SUM OF ERROR**2= 0.434 STAND. DEV.= 0.104

MAX. & MIN. POSITIONS
6.338 6.426 6.514 6.602 6.690

SECOND ORDER QUADRATURE FIT

K= 8.955 L= 0.702
MEAN= -0.224
A= -0.151 B= -0.464 S= 0.488
SUM OF ERROR**2= 0.616 STAND. DEV.= 0.124

MAX. & MIN. POSITIONS
5.753 6.104 6.455 6.806 7.156

ADDITIONAL TERM

K= 34.727 L= 0.181
MEAN= 0.005
A= 0.029 B= -0.126 S= 0.129
SUM OF ERROR**2= 0.253 STAND. DEV.= 0.080

MAX. & MIN. POSITIONS
6.294 6.384 6.475 6.565 6.656

(fig. 5-14)

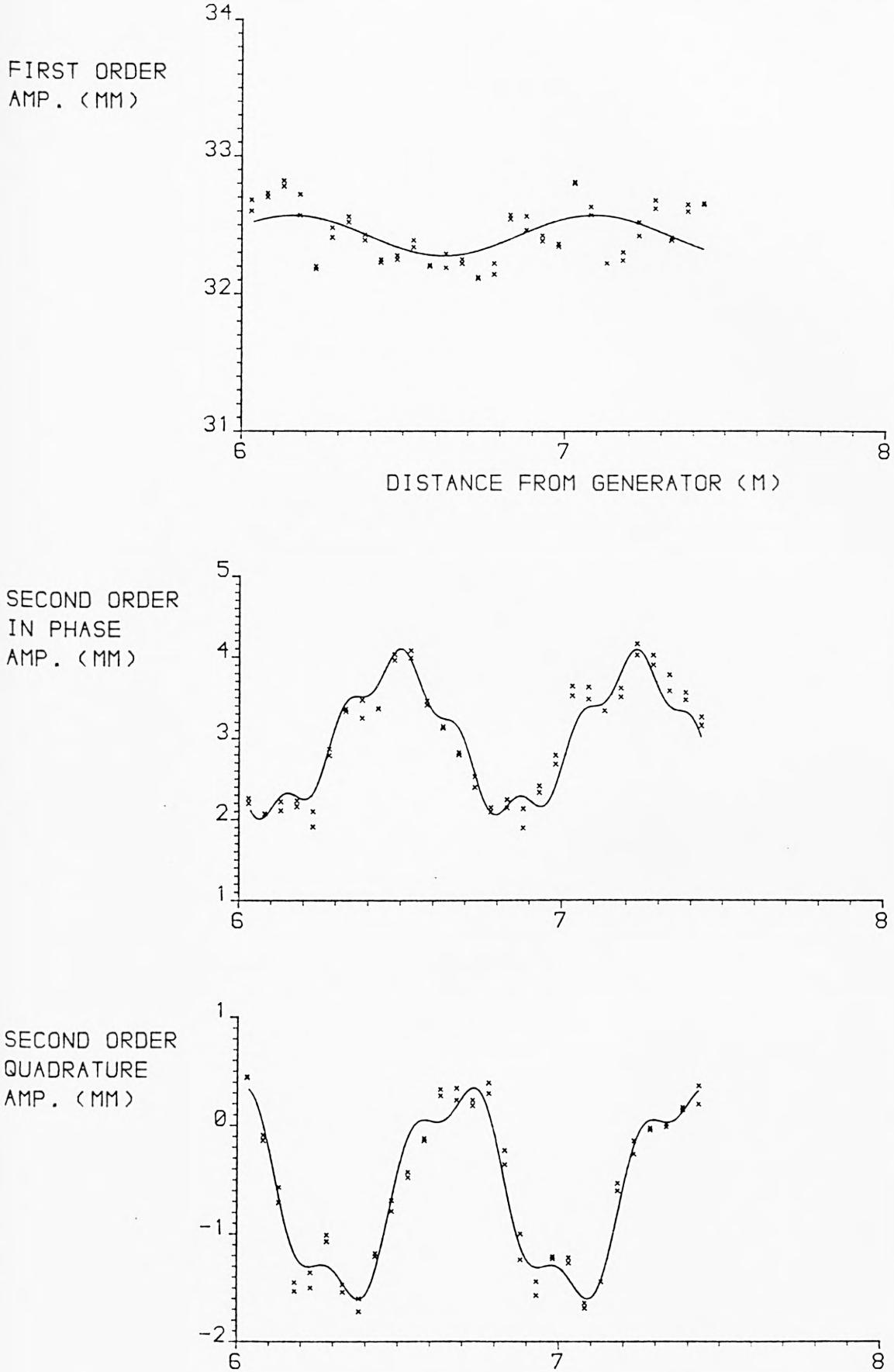

WAVEFORM VARIATION: WEDGE AMP. 40.0MM; FREQ. 1.172HZ
WATER DEPTH 500.0MM; WAVELENGTH 1160.0MM

Figure 5.15

WAVEFORM VARIATION: WEDGE AMP. 40.0MM; FREQ. 1.172HZ
WATER DEPTH 500.0MM; WAVELENGTH 1160.0MM

FIRST ORDER FIT

K= 5.083 L= 1.236
MEAN= 32.424
A= 0.114 B= -0.131 S= 0.174
SUM OF ERROR**2= 1.386 STAND. DEV.= 0.156

MAX. & MIN. POSITIONS
5.394 6.012 6.630 7.248 7.866

SECOND ORDER IN PHASE FIT

K= 8.458 L= 0.743
MEAN= 3.013
A= -0.118 B= -0.904 S= 0.912
SUM OF ERROR**2= 3.520 STAND. DEV.= 0.249

MAX. & MIN. POSITIONS
5.742 6.113 6.484 6.856 7.227

ADDITIONAL TERM

K= 34.588 L= 0.182
MEAN= -0.003
A= 0.065 B= -0.180 S= 0.191
SUM OF ERROR**2= 2.488 STAND. DEV.= 0.209

MAX. & MIN. POSITIONS
6.323 6.414 6.504 6.595 6.686

SECOND ORDER QUADRATURE FIT

K= 8.854 L= 0.710
MEAN= -0.622
A= -0.772 B= 0.543 S= 0.944
SUM OF ERROR**2= 3.120 STAND. DEV.= 0.234

MAX. & MIN. POSITIONS
5.963 6.318 6.672 7.027 7.382

ADDITIONAL TERM

K= 26.524 L= 0.237
MEAN= -0.007
A= -0.223 B= -0.072 S= 0.234
SUM OF ERROR**2= 1.592 STAND. DEV.= 0.167

MAX. & MIN. POSITIONS
6.289 6.408 6.526 6.645 6.763

(fig. 5.15)

Freq. (Hz)	WA (mm)	L_{meas} (mm)	a_I (mm)	a_R (mm)	a_2 (mm)	$a_{22(I)}$ (mm)	$a_{22(Q)}$ (mm)	$a_{22R(I)}$ (mm)	$a_{22R(Q)}$ (mm)
0.586	50	3350	14.54	0.59	0.61	1.39	1.42	0.22	0.22
0.586	60	3360	18.38	0.90	0.87	2.07	2.03	0.31	0.27
0.586	70	3335	21.70	1.02	1.11	2.69	2.79	0.14	0.14
0.684	40	2720	11.22	0.21	0.31	1.12	1.13	0.15	0.18
0.684	50	2720	13.89	0.22	0.41	1.56	1.55	0.11	0.10
0.684	60	2720	16.89	0.27	0.54	2.16	2.12	0.09	0.07
0.684	70	2720	20.03	0.36	0.84	2.63	2.54	0.17	0.19
0.781	30	2260	12.80	0.31	0.56	0.48	0.46	0.27	0.25
0.781	40	2260	17.57	0.23	1.31	0.66	0.65	0.23	0.25
0.781	50	2260	21.49	0.41	0.89	0.80	0.86	0.35	0.36
0.781	60	2270	25.59	0.51	1.49	1.27	1.26	0.42	0.43
0.781	70	2260	30.46	0.40	2.23	1.59	1.69	0.44	0.35
0.879	20	1870	10.52	0.07	0.13	0.27	0.23	0.24	0.24
0.879	30	1890	16.49	0.10	0.52	0.36	0.37	0.10	0.09
0.879	40	1885	22.25	0.20	0.97	0.48	0.40	0.21	0.18
0.879	50	1890	26.37	0.35	1.58	0.65	0.55	0.21	0.24
0.879	60	1880	32.58	0.28	2.09	0.73	0.72	0.27	0.15
0.879	70	1890	37.38	0.27	2.86	0.73	0.75	0.18	0.25
0.977	20	1570	12.60	0.34	0.25	0.24	0.24	0.08	0.07
0.977	30	1585	19.73	0.38	0.79	0.33	0.39	0.14	0.11
0.977	40	1585	26.47	0.75	1.37	0.32	0.29	0.11	0.10
0.977	50	1590	31.59	0.67	2.11	0.34	0.30	0.14	0.14
0.977	60	1590	38.83	1.06	3.14	0.48	0.60	0.29	0.47
0.977	70	1610	44.67	1.03	4.33	1.00	0.90	0.21	0.72
1.074	20	1330	14.22	0.21	0.39	0.23	0.26	0.13	0.14
1.074	30	1350	22.39	0.34	0.99	0.31	0.38	0.18	0.14
1.074	40	1340	29.20	0.69	1.84	0.26	0.40	0.29	0.22
1.074	50	1350	35.26	0.61	2.81	0.77	0.55	0.20	0.19
1.074	60	1350	43.10	1.02	4.60	1.15	1.15	0.37	0.31
1.172	20	1135	15.89	0.10	0.59	0.31	0.28	0.09	0.08
1.172	30	1140	24.78	0.19	1.48	0.46	0.49	0.10	0.13
1.172	40	1160	32.42	0.17	3.01	0.91	0.94	0.19	0.23
1.172	50	1170	38.42	0.30	5.97	0.79	0.97	0.34	0.31

Waveform Analysis Results

Table 5.1

5.1.1 Wave Amplitude Ratio

The wave amplitude ratio for a wedge type generator was shown by Wang (1974) to be;

$$\frac{a_I}{WA} = f(kb, b/d) \qquad (5\text{-}1)$$

Wang derived a relationship for the wave amplitude ratio for various values of b/d, which he presented in the form of curves against kb.

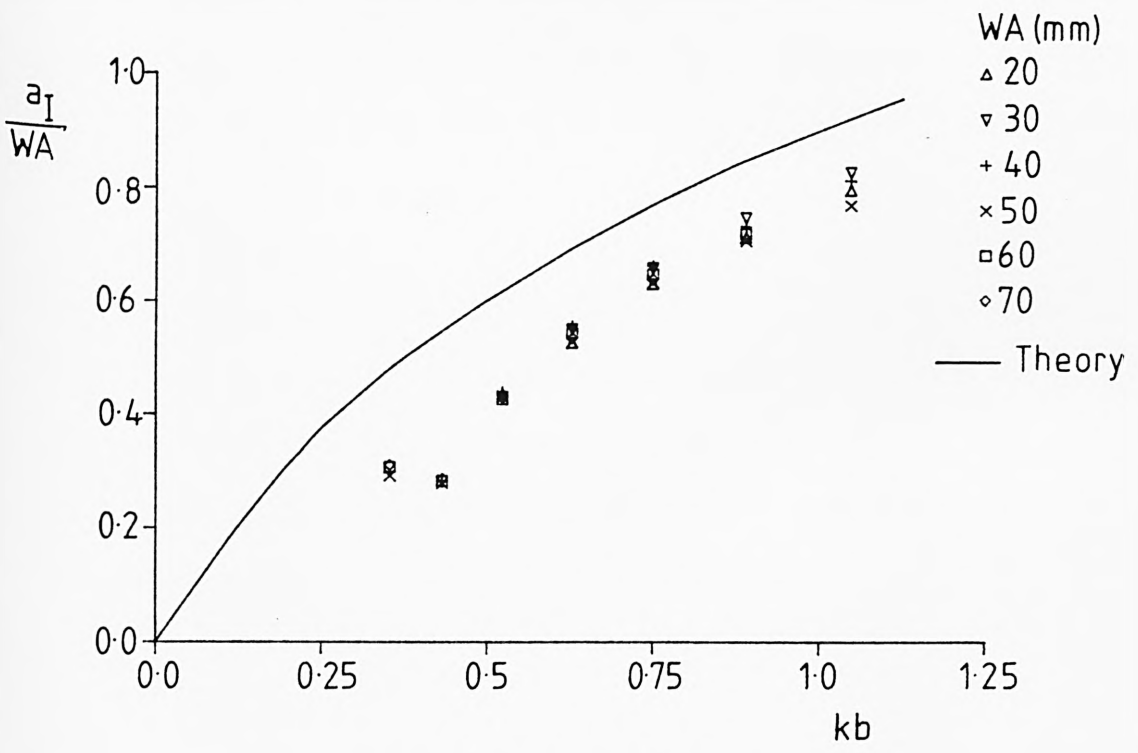

Wave Amplitude Ratio

Figure 5·16

The experimentally determined values of a_I/WA from this study are plotted against kb in Figure 5.16. Also shown is the theoretical curve for a d/b ratio of 1.6, found by interpolation between Wang's curves for d/b of 1.5 and 2.0.

The results show that the theory overestimates the wave amplitude ratio by typically 20%. The discrepancy is worse at lower frequencies, especially at 0.684 Hz, where the measured ratio is almost 50% less than theory. This is due, at least in part, to leakage underneath the wedge causing motion in the water behind it. A similar reduction in the wave amplitude ratio was found by Flick and Guza (1980) for a piston type wavemaker. They found that the wave amplitude ratio was up to 20% less than predicted, until the leaks around the piston were sealed, whereupon the agreement with theory became very good.

Wang's derivation is strictly only applicable to water of infinite depth, but this cannot account for the discrepancy. Theoretical work with circular cylindrical plungers on deep and shallow water by Kim (1969) showed that the wave amplitude becomes greater, rather than smaller, in shallower water.

5.1.2 First Order Reflection

In most cases the first order amplitude envelope was found to conform very well to the expected pattern. The obvious exceptions were those where the waves were unstable and results scattered, as in Figure 5.15.

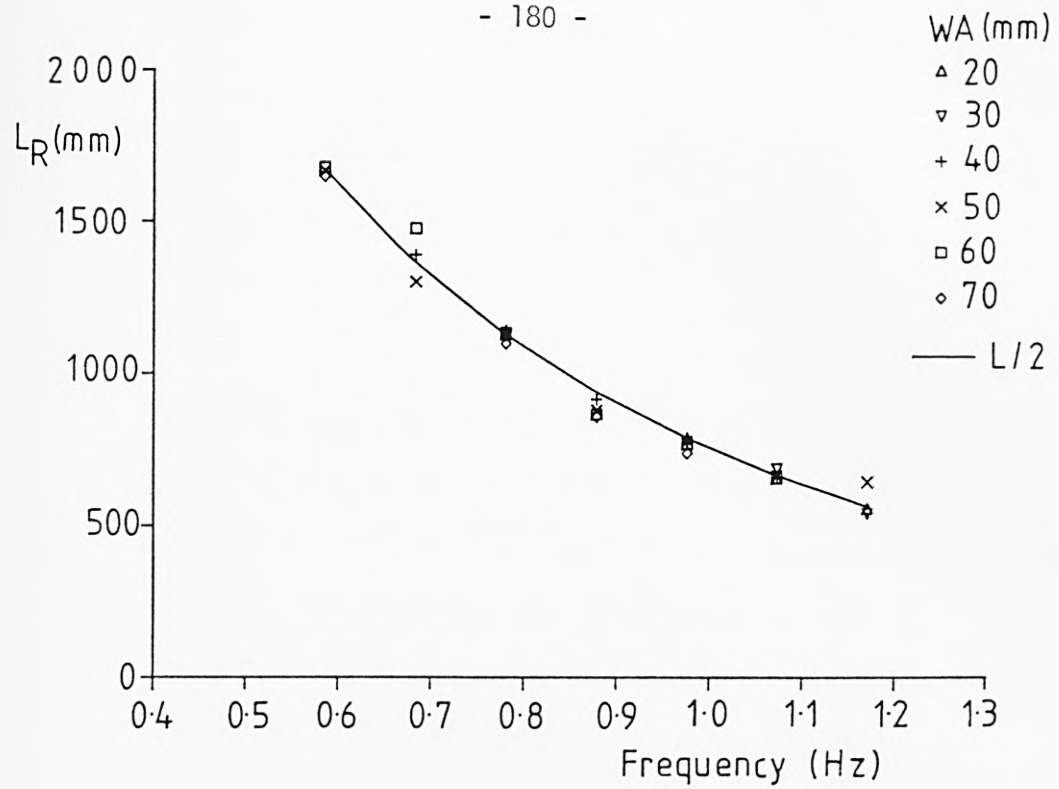

Reflection Beat Wavelength

Figure 5·17

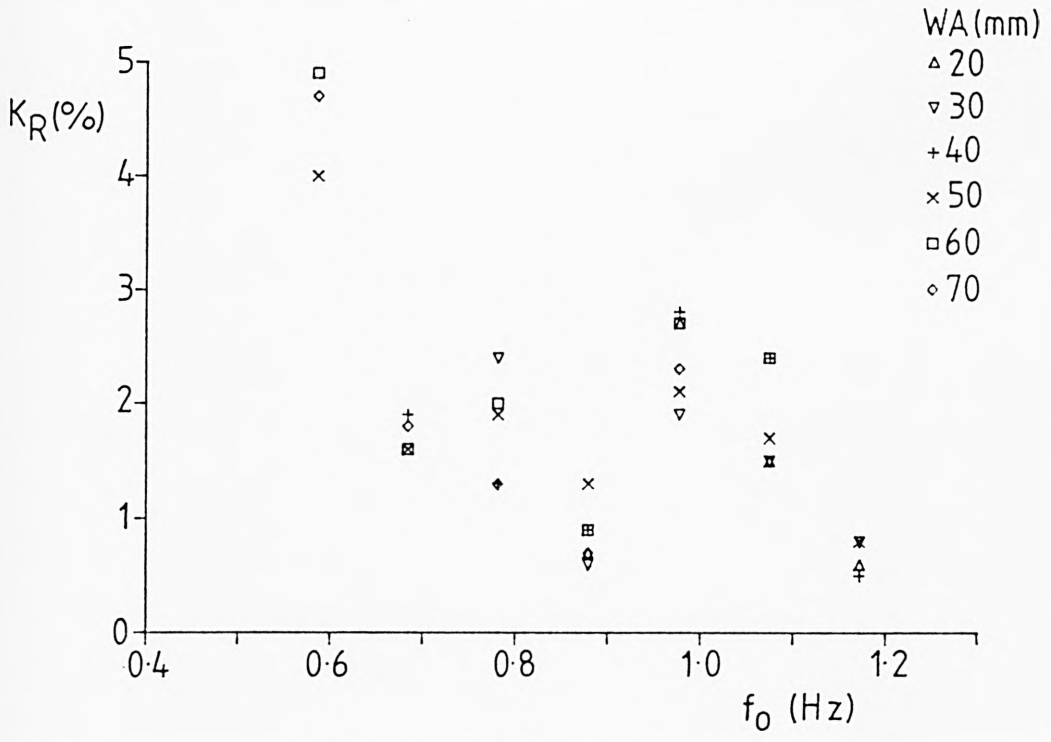

Reflection Coefficient

Figure 5·18

The measured values of the reflection beat wavelength, L_R, are shown in Figure 5.17, and generally agree to within 3% with the theoretical value of L/2.

The measured reflection coefficients, K_R, as given by (3-21) are shown in Figure 5.18. The results show that this beach arrangement is an efficient absorber of wave energy, with no more than 5% of the incident wave amplitude being reflected. There is a general trend for the shorter waves to be reflected less than the longer waves, but the scatter in the results means that the relationship cannot easily be inferred.

The results do not indicate any well defined variation of K_R with the wave steepness. For example, at 0.781 Hz the steepest wave has the lowest reflection coefficient, while the steepest wave at 1.074 Hz has the largest K_R

5.1.3 Second Order Stokes' Wave

The measured amplitude of the second order Stokes' component, a_2, was taken as the mean value of the second order in-phase amplitude in each case, as demonstrated in Figure 4.14. The measured results are compared with the theoretical values, as given by (3-10), in Figure 5.19. This figure is shown in two parts solely for the sake of clarity.

From the plotted results it can be seen that the measured values of a_2 closely follow the theoretical curves, but are on

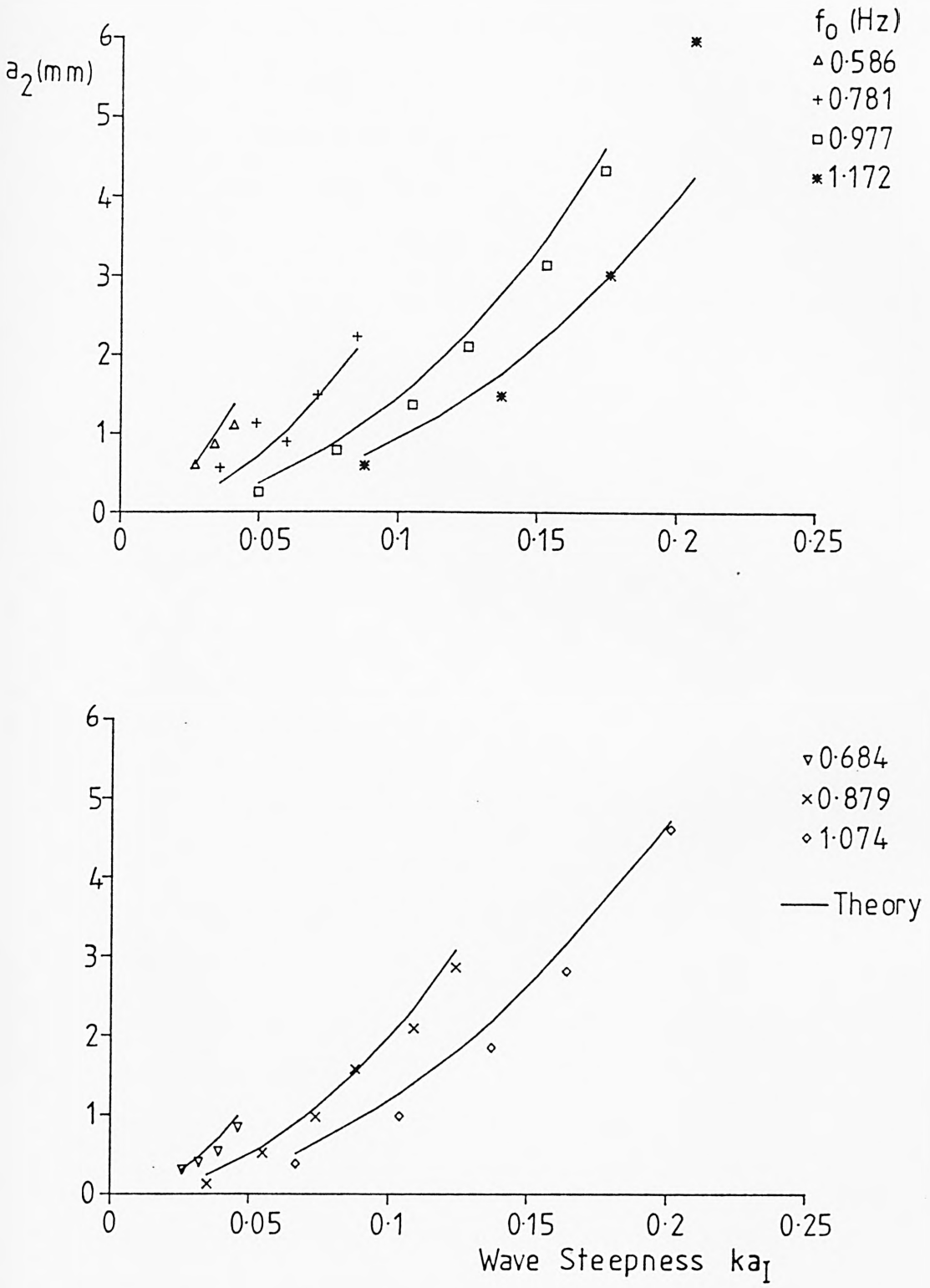

Second Order Stokes' Component

Figure 5.19

average approximately 10% less than predicted. The wave steepness, ka_I, and relative water depth, kh, are not beyond the limits of validity of Stokes' second order wave theory, so the reason for the difference is not clear. It may be indicative of systematic instrumental effects such as a non-linear gain response in one of the amplifier stages. This possibility has not been investigated, and it is noted that the actual magnitude of the discrepancy, being less than 0.5 mm, is less significant when compared with the total wave motion.

In their experiments with a paddle type wavemaker, Buhr Hansen and Svendsen (1974) found a similar order of deviation between the measured and theoretical second order Stokes' components.

5.1.4 Free Second Harmonic Wave

With a few exceptions, the in-phase and quadrature second order amplitude envelopes followed the expected pattern. In some cases, such as in Figures 5.1 to 5.4, the closeness of the fit to the data points was excellent. In others, such as Figures 5.6 and 5.8, the curves were less close to the individual points, but clearly followed their trends.

The two estimates in each case for L_B, a_{22}, L_{2R} and a_{22R} generally differed by only a few percent, meaning that the average value could be taken. The sinusoidal variation in the in phase envelope, due to beating between a_2 and a_{22}, was found to lead that in the quadrature envelope by almost exactly the expected $L_B/4$.

The maximum deviation from this was approximately 50 mm, or 3% of L_B.

As noted in Section 3.1.4, no adequate theory exists to predict the amplitude of the free second harmonic wave produced by a wedge. For this reason, it has only been possible to undertake a comparative study, in which the relative magnitudes of the free wave and the second order Stokes' component have been considered. The ratio a_{22}/a_2, with a_2 given by its theoretical value (3-10), is plotted against the wave steepness in Figure 5.20, from which a number of observations can be made.

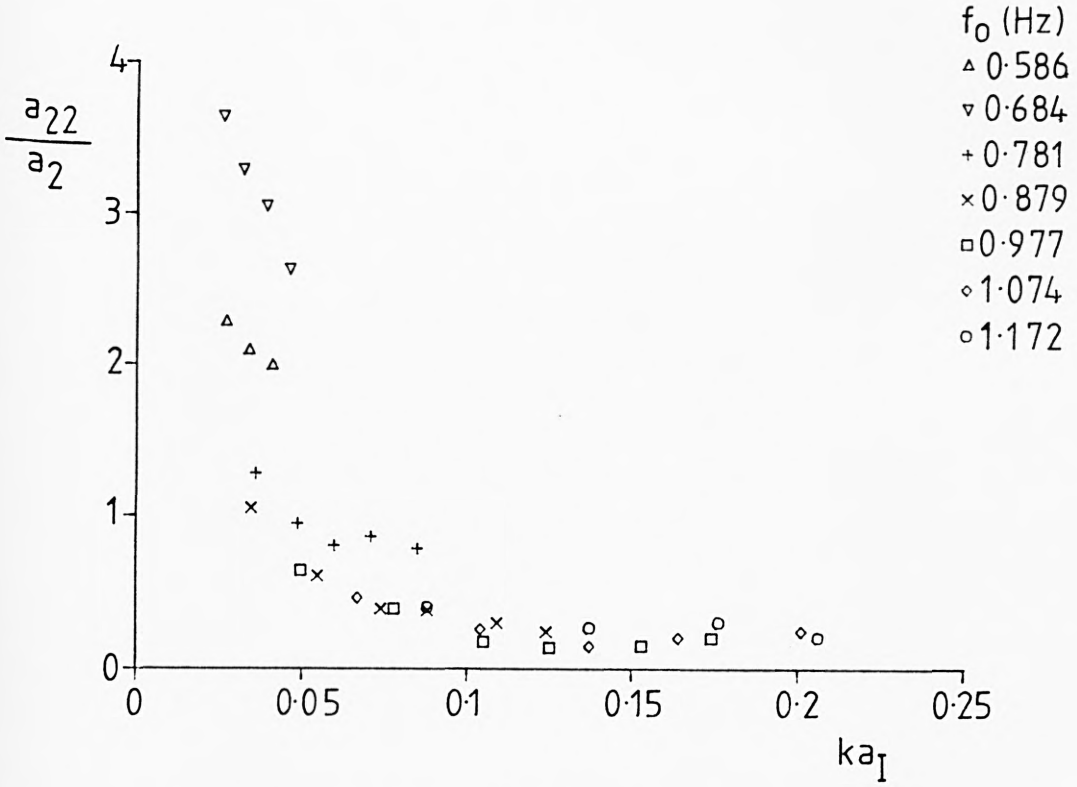

Free Second Harmonic Wave Amplitude

Figure 5.20

At the lower frequencies, particularly at f_o = 0.684 Hz, a_{22} is considerably greater than a_2. This conflicts with the results, both experimental and theoretical, Buhr Hansen and Svendsen (1974) and Madsen (1971), for piston type generators, which showed a_{22} to be always less than a_2. This represents a major disadvantage of wedge type wavemakers, since the free wave is an undesirable feature in most experimentation.

For the less steep waves, the ratio a_{22}/a_2 tends to fall with wave steepness. This is a logical result, since a_{22} is approximately proportional to the wedge amplitude and hence to a_I, while a_2 varies with a_I^2. Finally for the steeper waves, ka_I greater than 0.1, a_{22}/a_2 assumes a near constant value of between 0.15 and 0.25.

5.1.5 Free Wave Celerity

From the measured beat wavelength, L_B, it was possible to calculate the wavelength, and hence the celerity of the free wave.

$$\frac{1}{L_{22m}} = \frac{1}{L/2} - \frac{1}{L_B} \qquad (5\text{-}2)$$

$$C_{22m} = L_{22m} \times 2f_o \qquad (5\text{-}3)$$

These results were compared with the theoretical dispersion celerity, C_{22t}, given by (3-18). The ratio C_{22m}/C_{22t} is plotted against wave steepness, ka_I, in Figure 5.21.

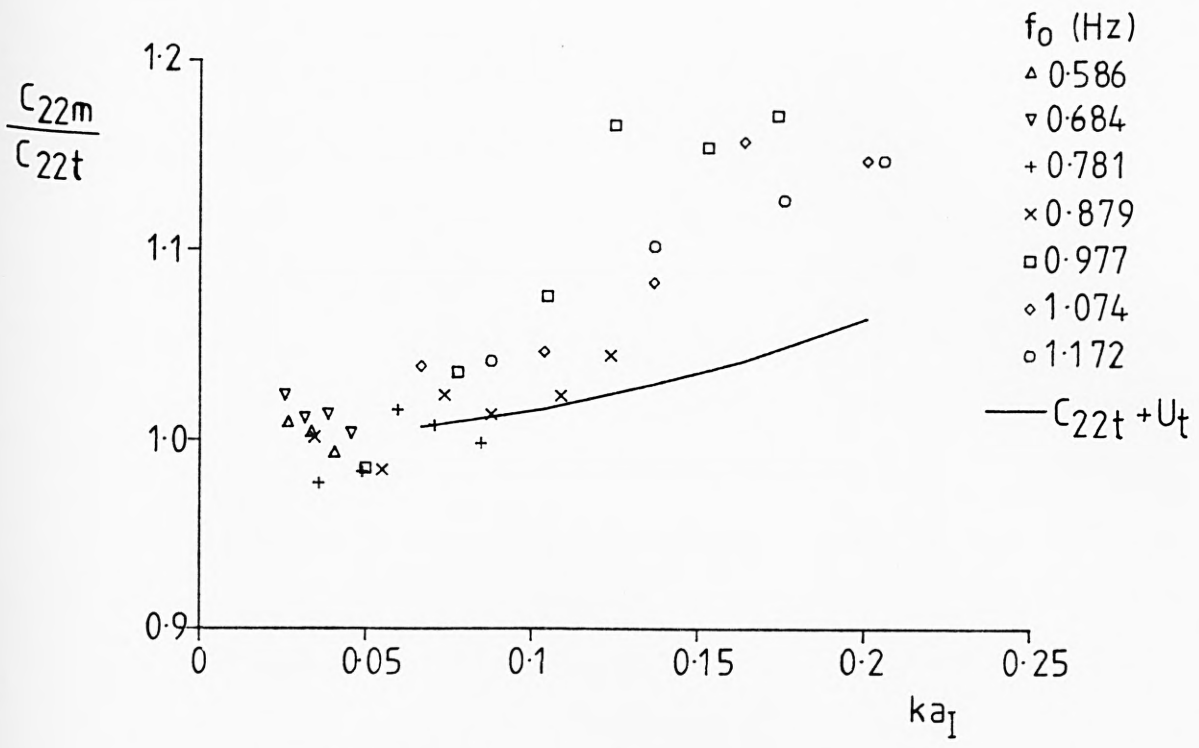

Free Wave Celerity

Figure 5.21

Although there is some scatter in the results, the free wave tends to travel faster than theoretically predicted, increasingly with wave steepness. This effect is borne out by the findings of Buhr Hansen and Svendsen (1974), who observed a similar increase in the celerity of the free wave produced by a piston. It is almost certainly due to the much larger wave through which the free wave travels. It would seem that the free wave is being carried along by the main wave to some extent, rather than travelling totally independently through it.

One possible explanation for this is the phenomenon of mass transport, as discussed in Section 3.1.3. The free wave activity is mainly in the surface region, thus the frame of reference through which it travels is subject to a net drift velocity, U_t (3-14). Assuming a simple superposition, the free wave can be considered to travel with a celerity equal to $C_{22t} + U_t$. The ratio $(C_{22t} + U_t)/C_{22t}$ has been calculated and is also shown in Figure 5.21. For clarity, only the curve for one typical fundamental frequency, f_o = 1.074 Hz, is shown, but the other curves all lie very close to this. Clearly the mass transport effect accounts for some, but not all, of the additional celerity of the free second harmonic wave.

A further explanation may be the effect which the main wave has on the surface boundary conditions applied to the free wave. In the linear solution for the free wave (3-16) and (3-17), the wave amplitude is assumed to be small and the surface boundary conditions are applied at the still water level, y=0. However, these assumptions can hardly be justified in the presence of the large surface displacement, η, and slope $\frac{\partial \eta}{\partial x}$, of the main wave.

5.1.6 Second Order Reflection

The presence of a second harmonic reflected wave is apparent from the additional terms in the second order waveform variations, Figures 5.1 to 5.15. The closeness of the fit in some cases, such as Figure 5.1, implies a higher degree of confidence in the measured values of a_{22R} and L_{2R}, than in those cases where the fit is not so good, e.g. Figure 5.12. In a very few cases, of which Figure 5.10

is an example, no beating effect due to reflected second harmonic waves was apparent, and the additional terms in the sine fitting are meaningless.

The equivalent second order reflection coefficients, defined by a_{22R}/a_{22} are shown in Figure 5.22. Their values, being typically between 30 and 40% are very large in comparison to the first order values of 1 to 5%. The reflected second harmonic waves are very probably due, not only to reflection of incident second harmonic components, but also the mechanism of the interaction between the beach and the first order waves.

The second order reflection beat wavelengths, L_{2R}, are shown in Figure 5.23, and compared with the theoretical value as given by;

$$\frac{1}{L_{2R}} = \frac{1}{L/2} + \frac{1}{L_{22}} \qquad (5\text{-}4)$$

The measured beat wavelengths agree very well with theory at the two lowest frequencies, but tend to be somewhat longer at the higher frequencies. The worst case of this is at a fundamental frequency of 0.781 Hz, where L_{2R} measured is 50% greater than theory. One possible explanation for this, that the reflected second harmonic wave travels 'locked-in' with the first order reflected wave, is implausible in view of the very small values of a_R. The second order Stokes' component associated with a_R would have an insignificant amplitude equal to $(k_R)^2 a_2$.

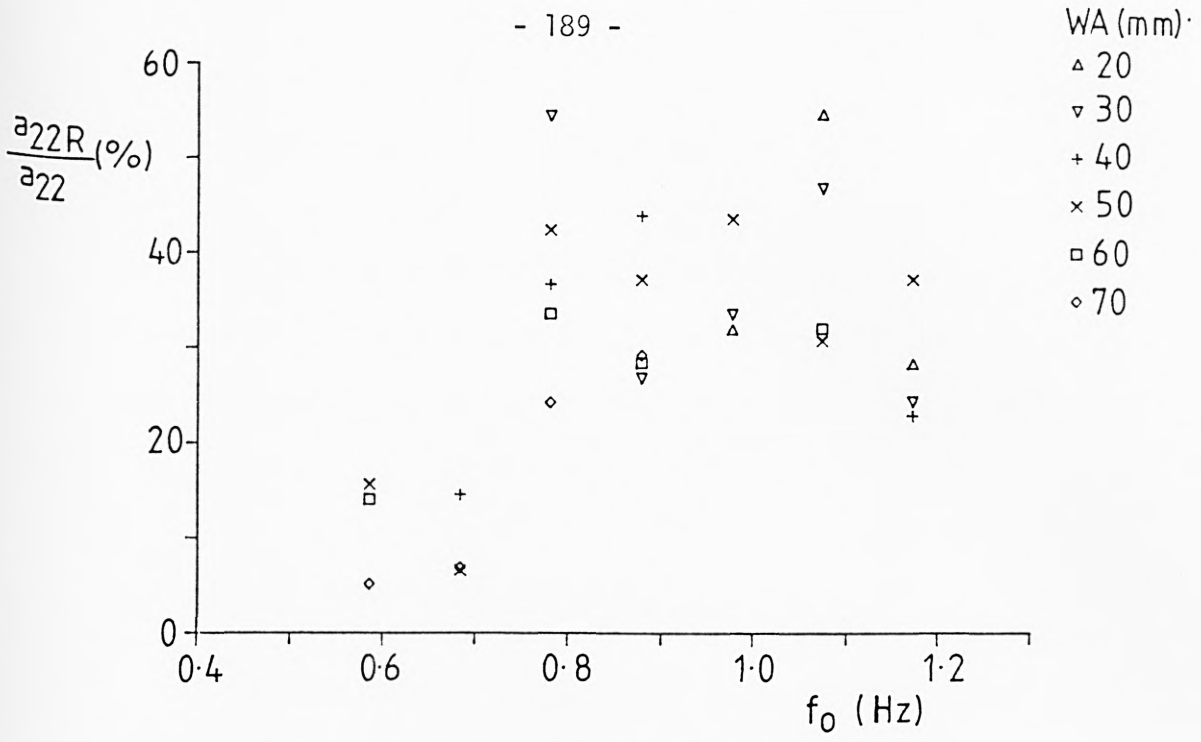

Second Order Reflection Coefficient

Figure 5·22

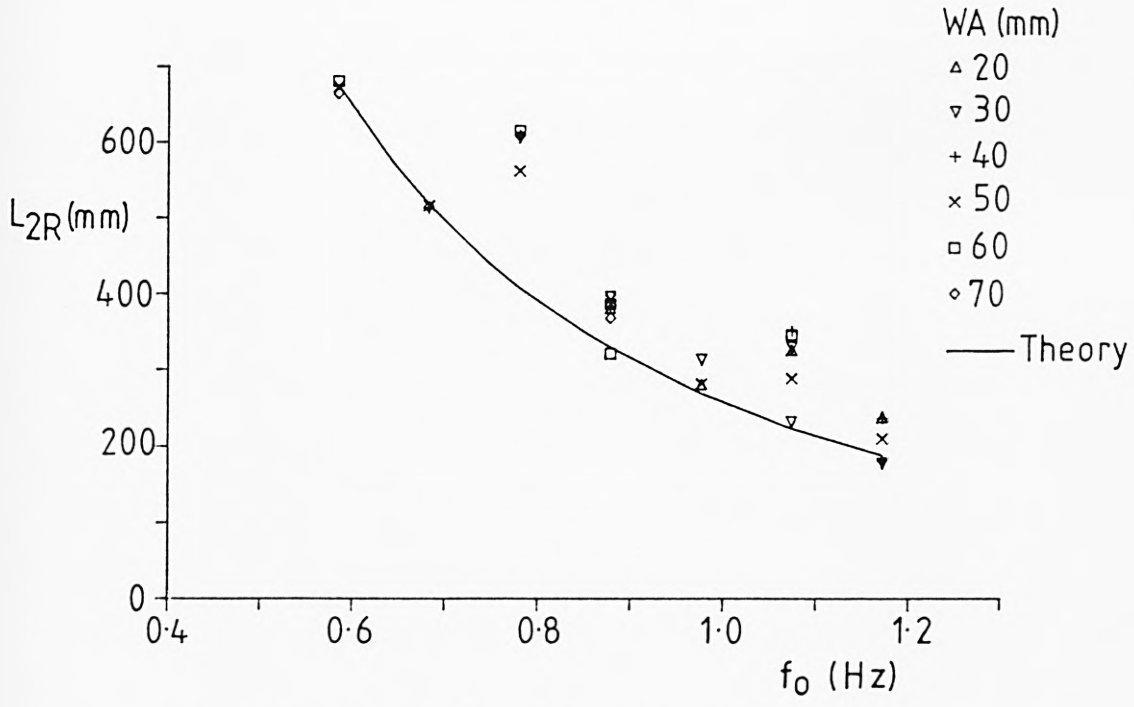

Second Order Reflection Wavelength

Figure 5·23

Referring to the tabulated results, Table 5.1, it can be seen that a_{22R} generally constitutes less than 1% of the total wave motion. In view of this, and of the uncertainties mentioned above, the reflected harmonic wave is neglected in the discussion of the wave cylinder interaction, in the remainder of this Chapter.

5.1.7 Wave Environment Around Test Cylinders

The waveform variations observed with the test cylinders in place were essentially of the same form as those without. There were, however, a few noticeable differences.

The wave amplitude, a_I, tended to reach a high maximum just upstream of the cylinder, and fall to an extreme low just downstream, as shown in Figure 5.24. This demonstrates the effect of the cylinder on the velocity potential under the wave, with the local high and low representing the exponentially decaying term of Havelock (1929).

A further effect of the cylinder on the wave is clearly visible in the first order variation in Figure 5.25. The wave amplitude is considerably reduced as it passes the cylinder. This is due to the energy lost by the wave in exerting the forces on the cylinder, and represents the blockage effect of the cylinder in the finite width of the flume. Quantitatively, a_I was found to be as much as 2% lower downstream of the cylinder than upstream.

Neither of these effects was accounted for in the analysis of the wave loading, and the waves were assumed to be described by

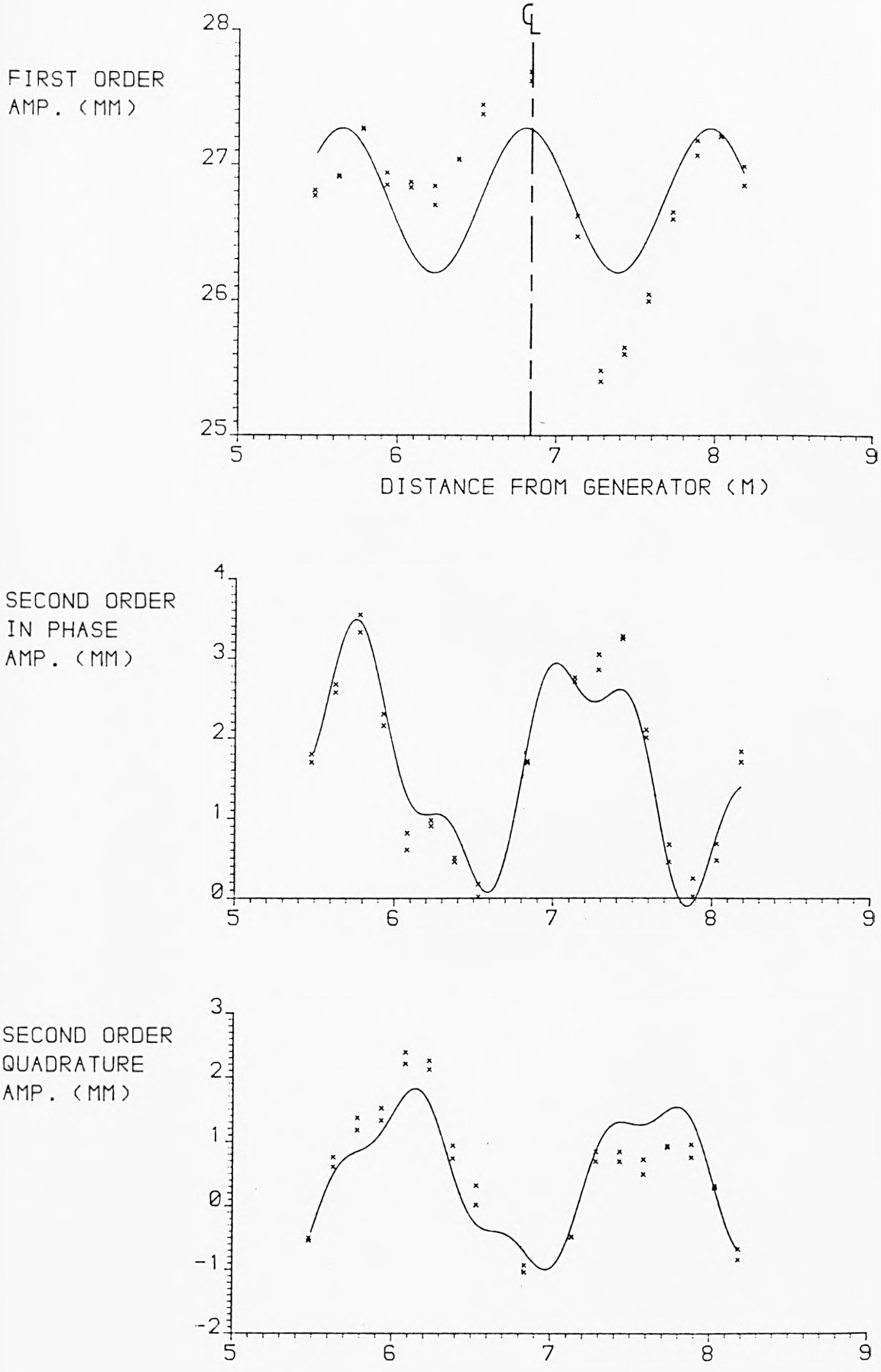

WAVEFORM VARIATION: WEDGE AMP. 60.0MM; FREQ. 0.781HZ
READINGS TAKEN AROUND 9.55 MM CYLINDER

Figure 5.24

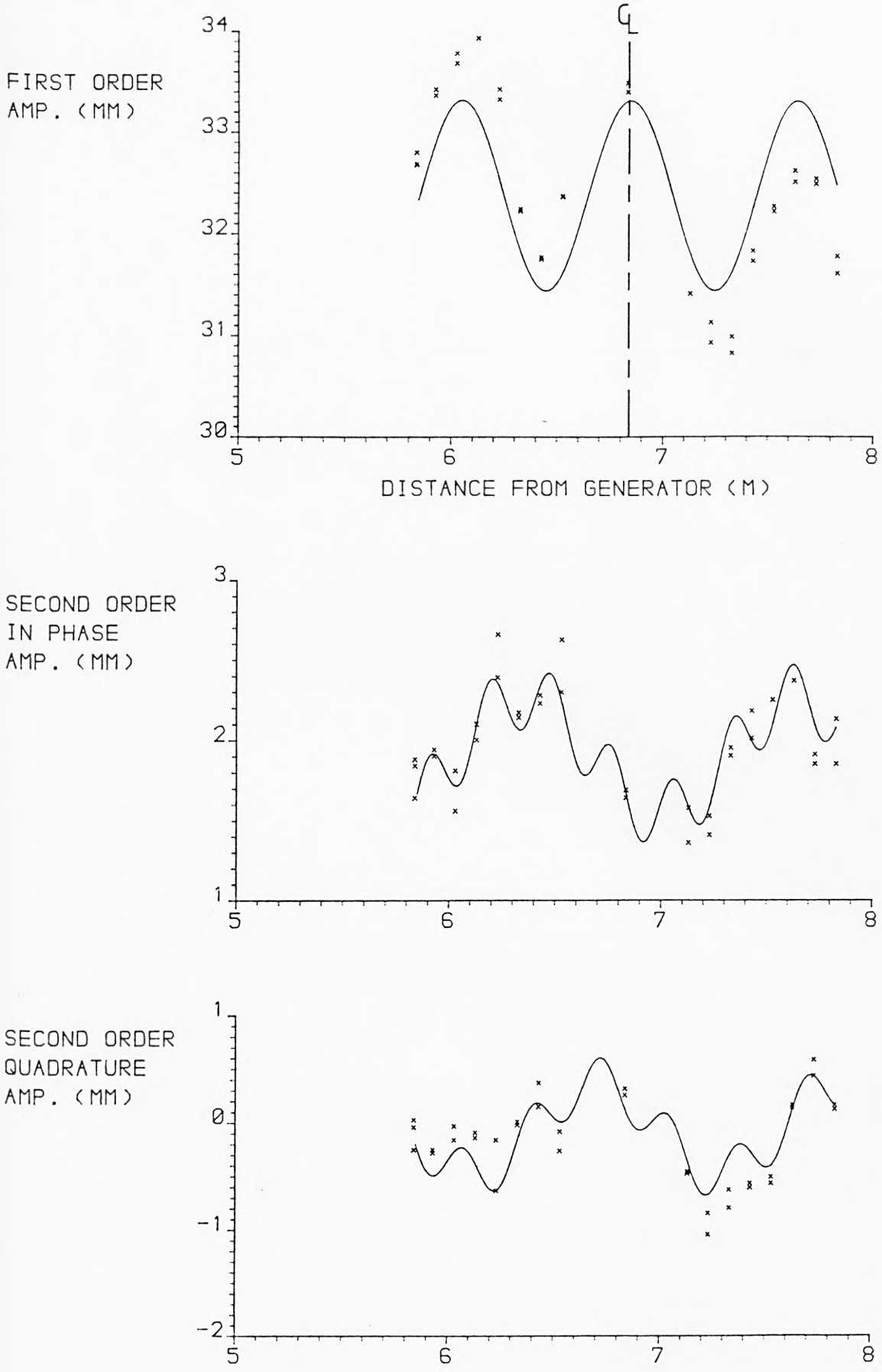

WAVEFORM VARIATION: WEDGE AMP. 50.0MM; FREQ. 0.977HZ
READINGS TAKEN AROUND 33.56 MM CYLINDER

Figure 5.25

Wave Setting		a_I(mm)			a_R(mm)			α (rads)			a_{22}(mm)			β (rads)		
WA(mm)	Freq(Hz)	(9.55)	(21.45)	(33.56)	(9.55)	(21.45)	(33.56)	(9.55)	(21.45)	(33.56)	(9.55)	(21.45)	(33.56)	(9.55)	(21.45)	(33.56)
50	0.586	16.81	17.12	17.11	0.79	0.87	0.91	0.95	0.95	0.85	1.96	2.09	2.09	-0.74	-0.83	-0.76
60	0.586	21.00	21.03	21.16	1.19	1.26	1.32	0.96	0.82	0.79	3.02	3.12	3.17	-0.79	-0.77	-0.71
70	0.586	24.82	25.08	25.00	1.53	1.61	1.62	0.93	0.95	0.96	3.68	3.76	3.79	-0.84	-0.88	-0.95
50	0.684	13.65	13.77	13.83	0.30	0.15	0.22	2.70	2.17	1.99	1.39	1.34	1.34	2.46	2.42	2.55
40	0.781	17.46	17.46	17.53	0.15	0.17	0.22	-0.22	-0.19	-0.04	0.58	0.53	0.58	4.44	4.42	4.48
50	0.781	22.01	22.44	22.12	0.35	0.42	0.39	-0.15	-0.39	0.00	0.97	0.96	1.05	4.76	-1.30	4.67
60	0.781	26.73	26.61	26.72	0.53	0.61	0.57	0.15	0.03	0.14	1.30	1.41	1.38	4.71	4.67	4.74
50	0.879	27.68	27.77	28.19	0.35	0.41	0.46	2.37	2.33	2.00	0.58	0.45	0.52	0.79	0.59	0.73
30	0.977	19.40	19.49	19.27	0.56	0.54	0.56	0.14	0.02	0.27	0.45	0.32	0.37	4.69	-0.95	-1.31
40	0.977	25.51	25.81	25.64	0.81	0.92	0.91	0.25	-0.16	0.05	0.44	0.24	0.26	4.30	3.73	4.14
50	0.977	32.61	32.41	32.37	0.88	0.95	0.94	-0.35	-0.43	-0.12	0.35	0.33	0.40	2.54	2.78	2.30
40	1.074	-	29.10	29.03	-	0.57	0.58	-	-0.56	-1.00	-	0.37	0.49	-	-0.86	-0.68
50	1.074	36.64	-	-	0.84	-	-	-1.18	-	-	0.91	-	-	1.35	-	-
20	1.172	16.62	16.76	16.95	0.18	0.26	0.30	-0.90	0.18	0.33	0.30	0.24	0.25	0.77	1.18	1.27
30.	1.172	24.44	24.58	24.54	0.30	0.39	0.33	0.03	0.21	0.24	0.56	0.50	0.57	3.36	3.27	3.82
40	1.172	31.90	31.70	32.12	0.33	0.36	0.38	4.11	4.34	-1.24	0.81	0.74	0.82	4.24	4.51	3.83

Cylinder Diameters (in brackets) in mm.

Waveform Results - Test Cylinders in Place

Table 5.2

the sine curves, as shown in Figures 5.24 and 5.25.

The full waveform results with the test cylinders in place are given in Table 5.2. Significant differences were recorded in the amplitudes and phases of the wave components under nominally identical wave conditions. This is symptomatic of the lack of repeatability noted in Section 4.5, and explains the need for a separate waveform run on every test.

5.2 Wave Loading Results

5.2.1 Wave and Force Time Variations

A number of the records taken from the wave probe and force transducers are presented graphically in Figures 5.26 to 5.37. The data is presented in an uncalibrated form, so that the shapes, but not the amplitudes, of the time variations are discernable. In those cases where the force transducer outputs were filtered, Figures 5.26 to 5.28, the traces have been corrected for the time delay only, by a simple shift along the time axis.

The relative importance of the drag and inertia forces is apparent from the phase differences between the wave and force traces. Where the Keulegan Carpenter number is relatively high, as in Figures 5.26 and 5.29, the force is approximately in phase with the wave profile indicating the dominance of drag loading. Conversely, at lower values of KCI, Figures 5.36 and 5.37, the force traces lead

the wave by almost $\pi/2$, indicating inertia dominance. In almost every case the bottom force fractionally leads the top force. This demonstrates that the inertia force has a greater resultant depth of action than the drag force, consistent with the results in Table 3.1.

The waterline force can be seen in the top transducer traces in Figures 5.29, 5.30, 5.32, 5.33, 5.36 and 5.37. For the 9.55 mm cylinder, Figures 5.29 and 5.30, the waterline force is dominated by FWD and the force traces show good agreement with the theoretical result of Figure 3.11. The inertia waterline force is evident in Figures 5.36 and 5.37, where the force traces follow the pattern of Figure 3.12. The waterline force on the 21.45 mm cylinder, Figures 5.32 and 5.33, is a combination of FWD and FWI.

The effect of the free second harmonic wave is shown in Figures 5.31, 5.34 and 5.35. In Figure 5.34, the free wave has a very noticeable effect on the observed wave profile as well as on the force traces. The importance of the phase of the free wave is demonstrated in Figure 5.31, where the force traces have flattened peaks and sharpened troughs. This effect is in contrast to the generally expected second order forces, and agrees with the predicted result of Figure 3.20. In Figure 5.35 the free wave forces and the waterline forces reinforce each other to give a pronounced effect on the force traces.

An important feature of the wave loading mechanism on a very small cylinder - vortex shedding - is visible in Figures 5.26 and 5.28.

In Figure 5.26, the Keulegan Carpenter number is high, particularly in the surface region, and the top transducer trace shows evidence of the shedding of 3 or 4 vortices in each wave cycle. The shedding of a vortex as a wave crest passes the cylinder can have a marked effect on the shape of the force traces, as demonstrated in Figure 5.28. This reduces the apparent phase difference between the wave profile and force trace and influences the measured values of the drag and inertia coefficients.

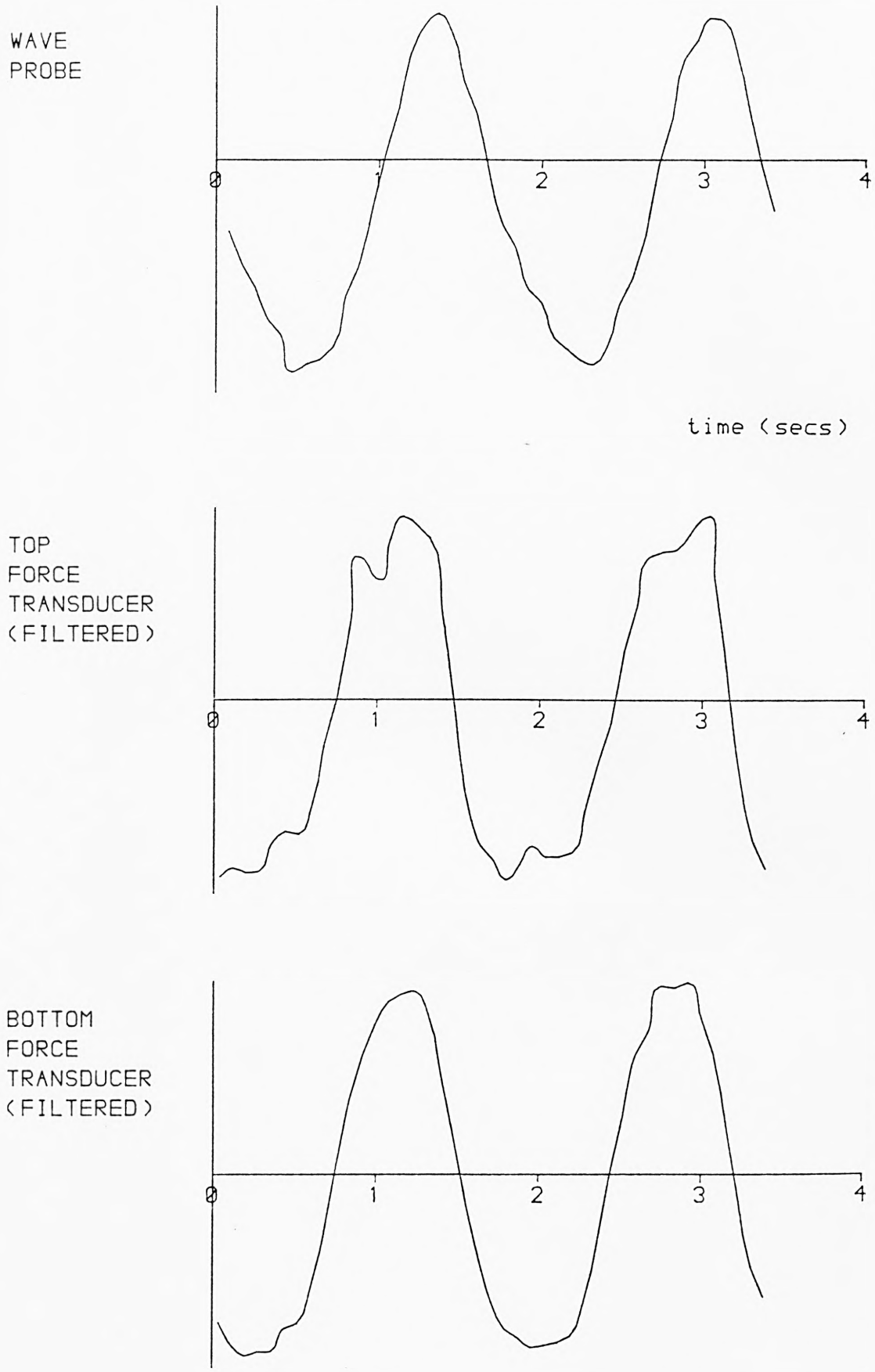

OUTPUT FROM WAVE PROBE AND FORCE TRANSDUCERS
LOADING ON 9.55 MM CYLINDER
WAVE CONDITIONS: WEDGE AMP. 50.0 MM, FREQ. .586 HZ

Figure 5.26

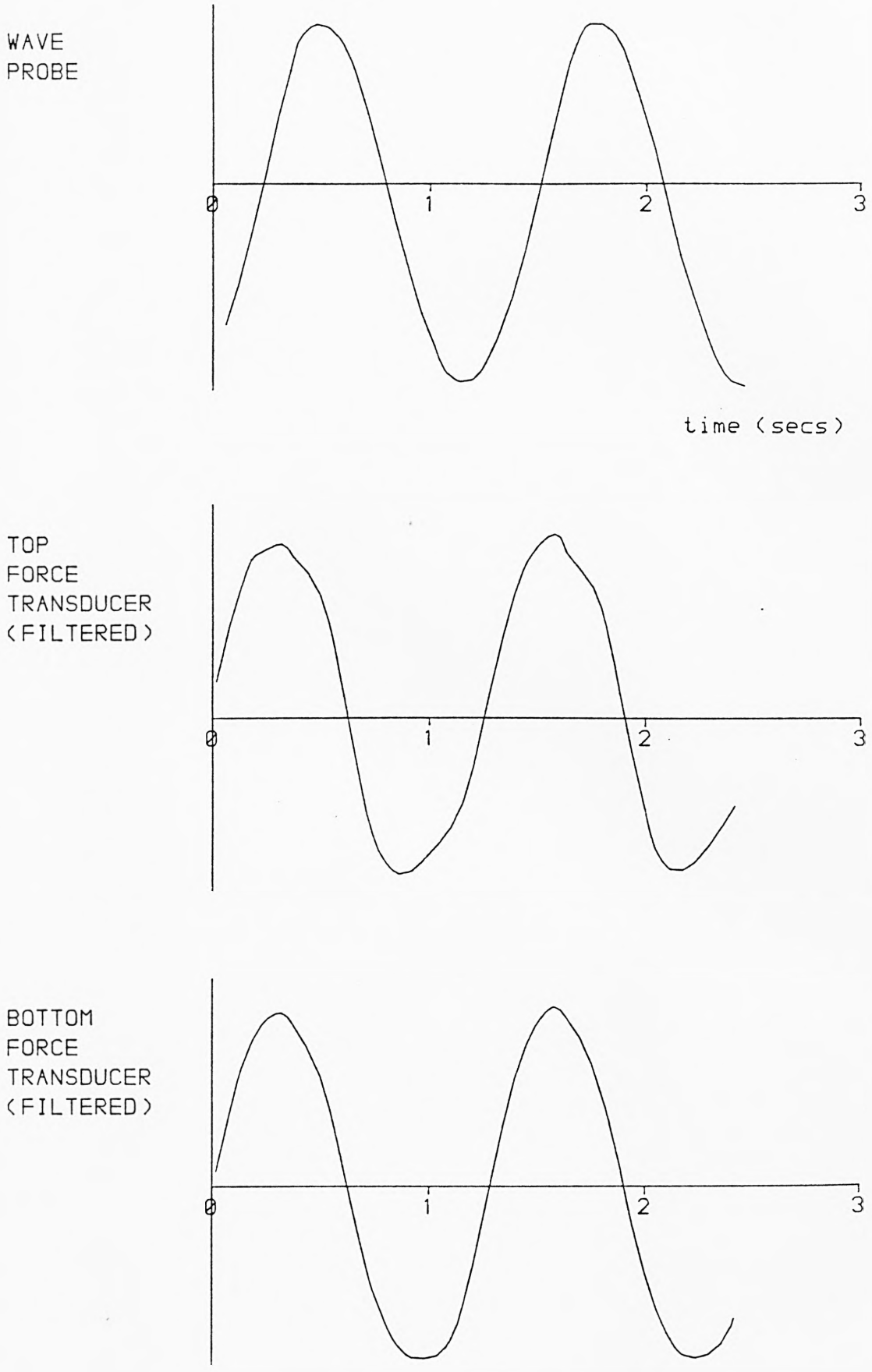

OUTPUT FROM WAVE PROBE AND FORCE TRANSDUCERS
LOADING ON 9.55 MM CYLINDER
WAVE CONDITIONS: WEDGE AMP. 40.0 MM, FREQ. .781 HZ

Figure 5.27

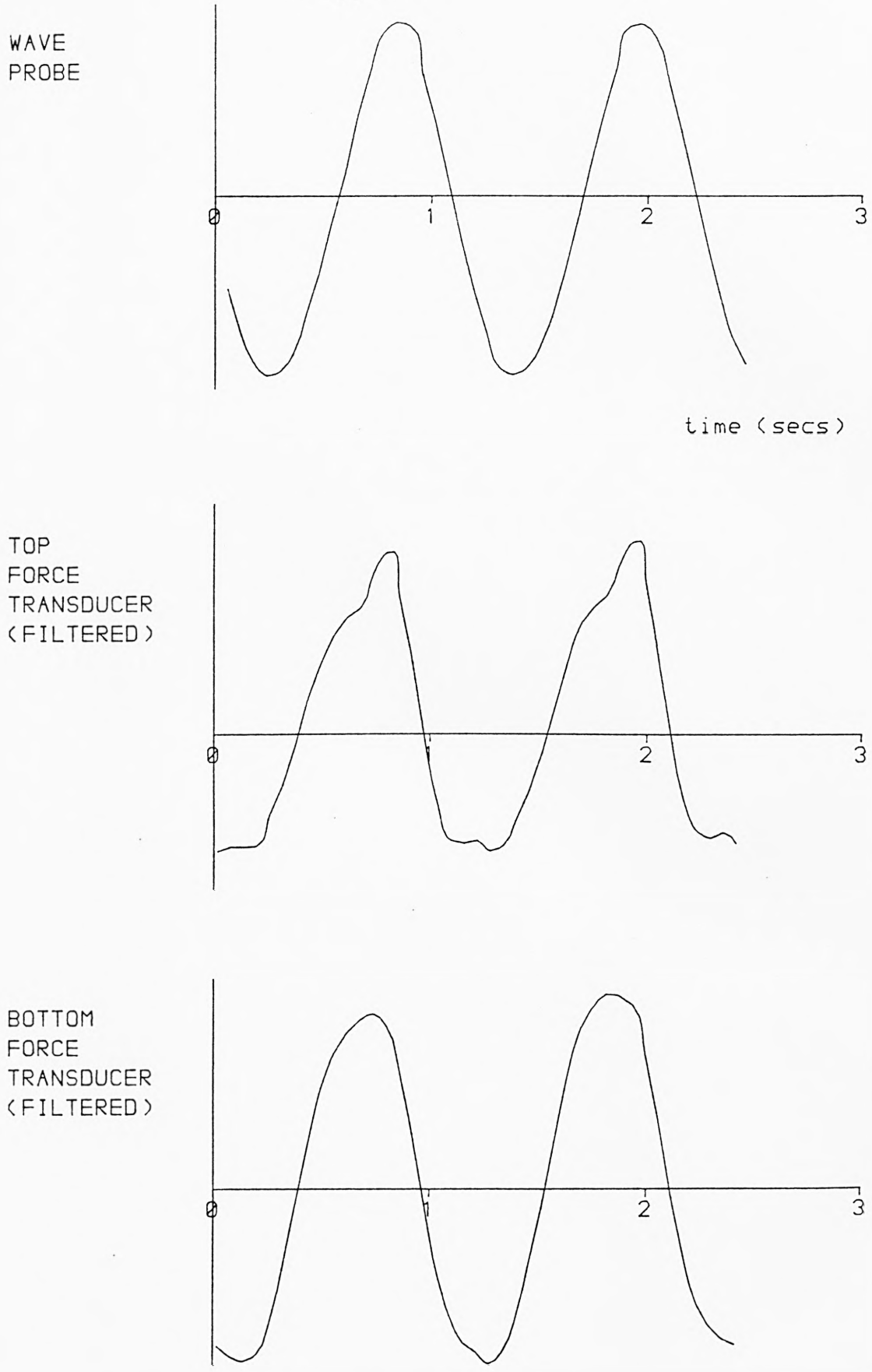

OUTPUT FROM WAVE PROBE AND FORCE TRANSDUCERS
LOADING ON 9.55 MM CYLINDER
WAVE CONDITIONS: WEDGE AMP. 50.0 MM, FREQ. .879 HZ

Figure 5.28

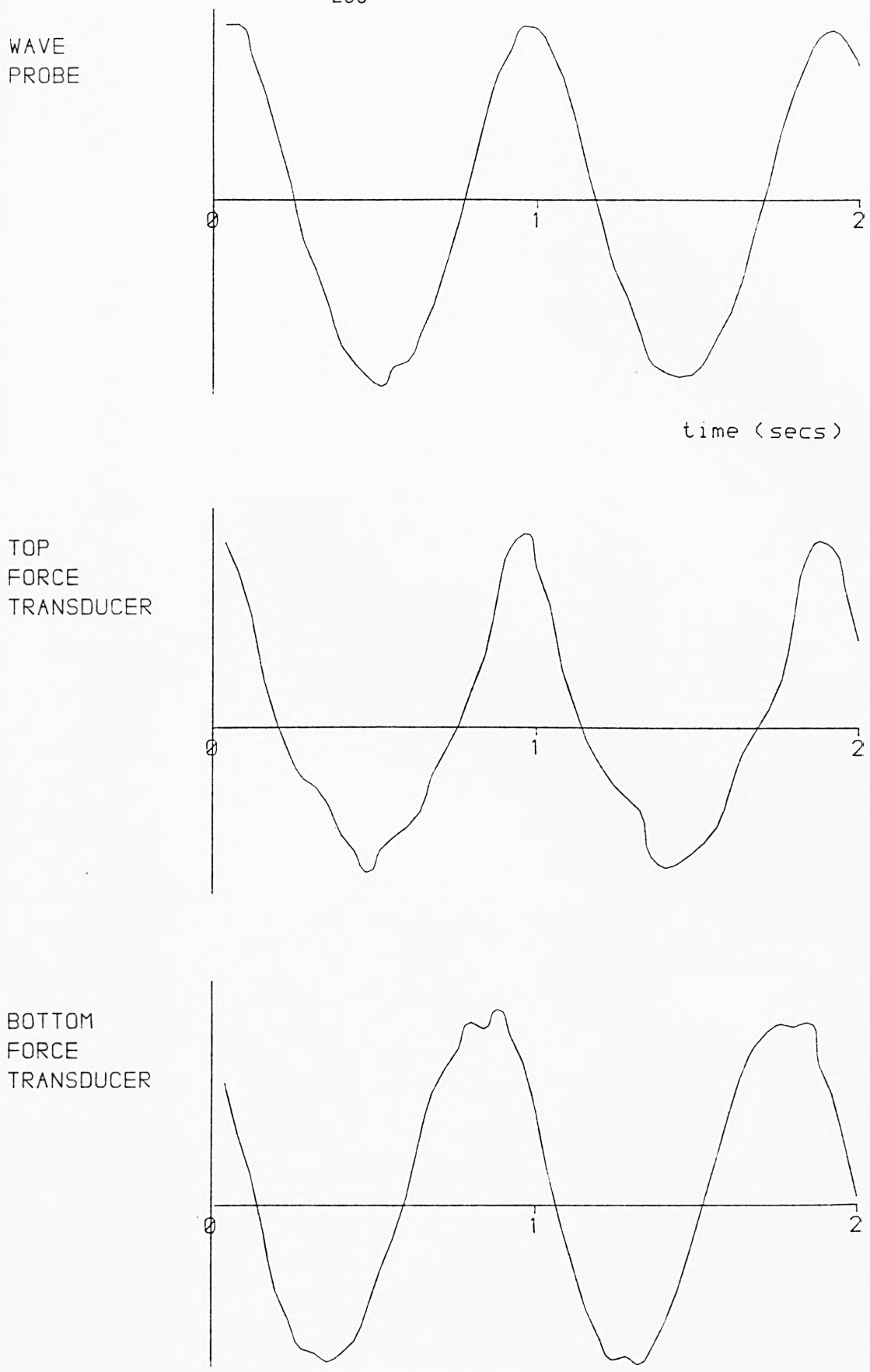

OUTPUT FROM WAVE PROBE AND FORCE TRANSDUCERS
LOADING ON 9.55 MM CYLINDER
WAVE CONDITIONS: WEDGE AMP. 50.0 MM, FREQ. 1.074 HZ

Figure 5.29

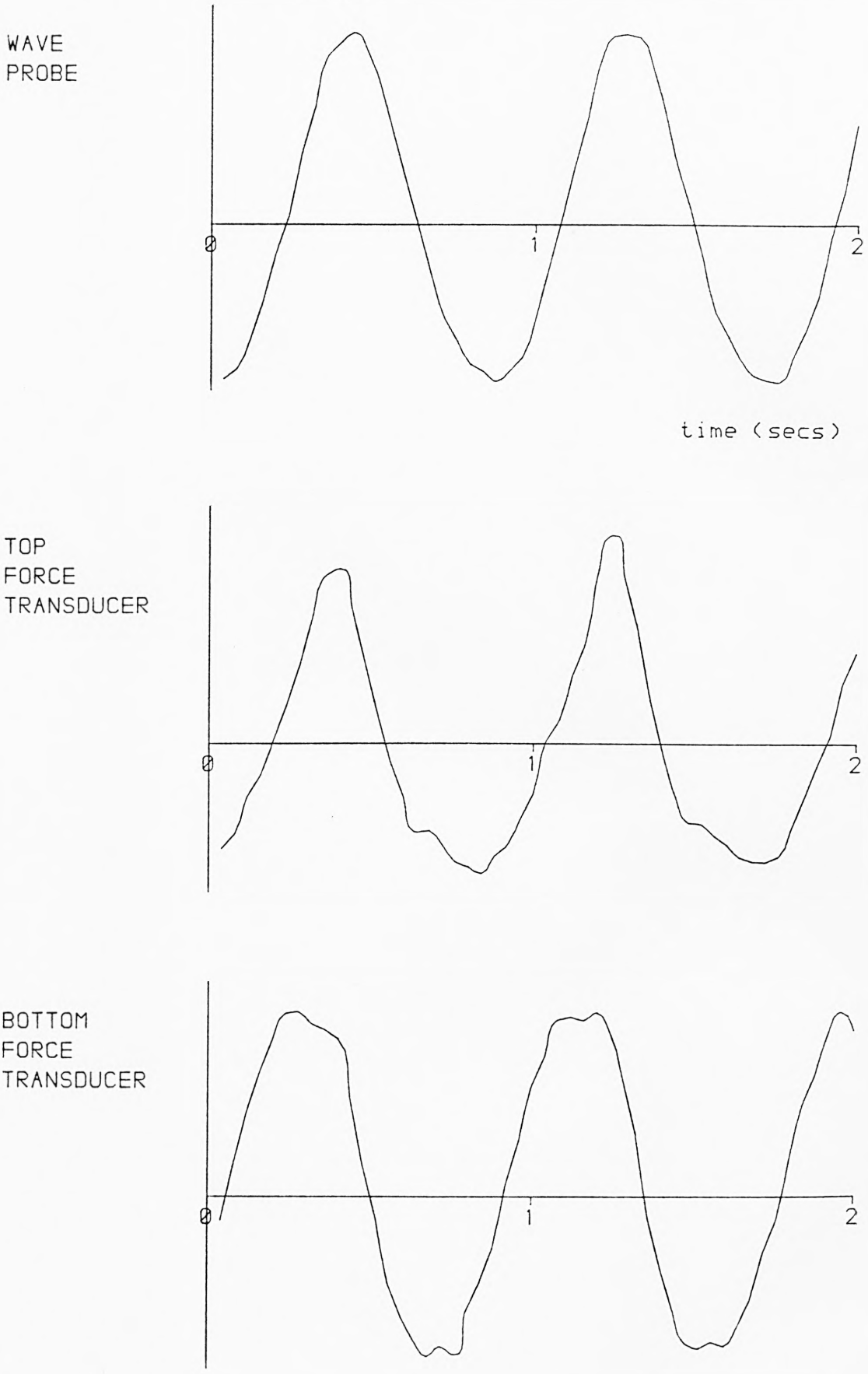

OUTPUT FROM WAVE PROBE AND FORCE TRANSDUCERS
LOADING ON 9.55 MM CYLINDER
WAVE CONDITIONS: WEDGE AMP. 40.0 MM, FREQ. 1.172 HZ

Figure 5.30

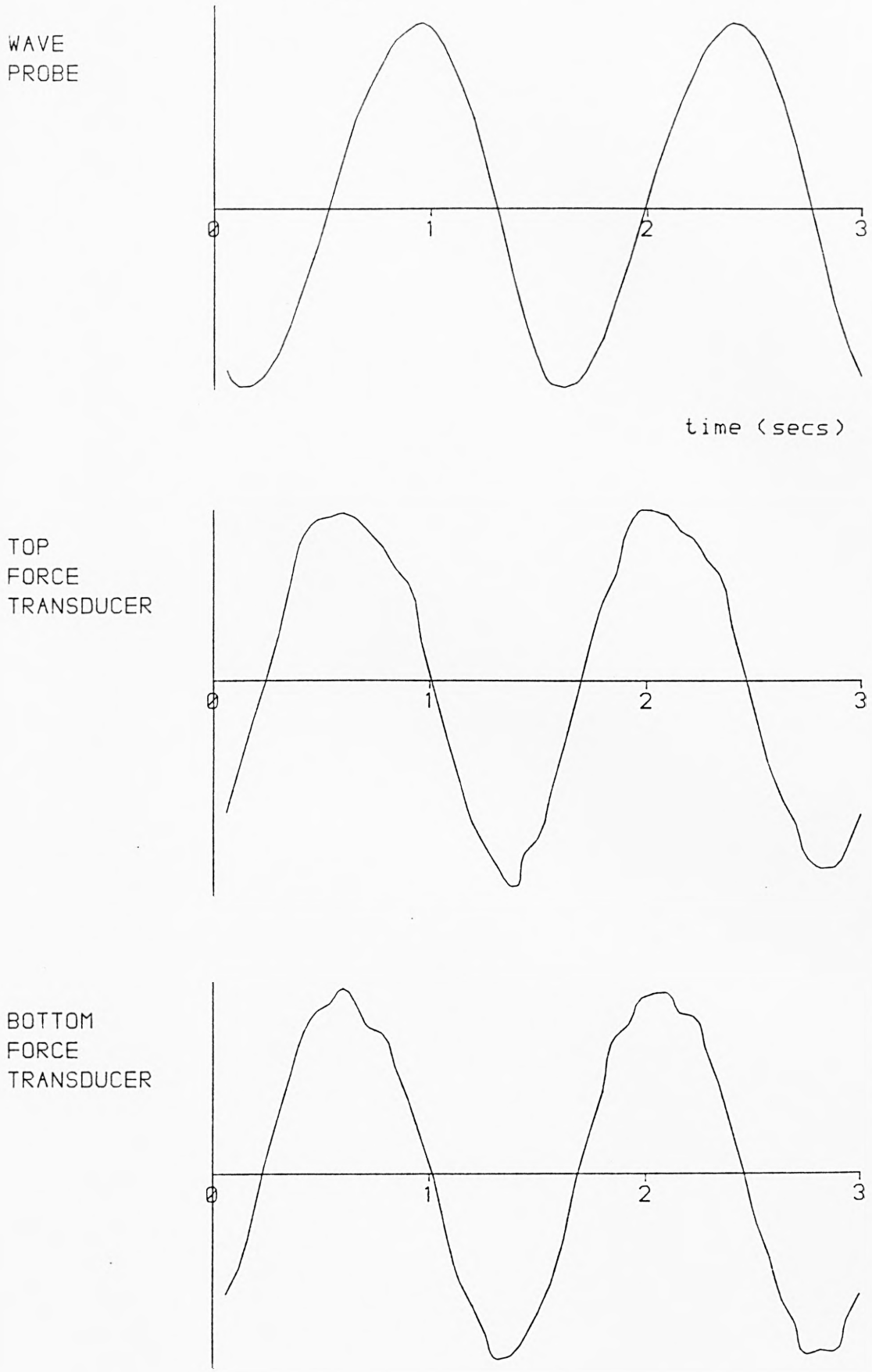

OUTPUT FROM WAVE PROBE AND FORCE TRANSDUCERS
LOADING ON 21.45 MM CYLINDER
WAVE CONDITIONS: WEDGE AMP. 50.0 MM, FREQ. .684 HZ

Figure 5.31

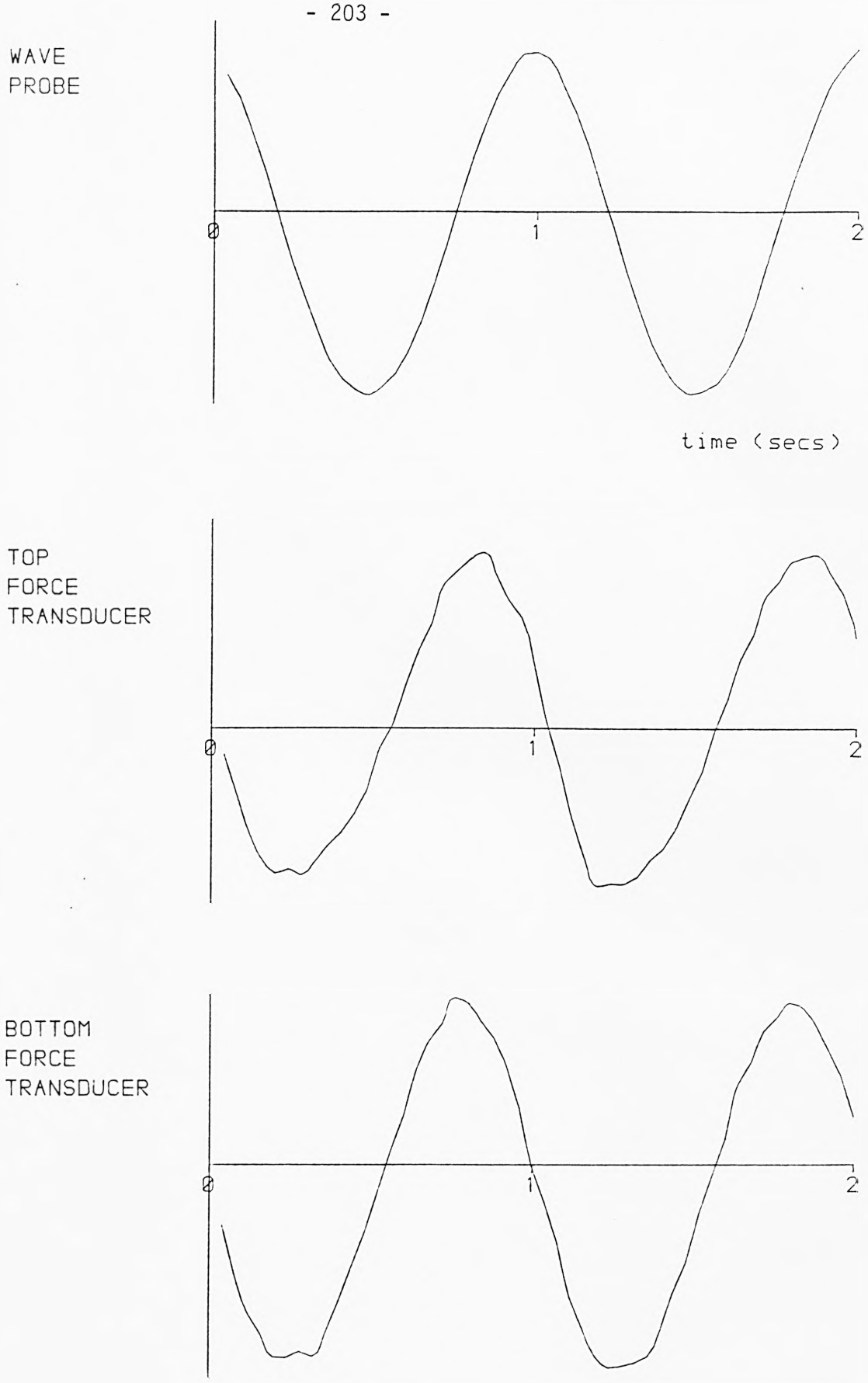

OUTPUT FROM WAVE PROBE AND FORCE TRANSDUCERS
LOADING ON 21.45 MM CYLINDER
WAVE CONDITIONS: WEDGE AMP. 40.0 MM, FREQ. .977 HZ

Figure 5.32

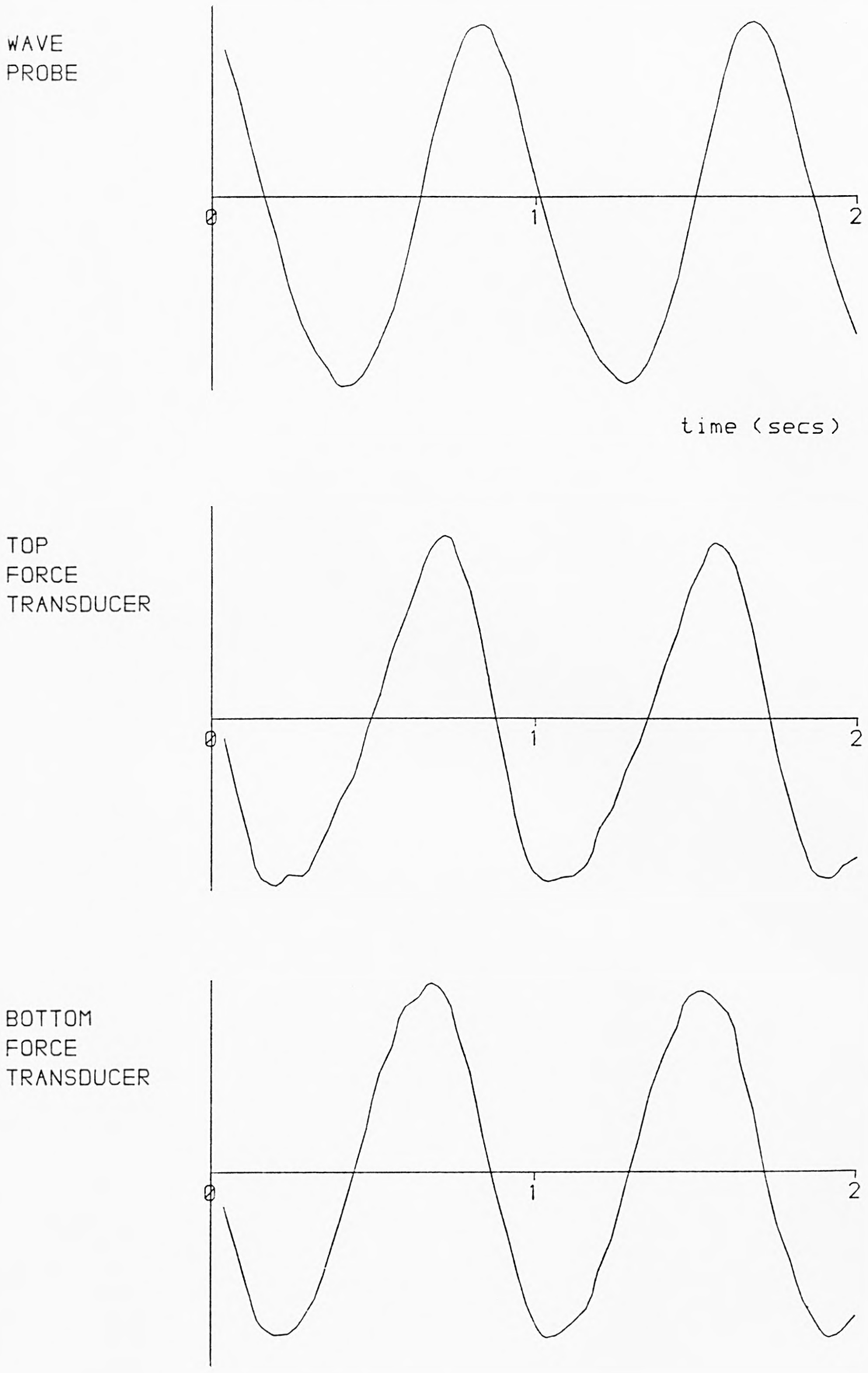

OUTPUT FROM WAVE PROBE AND FORCE TRANSDUCERS
LOADING ON 21.45 MM CYLINDER
WAVE CONDITIONS: WEDGE AMP. 40.0 MM, FREQ. 1.172 HZ

Figure 5.33

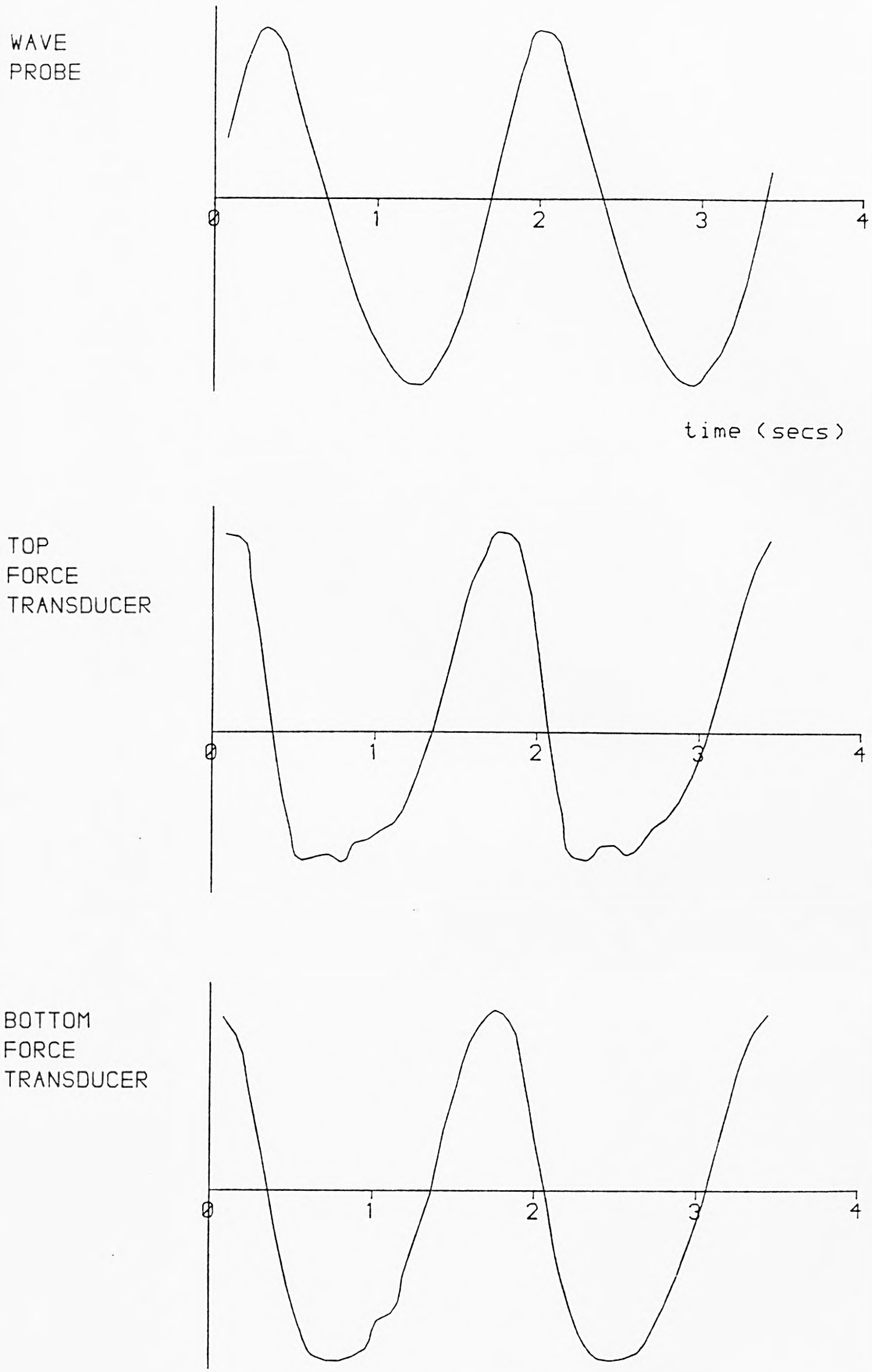

OUTPUT FROM WAVE PROBE AND FORCE TRANSDUCERS
LOADING ON 33.56 MM CYLINDER
WAVE CONDITIONS: WEDGE AMP. 50.0 MM, FREQ. .586 HZ

Figure 5.34

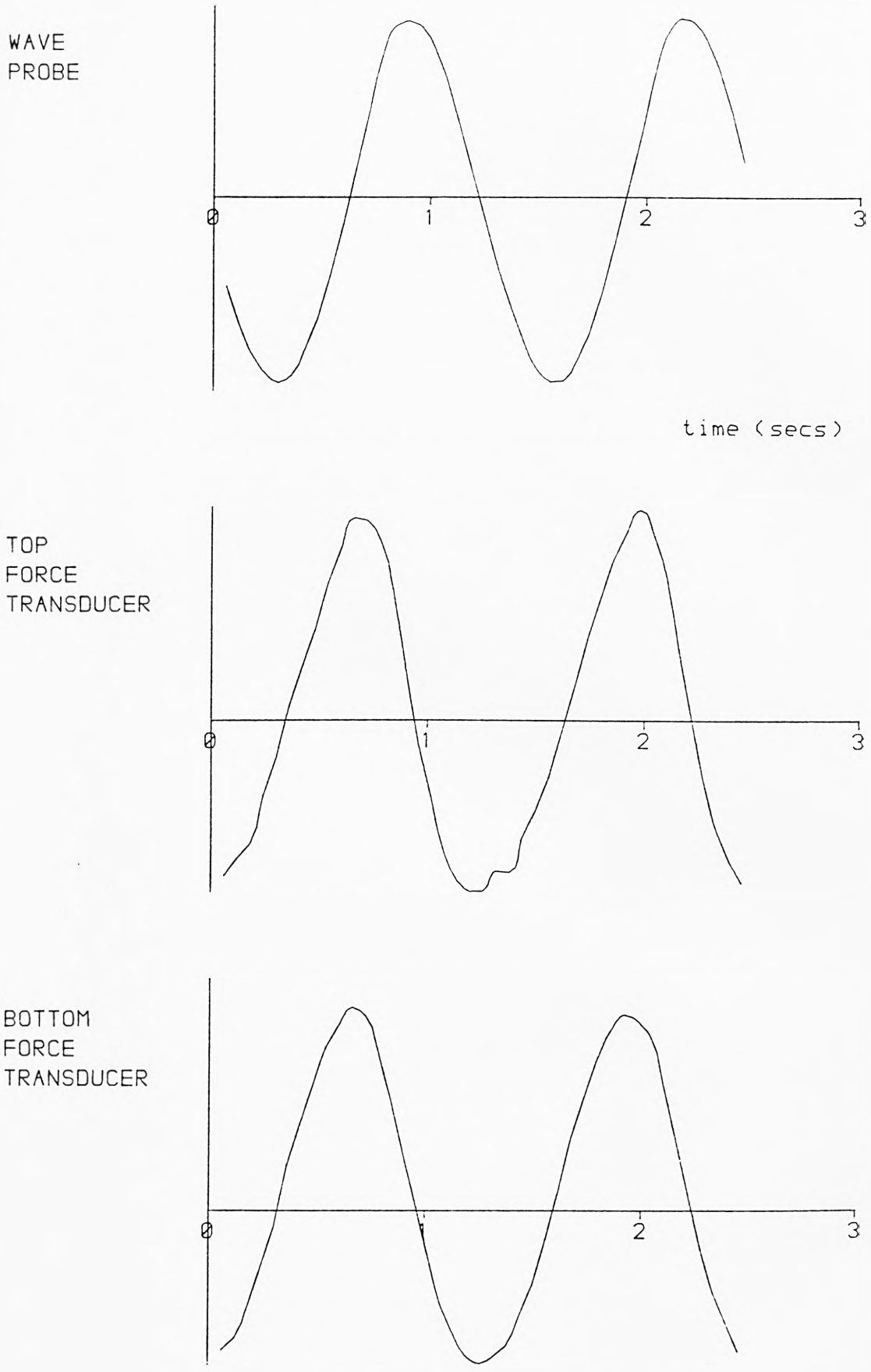

OUTPUT FROM WAVE PROBE AND FORCE TRANSDUCERS
LOADING ON 33.56 MM CYLINDER
WAVE CONDITIONS: WEDGE AMP. 50.0 MM, FREQ. .781 HZ

Figure 5.35

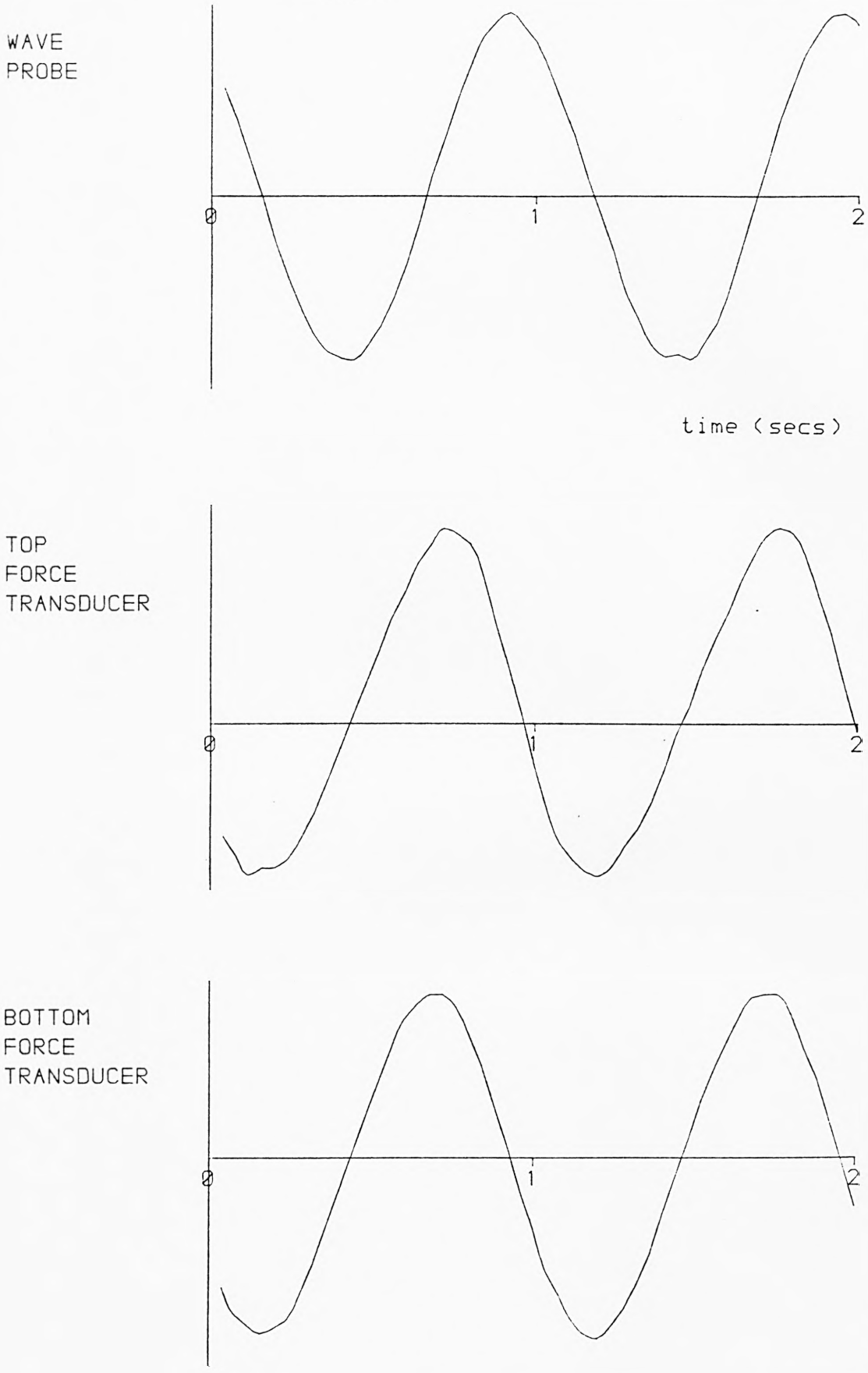

OUTPUT FROM WAVE PROBE AND FORCE TRANSDUCERS
LOADING ON 33.56 MM CYLINDER
WAVE CONDITIONS: WEDGE AMP. 40.0 MM, FREQ. .977 HZ

Figure 5.36

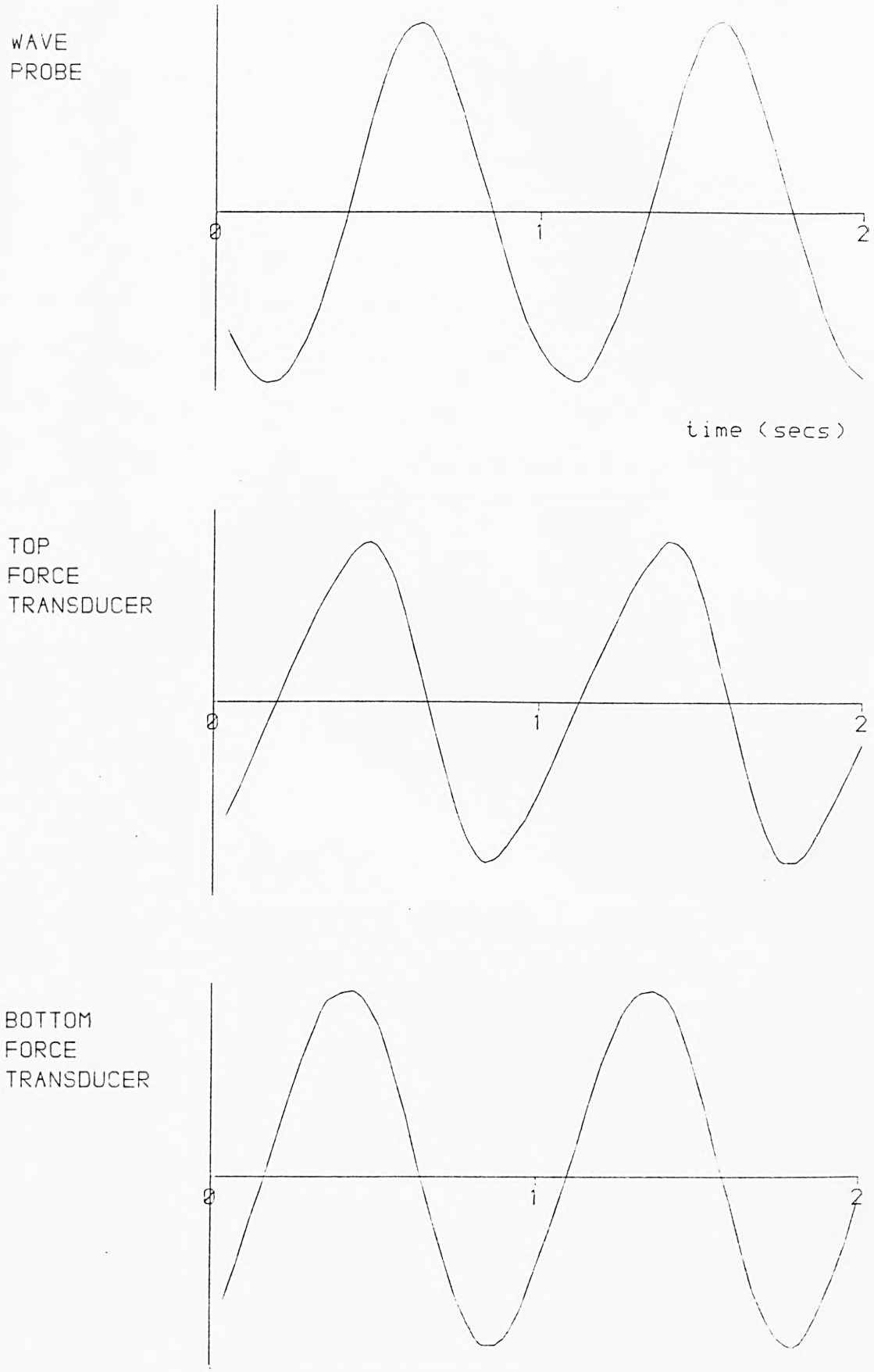

OUTPUT FROM WAVE PROBE AND FORCE TRANSDUCERS
LOADING ON 33.56 MM CYLINDER
WAVE CONDITIONS: WEDGE AMP. 40.0 MM, FREQ. 1.074 HZ

Figure 5.37

5.2.2 First Order Forces

As stated in Section 4.4.3.3, the force results were obtained in the form of six Fourier components of the total force, each with its respective depth of action. Three sets of results were obtained for each of the cylinder and wave combinations. These agreed to within 1% in most cases, allowing the average values to be taken for the force components. The first order force results, then, consisted of the $\cos\omega t$ and $\sin\omega t$ components and their depths of action.

The measured forces were equated with the theoretical first order forces, as calculated from the measured wave conditions, in order to give estimates for the drag and inertia coefficients. The theoretical forces acting at the fundamental frequency are the linear Morison forces, FI and FD((3-33) and (3-32)),and the forces due to the reflected wave, FIR and FDR ((3-63) and (3-62)).

The calculated values of FD and FDR were multiplied by the appropriate factors from their Fourier series, Table 3.2, to obtain their first order components. A correction was also made to the theoretical forces to allow for the fact that the cylinder did not extend right to the bottom of the flume, Figure 4.6. The cylinder was assumed to end 75 mm above the bottom in each case. This effectively changed the bottom limit of integration in (3-31) from -h to -0.85 h and introduced correction factors into the drag and inertia forces given by;

$$CORR_D = 1 - \frac{\sinh 0.3\ kh + 0.3\ kh}{\sinh 2\ kh + 2kh} \qquad (5\text{-}5)$$

$$CORR_I = 1 - \frac{\sinh 0.15\ kh}{\sinh kh} \qquad (5\text{-}6)$$

In the limit of deep or shallow water, $CORR_D$ and $CORR_I$ have identical values which tend towards 1.0 or 0.85 respectively. At intermediate depths, $CORR_I$ is somewhat lower than $CORR_D$.

Having obtained expressions for the theoretical first order forces, C_m and C_d were easily calculated from the measured forces, and the results are given in Table 5.3 a, b, and c. Also shown in Table 5.3 are the Keulegan Carpenter number, KCI, given by (3-40) and the Reynolds' number, calculated using the free surface particle velocity;

$$Re = \frac{U_m d}{\upsilon}$$

$$= \frac{a_I g k D}{\omega\ \upsilon} \qquad (5\text{-}7)$$

with the kinematic viscosity, υ, taken as 1.1×10^{-6} m^2/s.

5.2.2.1 Inertia Coefficient

The measured inertia coefficients are plotted against the Keulegan Carpenter number in Figure 5.38. Also shown are the results of Sarpkaya (1976a). obtained from U-tube tests, and Chakrabarti's (1980a) results from elements of vertical cylinders.

Wave Setting		KCI	Re	In Phase Component		Quadrature Component		C_m	C_d
WA (mm)	Freq (Hz)			Force (mN)	Depth (mm)	Force (mN)	Depth (mm)		
50	0.586	11.94	731	15.94	288	-20.16	253	2.83	2.02
60	0.586	14.91	913	24.49	288	-24.18	242	2.77	2.01
70	0.586	17.63	1079	34.49	282	-27.76	242	2.74	2.06
50	0.684	8.04	623	10.65	286	-20.61	260	2.95	2.05
40	0.781	8.76	842	15.99	269	-26.03	254	2.72	2.17
50	0.781	11.04	1062	25.89	261	-30.07	255	2.51	2.24
60	0.781	13.41	1290	36.09	262	-36.15	243	2.51	2.12
50	0.879	12.10	1425	37.66	239	-38.66	257	2.37	2.07
30	0.977	7.60	1073	14.87	106	-20.62	412	1.77	1.90
40	0.977	10.00	1411	25.67	118	-24.41	440	1.61	1.90
50	0.977	12.78	1804	41.50	128	-30.56	431	1.53	1.89
50	1.074	13.30	2185	50.25	97	-35.48	369	1.47	1.84
20	1.172	5.74	1071	9.55	36	-21.87	251	2.00	1.75
30	1.172	8.45	1575	21.42	40	-29.01	269	1.82	1.80
40	1.172	11.02	2055	38.94	56	-35.35	278	1.65	1.86

First Order Measured Forces - 9.55 mm Cylinder

Table 5.3 a

Wave Setting		KCI	Re	In Phase Component		Quadrature Component		C_m	C_d
WA (mm)	Freq (Hz)			Force (mN)	Depth (mm)	Force (mN)	Depth (mm)		
50	0.586	5.42	1673	31.61	188	-65.17	217	1.77	1.68
60	0.586	6.65	2054	50.93	182	-71.16	218	1.60	1.86
70	0.586	7.93	2450	80.35	182	-77.10	222	1.48	2.07
50	0.684	3.61	1410	18.48	178	-67.87	205	1.93	1.58
40	0.781	3.90	1892	25.13	154	-92.50	195	1.92	1.53
50	0.781	5.01	2432	43.86	159	-108.94	206	1.77	1.66
60	0.781	5.94	2884	67.20	153	-119.53	201	1.65	1.79
50	0.879	5.40	3211	73.80	139	-144.54	197	1.74	1.77
30	0.977	3.40	2422	27.18	130	-106.52	184	1.80	1.54
40	0.977	4.50	3206	50.11	126	-135.74	191	1.74	1.67
50	0.977	5.66	4026	87.31	124	-163.15	189	1.64	1.82
40	1.074	4.70	3897	61.70	95	-165.10	175	1.77	1.64
20	1.172	5.78	2425	18.76	101	-106.97	156	1.94	1.47
30	1.172	3.78	3556	41.75	87	-153.71	156	1.91	1.53
40	1.172	4.88	4587	82.40	82	-189.20	161	1.78	1.81

First Order Measured Forces - 21.45 mm Cylinder

Table 5.3 b

Wave Setting		KCI	Re	In Phase Component		Quadrature Component		C_m	C_d
WA (mm)	Freq (Hz)			Force (mN)	Depth (mm)	Force (mN)	Depth (mm)		
50	0.586	3.46	2615	46.27	203	-182.92	222	2.01	1.44
60	0.586	4.28	3233	74.56	192	-217.65	222	1.97	1.60
70	0.586	5.05	3820	110.92	190	-252.93	223	1.93	1.70
50	0.684	2.32	2217	24.97	204	-182.15	213	2.10	1.25
40	0.781	2.50	2973	31.01	165	-243.97	204	2.07	1.20
50	0.781	3.16	3750	53.25	168	-299.45	206	2.02	1.30
60	0.781	3.81	4531	88.19	161	-357.49	208	2.01	1.47
50	0.879	3.51	5098	98.35	140	-408.79	196	1.98	1.41
30	0.977	2.15	3745	29.79	66	-284.80	182	1.99	1.02
40	0.977	2.86	4983	59.51	84	-370.19	184	1.96	1.25
50	0.977	3.61	6292	106.12	88	-458.35	184	1.90	1.42
40	1.074	3.00	6083	70.71	40	-441.02	167	1.93	1.28
20	1.172	1.67	3837	16.74	-9	-275.29	153	2.02	0.77
30	1.172	2.41	5555	50.48	31	-395.46	152	2.00	1.17
40	1.172	3.16	7270	102.20	38	-503.76	153	1.93	1.47

First Order Measured Forces - 33.56 mm Cylinder

Table 5.3 c

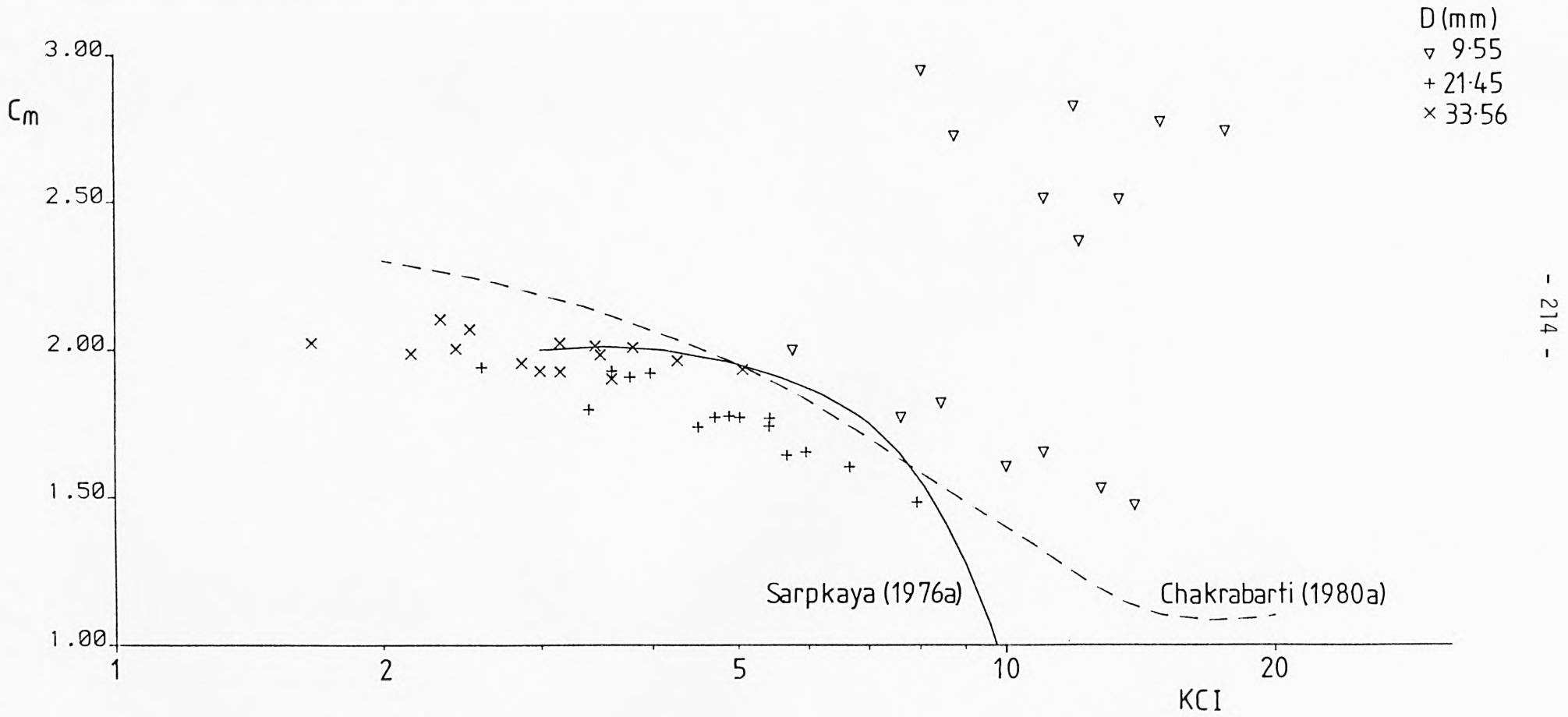

Inertia Coefficient vs. Keulegan Carpenter Number

Figure 5·38

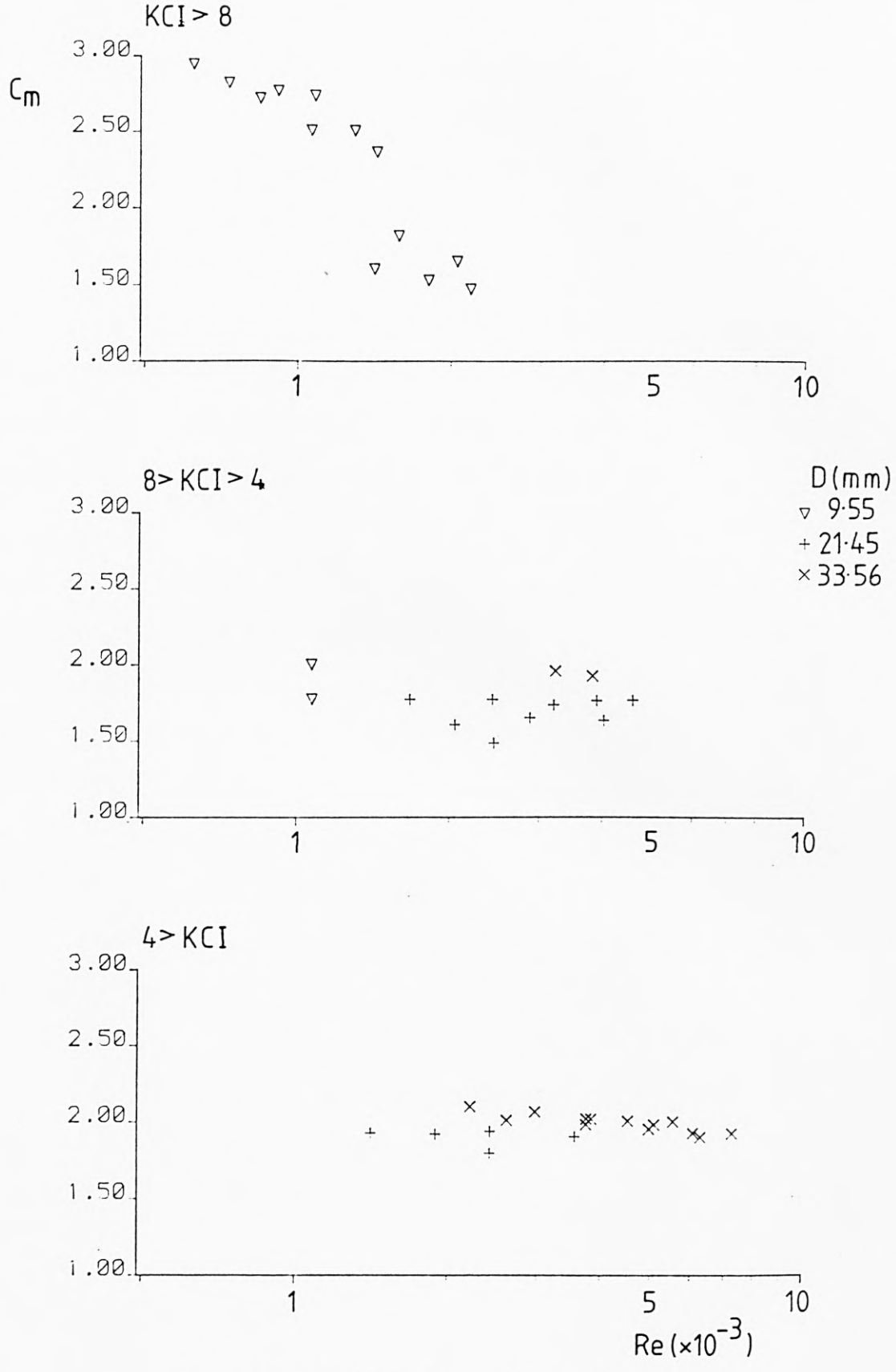

Inertia Coefficient vs. Reynolds' Number

Figure 5.39

At low values of KCI, C_m approaches its theoretical value of 2.0. This agrees with the results of Sarpkaya and of Jen (1968). Chakrabarti's results for vertical elements have a slightly larger value of C_m at the limit of low KC.

As the Keulegan Carpenter number increases, C_m tends to become lower. This trend is displayed in both Sarpkaya's and Chakrabarti's results, although the rate at which C_m falls is somewhat less in this case.

A number of high values for C_m have been found for the 9.55 mm cylinder at the higher values of KCI. These may be due to the dependence of C_m on the Reynolds' number. At this range of KCI, C_m was found to be very dependent on Re, Figure 5.39. Although Sarpkaya (1976a) found C_m to be independent of Reynolds' number for Re below 20,000, the typical Re in this study is a full order of magnitude below that value. Thus at high KCI, C_m was found to be dependent on Re, for values of Re below those covered by previous published work.

Apart from these few high points, the measured inertia coefficients follow the generally accepted trends, and are well within the limits of previous results.

5.2.2.2 Drag Coefficient

The measured drag coefficients are plotted against Keulegan Carpenter number in Figure 5.40, and against Reynolds' number in Figure 5.41. Also shown on Figure 5.40, as for the inertia

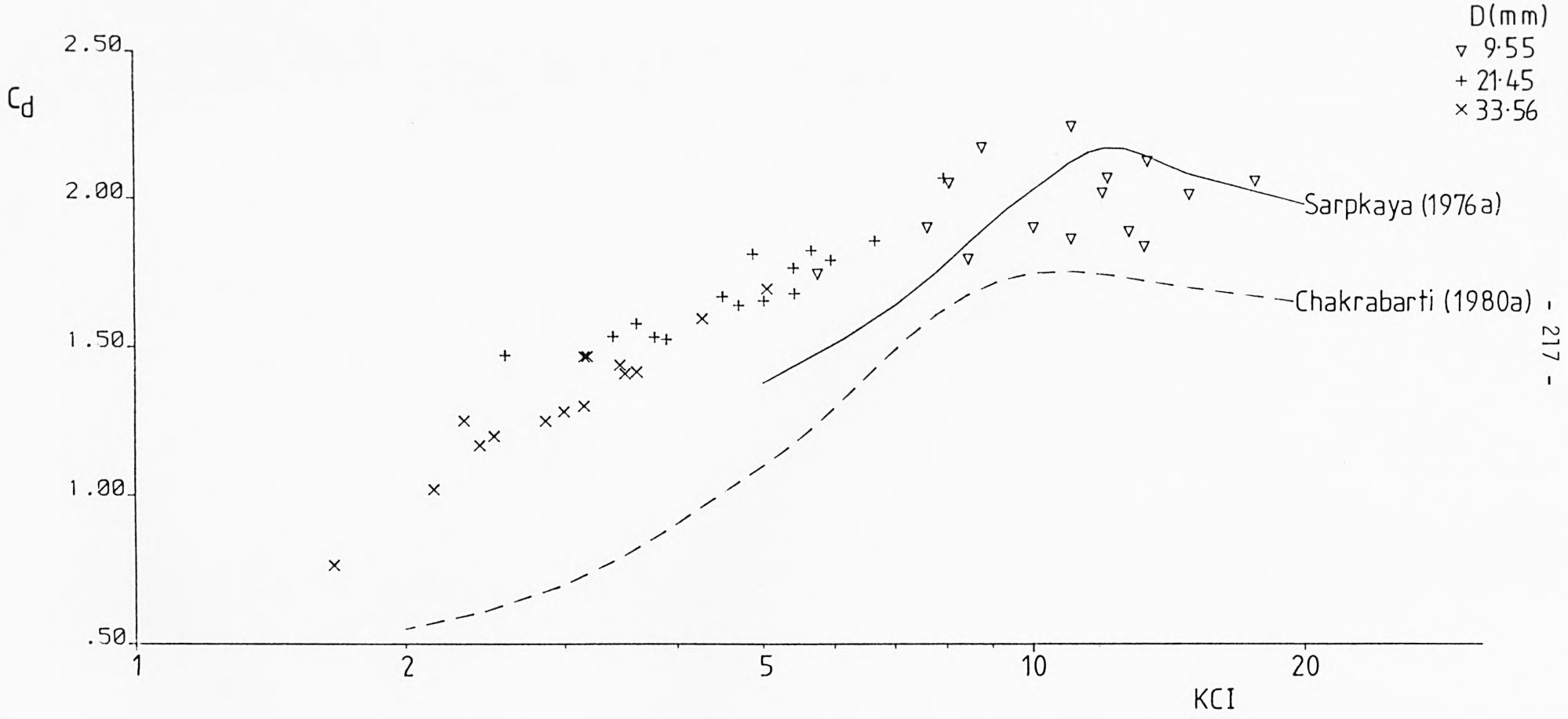

Drag Coefficient vs. Keulegan Carpenter Number

Figure 5.40

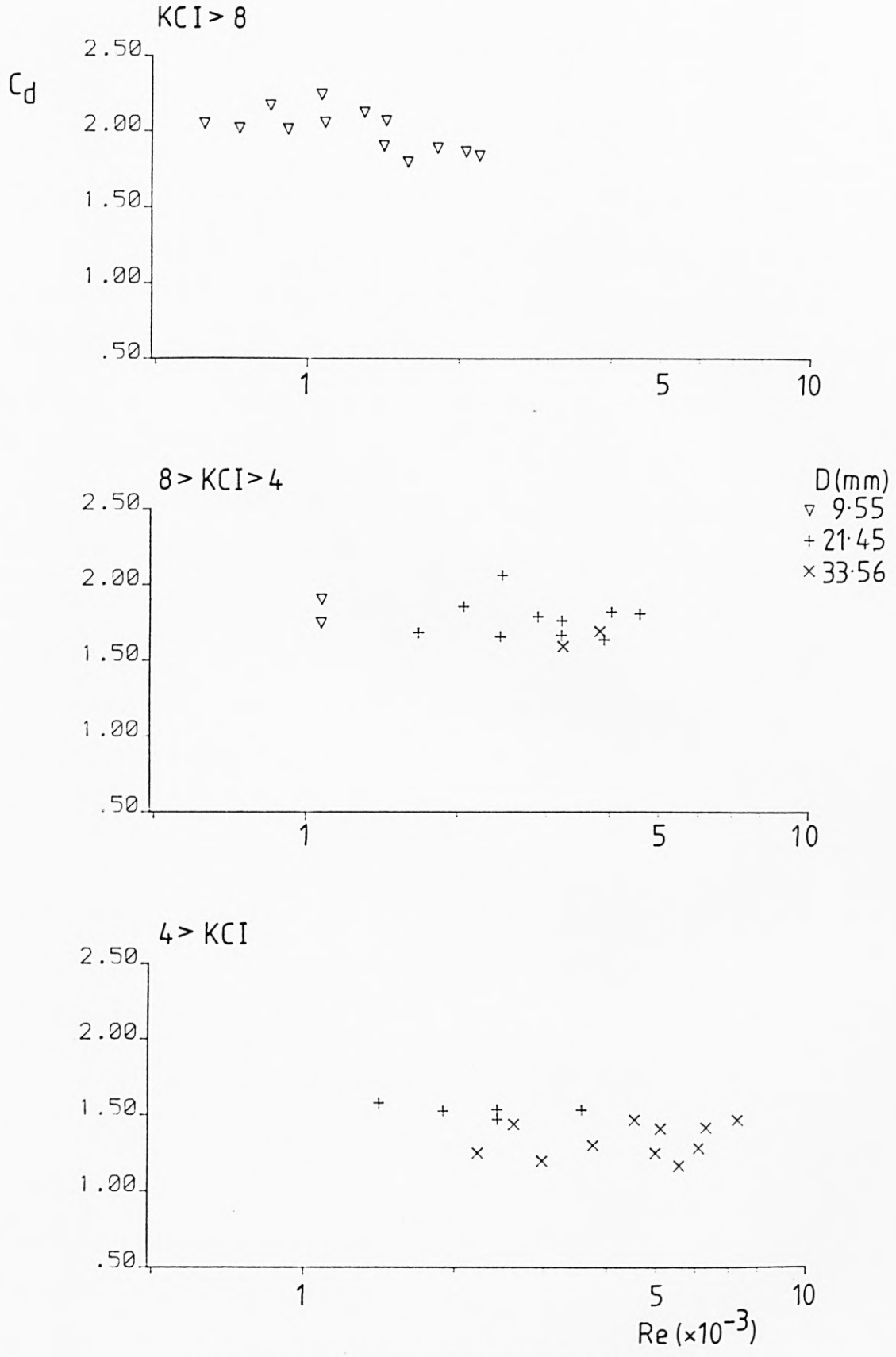

Drag Coefficient vs. Reynolds' Number

Figure 5·41

coefficient, are the results of Sarpkaya (1976a) and Chakrabarti (1980a).

The variation of C_d with KCI is well defined. At low Keulegan Carpenter numbers C_d is small; the drag coefficient then increases with KCI, before reaching a peak value for KCI about 15. This trend agrees with the results of both Sarpkaya and Chakrabarti, although the observed values of C_d are generally higher in this study.

The difference between the values of C_d from this study and from the previous results is due to its dependence on the Reynolds' number. Although C_d does not appear to vary with Re over the range covered by this work, Figure 5.41, over a much wider range C_d tends to fall with Re. Thus the drag coefficients measured in these tests, with typical Reynolds' numbers of 1,000 to 5,000, are higher than those from the previous work, where Re was approximately 30,000.

5.2.3 Second Order Forces

The measured second order forces consisted of cos $2\omega t$ and sin $2\omega t$ force components and their depths of action. The theoretical second order force components were calculated from the measured wave data using the first order values for C_m and C_d. The forces having components at the second harmonic frequency were; FI2 (3-43), FD2 (3-47), FWD (3-54), FWI (3-55), FDP (3-58), FD22 (3-67) and FI22 (3-68). Because of the number of theoretical forces contributing to the two measured components, it was not possible to directly

evaluate the magnitude of any one of them from the experimental results.

As a first stage in the analysis of the second order forces, the measured and theoretical force components are compared in Figures 5.42 to 5.62. These figures cover the three cylinder diameters at each of the seven fundamental frequencies. The theoretical forces are presented pictorially, with each of the force components and their depths of action (calculated from Table 3.1) shown approximately to scale. Comparison of the measured and theoretical resultant forces allows a number of observations to be made.

In considering the ratios of measured to theoretical forces given in Figures 5.42 to 5.62, it must be remembered that the second order loading generally constitutes less than 10% of the total loading. Thus a difference of 10% between the measured and theoretical second order forces amounts to only 1% of the total loading on the cylinder.

In a significant number of the results, for example Figures 5.46, 5.48, 5.52, 5.58 and 5.60, both components of the measured second order force agree very well with the theoretical resultant force, in both magnitude and position of action.

Where the phase of the free wave, β, varies significantly from zero, the forces FI22 and FD22 have components of the opposite sign to the second order forces due to the main wave. This has the effect, for example on the cos $2\omega t$ components in Figures 5.44, 5.49,

5.51 and 5.62, of giving a resultant equal to the small difference between large forces of opposite sign. In these cases the resultant force is subject to much larger relative errors, and the agreement between theory and experiment is, not unexpectedly, poor.

The measured force tends to be somewhat less than the theoretical resultant, in those cases where the second order loading is dominated by the forces due to the free wave, as in Figures 5.42, 5.43, 5.49 and 5.56. This shows that the free wave does not exert as great a force on the cylinder as it would in the absence of the main wave. If the force due to the free wave could be isolated from the overall second order loading, the difference could be accounted for by introducing different drag and inertia coefficients for FD22 and FI22.

In one or two cases, such as the cos $2\omega t$ component in Figure 5.53 and the sin $2\omega t$ component in Figure 5.45, there is no obvious explanation for the large discrepancy between theory and experiment.

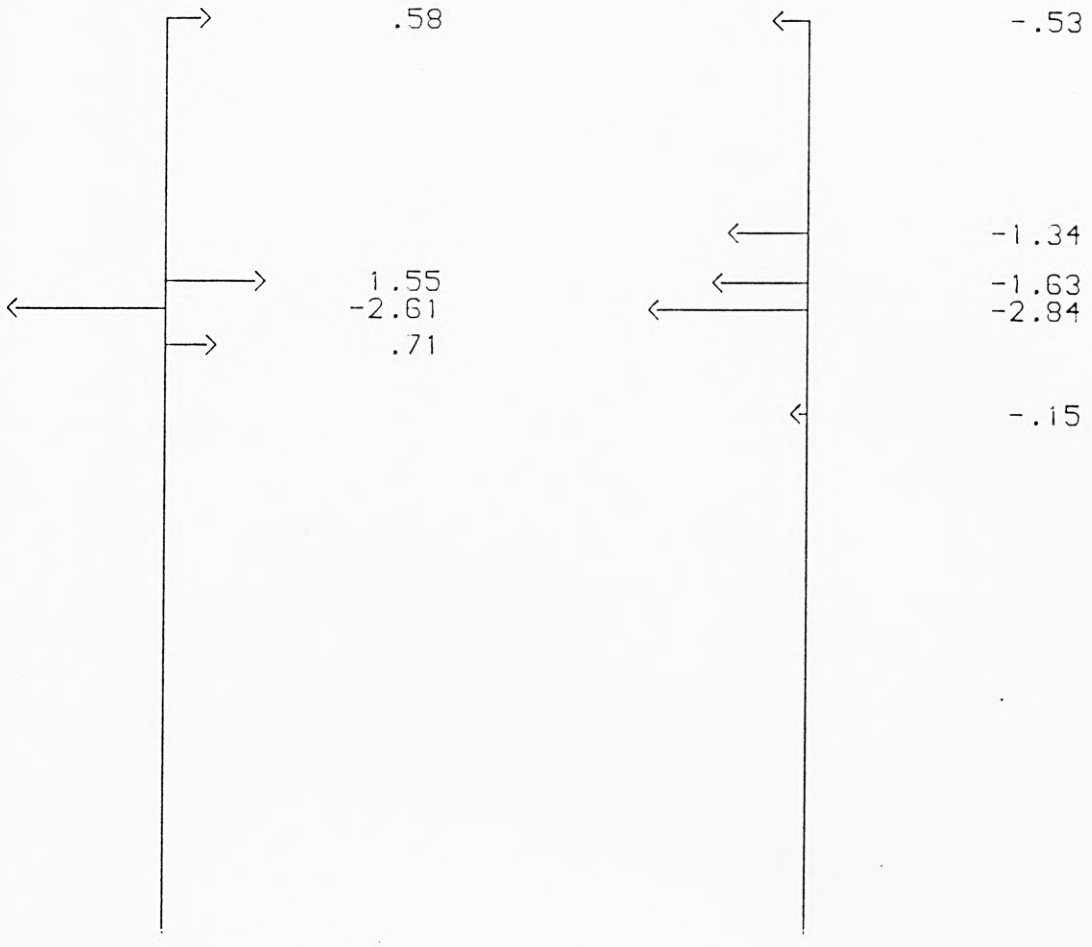

Theoretical Forces For CM = 2.825 and CD = 2.018

cos2wt Forces		sin2wt Forces	
Resultant Force =	.24 mN	Resultant Force =	-6.49 mN
Depth =	-261. mm	Depth =	135. mm
Measured Force =	.17 mN	Measured Force =	-4.18 mN
Depth =	-537. mm	Depth =	219. mm
Measured/Theory =	.711	Measured/Theory =	.644

Second Order Morison Coefficients :
CM2 = 1.791 ; CD2 = 1.293

SECOND ORDER WAVE LOADING ON 9.55 MM CYLINDER
WAVE CONDITIONS: WEDGE AMP. 50.0 MM, FREQ. .586 HZ

Figure 5.42

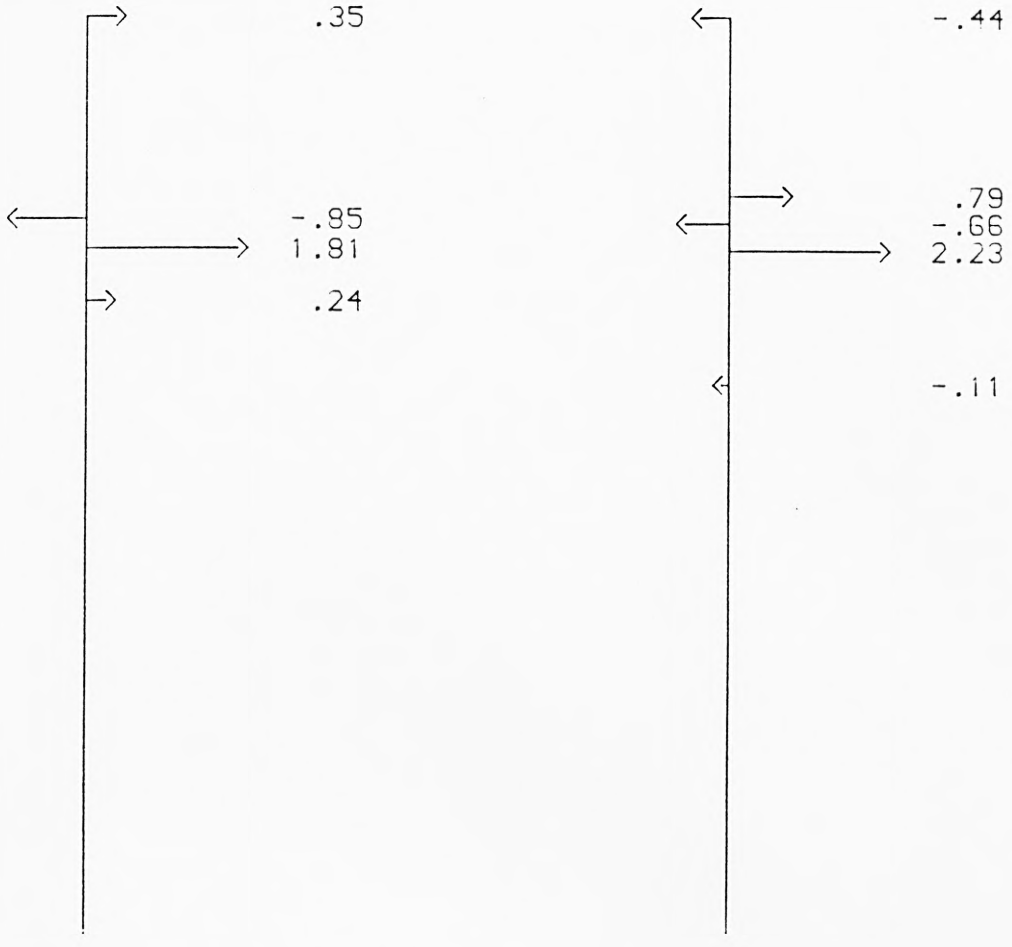

Theoretical Forces For CM = 2.947 and CD = 2.050

cos2wt Forces		sin2wt Forces	
Resultant Force =	1.54 mN	Resultant Force =	1.81 mN
Depth =	111. mm	Depth =	151. mm
Measured Force =	.94 mN	Measured Force =	1.23 mN
Depth =	103. mm	Depth =	148. mm
Measured/Theory =	.606	Measured/Theory =	.682

Second Order Morison Coefficients :
CM2 = 1.866 ; CD2 = 1.632

SECOND ORDER WAVE LOADING ON 9.55 MM CYLINDER
WAVE CONDITIONS: WEDGE AMP. 50.0 MM, FREQ. .684 HZ

Figure 5.43

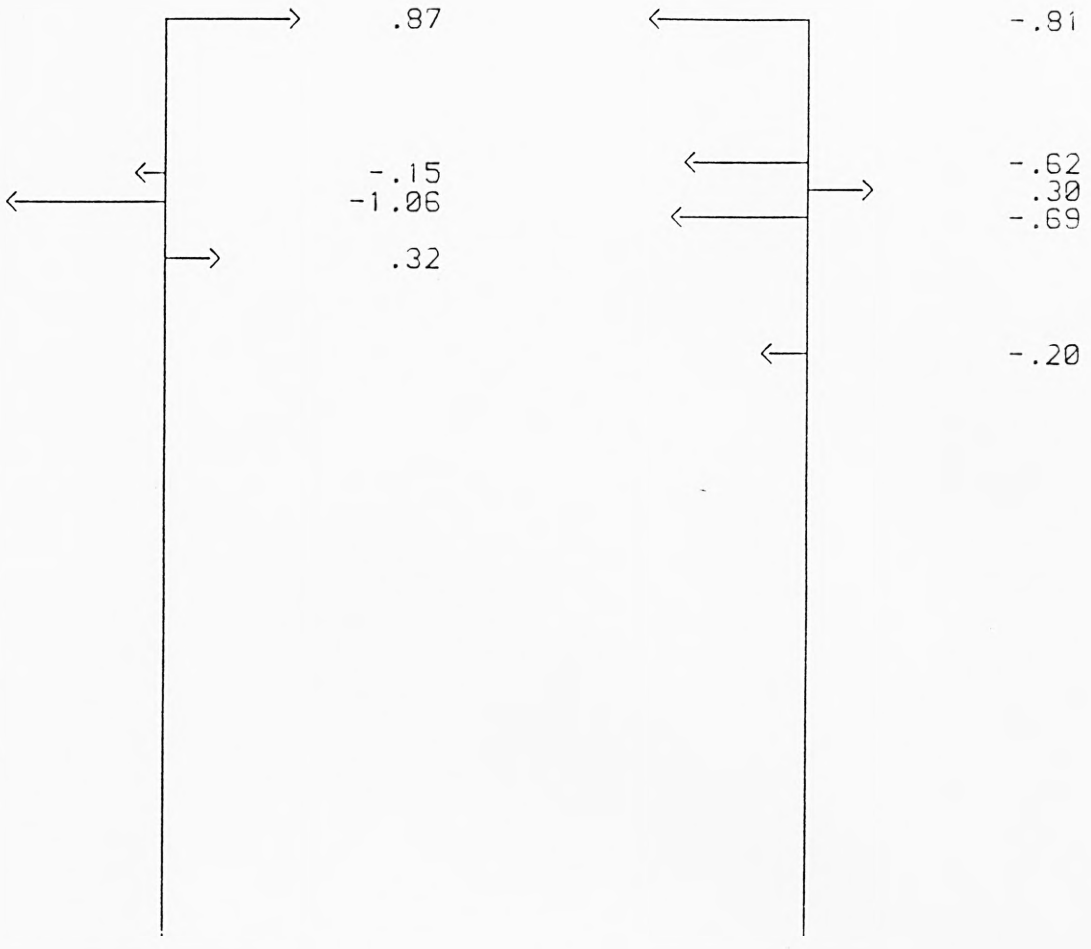

Theoretical Forces For CM = 2.724 and CD = 2.170

cos2wt Forces		sin2wt Forces	
Resultant Force =	-.03 mN	Resultant Force =	-2.02 mN
Depth =	2963. mm	Depth =	66. mm
Measured Force =	.47 mN	Measured Force =	-1.39 mN
Depth =	-306. mm	Depth =	58. mm
Measured/Theory =	******	Measured/Theory =	.689

Second Order Morison Coefficients :
CM2 = 1.348 ; CD2 = 2.096

SECOND ORDER WAVE LOADING ON 9.55 MM CYLINDER
WAVE CONDITIONS: WEDGE AMP. 40.0 MM, FREQ. .781 HZ

Figure 5.44

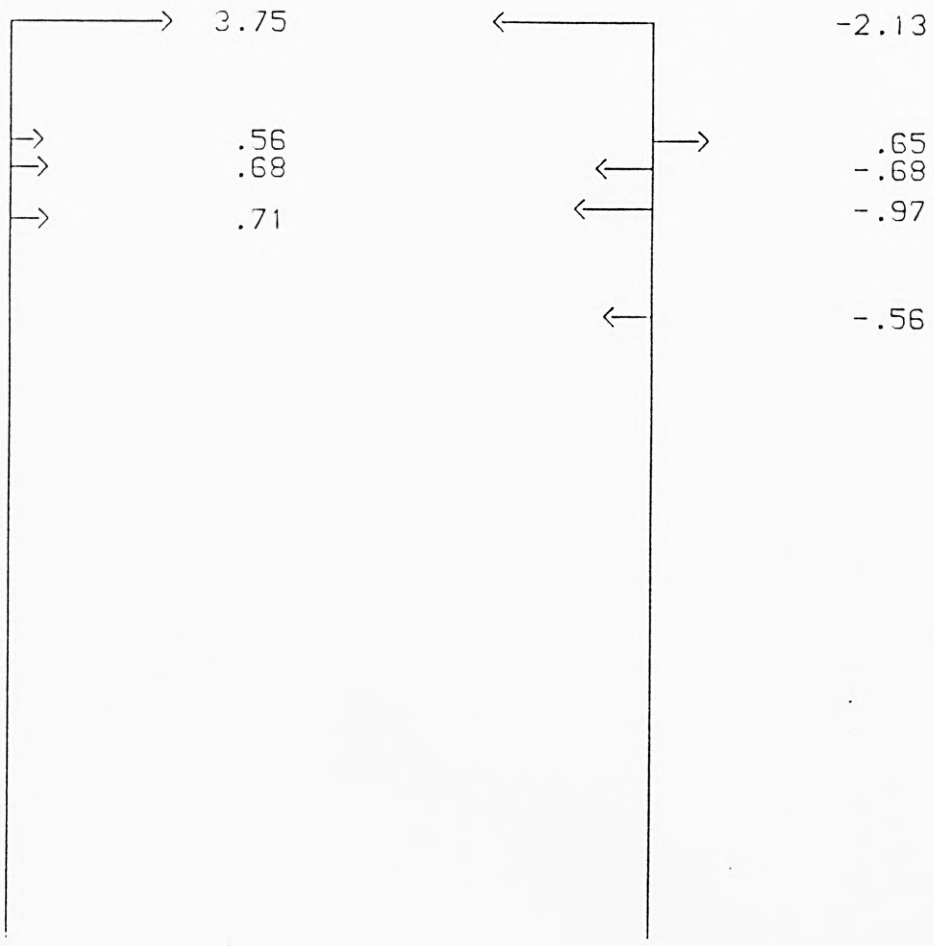

Theoretical Forces For CM = 2.367 and CD = 2.068

cos2wt Forces		sin2wt Forces	
Resultant Force =	5.70 mN	Resultant Force =	-3.69 mN
Depth =	30. mm	Depth =	54. mm
Measured Force =	3.95 mN	Measured Force =	-1.98 mN
Depth =	-17. mm	Depth =	48. mm
Measured/Theory =	.693	Measured/Theory =	.509

Second Order Morison Coefficients :
CM2 = 1.121 ; CD2 = 1.495

SECOND ORDER WAVE LOADING ON 9.55 MM CYLINDER
WAVE CONDITIONS: WEDGE AMP. 50.0 MM, FREQ. .979 HZ

Figure 5.45

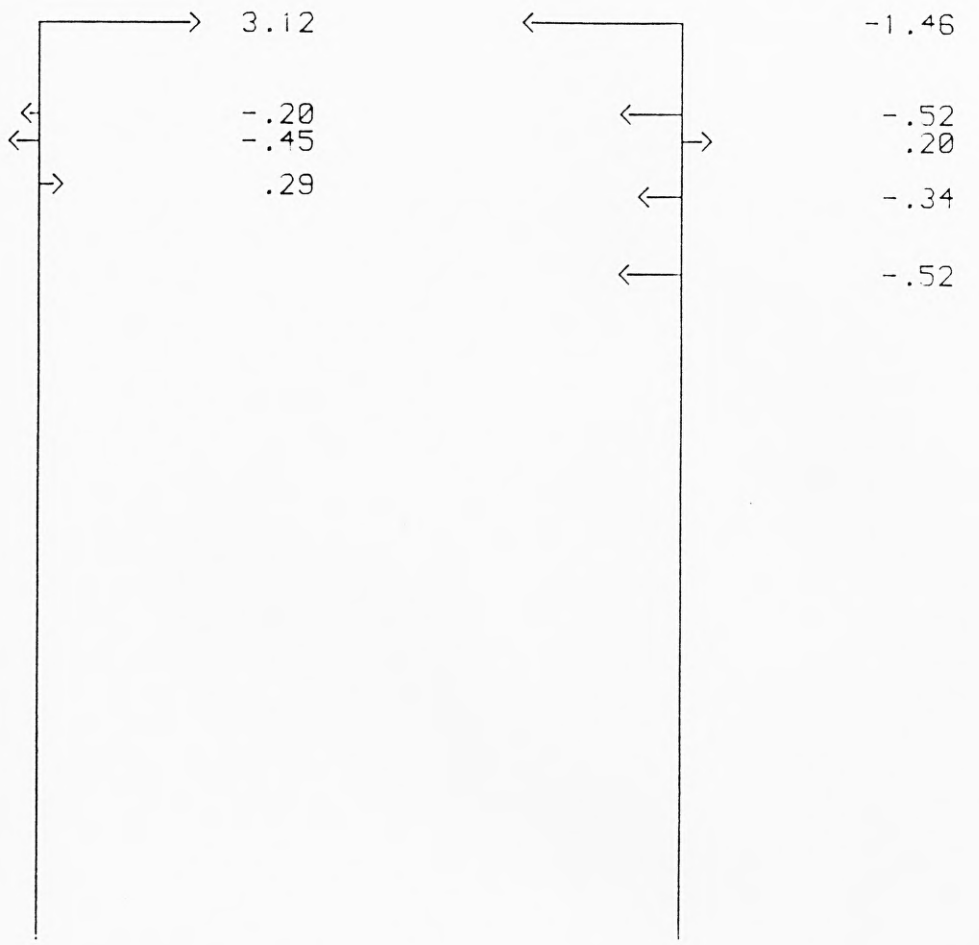

Theoretical Forces For CM = 1.605 and CD = 1.901

cos2wt Forces		sin2wt Forces	
Resultant Force =	2.76 mN	Resultant Force =	-2.65 mN
Depth =	-5. mm	Depth =	45. mm
Measured Force =	2.19 mN	Measured Force =	-2.40 mN
Depth =	37. mm	Depth =	33. mm
Measured/Theory =	.795	Measured/Theory =	.907

Second Order Morison Coefficients :
CM2 = 1.456 ; CD2 = 1.541

SECOND ORDER WAVE LOADING ON 9.55 MM CYLINDER
WAVE CONDITIONS: WEDGE AMP. 40.0 MM, FREQ. .977 HZ

Figure 5.46

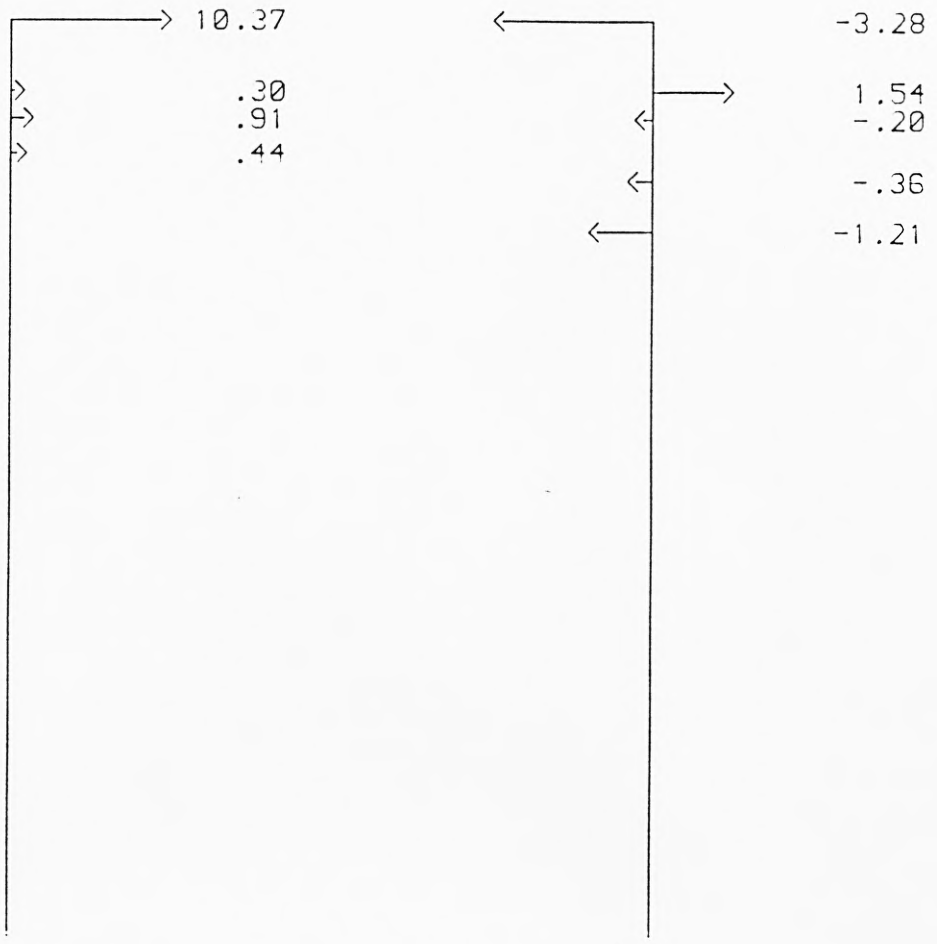

Theoretical Forces for CM = 1.473 and CD = 1.838

cos2wt Forces		sin2wt Forces	
Resultant Force =	12.03 mN	Resultant Force =	-3.51 mN
Depth =	8. mm	Depth =	33. mm
Measured Force =	8.46 mN	Measured Force =	-4.59 mN
Depth =	2. mm	Depth =	25. mm
Measured/Theory =	.703	Measured/Theory =	1.310

Second Order Morison Coefficients :
CM2 = 1.691 ; CD2 = 1.225

SECOND ORDER WAVE LOADING ON 9.55 MM CYLINDER
WAVE CONDITIONS: WEDGE AMP. 50.0 MM, FREQ. 1.074 HZ

Figure 5.47

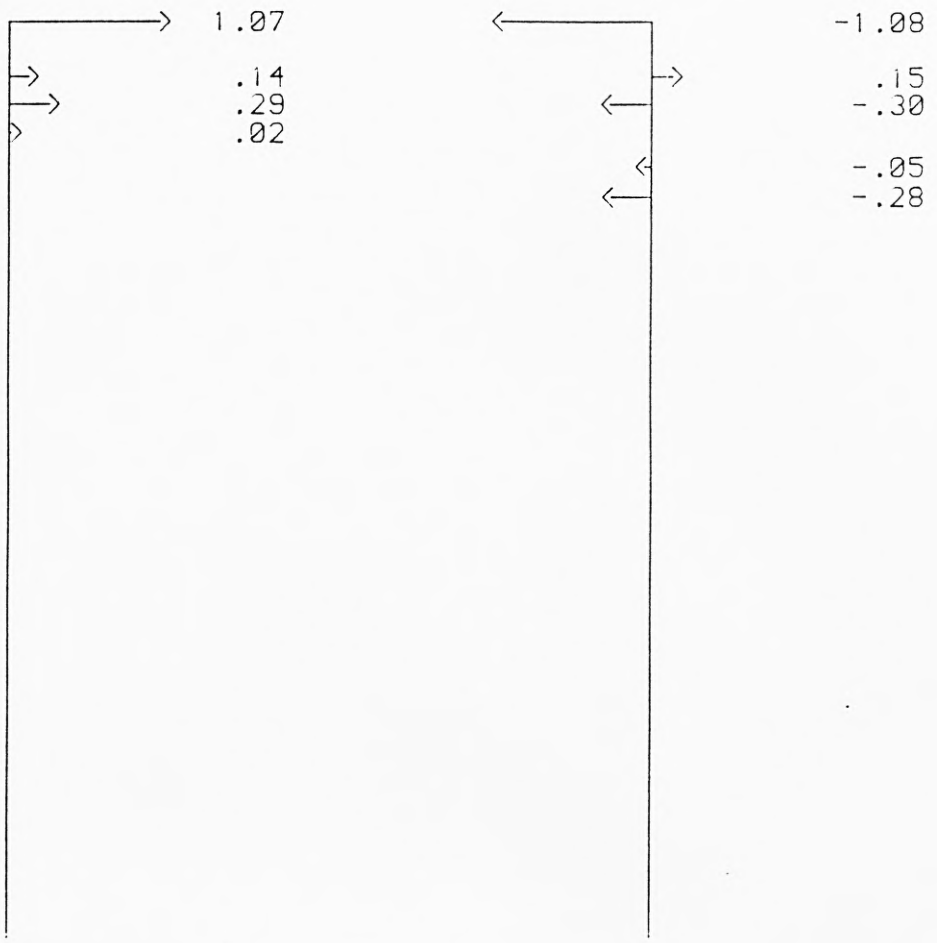

Theoretical Forces For CM = 1.998 and CD = 1.745

cos2wt Forces		sin2wt Forces	
Resultant Force =	1.52 mN	Resultant Force =	-1.56 mN
Depth =	13. mm	Depth =	25. mm
Measured Force =	1.26 mN	Measured Force =	-1.34 mN
Depth =	-47. mm	Depth =	-17. mm
Measured/Theory =	.829	Measured/Theory =	.862

Second Order Morison Coefficients :
CM2 = 1.661 ; CD2 = 1.447

SECOND ORDER WAVE LOADING ON 9.55 MM CYLINDER
WAVE CONDITIONS: WEDGE AMP. 20.0 MM, FREQ. 1.172 HZ

Figure 5.48

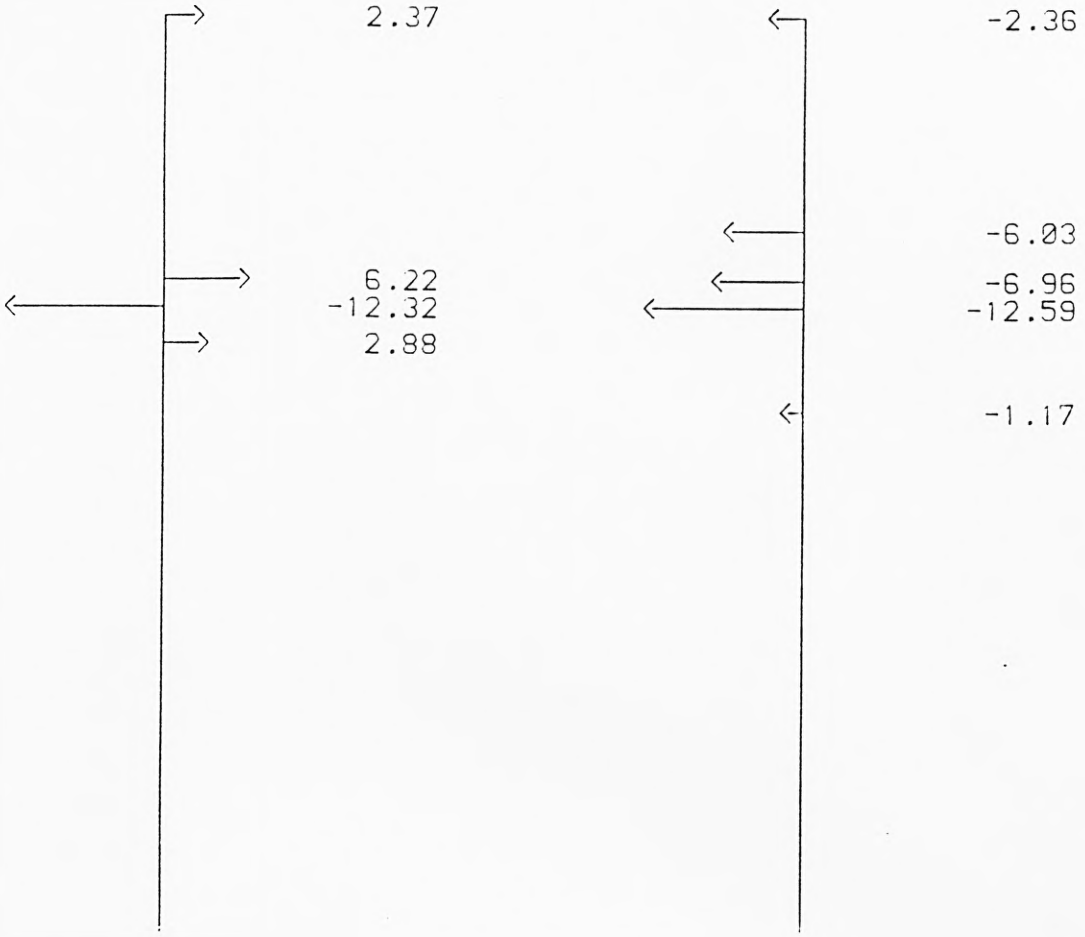

Theoretical Forces For CM = 1.604 and CD = 1.856

cos2wt Forces		sin2wt Forces	
Resultant Force =	-.85 mN	Resultant Force =	-29.11 mN
Depth =	640. mm	Depth =	136. mm
Measured Force =	-6.22 mN	Measured Force =	-20.96 mN
Depth =	190. mm	Depth =	127. mm
Measured/Theory =	7.297	Measured/Theory =	.720

Second Order Morison Coefficients :
CM2 = 1.328 ; CD2 = .645

SECOND ORDER WAVE LOADING ON 21.45 MM CYLINDER
WAVE CONDITIONS: WEDGE AMP. 60.0 MM, FREQ. .586 HZ

Figure 5.49

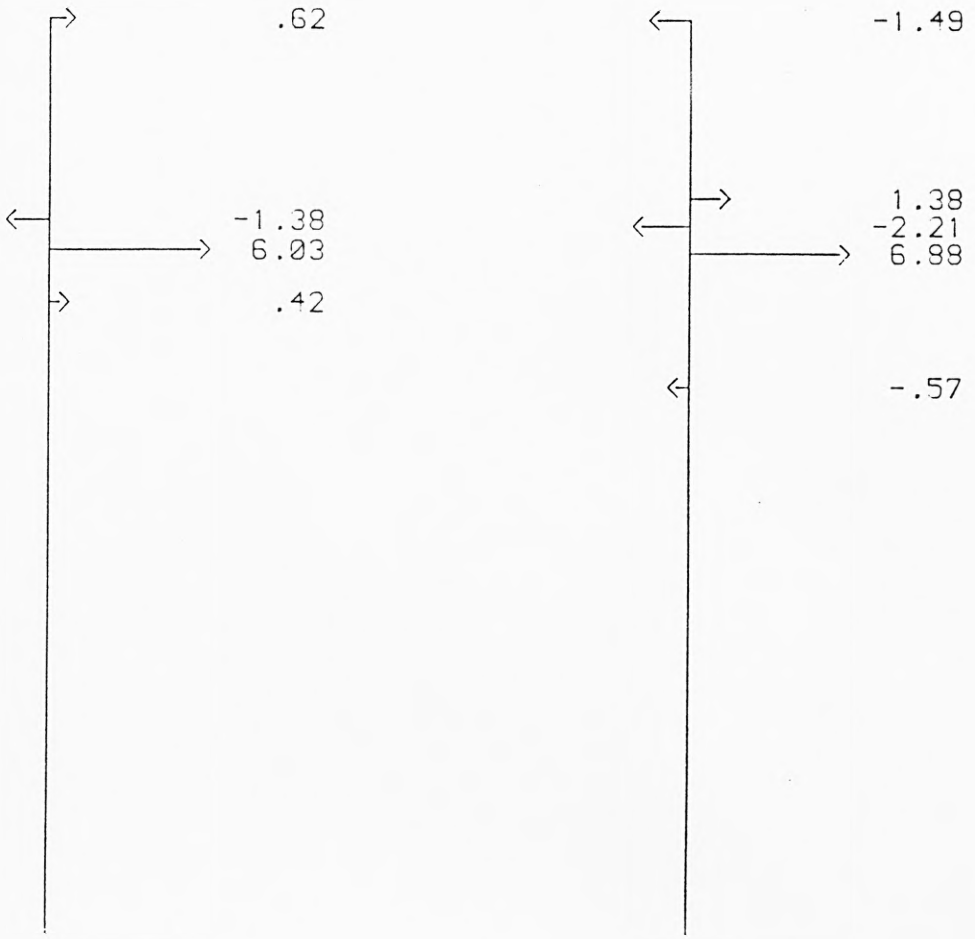

Theoretical Forces For CM = 1.929 and CD = 1.578

cos2wt Forces		sin2wt Forces	
Resultant Force =	5.69 mN	Resultant Force =	4.00 mN
Depth =	119. mm	Depth =	165. mm
Measured Force =	4.59 mN	Measured Force =	3.70 mN
Depth =	116. mm	Depth =	140. mm
Measured/Theory =	.806	Measured/Theory =	.925

Second Order Morison Coefficients :
CM2 = 1.596 ; CD2 = 1.861

SECOND ORDER WAVE LOADING ON 21.45 MM CYLINDER
WAVE CONDITIONS: WEDGE AMP. 50.0 MM, FREQ. .684 HZ

Figure 5.50

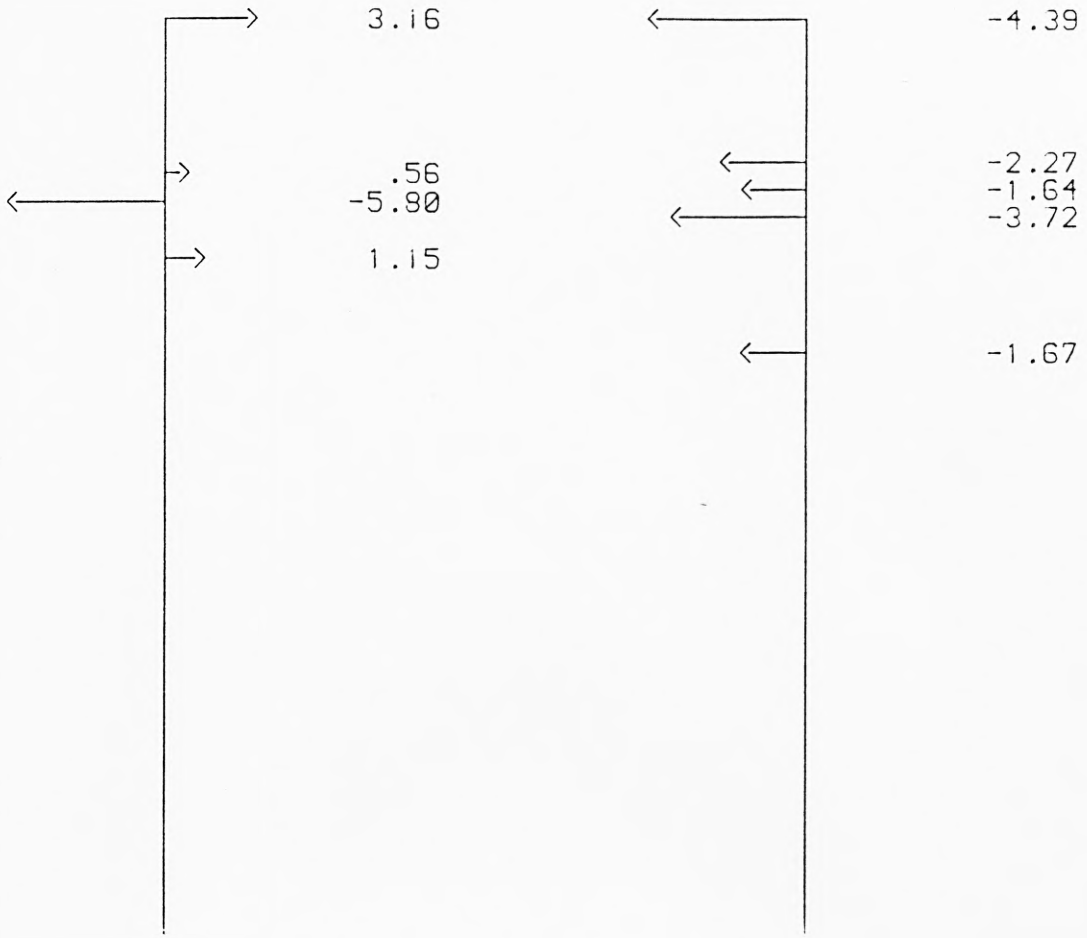

Theoretical Forces For CM = 1.771 and CD = 1.656

cos2wt Forces		sin2wt Forces	
Resultant Force =	-.93 mN	Resultant Force =	-13.69 mN
Depth =	412. mm	Depth =	78. mm
Measured Force =	-.51 mN	Measured Force =	-12.66 mN
Depth =	697. mm	Depth =	77. mm
Measured/Theory =	.546	Measured/Theory =	.924

Second Order Morison Coefficients :
CM2 = 1.596 ; CD2 = 1.605

SECOND ORDER WAVE LOADING ON 21.45 MM CYLINDER
WAVE CONDITIONS: WEDGE AMP. 50.0 MM, FREQ. .781 HZ

Figure 5.51

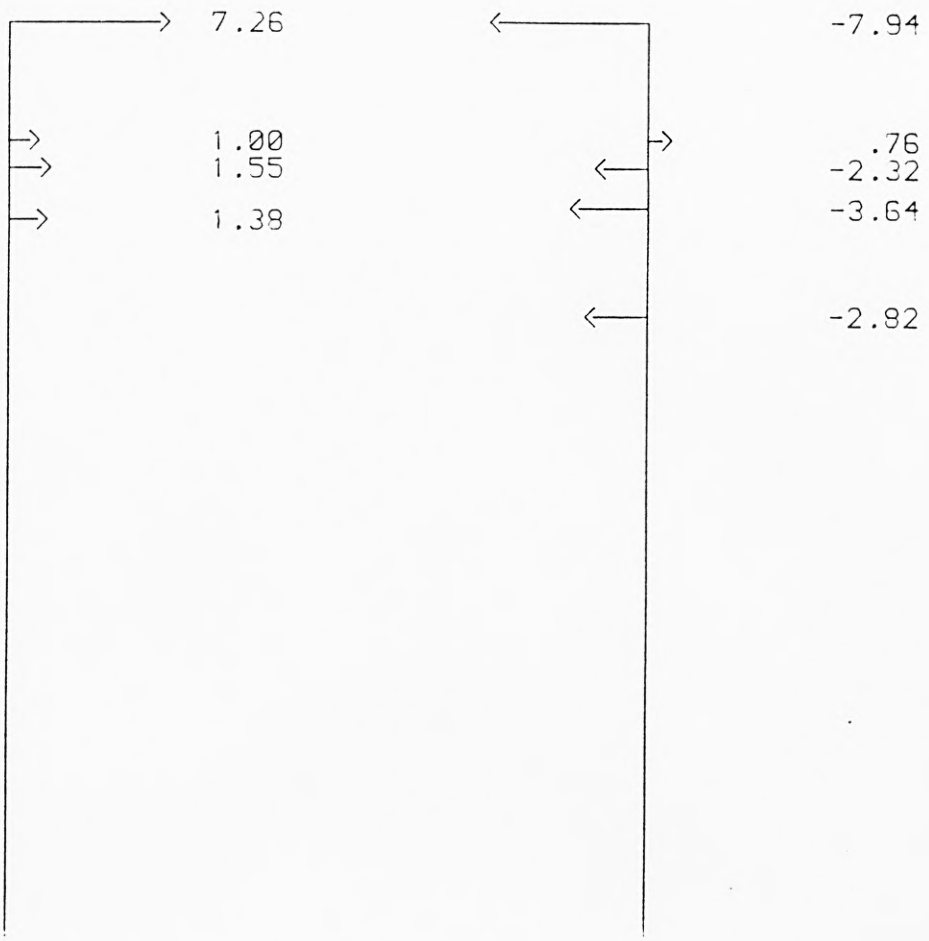

Theoretical Forces For CM = 1.741 and CD = 1.766

cos2wt Forces		sin2wt Forces	
Resultant Force =	11.20 mN	Resultant Force =	-15.96 mN
Depth =	30. mm	Depth =	60. mm
Measured Force =	9.87 mN	Measured Force =	-12.53 mN
Depth =	19. mm	Depth =	53. mm
Measured/Theory =	.882	Measured/Theory =	.785

Second Order Morison Coefficients :
CM2 = 1.301 ; CD2 = 1.595

SECOND ORDER WAVE LOADING ON 21.45 MM CYLINDER
WAVE CONDITIONS: WEDGE AMP. 50.0 MM, FREQ. .979 HZ

Figure 5.52

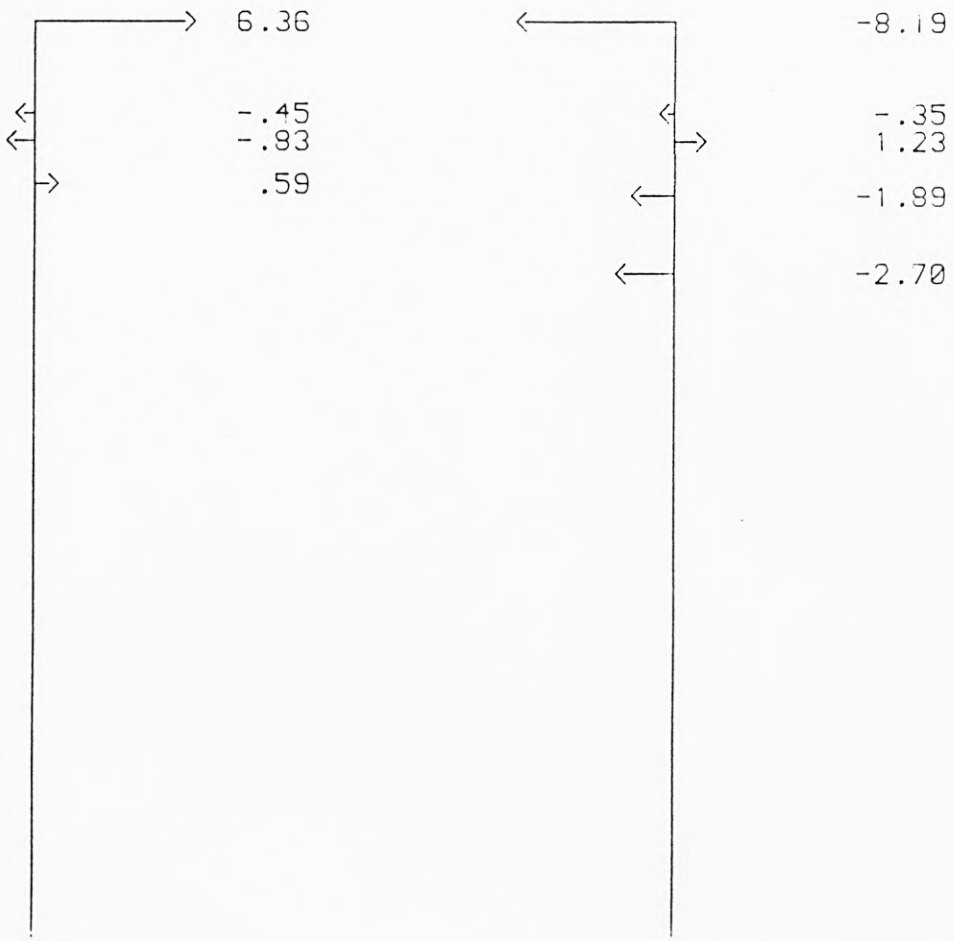

Theoretical Forces for CM = 1.739 and CD = 1.669

cos2wt Forces		sin2wt Forces	
Resultant Force =	5.67 mN	Resultant Force =	-11.89 mN
Depth =	-4. mm	Depth =	41. mm
Measured Force =	1.67 mN	Measured Force =	-12.32 mN
Depth =	-295. mm	Depth =	46. mm
Measured/Theory =	.294	Measured/Theory =	1.036

Second Order Morison Coefficients :
CM2 = 1.865 ; CD2 = .657

SECOND ORDER WAVE LOADING ON 21.45 MM CYLINDER
WAVE CONDITIONS: WEDGE AMP. 40.0 MM, FREQ. .977 HZ

Figure 5.53

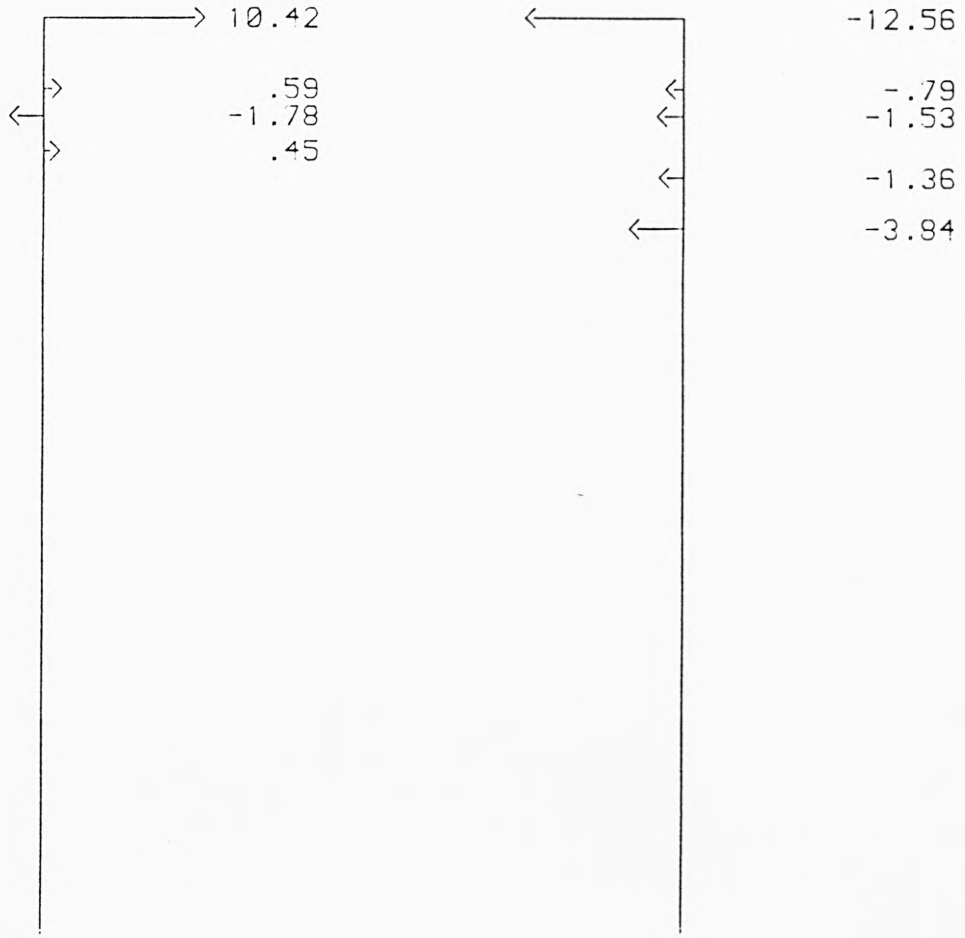

Theoretical Forces For CM = 1.772 and CD = 1.641

cos2wt Forces		sin2wt Forces	
Resultant Force =	9.67 mN	Resultant Force =	-20.09 mN
Depth =	-4. mm	Depth =	34. mm
Measured Force =	6.70 mN	Measured Force =	-18.05 mN
Depth =	-72. mm	Depth =	37. mm
Measured/Theory =	.693	Measured/Theory =	.899

Second Order Morison Coefficients :
CM2 = 1.564 ; CD2 = 1.186

SECOND ORDER WAVE LOADING ON 21.45 MM CYLINDER
WAVE CONDITIONS: WEDGE AMP. 40.0 MM, FREQ. 1.074 HZ

Figure 5.54

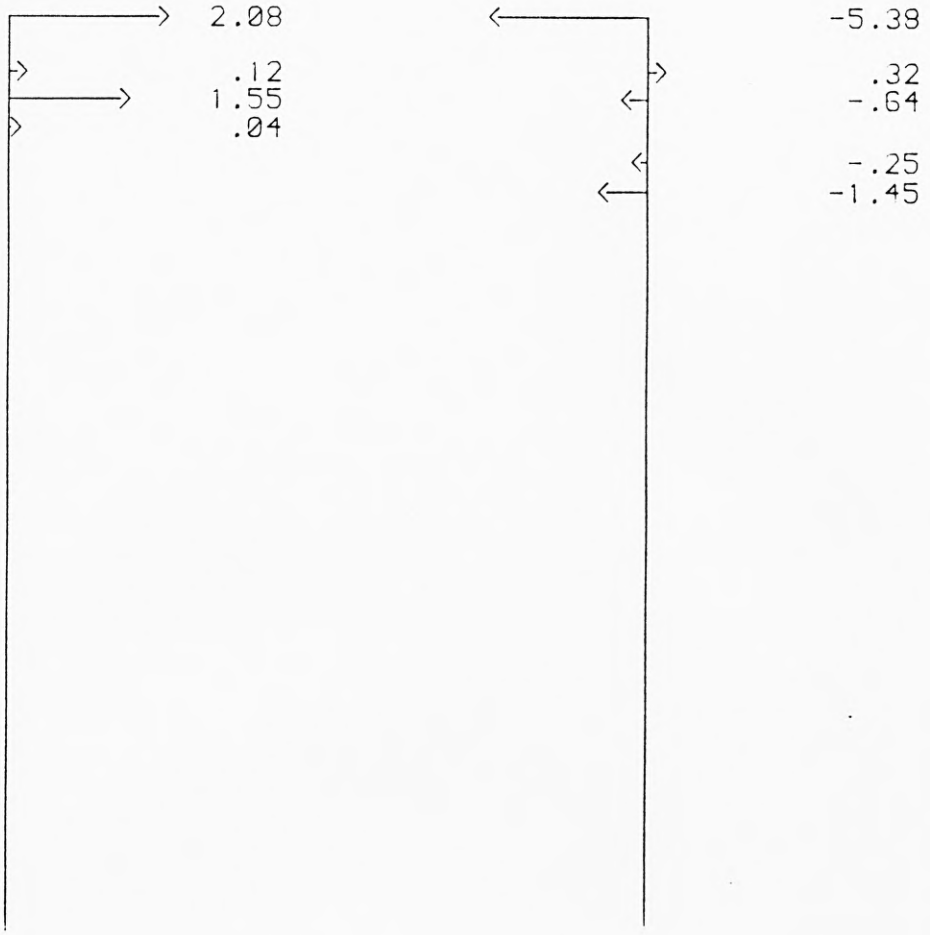

Theoretical Forces For CM = 1.941 and CD = 1.471

cos2wt Forces		sin2wt Forces	
Resultant Force =	3.79 mN	Resultant Force =	-7.40 mN
Depth =	20. mm	Depth =	24. mm
Measured Force =	4.94 mN	Measured Force =	-6.28 mN
Depth =	37. mm	Depth =	-2. mm
Measured/Theory =	1.304	Measured/Theory =	.849

Second Order Morison Coefficients :
CM2 = 1.656 ; CD2 = 2.380

SECOND ORDER WAVE LOADING ON 21.45 MM CYLINDER
WAVE CONDITIONS: WEDGE AMP. 20.0 MM, FREQ. 1.172 HZ

Figure 5.55

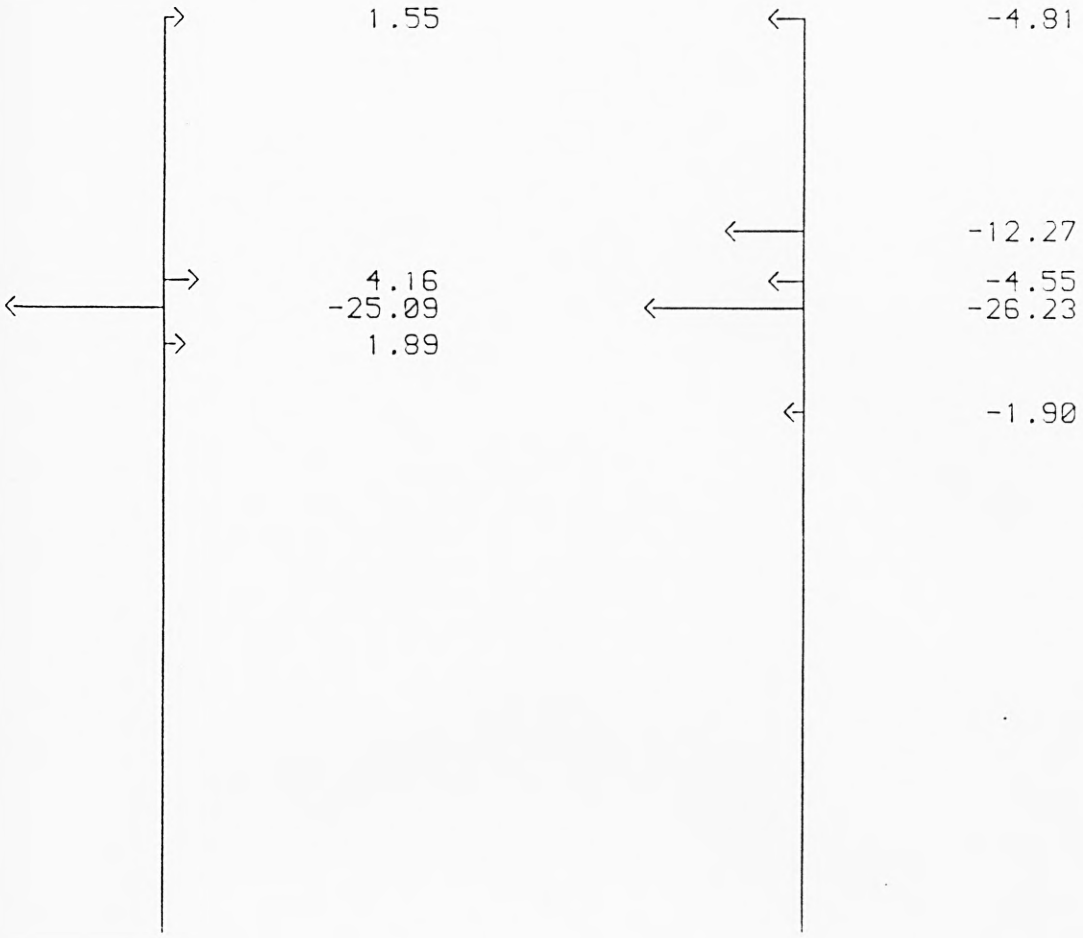

Theoretical Forces for CM = 2.014 and CD = 1.439

cos2wt Forces		sin2wt Forces	
Resultant Force =	-17.50 mN	Resultant Force =	-49.76 mN
Depth =	174. mm	Depth =	134. mm
Measured Force =	-19.37 mN	Measured Force =	-37.80 mN
Depth =	176. mm	Depth =	130. mm
Measured/Theory =	1.107	Measured/Theory =	.760

Second Order Morison Coefficients :
CM2 = 1.640 ; CD2 = .201

SECOND ORDER WAVE LOADING ON 33.56 MM CYLINDER
WAVE CONDITIONS: WEDGE AMP. 50.0 MM, FREQ. .586 HZ

Figure 5.56

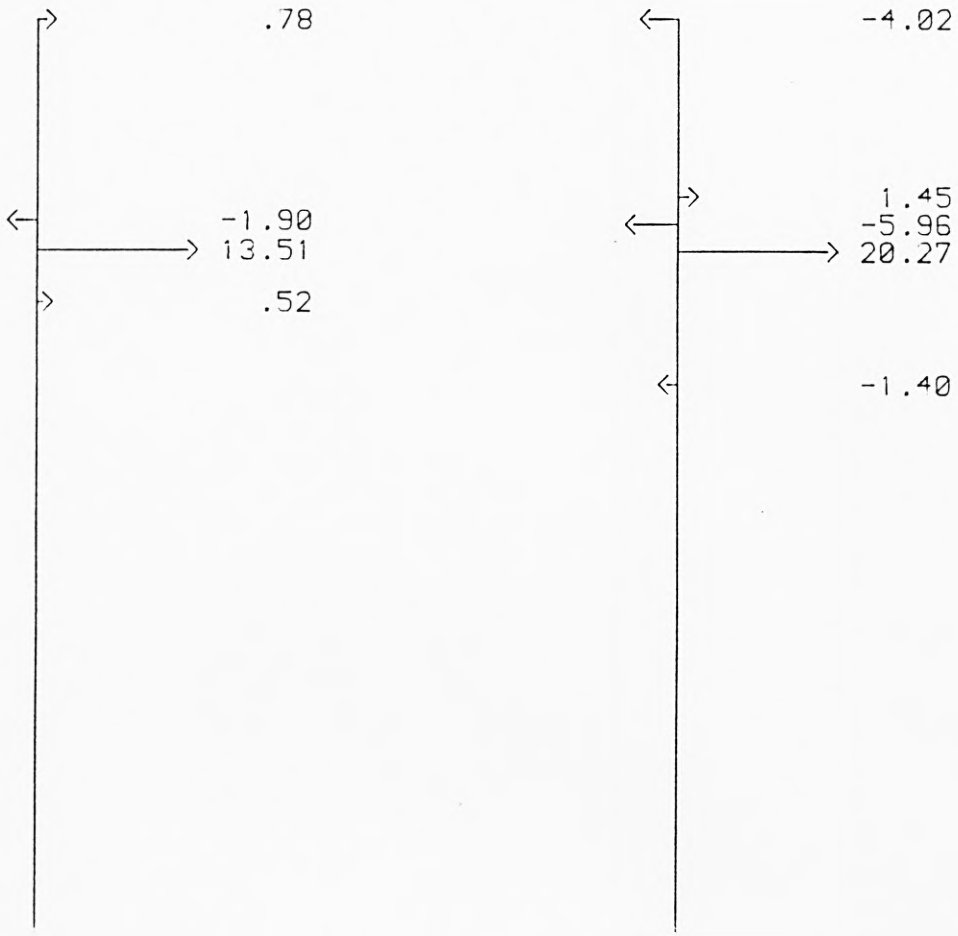

Theoretical Forces For CM = 2.103 and CD = 1.250

cos2wt Forces		sin2wt Forces	
Resultant Force =	12.92 mN	Resultant Force =	10.34 mN
Depth =	123. mm	Depth =	172. mm
Measured Force =	10.43 mN	Measured Force =	11.39 mN
Depth =	105. mm	Depth =	135. mm
Measured/Theory =	.808	Measured/Theory =	1.101

Second Order Morison Coefficients :
CM2 = 1.860 ; CD2 = 3.186

SECOND ORDER WAVE LOADING ON 33.56 MM CYLINDER
WAVE CONDITIONS: WEDGE AMP. 50.0 MM, FREQ. .684 HZ

Figure 5.57

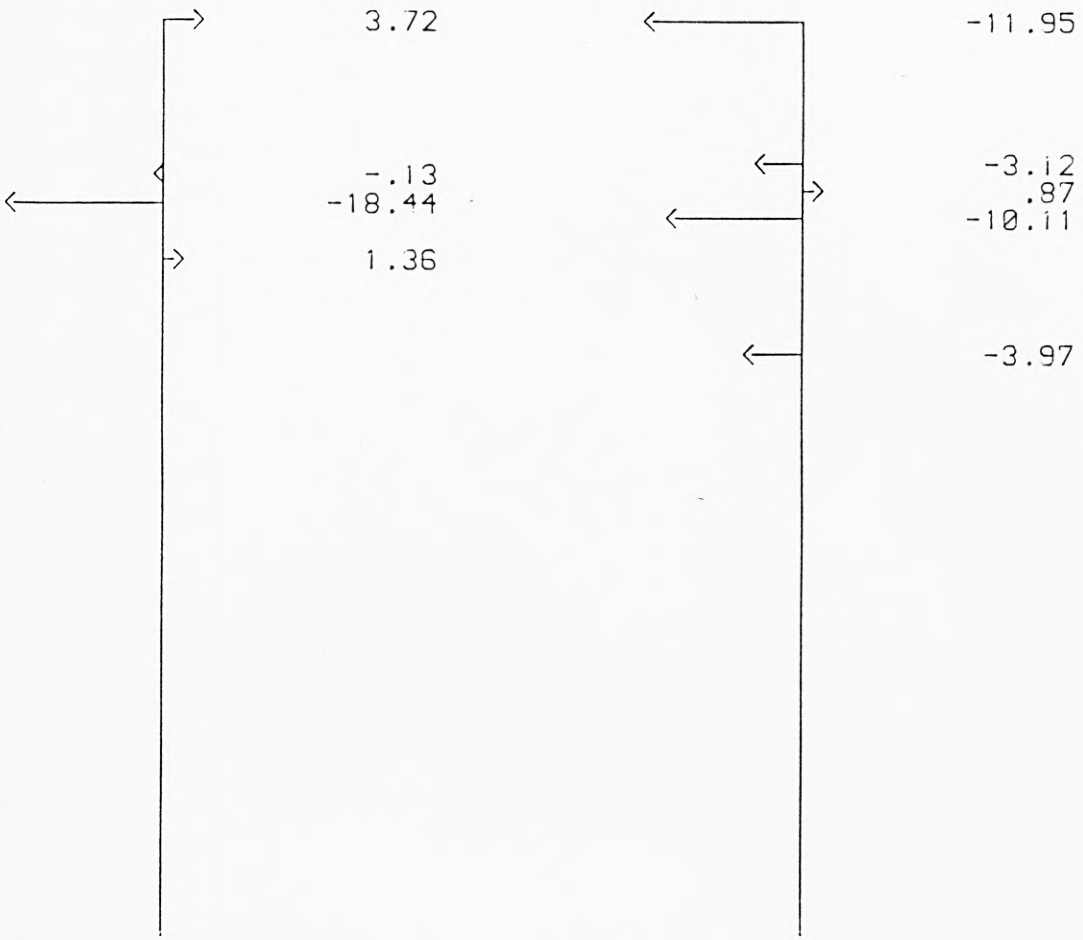

Theoretical Forces For CM = 2.024 and CD = 1.301

cos2wt Forces		sin2wt Forces	
Resultant Force =	-13.49 mN	Resultant Force =	-28.27 mN
Depth =	125. mm	Depth =	70. mm
Measured Force =	-13.08 mN	Measured Force =	-31.95 mN
Depth =	160. mm	Depth =	67. mm
Measured/Theory =	.969	Measured/Theory =	1.130

Second Order Morison Coefficients :
CM2 = 2.235 ; CD2 = 1.916

SECOND ORDER WAVE LOADING ON 33.56 MM CYLINDER
WAVE CONDITIONS: WEDGE AMP. 50.0 MM, FREQ. .781 HZ

Figure 5.58

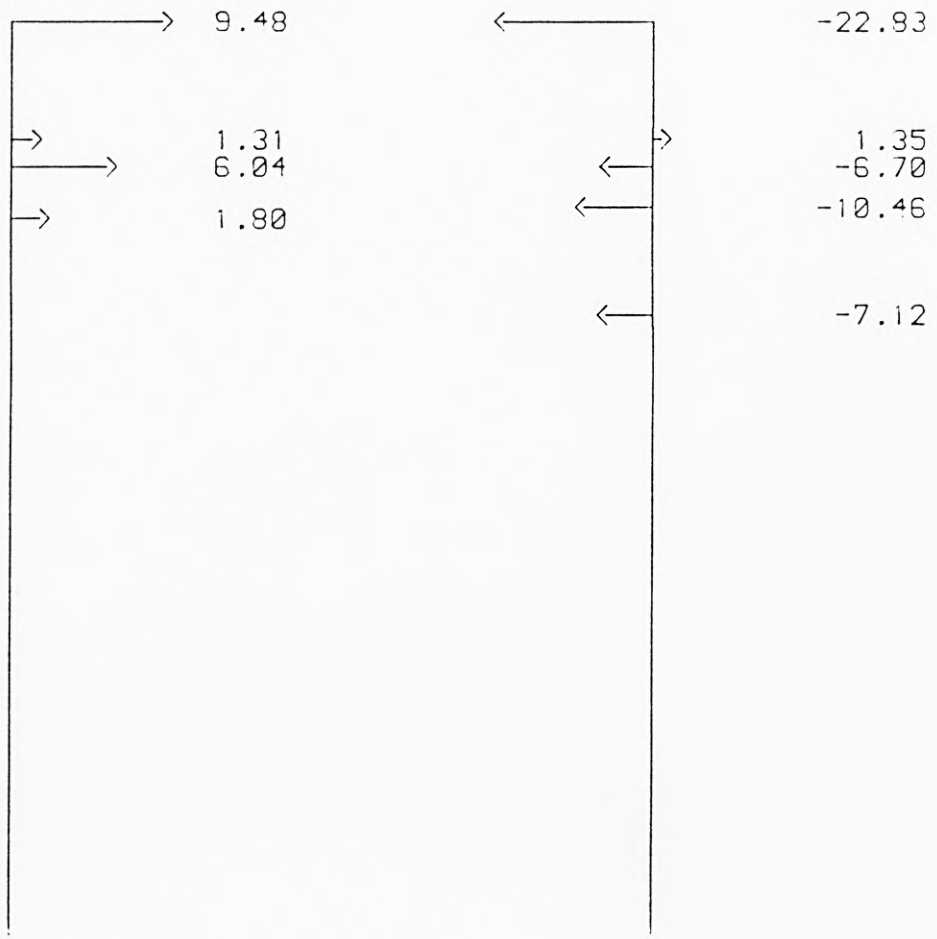

Theoretical Forces For CM = 1.984 and CD = 1.410

cos2wt Forces		sin2wt Forces	
Resultant Force =	18.64 mN	Resultant Force =	-45.76 mN
Depth =	41. mm	Depth =	58. mm
Measured Force =	16.66 mN	Measured Force =	-34.03 mN
Depth =	-11. mm	Depth =	36. mm
Measured/Theory =	.894	Measured/Theory =	.744

Second Order Morison Coefficients :
CM2 = 1.401 ; CD2 = 1.397

SECOND ORDER WAVE LOADING ON 33.56 MM CYLINDER
WAVE CONDITIONS: WEDGE AMP. 50.0 MM, FREQ. .979 HZ

Figure 5.59

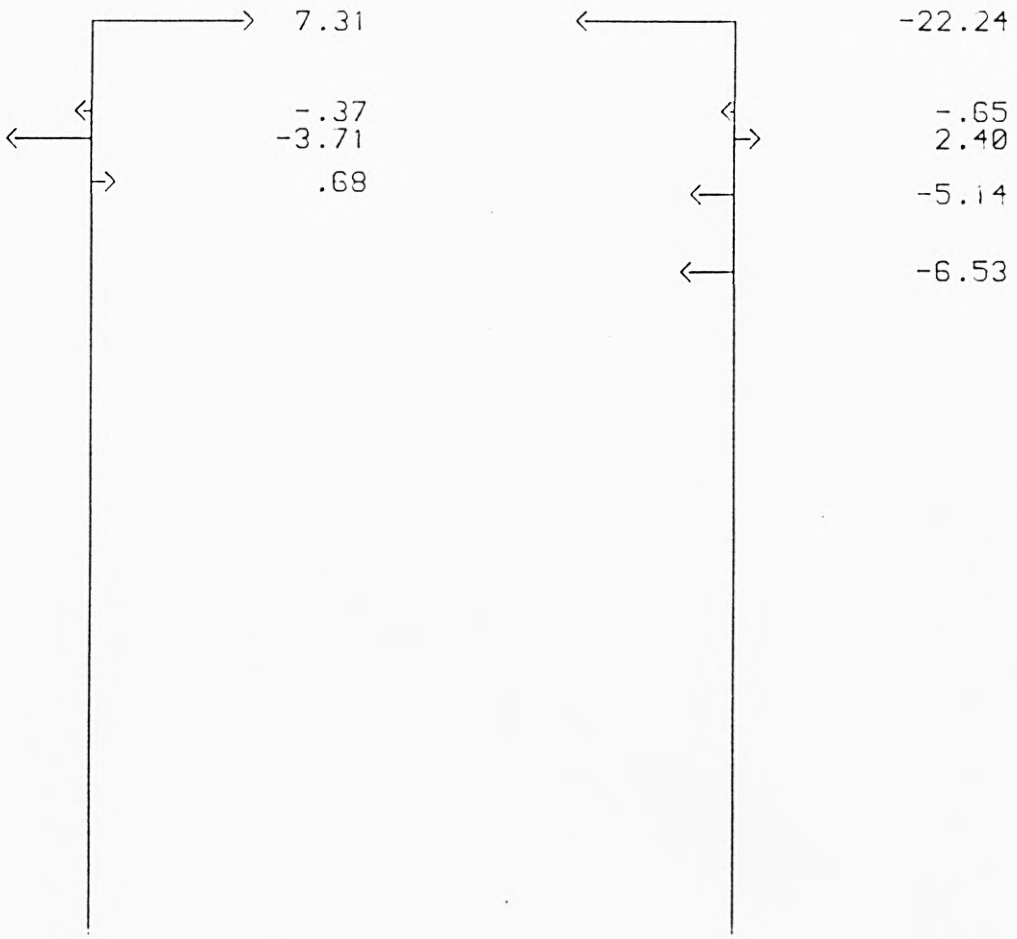

Theoretical Forces for CM = 1.956 and CD = 1.250

cos2wt Forces		sin2wt Forces	
Resultant Force =	3.92 mN	Resultant Force =	-32.16 mN
Depth =	-51. mm	Depth =	39. mm
Measured Force =	3.80 mN	Measured Force =	-27.79 mN
Depth =	-82. mm	Depth =	25. mm
Measured/Theory =	.972	Measured/Theory =	.864

Second Order Morison Coefficients :
CM2 = 1.619 ; CD2 = 1.128

SECOND ORDER WAVE LOADING ON 33.56 MM CYLINDER
WAVE CONDITIONS: WEDGE AMP. 40.0 MM, FREQ. .977 HZ

Figure 5.60

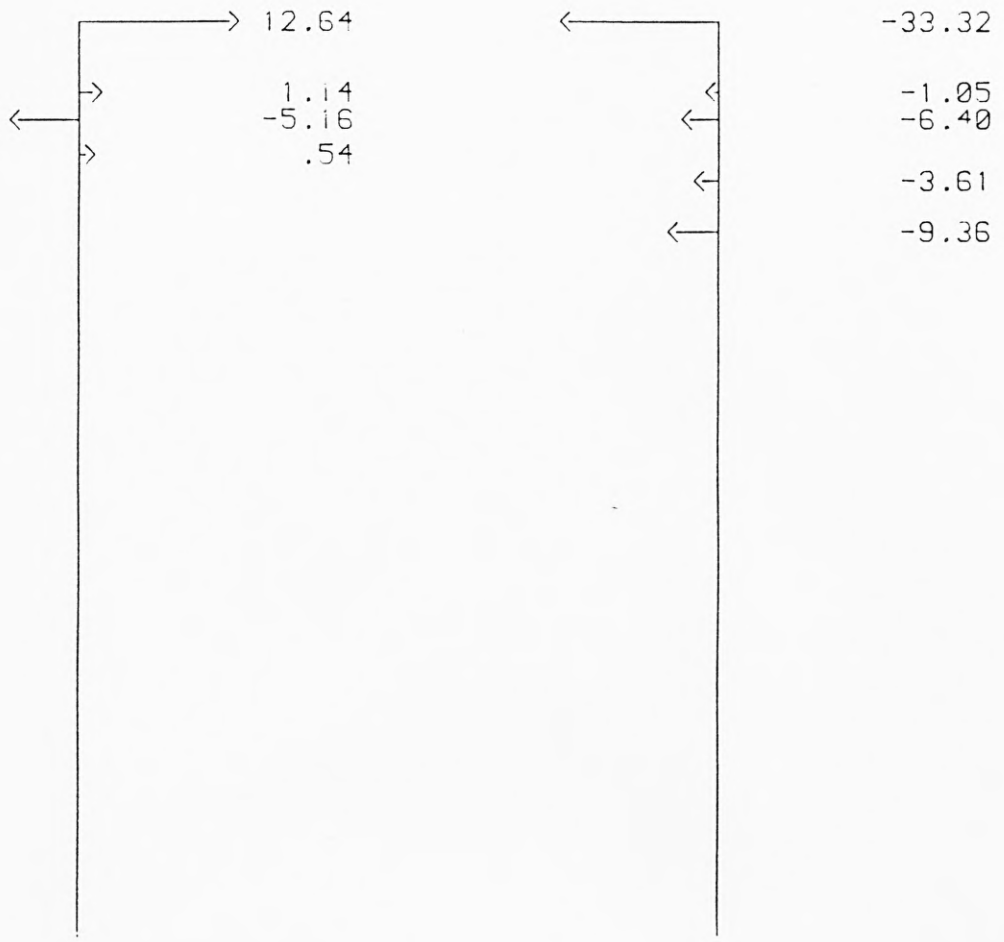

Theoretical Forces For CM = 1.929 and CD = 1.282

cos2wt Forces		sin2wt Forces	
Resultant Force =	9.17 mN	Resultant Force =	-53.73 mN
Depth =	-21. mm	Depth =	33. mm
Measured Force =	21.08 mN	Measured Force =	-39.69 mN
Depth =	-1. mm	Depth =	16. mm
Measured/Theory =	2.300	Measured/Theory =	.739

Second Order Morison Coefficients :
CM2 = 1.270 ; CD2 = 2.191

SECOND ORDER WAVE LOADING ON 33.56 MM CYLINDER
WAVE CONDITIONS: WEDGE AMP. 40.0 MM, FREQ. 1.074 HZ

Figure 5.61

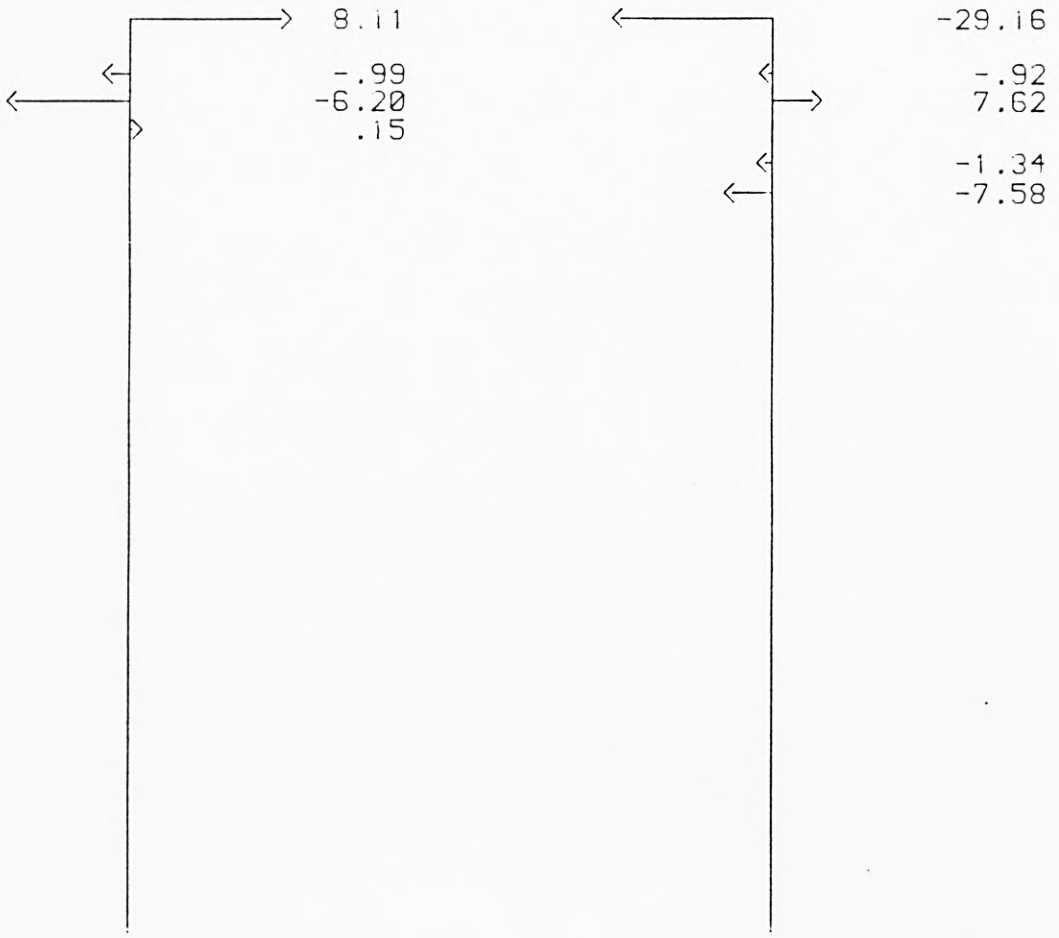

Theoretical Forces For CM = 2.004 and CD = 1.167

cos2wt Forces		sin2wt Forces	
Resultant Force =	1.07 mN	Resultant Force =	-31.39 mN
Depth =	-288. mm	Depth =	17. mm
Measured Force =	-2.52 mN	Measured Force =	-26.72 mN
Depth =	301. mm	Depth =	-2. mm
Measured/Theory =	-2.366	Measured/Theory =	.851

Second Order Morison Coefficients :
CM2 = 1.648 ; CD2 = .413

SECOND ORDER WAVE LOADING ON 33.56 MM CYLINDER
WAVE CONDITIONS: WEDGE AMP. 30.0 MM, FREQ. 1.172 HZ

Figure 5.62

A second method used for comparing the measured and theoretical second order forces involved the use of equivalent second order Morison coefficients. The first order coefficients, C_m and C_d, were replaced by C_{m2} and C_{d2} in the expressions for the theoretical second order forces. Equating the measured and theoretical cos $2\omega t$ and sin $2\omega t$ resultant forces then gave values for C_{m2} and C_{d2}. The full second order force results, including the measured and theoretical forces, and second order Morison coefficients are given in Table 5.4 a, b and c. In a few of the tests, for example Figures 5.43, 5.50, 5.56 and 5.57, both the cos $2\omega t$ and sin $2\omega t$ components are dominated by inertia forces. Thus, the solutions for C_{d2} in these cases are ill-conditioned, and the values obtained are unreliable.

The remainder of the values of C_{m2} and C_{d2} are shown plotted against KCI in Figure 5.63. The results show a considerable degree of scatter and no clear trends. Obviously having a total of nine unknown forces contributing to the two second order force components makes any quantitative analysis difficult.

The second order results do show that, in those cases where the resultant is not the difference between forces of opposite sign, the resultant measured forces agree well with theory. The agreement is generally at its best where the free wave forces are small and the waterline and dynamic pressure forces, suggested by Lighthill (1979), are dominant.

Wave Setting		In Phase Component					Quadrature Component						
WA	Freq	Theoretical		Measured		meas.	Theoretical		Measured		meas.	C_{m2}	C_{d2}
(mm)	(Hz)	Force (mN)	Depth (mm)	Force (mN)	Depth (mm)	theory	Force (mN)	Depth (mm)	Force (mN)	Depth (mm)	theory		
50	0.586	0.24	-261	0.17	-537	0.71	-6.49	135	-4.18	219	0.64	1.79	1.29
60	0.586	1.24	2	0.49	-424	-	10.49	135	-6.03	218	0.58	1.08	-
70	0.586	3.01	53	1.40	-208	0.47	-14.06	134	-8.29	219	0.59	1.64	1.13
50	0.684	1.54	111	0.94	103	0.61	1.81	151	1.23	148	0.68	1.87	-
40	0.781	-0.03	-	0.47	-	-	-2.02	66	-1.39	58	0.69	1.35	-
50	0.781	0.79	-102	1.67	-31	2.10	-4.00	73	-2.69	74	0.67	1.12	-
60	0.781	1.85	-46	1.62	-164	0.87	-5.86	73	-3.92	121	0.67	1.48	1.52
50	0.879	5.70	30	3.95	-17	0.69	-3.69	54	-1.88	48	0.51	1.12	1.50
30	0.977	0.93	-28	1.08	-10	1.17	-1.88	45	-1.56	15	0.83	1.28	1.90
40	0.977	2.76	-5	2.19	37	0.80	-2.65	45	-2.40	33	0.91	1.46	1.54
50	0.977	6.87	7	5.07	31	0.74	-3.03	43	-3.64	64	1.20	1.85	1.37
50	1.074	12.03	8	8.46	2	0.70	-3.51	33	-4.59	25	1.31	1.69	1.23
20	1.172	1.52	13	1.26	-47	0.83	-1.56	25	-1.34	-17	0.86	1.66	1.45
30	1.172	2.89	-8	2.53	-43	0.88	-2.28	17	-2.85	-13	1.25	-	1.62
40	1.172	6.91	-7	5.07	-34	0.73	-5.16	26	-5.67	-29	1.10	2.06	1.47

Second Order Force Results - 9.55 mm Cylinder

Table 5.4 a

Wave Setting		In Phase Component					Quadrature Component						
WA	Freq	Theoretical		Measured			Theoretical		Measured			C_{m2}	C_{d2}
(mm)	(Hz)	Force (mN)	Depth (mm)	Force (mN)	Depth (mm)	meas. / theory	Force (mN)	Depth mm)	Force (mN)	Depth (mm)	meas. / theory		
50	0.586	-4.17	206	-6.40	174	1.53	-19.27	134	-15.15	144	0.79	1.55	-
60	0.586	-0.85	640	-6.22	190	-	-29.11	136	-20.96	127	0.72	1.33	-
70	0.586	3.55	-47	-5.90	229	-	-37.44	134	-26.69	124	0.71	1.28	-
50	0.684	5.69	119	4.59	116	0.81	4.00	165	3.70	140	0.93	1.60	-
40	0.781	-1.81	166	-3.21	120	1.78	-6.17	68	-5.53	72	0.90	1.96	-
50	0.781	-0.93	412	-0.51	697	0.55	-13.69	78	-12.66	77	0.92	1.60	1.61
60	0.781	-0.62	917	-3.72	266	-	-17.11	76	-16.87	84	0.99	1.82	1.26
50	0.879	11.20	30	9.87	19	0.88	-15.96	60	-12.53	53	0.79	1.30	1.60
30	0.977	1.41	-50	0.54	-465	0.38	-9.11	46	-10.20	32	1.12	2.10	1.23
40	0.977	5.67	-4	1.67	-295	-	-11.89	41	-12.32	46	1.04	1.87	-
50	0.977	14.77	7	8.01	-92	0.54	-17.07	42	-17.10	67	1.00	1.62	0.95
40	1.074	9.67	-4	6.70	-72	0.69	-20.09	34	-18.05	37	0.90	1.56	1.19
20	1.172	3.79	20	4.94	37	1.30	-7.40	24	-6.28	-2	0.85	1.66	-
30	1.172	5.59	-8	-0.17	-	-	-11.82	16	-12.15	-4	1.03	2.01	-
40	1.172	12.70	-16	6.02	-172	0.47	-25.09	24	-23.63	31	0.94	1.73	1.10

Second Order Force Results - 21.45 mm Cylinder

Table 5.4 b

Wave Setting		In Phase Component					Quadrature Component						
WA	Freq	Theoretical		Measured			Theoretical		Measured			C_{m2}	C_{d2}
(mm)	(Hz)	Force (mN)	Depth (mm)	Force (mN)	Depth (mm)	meas. / theory	Force (mN)	Depth (mm)	Force (mN)	Depth (mm)	meas. / theory		
50	0.586	-17.50	174	-19.37	176	1.11	-49.76	134	-37.80	130	0.76	1.64	-
60	0.586	-18.63	189	-22.10	194	1.19	-77.90	135	-59.04	136	0.76	1.57	-
70	0.586	-28.25	191	-28.72	201	1.02	-92.54	130	-70.99	137	0.77	1.56	0.93
50	0.684	12.92	123	10.45	105	0.81	10.34	172	11.39	135	1.10	1.86	-
40	0.781	-8.08	119	-7.24	129	0.90	-15.52	66	-14.18	59	0.91	1.86	1.08
50	0.781	-13.49	125	-13.08	160	0.97	-28.27	70	-31.95	67	1.13	2.24	1.92
60	0.781	-13.90	148	-13.44	201	0.97	-43.91	72	-41.79	68	0.95	1.90	1.35
50	0.879	18.64	41	16.66	-11	0.89	-45.76	58	-34.03	36	0.74	1.40	1.39
30	0.977	-3.29	114	-2.87	127	0.87	-21.72	43	-22.33	32	1.03	2.04	1.22
40	0.977	3.92	-51	3.80	-82	0.97	-32.16	39	-27.79	25	0.86	1.62	1.13
50	0.977	22.07	18	17.24	-17	0.78	-47.22	39	-35.45	19	0.75	1.30	1.14
40	1.074	9.17	-21	21.08	-1	2.30	-53.73	33	-39.69	16	0.74	1.27	2.19
20	1.172	6.10	32	10.85	48	1.78	-19.34	23	-13.47	2	0.70	1.40	-
30	1.172	1.07	-288	-2.52	301	-	-31.39	17	-26.72	-2	0.85	1.65	-
40	1.172	12.22	-37	14.16	-89	1.16	-54.98	19	-49.18	11	0.90	1.64	1.51

Second Order Force Results - 33.56 mm Cylinder

Table 5.4 c

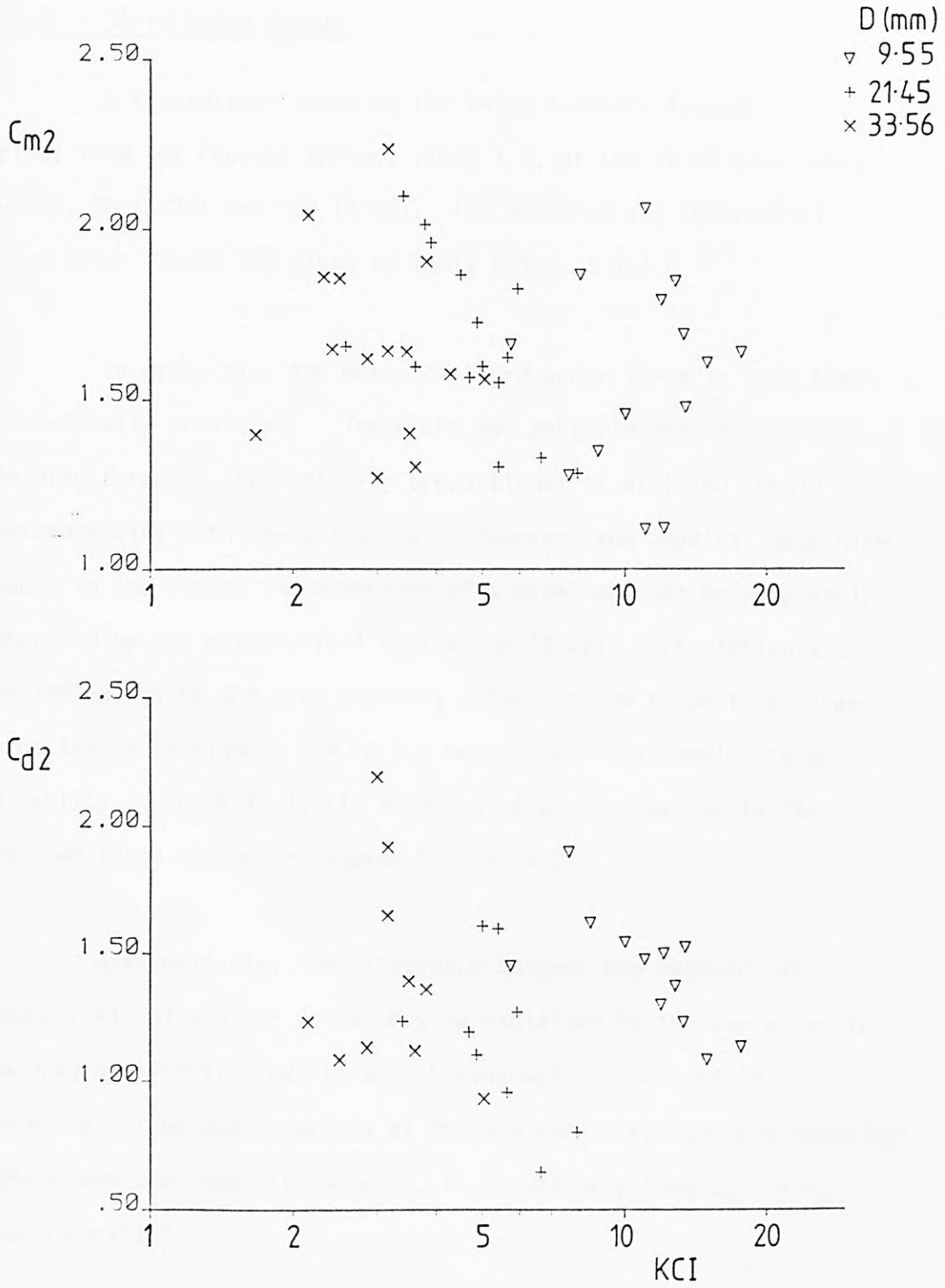

Second Order Inertia and Drag Coefficients

Figure 5·63

5.2.4 Third Order Forces

A theoretical force at the third harmonic frequency arises from the Fourier series, Table 3.2, of the first order drag forces, FD (3-32) and FDR (3-62). The measured and theoretical third order forces are given in Table 5.5 a, b and c.

In every case the measured third order force is less than theoretically predicted. There are two possible reasons for this. The drag force is theoretically proportional to $u|u|$ and should therefore vary with $\cos \omega t|\cos \omega t|$. However, the physical mechanism producing the force, the formation of a wake, may not be completely described by the mathematical expression (3-32). In particular, the inflexions at the zero crossing points in the theoretical drag force traces in Figures 3.4 to 3.6 may not be so strongly present in reality. There is little evidence of any inflexions in the measured force traces in Figures 5.26 to 5.37.

Alternatively, the difference between the measured and theoretical third order forces may be explained by the variation in the drag and inertia coefficients throughout the wave cycle. Since the instantaneous values of the Keulegan Carpenter and Reynolds' numbers are continuously changing, it is unlikely that C_m and C_d remain constant.

Keulegan and Carpenter (1958) suggested that the difference between the measured and theoretical forces should be termed the remainder force, of the form;

$$\Delta R_e = \rho u_m^2 \, D \, A_3 \cos 3\omega t \, \delta y + \rho u_m^2 D B_3 \sin 3\omega t \, \delta y \qquad (5\text{-}8)$$

Keulegan and Carpenter's experiments were carried out on a horizontal cylinder under the node of a standing wave. Thus the velocity u_m did not vary along the length of the cylinder, and replacing δy by the cylinder length gave the total remainder force ΔR. The equivalent expression for a vertical cylinder is found by integrating (5-8) between the bottom and the surface.

$$\Delta R = \tfrac{1}{2} \rho D a_I^2 g \left(\frac{\sinh 2kh + 2kh}{\sinh 2kh} \right) (A_3 \cos 3\omega t + B_3 \sin 3\omega t) \qquad (5\text{-}9)$$

The remainder force, ΔR, and the coefficients, A_3 and B_3, are given in Table 5.5, and the remainder force coefficients are plotted against KCI in Figures 5.64 and 5.65, together with the results of Keulegan and Carpenter (1958).

The cos $3\omega t$ coefficient, A_3, in Figure 5.64 is negative for all values of KCI. At low values of KCI, A_3 falls sharply reaching a minimum at KCI of approximately 4. A_3 then increases gradually with KCI and may be expected to tend toward zero for very high Keulegan Carpenter numbers.

The measured values of the sin $3\omega t$ coefficient, Figure 5.65, have a large degree of scatter which disguises any definite trends. B_3 tends to be close to zero for KCI less than 3 or greater than 10, and there is some evidence of a weak minimum in between.

Neither of the coefficients displays a trend which agrees with the results of Keulegan and Carpenter (1958). However, the experimental arrangement is very different in the two sets of

experiments, especially with regard to the variation in velocity along the cylinder length. Also, no account is taken of third order particle kinematics in either study.

Wave Setting		Theoretical Force		Measured Force		Remainder Force		A_3	B_3
WA (mm)	Freq (Hz)	In Phase (mN)	Quad (mN)	In Phase (mN)	Quad (mN)	In Phase (mN)	Quad (mN)		
50	0.586	3.03	0.36	1.83	-0.33	-1.20	-0.69	-0.057	-0.033
60	0.586	4.65	0.67	2.65	-1.01	-2.00	-1.68	-0.061	-0.051
70	0.586	6.60	1.01	4.24	-1.72	-2.36	-2.73	-0.052	-0.060
50	0.684	2.09	0.06	0.78	-0.16	-1.31	-0.24	-0.102	-0.017
40	0.781	3.21	-0.02	1.70	0.66	-1.51	0.68	-0.079	0.036
50	0.781	5.19	-0.04	3.38	1.09	-1.81	1.13	-0.060	0.037
60	0.781	7.20	0.07	4.59	0.55	-2.61	0.48	-0.058	0.011
50	0.879	7.47	0.19	4.65	0.90	-2.82	0.71	-0.063	0.016
30	0.977	2.96	0.04	1.70	0.25	-1.26	0.21	-0.062	0.010
40	0.977	5.09	0.13	2.76	0.34	-2.33	0.21	-0.069	0.006
50	0.977	8.36	-0.24	4.29	-0.21	-4.07	0.03	-0.071	0.001
50	1.074	10.20	-0.65	6.95	-0.22	-3.25	0.43	-0.048	0.006
20	1.172	1.95	-0.05	0.81	-0.26	-1.14	-0.21	-0.084	-0.015
30	1.172	4.28	0.01	2.44	-0.63	-1.84	-0.64	-0.063	-0.022
40	1.172	7.85	-0.20	5.35	-1.32	-2.50	-1.12	-0.050	-0.026

Third Order Force Results - 9.55 mm Cylinder

Table 5.5 a

Wave Setting		Theoretical Force		Measured Force		Remainder Force		A_3	B_3
WA (mm)	Freq (Hz)	In Phase (mN)	Quad (mN)	In Phase (mN)	Quad (mN)	In Phase (mN)	Quad (mN)		
50	0.586	5.80	0.69	1.52	-3.95	-4.28	-4.64	-0.087	-0.095
60	0.586	9.51	1.31	3.79	-5.18	-5.72	-6.49	-0.078	-0.088
70	0.586	15.19	2.48	6.07	-2.84	-9.12	-5.32	-0.087	-0.051
50	0.684	3.58	0.09	0.90	-1.08	-2.68	-1.17	-0.092	-0.040
40	0.781	5.06	-0.03	0.25	-1.86	-4.81	-1.83	-0.111	-0.043
50	0.781	8.93	-0.19	0.80	-2.30	-8.13	-2.11	-0.114	-0.030
60	0.781	13.42	0.03	4.28	-1.19	-9.14	-1.22	-0.091	-0.012
50	0.879	14.45	0.45	5.67	-2.45	-8.78	-2.90	-0.088	-0.029
30	0.977	5.42	0.01	0.63	-2.24	-4.79	-2.25	-0.105	-0.049
40	0.977	10.18	-0.18	2.14	-1.18	-8.04	-1.00	-0.100	-0.012
50	0.977	17.87	-0.67	4.72	0.87	-13.15	1.54	-0.104	-0.012
40	1.074	12.69	-0.40	2.92	-1.78	-9.77	-1.38	-0.101	-0.014
20	1.172	3.70	0.02	0.64	-0.95	-3.06	-0.97	-0.099	-0.032
30	1.172	8.25	0.08	0.13	0.08	-8.12	0.00	-0.123	0.000
40	1.172	16.88	-0.53	-0.13	-1.85	-17.01	-1.32	-0.154	-0.012

Third Order Force Results - 21.45 mm Cylinder

Table 5.5 b

Wave Setting		Theoretical Force		Measured Force		Remainder Force		A_3	B_3
WA (mm)	Freq (Hz)	In Phase (mN)	Quad (mN)	In Phase (mN)	Quad (mN)	In Phase (mN)	Quad (mN)		
50	0.586	7.73	0.96	-1.92	-10.64	-9.65	-11.60	-0.126	-0.152
60	0.586	12.87	1.79	-3.36	-18.39	-16.23	-20.18	-0.139	-0.173
70	0.586	19.35	3.18	-7.57	-24.11	-26.92	-27.29	-0.165	-0.167
50	0.684	4.48	0.19	0.70	1.48	-3.78	1.29	-0.082	-0.028
40	0.781	6.23	-0.01	-1.56	-3.29	-7.79	-3.30	-0.114	-0.048
50	0.781	10.65	0.00	-4.54	-7.12	-15.19	-7.12	-0.140	-0.066
60	0.781	17.42	0.16	-6.42	-6.37	-23.84	-6.53	-0.151	-0.041
50	0.879	18.47	0.81	3.74	-8.09	-14.73	-8.90	-0.090	-0.055
30	0.977	5.51	0.13	0.15	-2.85	-5.36	-2.98	-0.076	-0.042
40	0.977	11.78	0.06	-1.95	-1.95	-13.73	-2.01	-0.111	-0.016
50	0.977	21.55	-0.23	0.63	-3.31	-20.92	-3.08	-0.106	-0.016
40	1.074	15.62	-0.79	-1.08	3.28	-16.70	4.07	-0.111	0.027
20	1.172	3.07	0.05	1.56	-0.92	-1.51	-0.97	-0.031	-0.020
30	1.172	9.84	0.10	-1.66	-0.05	-11.50	-0.15	-0.111	-0.001
40	1.172	21.58	-0.73	-5.89	1.78	-27.47	2.51	-0.155	0.014

Third Order Force Results - 33.56 mm Cylinder

Table 5.5 c

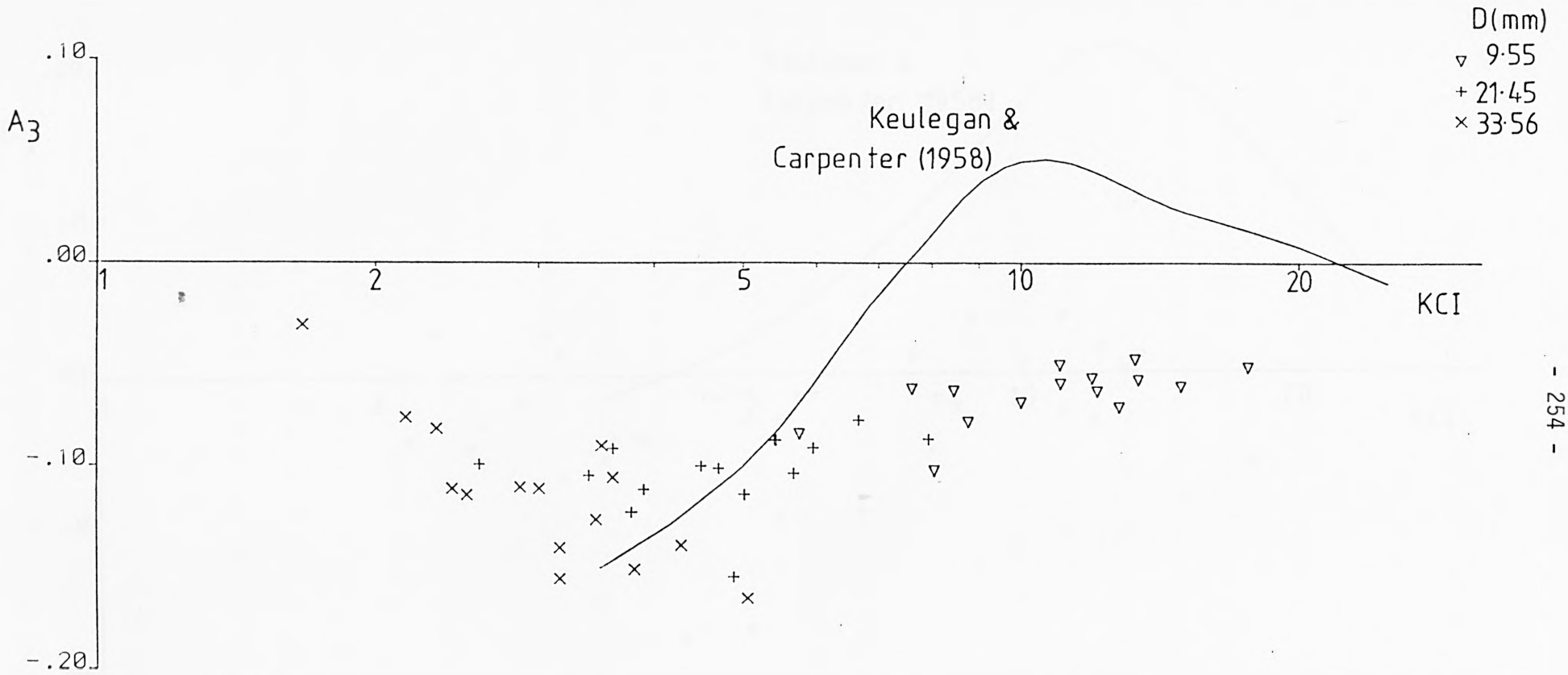

Remainder Force - cos 3wt Coefficient

Figure 5·64

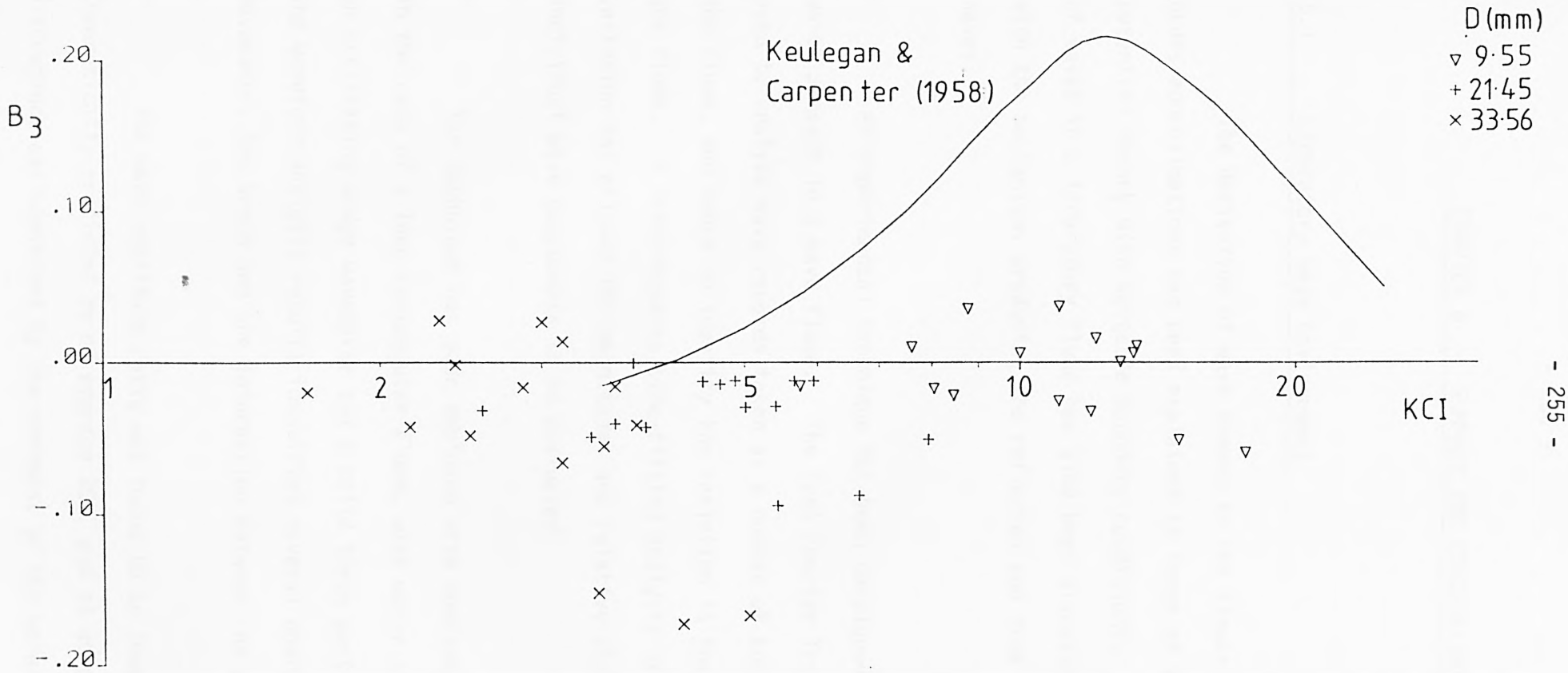

Remainder Force - sin 3wt Coefficient

Figure 5·65

CHAPTER 6 - SUMMARY AND CONCLUSIONS

6.1 Laboratory Wave Environment

The derivation of wave theory to its linear and second order approximations has been explained in terms of velocity potential theory with suitable boundary conditions. The generation of waves in a laboratory flume has also been discussed, together with the mechanisms producing the reflected and free second harmonic waves.

An experimental technique has been developed to measure the waves present in a wave flume. The Fast Fourier Transform has been used to analyse wave records taken at a number of known positions in the flume, and hence to identify the variation in the waveform down the flume. A least-squares sine-fitting analysis of the waveform variation has allowed the magnitudes and relative phases of the individual wave components to be evaluated.

The technique has been employed with considerable success in the case of a long rectangular flume, with water of constant depth, an oscillating wedge wavemaker and a solid three part absorbing beach. The waveform analysis results identified several characteristics of the wavemaker, the beach and the interaction between the wave components.

The wave amplitude ratio was found to be lower than theoretically predicted by on average 20%, and at worst 50%. This discrepancy was explained by the movement of the water in the region behind the wedge.

The wedge wavemaker was shown to produce a significant free second harmonic wave, especially at lower frequencies, where its amplitude was as much as 12% of the total wave motion. This demonstrates that the free wave cannot be neglected in any experimentation carried out in this flume.

The interaction between the wave components was highlighted in the celerity of the free second harmonic wave, which was found to be greater than the dispersion value it would have had in the absence of the main wave. The free wave was being carried along by the main wave, with the effect of being accounted for in part by the phenomenon of mass transport.

The beach was found to be an efficient absorber of wave energy, with no more than 5% of the first order incident wave amplitude being reflected. The reflection coefficient was generally lower at higher frequencies, but no obvious relationship could be inferred from the results. The reflected second harmonic wave had a disproportionately large amplitude, when compared to the incident free second harmonic wave. It was, however, found to be small enough, relative to the total wave motion, to be neglected.

The wave environment was not substantially altered by the presence of a test cylinder, but two effects were noted. In the immediate vicinity of the cylinder the wave amplitude tended towards local high or low values. The wave amplitude was found to be slightly reduced as it passed the cylinder, this being a blockage effect due to the energy lost by the wave in exerting the forces on the cylinder.

6.2 Non Linear Wave Loading

The theoretical wave induced loading on a vertical surface piercing cylinder has been developed from its linear approximation by considering the effect of various non-linear forces, both individually and collectively.

The linear approximation to the loading was found by using Morison's equation, to give the drag and inertia forces on an element of the cylinder. Linear wave theory was used to calculate the particle kinematics, and the total force was found by integrating up to the still water level.

The use of drag and inertia coefficients in determining the elemental force has been explained, and the relative importance of the drag and inertia forces has been shown to depend on the Keulegan Carpenter number. An alternative expression for the Keulegan Carpenter number, giving its integrated average value, has been proposed for the case of a vertical cylinder.

As a next approximation, the particle kinematics were described by Stokes' second order wave theory. This correction predicted significant forces at the second harmonic frequency under the conditions of steep waves in shallow water.

The use of the local fluid acceleration in calculating the inertia force was investigated by considering the effect of including the convective acceleration. Under all except the steepest shallow water waves, the force due to the convective acceleration was shown to be negligible.

The use of undisturbed water level as the upper limit for the integration of the elemental forces was shown to be an oversimplification. The velocities and accelerations in the waterline region were found to produce significant second order drag and inertia forces, termed the waterline forces.

A further second order force was derived from the variation in the dynamic pressure around the cylinder circumference. The dynamic pressure force was shown to have a similar form to, but be somewhat smaller than, the waterline inertia force.

The effect that the additional wave components present in a laboratory flume have on a test cylinder was also investigated. The importance of considering the phases, as well as the amplitudes, of the free and reflected waves was established.

The Fourier compositions and depths of action of the force components were evaluated to allow the theoretical resultant force acting at each harmonic frequency to be determined.

The total linear and non-linear forces acting on a cylinder, under both measured laboratory conditions and design wave conditions, were calculated. The results demonstrated that the non linear forces make a very significant contribution to the total loading.

A series of experiments have been conducted to measure the wave forces on vertical cylinders of three diameters. In each case the cylinder was simply-supported between force transducers to allow the resultant force components and their depths of action to be

computed. A Fast Fourier Transform technique was employed to separate the harmonics of the total force and determine their phase relationships. The amplitudes and phases of the various wave components were measured at the same time, so that their effect on the loading could be considered.

Graphical examination of the force transducer outputs identified a number of features of the wave loading. The phase difference between the wave and force traces indicated the relative importance of the drag and inertia forces in each case. Under appropriate wave conditions, the drag and inertia waterline forces and the forces due to the free wave were observed in the transducer outputs, whose time variations showed good agreement with the theoretical predictions.

The graphical records of the forces on the smallest cylinder also highlighted the phenomenon of vortex shedding and its effect on the total loading.

The numerical force results were analysed by considering the first, second and third order forces separately. The measured first order forces and wave data were used to calculate values for the drag and inertia coefficients. Both of these coefficients showed good correlation with the Keulegan Carpenter number, and their general trends agreed with those found by previous investigators. A few high values of C_m, and the generally slightly higher values of C_d, were explained by the dependence of the coefficients on the Reynolds' number.

The measured second order force components were compared with the theoretical forces, calculated using the measured wave data and the first order Morison coefficients. In a good number of cases the measured and theoretical forces agreed to within 20% of the second order force, equivalent to 2% of the total force. The measured second order force was somewhat less than theory in those cases where it was dominated by the forces due to the free second harmonic wave, indicating that the first order Morison coefficients may be inappropriate in calculating those forces. In a few unavoidable instances the resultant force was given by the small difference between forces of opposite sign, leading to a poor agreement between theory and experiment.

Because of the large number of theoretical forces contributing to the second order components, it was not possible to quantify them individually. Attempts to assign equivalent second order Morison coefficients gave scattered results and no clear trends.

The measured third order forces were compared with the theoretical components arising from the Fourier series of the first order drag forces. The measured force was less than theory in every case, indicating the inadequacy of the mathematical description of the drag force.

6.3 Limitations and Recommendations for Further Work

The experimental work carried out in this study was subject to a number of limitations, which were features of the facilities used. The wedge wavemaker was found to produce a very significant

free second harmonic wave. This in turn imposed a large second order force on the test cylinder, in some cases outweighing the other non linear components, and necessitated a lengthy procedure to measure its amplitude and phase in each case. In an experimental study aiming to identify the non-linear forces proposed by Lighthill (1979), the free wave is an undesirable feature, and two possible remedies exist. Either the experimental conditions should be limited to those in which the free wave is small, or the free wave amplitude should be reduced by introducing a second harmonic component into the wedge motion, in a similar manner to that used by Buhr Hansen and Svendsen (1974) for a piston.

The very small scale of the testing gave rise to a number of limitations, which could be reduced by working in a larger facility. The Reynolds' numbers covered by this study were as much as 1000 times smaller than those encountered in real sea conditions. This means that the measured drag and inertia coefficients, and possibly the observed second order effects, cannot be extrapolated to design conditions.

The very small forces exerted on the cylinders required highly sensitive equipment for their detection. Even with the equipment used the forces on the smallest cylinder were only just measurable, and no cylinder smaller than this could be used. This limited the Keulegan Carpenter number to values below 20. Larger scale testing could use cylinders of smaller relative diameter, and hence cover a wider range of conditions.

A further feature of the force measurement which might be eliminated by larger scale testing is instrumental drift. Where the force outputs do not need such powerful amplification the Wheatstone bridge balance point may be more stable, allowing the time averaged force to be measured.

APPENDIX 1 - THE FAST FOURIER TRANSFORM

Fourier's Theorem states that any periodic function may be represented by the sum of an infinite number of trigonometric functions at its harmonic frequencies.

$$x(t) = a_o + 2 \sum_{m=1}^{\infty} \left(a_m \cos \frac{2\pi mt}{T} + b_m \sin \frac{2\pi mt}{T}\right) \qquad \text{(A1-1)}$$

where a_o is the mean value of the function, and a_m and b_m are the Fourier coefficients given by;

$$a_m = \frac{1}{T} \int_0^T x(t) \cos \frac{2\pi mt}{T} \, dt$$

$$b_m = \frac{1}{T} \int_0^T x(t) \sin \frac{2\pi mt}{T} \, dt \qquad \text{(A1-2)}$$

Complex notation is used to combine (A1-2) into a single equation for each frequency by defining;

$$X_m = a_m - ib_m \qquad \text{(A1-3)}$$

and de Moivre's theorem gives;

$$X_m = \frac{1}{T} \int_0^T x(t) e^{-i(2\pi mt/T)} \, dt \qquad \text{(A1-4)}$$

In a digitized experimental record, the continuous function $x(t)$ is represented by a number of sample points - a discrete time series $\{x_r\}$, $r = 0,1,2,....(N-1)$, where $t = r\Delta$ and $\Delta = T/N$. Equation (A1-4) is modified as the integral becomes a summation;

$$X_m = \frac{1}{N} \sum_{r=0}^{N-1} x_r e^{-i(2\pi mr/N)} \qquad \text{(A1-5)}$$

The real and imaginary parts of $\{x_m\}$ in (A1-5) define the discrete Fourier Transform (D.F.T.) of the time series $\{x_r\}$. The D.F.T. does not contain enough information for the continuous fuction $x(t)$ to be obtained, but the discrete time series can be reconstructed exactly using the inverse D.F.T.;

$$x_r = 2 \sum_{m=0}^{N-1} X_m e^{i(2\pi mr/N)} \qquad \text{(A1-6)}$$

The number of complex calculations required to evaluate the complete D.F.T. of the series is N for each of the N components, giving a total of N^2. Since N can run into thousands, this involves a great deal of computer processor time. The Fast Fourier Transform (F.F.T.) technique reduces this workload by dividing the full time series into a number of shorter sequences and determining their D.F.T.s. These are then combined to give the D.F.T. of the full sequence.

Consider a discrete time series $\{x_r\}$ divided into two shorter sequences $\{y_r\}$ and $\{z_r\}$, such that they take alternate

terms from the full sequence;

$$y_r = x_{2r}$$

$$z_r = x_{2r+1} \qquad \text{(A1-7)}$$

The D.F.T.s of these sequences are;

$$Y_m = \frac{1}{N/2} \sum_{r=0}^{N/2-1} y_r \, e^{-i2\pi mr/(N/2)} \qquad \text{(A1-8)}$$

$$z_m = \frac{1}{N/2} \sum_{r=0}^{N/2-1} z_r \, e^{-i2\pi mr/(N/2)}$$

The D.F.T.s of the full and half sequences are related by;

$$X_m = \tfrac{1}{2}(Y_m + e^{-i2\pi m/N} Z_m) \qquad \text{(A1-9)}$$

In a similar manner the transforms $\{Y_m\}$ and $\{Z_m\}$ can be found by sub-dividing the sequence into quarters. In the limit, provided N is a power of 2 (a requirement for the F.F.T.), the time series can be repeatedly divided until the sub-sequences contain only one term each.

The D.F.T. of a sequence containing only one term is;

$$X_m = \frac{1}{N} \sum_{r=0}^{N-1} x_r e^{-i2\pi mr/N} \qquad \text{(A1-10)}$$

$$= x_o \qquad \text{for } N=1,\ r=0$$

Thus, the D.F.T. of a single term sequence is simply the term itself.

The subroutine DFT4 employed in this study represents a logical procedure for combining single term D.F.T.s to give the overall transform for the full series.

Numerous texts have been written, for example Newland (1975), where discuss the limitations and applications of the Fast Fourier Transform. A variety of computer algorithms have been developed, each having a particular application and inherent time saving.

```
      SUBROUTINE DFT4
C      DATE 7-MAY-82
C
C  PERFORM A FAST FOURIER TRANSFORM ON N DATA POINTS STORED
C  AS TWO DATA SETS EACH 'NN=N/2' POINTS LONG
C
C  DATA= DATA POINT ARRAY
C  N= NUMBER OF DATA POINTS (WHERE N=2**M)
C  RX= REAL PART (IN PHASE) OF TRANSFORM
C  AIX= IMAGINARY PART (OUT OF PHASE) OF TRANSFORM
C
      DIMENSION DATA(128),RX(65),AIX(65),RFI(64),AIFI(64)
      DIMENSION IR(128)
      COMMON/DFT4A/N,DATA,RX,AIX
C
      TYPE 50,N
   50 FORMAT(/,' START OF FFT FOR'I5,' DATA POINTS')
      NN=N/2
      IF(NN.GT.512) GO TO 120
  100 M=0
      L=1
  110 L=2*L
      M=M+1
      IF(L-NN) 110,130,120
  120 WRITE(7,1004)
 1004 FORMAT(' N IS LARGER THAN 1024 OR NOT AN INTEGER
     & POWER OF 2')
      STOP 'DFT1 ERROR'
  130 CONTINUE
C
C  FIND NN/2 ROOTS OF UNITY AND NN/4 INTEGERS IN REVERSE
C  BINARY ORDER
C
      PI=3.14159
      IR(1)=1
      RFI(1)=1
      AIFI(1)=0.0
      RFI(2)=0.0
      AIFI(2)=1.0
```

/CONT'D OVER

```
C
      II=NN/2
      KJ=NN/2
      JO=M-2
      DO 140 J=1,JO
      KO=KJ/II
      II=II/2
      RC=COS(PI/4.0/FLOAT(KO))
      AIC=SIN(PI/4.0/FLOAT(KO))
      DO 140 K=1,KO
      KK=K+KO
      IR(KK)=II+IR(K)
      RFI(2*KK-1)=RC*RFI(2*K-1)-AIC*AIFI(2*K-1)
      AIFI(2*KK-1)=RC*AIFI(2*K-1)+AIC*RFI(2*K-1)
      RFI(2*KK)=RC*RFI(2*K)-AIC*AIFI(2*K)
      AIFI(2*KK)=RC*AIFI(2*K)+AIC*RFI(2*K)
  140 CONTINUE
C
C  STORE 2NN REAL NUMBERS AS NN 'COMPLEX NUMBERS
      DO 150 I=1,NN
      RX(I)=DATA(2*I-1)
      AIX(I)=DATA(2*I)
  150 CONTINUE
C
C  PERFORM DISCRETE FOURIER TRANSFORM ON 2NN DATA POINTS
C
C  RESULT WILL BE IN REVERSE BINARY ORDER
C
      JO=NN
      DO 160L=1,M
      KO=NN/JO
      JO=JO/2
      J2=0
      DO 160 K=1,KO
      RC=RFI(K)
      AIC=AIFI(K)
      J1=J2
      DO 160 J=1,JO
      J1=J1+1
      J2=J1+JO
      RA=RX(J1)
      AIA=AIX(J1)
      RB=RX(J2)
      AIB=AIX(J2)
      RBC=RB*RC-AIB*AIC
      AIBC=RB*AIC+AIB*RC
      RX(J1)=RA+RBC
      AIX(J1)=AIA+AIBC
      RX(J2)=RA-RBC
      AIX(J2)=AIA-AIBC
  160 CONTINUE
```

/CONT'D OVER

```
C
C  UNSCRAMBLE TO CORRECT ORDER
C
      KK=NN/2
      KO=NN/4
      DO 180 K=1,KO
      K1=2*K-1
      K2=IR(K)
      J1=K1+1
      J2=K2+KK
      RA=RX(J1)
      AIA=AIX(J1)
      RX(J1)=RX(J2)
      AIX(J1)=AIX(J2)
      RX(J2)=RA
      AIX(J2)=AIA
      IF(K2.LE.K1) GO TO 180
      RA=RX(K1)
      AIA=AIX(K1)
      RX(K1)=RX(K2)
      AIX(K1)=AIX(K2)
      RX(K2)=RA
      AIX(K2)=AIA
C
      J1=K1+KK+1
      J2=K2+KK+1
      RA=RX(J1)
      AIA=AIX(J1)
      RX(J1)=RX(J2)
      AIX(J1)=AIX(J2)
      RX(J2)=RA
      AIX(J2)=AIA
  180 CONTINUE
```

/CONT'D OVER

```
C
C UNSCRAMBLE 2NN POINT TRANSFORM TO NN COMPLEX FOURIER
C  COMPONENTS
C
      XN=0.25/FLOAT(NN)
      RPSI=COS(PI/FLOAT(NN))
      AIPSI=SIN(PI/FLOAT(NN))
      RAI=0.0
      AIAI=1.0
      RX(NN+1)=RX(1)
      AIX(NN+1)=AIX(1)
      NNI=NN/2+1
      DO 190 I=1,NNI
      NI=NN-I+2
      RA1=XN*RX(I)
      AIA1=XN*AIX(I)
      RA2=XN*RX(NI)
      AIA2=-XN*AIX(NI)
      RB1=RA1+RA2
      AIB1=AIA1+AIA2
      RB2=(RA1-RA2)*RAI-(AIA1-AIA2)*AIAI
      AIB2=(RA1-RA2)*AIAI+(AIA1-AIA2)*RAI
      RX(NI)=RB1+RB2
      AIX(NI)=AIB1+AIB2
      RX(I)=RB1-RB2
      AIX(I)=AIB2-AIB1
      RAI1=RAI*RPSI-AIAI*AIPSI
      AIAI=RAI*AIPSI+AIAI*RPSI
      RAI=RAI1
  190 CONTINUE
C
C HALVE THE NN+1 COMPONENTS FOR POSITVE FREQUENCIES ONLY
C
      RX(NN+1)=0.5*RX(NN+1)
      AIX(NN+1)=0.5*AIX(NN+1)
C
C     DOUBLE ALL CPTS FOR SINGLE SIDED SPECTRUM
C
      DO 20 I=1,NN
      RX(I)=RX(I)*2.0
      AIX(I)=AIX(I)*2.0
  20  CONTINUE
      TYPE 70
   70 FORMAT(' FFT ENDS')
      RETURN
     END
```

APPENDIX 2 - LEAST SQUARES SINE FITTING

A2.1 Least Squares Formulation

Consider a function which has the form of a sine wave of unknown amplitude, wavelength and phase superimposed on an unknown mean value. The function is approximated by a series of discrete data points $\{x_i, y_i\}$, i=1,n as shown in Figure A2.1.

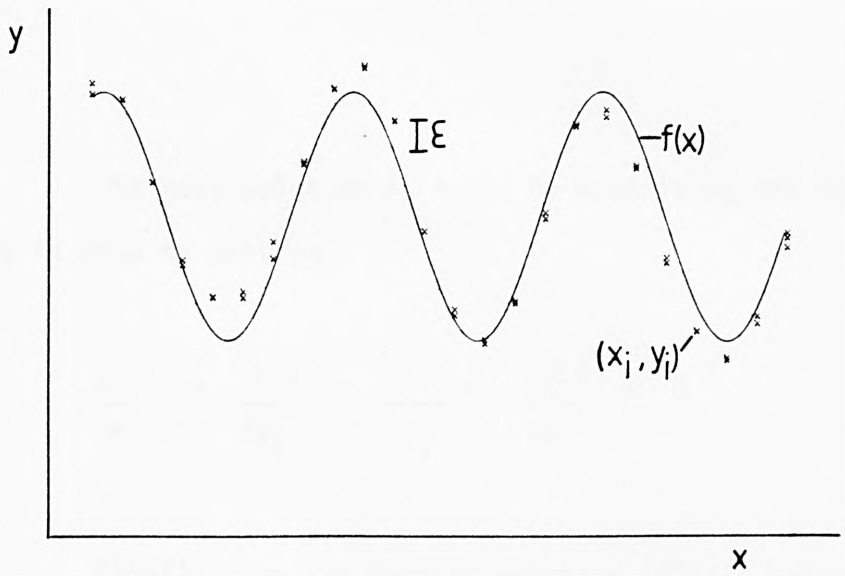

Sine Fitting

Figure A2.1

The requirement is to assign values to the parameters of the sine curve, such that it gives the best fit to the n data points.

$$f(x) = a_0 + a_1 \cos kx + b_1 \sin kx \qquad \text{(A2-1)}$$

At each data point, x_i, there will be a difference between $f(x)$ and the measured y_i;

$$\varepsilon = y_i - f(x) = y_i - a_0 - a_1 \cos kx_i - b_1 \sin kx_i \qquad \text{(A2-2)}$$

The sum of the squares of the errors for all of the data points (dropping the suffix i) is;

$$\Sigma\varepsilon^2 = \Sigma y^2 - 2a_0\Sigma y - 2a_1\Sigma y\cos kx - 2b_1\Sigma y\sin kx + na_0^2 + 2a_0a_1\Sigma\cos kx + 2a_0b_1\Sigma\sin kx + a_1^2\Sigma\cos^2 kx + b_1^2\Sigma\sin^2 kx + 2a_1b_1\Sigma\cos kx\sin kx \qquad \text{(A2-3)}$$

The best solution is found by minimizing the value of $\Sigma\varepsilon^2$. This is done by putting;

$$\frac{\partial\Sigma\varepsilon^2}{\partial a_0} = \frac{\partial\Sigma\varepsilon^2}{\partial a_1} = \frac{\partial\Sigma\varepsilon^2}{\partial b_1} = \frac{\partial\Sigma\varepsilon^2}{\partial k} = 0 \qquad \text{(A2-4)}$$

Clearly from the form of equation (A2-3), there will be no explicit solution for k. Initially, therefore, k is assumed to be known and the problem is solved for a_0, a_1 and b_1.

A2.2 Solution for Known k

Where k is assumed to be known, (A2-3) and (A2-4) yield three simultaneous equations;

$$\frac{\partial \Sigma\varepsilon^2}{\partial a_0} = -2\Sigma y + 2na_0 + 2a_1\Sigma\cos kx + 2b_1\Sigma\sin kx = 0 \qquad \text{(A2-5)}$$

$$\frac{\partial \Sigma\varepsilon^2}{\partial a_1} = -2\Sigma y\cos kx + 2a_0\Sigma\cos kx + 2b_1\Sigma\sin kx\cos kx + 2a_1\Sigma\cos^2 kx = 0 \qquad \text{(A2-6)}$$

$$\frac{\partial \Sigma\sigma^2}{\partial b_1} = -2\Sigma y\cos kx + 2a_0\Sigma\sin kx + 2a_1\Sigma\sin kx\cos kx + 2b_1\Sigma\sin^2 kx = 0 \qquad \text{(A2-7)}$$

These equations are readily solved to give the optimum values of a_0, a_1 and b_1. A measure of the closeness of the fit is given by the residual sum of squares of errors.

$$SE = \Sigma(y - a_0 - a_1\cos kx - b_1\sin kx)^2 \qquad \text{(A2-8)}$$

The subroutine SINFIT forms a matrix for the solution of equations (A2-5), (A2-6) and (A2-7) using the given data points $\{x_i, y_i\}$ and the assumed value of k. It returns values for a_0, a_1, b_1 and SE.

A2.3 Determination of k

The optimum value of k is found by a technique of successive approximations. The procedure adopted in the subroutine KFIND is as follows.

(i) For a wide range of values of k, separated by intervals of Δk, the associated values of a_0, a_1, b_1 and SE are found using the

procedure described above (SINFIT).

(ii) The first approximation to k is taken as being the one with the smallest residual error, SE.

(iii) The process is repeated for a range of values of k in the vicinity of the first approximation, with a smaller value of Δk, to give a second approximation.

(iv) Successive iterations are carried out to determine k to the required accuracy.

The optimum value of k, and the associated values of a_0, a_1, and b_1 define the best-fit sine wave, f(x) to the data points. The residual of SE is now a measure of how closely the sine function follows the given data points.

A2.4 Second Sine Component

Consider the case where the expected form of the data is the sum of two unknown sine waves. The function to be fitted is

$$h(x) = f(x) + g(x) \qquad \text{(A2-9)}$$

where $$f(x) = a_0 + a_1\cos kx + b_1\sin kx \qquad \text{(A2-1)}$$

$$g(x) = a_0' + a_1'\cos k'x + b_1'\sin k'x \qquad \text{(A2-10)}$$

Treating the data as in Sections A2.2 and A2.3 gives f(x) as the more significant of the two sine wave components, with a relatively large residual error, SE.

The data points are then adjusted to take out the first sine wave;

$$y'_i = y_i - f(x_i) \quad \text{for all data points} \tag{A2-11}$$

The function g(x) is found by fitting a sine curve to y' in a similar manner. a_1', b_1' and k_1' describe the second sine components, while a_0' represents a small correction to the mean value.

It would be possible to continue to include a third term. However, with experimental errors and the smoothing effect of the first two terms it is likely to be both small and meaningless.

```
      SUBROUTINE SINFIT(N,X,Y,RK,C,SE)
      DOUBLE PRECISION A(3,3),B(3),C(3),AA(3,3),
     &WKS1(3),WKS2(3)
      DIMENSION X(N),Y(N)
C
C     SET UP ARRAYS A(3,3) & B(3) TO SOLVE FOR
C     BEST SIN FIT
C
      DO 10 I=1,3
      B(I)=0.0
      DO 10 J=1,3
      A(I,J)=0.0
   10 CONTINUE
      A(1,1)=N
      DO 20 I=1,N
      CO=COS(RK*X(I))
      SI=SIN(RK*X(I))
      A(1,2)=A(1,2)+CO
      A(1,3)=A(1,3)+SI
      A(2,2)=A(2,2)+CO**2
      A(2,3)=A(2,3)+CO*SI
      A(3,3)=A(3,3)+SI**2
      B(1)=B(1)+Y(I)
      B(2)=B(2)+Y(I)*CO
      B(3)=B(3)+Y(I)*SI
   20 CONTINUE
      A(2,1)=A(1,2)
      A(3,1)=A(1,3)
      A(3,2)=A(2,3)
C
C     CALL NAG ROUTINE TO SOLVE
C     ANSWERS IN C MATRIX
C
      IFAIL=0
      CALL F04ATF(A,3,B,3,C,AA,3,WKS1,WKS2,IFAIL)
      IF(IFAIL.EQ.0) GO TO 30
      PRINT 40,IFAIL
   40 FORMAT(/,' FAIL AT',I2)
      STOP
   30 CONTINUE
C
C     COMPUTE RESIDUAL SUM OF ERRORS**2
C
      SE=0.0
      DO 50 I=1,N
      SE=SE+(Y(I)-C(1)-C(2)*COS(RK*X(I))-
     &C(3)*SIN(RK*X(I)))**2
   50 CONTINUE
      RETURN
      END
```

```
      SUBROUTINE KFIND(M,X,Y,RKOPT,C,SE)
      DOUBLE PRECISION C(3)
      DIMENSION X(M),Y(M)
      N=M
C
C     FIND OPT. VAL. OF K BY SUCCESSIVE APPROX.
C     INITIALLY CONSIDER K=1,36,1 FIND CLOSEST FIT
C     (ALLOWABLE VALUES OF K DEPEND ALSO ON TOTAL
C      LENGTH OF SAMPLE AND SAMPLING INTERVAL)
C     THEN REDUCE INTERVAL IN K
C
C     FIND RANGE OF X VALUES
C
      XMAX=0.0
      XMIN=100.0
      DO 5 I=1,N
      IF(X(I).LT.XMAX) GO TO 6
      XMAX=X(I)
    6 IF(X(I).GT.XMIN) GO TO 5
      XMIN=X(I)
    5 CONTINUE
C
C     CALC. MAX & MIN ALLOWABLE VALUES OF K
C
      RKMIN=2.0*3.1415/(XMAX-XMIN)
      RKMAX=RKMIN*0.25*N
      RKOPT=10.0
      DO 10 J=1,5
      RINT=10.0**(1-J)
      SMIN=10.0**6
      NINT=19
      IF(J.EQ.1) NINT=NINT+16
      DO 20 I=1,NINT
      RK=RKOPT+(I-10)*RINT
      IF(RK.LT.RKMIN.OR.RK.GT.RKMAX) GO TO 20
C
C     FOR EACH K FIND LEAST SQUARES SINE FIT
C     AND RESIDUAL SUM OF ERRORS**2
C
      CALL SINFIT(N,X,Y,RK,C,S)
      IF(S.GE.SMIN) GO TO 20
      IOPT=I
      SMIN=S
   20 CONTINUE
      RKOPT=RKOPT+(IOPT-10)*RINT
   10 CONTINUE
C
C     FOR OPT K. EVALUATE A0,A1,B1&SE
C
      CALL SINFIT(N,X,Y,RKOPT,C,SE)
      RETURN
      END
```

APPENDIX 3 - SIMPLIFICATION OF TRIGONOMETRIC EXPRESSIONS

A simplification is required for the trigonometric expressions which arise from $u|u|$ in the determination of the drag force components. These are of the form;

$$(a\cos\theta + f(\theta))|a\cos\theta + f(\theta)| \tag{A3-1}$$

The simplification is found by considering the combinations of positive and negative values of $\cos\theta$ and $f(\theta)$. In order that a single expression can be used for all of the combinations, two limiting assumptions must be made. These are;

$$f << a \tag{A3-2}$$

such that $f^2(\theta)$ is negligible, and where $\cos\theta$ and $f(\theta)$ are of opposite sign;

$$|f(\theta)| < |a\cos\theta| \tag{A3-3}$$

Subject to these limitations, (A3-1) is simplified by;

$$(a\cos\theta + f(\theta))|a\cos\theta + f(\theta)| = a^2\cos\theta|\cos\theta| + 2a|\cos\theta|f(\theta) \tag{A3-4}$$

The validity of this approximation is demonstrated in Figure A3.1, for $a=1$ and $f(\theta)=0.1\ (\sin\theta + \sin2\theta + \cos2\theta)$, representing the extreme of the range of its use in this study.

The approximation breaks down in two regions; firstly at the peak values where $f^2(\theta)$ is not negligible, and secondly at the zero crossing point where the condition (A3-3) is not satisfied. In spite of these deviations, the overall fit shown in Figure A3.1 is very good, and for practical purposes, (A3-4) is a valid simplification.

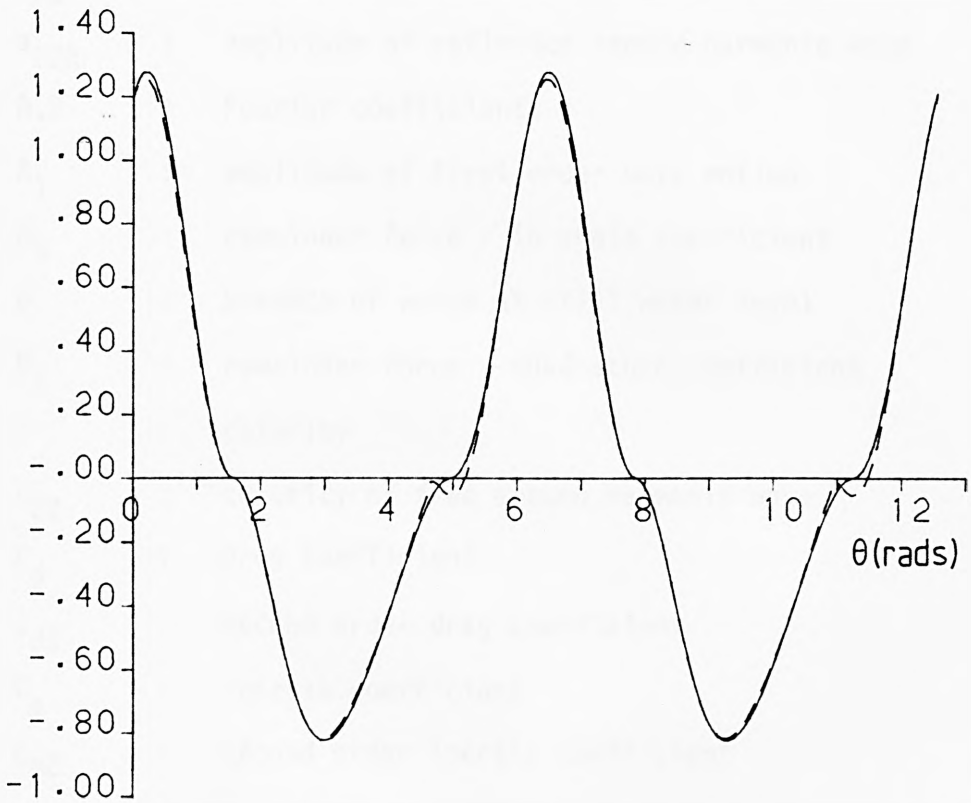

——— $(\cos\theta + 0{\cdot}1(\sin\theta + \sin 2\theta + \cos 2\theta)) \times |\cos\theta + 0{\cdot}1(\sin\theta + \sin 2\theta + \cos 2\theta)|$

– – – $\cos\theta\,|\cos\theta| + 0{\cdot}2(\sin\theta + \sin 2\theta + \cos 2\theta)|\cos\theta|$

Simplification of a Trigonometric Expression

Figure A3.1

NOMENCLATURE

a_I	:	amplitude of first order incident wave
a_R	:	amplitude of first order reflected wave
a_2	:	amplitude of second order Stokes' component
a_{22}	:	amplitude of free second harmonic wave
a_{22R}	:	amplitude of reflected second harmonic wave
A,B	:	Fourier coefficients
A_1	:	amplitude of first order wave motion
A_3	:	remainder force - in phase coefficient
b	:	breadth of wedge at still water level
B_3	:	remainder force - quadrature coefficient
c	:	celerity
c_{22}	:	celerity of free second harmonic wave
C_d	:	drag coefficient
C_{d2}	:	second order drag coefficient
C_m	:	inertia coefficient
C_{m2}	:	second order inertia coefficient
C_F	:	total force coefficient
C_L	:	lift coefficient
$CORR_D$	:	correction to drag force
$CORR_I$	:	correction to inertia force
d	:	mean submergence of wedge
D	:	cylinder diameter
f_o	:	fundamental wave frequency
F_e	:	elemental force
F_d	:	elemental drag force
F_i	:	elemental inertia force

F_{dp} : elemental dynamic pressure force

FT : total force

FD : drag force

FI : inertia force

FD2 : drag force due to Stokes' second order wave

FI2 : inertia force due to Stokes' second order wave

FCA : convective acceleration force

FWD : waterline drag force

FWI : waterline inertia force

FDP : dynamic pressure force

FDR : drag force due to reflected wave

FIR : inertia force due to reflected wave

FD22 : drag force due to free wave

FI22 : inertia force due to free wave

g : acceleration due to gravity

h : water depth

H : wave height

k : wave number

k_{22} : wave number of free second harmonic

k_B : wave number of second order beat wavelength

k_{2R} : wave number of second order reflection beat wavelength

K_R : reflection coefficient

KC : Keulegan Carpenter number

KCS : surface value of KC

KCI : integrated average of KC

L : wavelength

L_{22} : wavelength of free second harmonic

L_R : first order reflection beat wavelength

L_B : second order beat wavelength

L_{2R} : second order reflection beat wavelength

M : moment

M_a : added mass

N : number of vortices shed per half wave cycle

P : pressure

P_d : dynamic pressure

Re : Reynolds' number

S : amplitude of best fit sine component

SE : residual sum of squares of errors

t : time

T : wave period

u : horizontal particle velocity

u_o : horizontal velocity at free surface

u_1 : first order horizontal velocity

u_2 : second order component of horizontal velocity

u_R : horizontal velocity due to reflected wave

u_{22} : horizontal velocity due to free wave

u_t : mass transport velocity

U_t : surface value of mass transport velocity

v : vertical particle velocity

V : volume of element of cylinder

WA : amplitude of wedge oscillations

WL : wavelength

x,y : cartesian coordinates

x_r : term in a discrete time series

X_m : term in a discrete Fourier transform

$\bar{y}$: depth of action

α,β,γ : phase angles

β : frequency parameter

δ : phase angle between incident and total wave motion

ε : residual error

η : free surface displacement

θ : polar coordinate

λ : perturbation parameter

ν : kinematic viscosity

ρ : density

ϕ : velocity potential

ω : angular frequency

Ω : orbital shape parameter

REFERENCES

Bidde, D. (1971): Laboratory study of lift forces on circular piles - J. Water. Harb. & Coast. Eng. Div., ASCE, Vol. 97, WW4.

Buhr Hansen, J. and Svendsen, I. (1974): Laboratory generation of waves of constant form - Proc. 14th Conf. Coast. Eng.

Chakrabarti, S., Wolbert, A. and Tam, W. (1976): Wave forces on vertical circular cylinder - J. Water. Harb. & Coast. Eng. Div., ASCE, Vol. 102, WW2.

Chakrabarti, S. (1980a): Inline forces on fixed vertical cylinders in waves - J. Water. Port Coast. & Ocean Div., ASCE, WW2.

Chakrabarti, S. (1980b): Laboratory generated waves and wave theories - J. Water. Port Coast. & Ocean Div., ASCE, WW3.

Dean, R. (1965): Stream function representation of non linear ocean waves - J. Geophys. Res., Vol. 70, p 4561 - 4572.

Dean, R. (1970): Relative validities of water wave theories - J. Water. Harb. & Coast. Eng. Div., ASCE, Vol. 96, WW1.

Eagleson, P. and Dean, R. (1966); and Dean and Eagleson (1966): from Estuary and Coastline Hydrodynamics (Ippen A. ed.), McGraw-Hill.

Ellix, D. and Arumugam, K. (1984): An experimental study of waves generated by an oscillating wedge - J. Hyd. Res. , Vol. 22, No.5.

Evans, D. (1969): Analysis of wave force data - Off. Tech. Conf., paper 1005.

Flick, R. and Guza, R. (1980): Paddle generated waves in laboratory channels - J. Water. Port Coast. & Ocean Div., ASCE, WW1.

Garrison, C., Field , J., and May, M. (1977): Drag and inertia forces on a cylinder in periodic flow - J. Water. Port Coast. & Ocean Div., ASCE, Vol. 103, WW2.

Gaston, J. and Ohmart, R. (1979): Effects of surface roughness on drag coefficients - Civ. Eng. in Oceans IV, ASCE, p 611 - 621.

Goda, Y. and Suzuki, Y. (1976): Estimation of incident and reflected waves in random wave experiments - Proc. 15th Conf. Coast. Eng.

Havelock, T. (1929): Forced surface waves on water - Phil. Mag. Series 7, Vol. 8, p 569 - 576.

Hogben, N., Miller, B., Searle, J. and Ward, G. (1977): Estimation of fluid loading on offshore structures - Proc. Inst.Civ. Eng. Pt. 2, 63, p 515 - 562.

Hydraulics Research Station (1981): Wave force on cylinders - simulation of high Reynolds' numbers - Report No. EX 996.

Isaacson, M. and Maull, D. (1976): Transverse forces on circular cylinders in waves - J. Water. Harb. & Coast. Eng. Div., ASCE, WW1.

Isaacson, M. (1979): Nonlinear inertia forces on bodies - J. Water. Port. Coast. & Ocean Div., ASCE, Vol. 105, WW3.

Iwagaki, Y. and Sakai, T. (1970): Horizontal water particle velocity of finite amplitude waves - Proc. 10th Conf. Coast. Eng.

Jen, Y. (1968): Laboratory study of inertia forces on a pile - J. Water. & Harb. Div., ASCE, WW1.

Keulegan, G. and Carpenter, L. (1958): Forces on cylinders and plates in an oscillating fluid - J. Res. Nat. Bur. Stand., Vol. 60, No. 5, paper 2857.

Kim, C. (1969): Hydrodynamic forces and moments for heaving, swaying and rolling cylinders on water of finite depth - J. Ship Res., Vol. 1, No. 3.

Korteweg, D. and De Vries, G. (1895): On the change of form of long waves advancing in a rectangular channel, and on a new type of long stationary waves - Phil. Mag., 5th Series, Vol. 39.

Lamb, Sir H. (1932): Hydrodynamics, 6th ed., Camb. Univ. Press.

Lighthill, J. (1979): Waves and hydrodynamic loading - Proc. 2nd Int. Conf. B.O.S.S., London, Vol. 1, p 1 - 40.

MacCamy, R. and Fuchs, R. (1954): Wave forces on piles: a diffraction theory - U.S. Army Corps of Eng., Beach Erosion Board, Tech. Memo 69.

Madsen, O. (1970): Waves generated by a piston-type wavemaker - Proc. 12th Conf. Coast. Eng.

Madsen, O. (1971): On the generation of long waves - J. Geophys. Res., Vol. 36.

Mahony, J. and Pritchard, W. (1980): Wave reflexion from beaches - J. Fluid Mech., Vol. 101, p 809 - 832.

Maull, D. and Milliner, M. (1978): Sinusoidal flow past a circular cylinder - Coast Eng., Vol. II, No. 2, p. 149 - 168.

Morison, J., O'Brien, M., Johnson J. and Schaaf, S. (1950): The forces exerted by surface waves on piles - Petroleum Trans. AIME, Vol. 189, p 149 - 157.

Newland, D. (1975): Random vibrations and spectral analysis, Longman.

Ramberg, S. and Niedzwecki, J. (1979): Some uncertainties and errors in wave force computations - Off. Tech. Conf., paper OTC 3597.

Sarpkaya, T. (1976a): In-line and transverse forces on cylinders in oscillatory flow at high Reynolds' numbers - Off. Tech. Conf., paper OTC 2533.

Sarpkaya, T. (1976b): Forces on rough walled circular cylinders - Proc. 15th Conf. Coast. Eng.

Sarpkaya, T. and Isaacson, M. (1981): Mechanics of Wave Forces on Offshore Structures - Van Nostrand Reinhold.

Scott-Russell, J. (1844): Report on waves - 14th Meet. Brit. Ass. Adv. Sci., p 311 - 390.

Skjelbreia, L. and Hendrickson, J. (1961): Fifth order gravity wave theory - Proc. 7th Conf. Coast. Eng.

Stansby, P., Bullock, G. and Short, I. (1983): Quasi - 2-D forces on a vertical cylinder in waves - J. Water. Port Coast. & Ocean Eng., ASCE, Vol. 109, No. 1.

Stokes, G. (1847): On the theory of oscillatory waves - Trans. Camb. Phil. Soc., Vol. 8, p 441 - 455.

Ursell, F. (1949): On the heaving motion of a circular cylinder on the surface of a fluid - Quart. J. Mech. & App. Math., Vol. 2.

Ursell, F., Dean, R. and Yu, Y. (1960): Forced small-amplitude water waves: a comparison of theory and experiment - J. Fluid Mech., Vol. 7.

Verley, R. (1975): Wave forces on structures - an introduction - B.H.R.A., Rep. No. TN 1319.

Wang, S. (1974): Plunger-type wavemakers: theory and experiment - J. Hyd. Res., Vol. 12.

Wiegel, R., Beebe, K. and Moon, J. (1957): Ocean wave forces on circular cylindrical piles - J. Hyd. Div. ASCE, Vol. 83, HY2.